

**SYNTHESIS AND CHARACTERIZATION OF SOME METAL  
OXIDE NANOPARTICLES USING NEWLY DEVELOPED  
GREEN SOLVENTS**

**THESIS SUBMITTED TO BHARATHIDASAN UNIVERSITY**



**In partial fulfilment of the requirement for the degree of  
DOCTOR OF PHILOSOPHY  
IN  
CHEMISTRY**

**By**

**K. SARJUNA, M. Sc., B.Ed. M.Phil.,**

**(Ref. No: 06926/Ph. D. K2/ Chemistry/ Full-Time/ April-2017)**

**Under the guidance of**

**Dr. D. ILANGESWARAN, M. Sc., M. Phil., Ph.D.,**

**Assistant Professor in Chemistry**



**DEPARTMENT OF CHEMISTRY  
RAJAH SERFOJI GOVERNMENT COLLEGE (AUTONOMOUS)  
THANJAVUR-613005  
TAMILNADU, INDIA**

**MARCH-2022**

Dr. D. Ilangeswaran, M.Sc., M.Phil., Ph.D.,  
**RESEARCH SUPERVISOR & CONVENER**  
*Department of Chemistry*  
**Rajah Serfoji Govt. College (Autonomous)**  
Thanjavur – 613005



**email: [ilangeswaran@rsgc.ac.in](mailto:ilangeswaran@rsgc.ac.in)**  
**Mobile: 8903853566, 9894716566**

### **CERTIFICATE**

This is to certify that the thesis entitled “**SYNTHESIS AND CHARACTERIZATION OF SOME METAL OXIDE NANOPARTICLES USING NEWLY DEVELOPED GREEN SOLVENTS**” submitted by **K. SARJUNA (Ref. No: 06926/Ph. D. K2/ Chemistry/ Full-Time/ April-2017)** for the award of the Degree of Doctorate of Philosophy in Chemistry is a record of research work done under my supervision during the period from April 2017-December 2021 and the thesis has not formed the basis of award of any Degree, Diploma, Associateship, and Fellowship or any other similar title of any University or Institution. Also, certify that the thesis represents an independent work on the part of the candidate.

Date: [23.03.2022](#)

Place: [Thanjavur - 05](#)

Signature of the Research Supervisor

Dr.D. ILANGESWARAN, M.Sc.,M.Phil.,Ph.D.,  
*Assistant Professor,*  
P.G. & Research Dept. of Chemistry,  
Rajah Serfoji Govt. College (Autonomous),  
Thanjavur (Dt)-613 005

Dr. D. Ilangeswaran, M.Sc., M.Phil., Ph.D.,  
**RESEARCH SUPERVISOR & CONVENER**  
*Department of Chemistry*  
**Rajah Serfoji Govt. College (Autonomous)**  
Thanjavur – 613005



**email: ilangeswaran@rsgc.ac.in**  
**Mobile: 8903853566, 9894716566**

### CERTIFICATE OF PLAGIARISM

1	Name of the Research Scholar	<b>Mrs. K. SARJUNA</b>
2	Course of study	Ph.D – Chemistry ( Full time)
3	Ref.no.	<b>(Ref. No: 06926/Ph. D. K2/ Chemistry/ Full-Time/ April-2017)</b>
4	Title of the thesis/ Dissertation	Synthesis and Characterization of some metal oxide nanoparticles using newly developed green solvents
5	Name of the Research Supervisor	<b>Dr. D. ILANGESWARAN</b>
6	Department / Institution / Research centre	Department of chemistry Rajah Serfoji Government College (autonomous) Thanjavur-613005
7	Acceptable Maximum limit	20 %
8	Percentage of similarity of content identified	0 %
9	Software used	URKUND
10	Date of verification	16-03-2022
11	Issued by	bdulib.bdu@analysis.urkund.com

Report on plagiarism check, item with % of similarity is identified.

Date: 23.03.2022

Place: Thanjavur - 05

Signature of the Research Supervisor

Dr.D. ILANGESWARAN, M.Sc., M.Phil., Ph.D.,  
*Assistant Professor,*  
P.G. & Research Dept. of Chemistry,  
Rajah Serfoji Govt. College (Autonomous),  
Thanjavur (Dt)-613 005





## Document Information

---

<b>Analyzed document</b>	K.SARJUNA.docx (D130522480)
<b>Submitted</b>	2022-03-16T06:37:00.0000000
<b>Submitted by</b>	Srinivasa ragavan S
<b>Submitter email</b>	bdulib@gmail.com
<b>Similarity</b>	0%
<b>Analysis address</b>	bdulib.bdu@analysis.arkund.com

## Sources included in the report

---

<b>W</b>	URL: <a href="https://xueshu.baidu.com/usercenter/paper/show?paperid=217c09d033dbaeb9662cf9c6c8d95c8b">https://xueshu.baidu.com/usercenter/paper/show?paperid=217c09d033dbaeb9662cf9c6c8d95c8b</a> Fetched: 2022-03-16T06:37:31.5930000		<b>1</b>
<b>W</b>	URL: <a href="https://www.mdpi.com/2076-3417/9/19/4169/pdf">https://www.mdpi.com/2076-3417/9/19/4169/pdf</a> Fetched: 2021-01-13T06:57:04.0530000		<b>3</b>
<b>W</b>	URL: <a href="http://121.199.17.194/paper/search/byFaculty/17612">http://121.199.17.194/paper/search/byFaculty/17612</a> Fetched: 2022-03-16T06:37:30.8170000		<b>1</b>
<b>W</b>	URL: <a href="https://pdfs.semanticscholar.org/b2a6/57a3f2ebc9d0920d846e357fe2767f4e2a16.pdf">https://pdfs.semanticscholar.org/b2a6/57a3f2ebc9d0920d846e357fe2767f4e2a16.pdf</a> Fetched: 2022-03-16T06:37:24.9430000		<b>6</b>

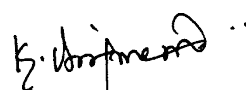
---

**K. SARJUNA M.Sc., B.Ed., M.Phil.,**  
**Research scholar**  
**Department of Chemistry**  
**Rajah Serfoji Government College (Autonomous),**  
**Thanjavur – 613 005.**  
**TAMIL NADU, INDIA**

---

## **DECLARATION**

I hereby declare that the thesis entitled “**SYNTHESIS AND CHARACTERIZATION OF SOME METAL OXIDE NANOPARTICLES USING NEWLY DEVELOPED GREEN SOLVENTS**” has been originally carried out by me at Research Lab II, Department of Chemistry, Rajah Serfoji Government College (Autonomous), Thanjavur, India, under the guidance of **Dr. D. Ilangeswaran**, Assistant Professor, Department of Chemistry, Rajah Serfoji Government College (Autonomous), Thanjavur, India. This work has not formed the basis for the award of any Degree, Diploma, Associateship, Fellowship, or another similar title of Bharathidasan University or any other University.

  
(K. SARJUNA)

Place: Thanjavur

Date: 23.03.2022

## ACKNOWLEDGEMENT

First and foremost, I owe my debt to my guide **Dr. D. ILANGESWARAN**, Assistant Professor, Department of Chemistry, Rajah Serfoji Govt College (Autonomous), Thanjavur, for his friendly guidance, constant care, and encouragement throughout the research program. I thank him for all his contributions of time, ideas, and funding to make my Ph.D. experience productive and stimulating. It would have been quite impossible to carry on the research work and make it into the final shape of a thesis without his able guidance. His affection for me is fondly remembered.

I convey my sincere thanks to my Doctoral Committee members Prof. Dr. S. VALARSELVAN, Assistant Professor, Department of Chemistry, H.H. The Rajah's College (Autonomous), Pudukottai and Prof. Dr. R. CHITRAVEL, Assistant Professor, Department of Chemistry, Rajah Serfoji Govt Arts College (Autonomous), Thanjavur for their insightful comments and encouragement throughout my course of work.

I am very grateful to thank Prof. S.P. ELANGO VAN the Head, Department of Chemistry, Rajah Serfoji Govt College (Autonomous), Thanjavur for his personal care, unstinted support, and constant encouragement.

I express gratitude to the Principal, Dr. V. SENTHAMILSELVI Rajah Serfoji Govt College (Autonomous), Thanjavur for providing me the necessary facilities to carry out this work.

I express my special thanks to Mr. BALAJI, Assistant Professor, Department of Chemistry, Rajah Serfoji Govt College (Autonomous), Thanjavur for his inestimable help throughout my work.

I would like to thank the Teaching, non-teaching staff members of Rajah Serfoji Govt College (Autonomous), Thanjavur for their timely help during my study.


I take this opportunity to thank my research colleague Mrs.K.Hemalatha, and Mr. P.G.Ramesh, for their fullest cooperation throughout the tenure of this work.

It is a great pleasure to express my special thanks to my friends Mrs.G.Jayabharathi, Research Scholar and Ms.S.Karthika, Research Scholar for motivating me to do research and all Research Students and Post Graduate Students in the Department of Chemistry, Rajah Serfoji Govt Arts College (Autonomous), Thanjavur.

On a personal front, a million words would be too short to say how grateful I am to my wonderful parents, Mr.R.Kannan & Mrs.K.Mangaiyarkarasi, my husband Mr.M.Amreetharasan, my adorable sister Mrs. K.Janani, my brothers K.Jawahar, K.Jegan Santosh, and my loving kids A.Abhinav Harshal, A.Hiranmayi Venba, for their outpouring love and affection, for supporting me through my trials and tribulations, for bearing the pain of separation as I pursued my dreams.

Last but not least I would like to thank my loveable family friends Dr.K.Raju, Mrs.S.Padmapriya, R.P.Shivaprashanth, Thank you from the bottom of my heart for being my first excellent cheerleader and the constant sounding boards while encouraging me towards excellence. You all are the reason I did this and the reason I thrive to be better.

Above all, I offer my thanks and praises to the Almighty God for his immense shower of Blessings.

  
(K.SARJUNA)

## CONTENTS

<b>Chapter</b>	<b>Title</b>	<b>Page No.</b>	
<b>I</b>	<b>1</b>	<b>Introduction</b>	<b>1</b>
	1.1	General introduction to deep eutectic solvents	1
	1.2	Definition of Deep Eutectic Solvents	4
	1.3	Physicochemical characteristics of DESs	6
	1.3.1	Freezing Point	6
	1.3.2	Density	6
	1.3.3	Viscosity	7
	1.3.4	Ionic conductivity	8
	1.3.5	Acidity or Alkalinity	8
	1.4	Binary Deep Eutectic Solvents	8
	1.4.1	Types of Binary Deep Eutectic Solvents	9
	1.5	Ternary Deep Eutectic Solvents	10
	1.6	Zinc Chloride based Deep Eutectic Solvents	11
	1.7	Malonic Acid-based Deep Eutectic Solvents	13
	1.8	Manganese based Deep Eutectic Solvents	14
	1.9	Sugar-based Deep Eutectic Solvents	14
	1.10	Significance of Deep Eutectic Solvents	15
	1.11	Comparison of ionic liquids with deep eutectic solvents	16
	1.12	Applications of Deep Eutectic Solvents	17
	1.12.1	Applications of Deep Eutectic Solvents in Nanotechnology	18
	1.13	Introduction to Nanoparticles	21
	1.13.1	Silver Nanoparticles	21
	1.13.2	Copper Nanoparticles	23
	1.13.3	Cadmium Nanoparticles	24



	1.13.4	Mercury Nanoparticles	25
<b>1.14</b>		<b>Review of Literature</b>	27
	1.14.1	Deep Eutectic Solvents- Synthesis and Characterization	27
	1.14.2	Copper Nanoparticles	27
	1.14.3	Silver Nanoparticles	30
	1.14.4	Cadmium Nanoparticles	32
	1.14.5	Mercury Nanoparticles	33
<b>1.15</b>		<b>Aim, scope, and objectives of the present work</b>	37
		References	39
<b>II</b>	<b>2</b>	<b>Materials and Methods</b>	
	2.1	Materials	69
	2.2	Experimental methods	70
	2.2.1	General method of preparation of Deep Eutectic Solvents	70
	2.2.2	General preparation of Ternary Deep Eutectic Solvents	71
	2.2.3	General procedure for the synthesis of nanoparticles	73
	2.2.3.1	Synthesis of copper nanoparticles	73
	2.2.3.2	Synthesis of silver nanoparticles	73
	2.2.3.3	Synthesis of cadmium and mercury nanoparticles	74
	2.2.4	Instrumentation used for the characterization of Deep Eutectic Solvents and nanoparticles	74
	2.2.4.1	pH meter	74
	2.2.4.2	Viscometer	74
	2.2.4.3	Conductivity meter	75
	2.2.4.4	Density calculation	75
	2.2.4.5	Fourier Transform Infrared Spectroscopy	75
	2.2.4.6	Ultraviolet-Visible spectroscopy	75

2.2.4.7	Scanning Electron Microscopy	76
2.2.4.8	X-Ray Diffractometer	76
2.2.4.9	Energy Dispersive X-Ray Analysis	76
2.2.5	Disc Diffusion method	76
	References	78

### **III Preparation and Characterization Studies of Malonic Acid-Based Binary Deep Eutectic Solvents**

3.	Malonic acid Based Binary Deep Eutectic Solvents (BDES)	
3.1	Introduction	79
3.2	Preparation of Malonic acid- Glucose (MA-GLU) BDES	79
3.3	Preparation of Malonic acid- Fructose (MA-FRU) BDES	79
3.4	Preparation of Malonic acid- Glycerol (MA-GCL) BDES	80
3.5	Results and Discussion	80
3.5.1	Characterization of Malonic Acid- Glucose BDES	80
3.5.1.1	Density and Conductivity	80
3.5.1.2	pH	81
3.5.1.3	Viscosity	81
3.5.1.4	FTIR spectral analysis of MA-GLU	81
3.5.2	Characterization of Malonic Acid- Fructose BDES	82
3.5.2.1	Density and Conductivity	82
3.5.2.2	pH	82
3.5.2.3	Viscosity	82
3.5.2.4	FTIR spectral analysis of MA-FRU	83
3.5.3	Characterization of Malonic Acid- Glycerol BDES	83
3.5.3.1	Density and Conductivity	83
3.5.3.2	pH	84

	3.5.3.3	Viscosity	84
	3.5.3.4	FTIR spectral analysis of MA-GCL	84
3.6		Conclusion	85
		References	86
<b>IV</b>		<b>Preparation and Characterization Studies of Zinc chloride- Based Binary Deep Eutectic Solvents</b>	
4.		Zinc chloride Based Binary Deep Eutectic Solvents (BDES)	93
4.1		Introduction	93
4.2		Preparation of Zinc chloride- Glucose (ZC-GLU) BDES	93
4.3		Preparation of Zinc chloride - Fructose (ZC-FRU) BDES	93
4.4		Preparation of Zinc chloride – Lactic Acid (ZC-LA) BDES	94
4.5		Results and Discussion	94
	4.5.1	Characterization of Zinc chloride - Glucose BDES	94
		4.5.1.1 Density and Conductivity	94
		4.5.1.2 pH	94
		4.5.1.3 Viscosity	95
		4.5.1.4 FTIR spectral analysis of ZC-GLU	95
	4.5.2	Characterization of Zinc Chloride- Fructose BDES	96
		4.5.2.1 Density and Conductivity	96
		4.5.2.2 pH	96
		4.5.2.3 Viscosity	96
		4.5.2.4 FTIR spectral analysis of ZC-FRU	96
	4.5.3	Characterization of Zinc Chloride- Lactic acid BDES	97
		4.5.3.1 Density and Conductivity	97
		4.5.3.2 pH	97
		4.5.3.3 Viscosity	97

	4.5.3.4	FTIR spectral analysis of ZC- LA	98
4.6		Conclusion	98
		References	99
<b>V</b>		<b>Preparation and Characterization Studies of Manganese chloride-Based Binary Deep Eutectic Solvents</b>	
5.		Manganese chloride Based Binary Deep Eutectic Solvents (BDES)	107
5.1		Introduction	107
5.2		Preparation of Manganese chloride-Glucose (MC-GLU) BDES	107
5.3		Preparation of manganese chloride - Fructose (MC-FRU) BDES	107
5.4		Preparation of manganese chloride – Citric Acid (MC-CA) BDES	108
5.5		Results and Discussion	108
	5.5.1	Characterization of Manganese chloride - Glucose BDES	108
		5.5.1.1 Density and Conductivity	108
		5.5.1.2 pH	108
		5.5.1.3 Viscosity	109
	5.5.2	Characterization of Manganese chloride - Fructose BDES	109
		5.5.2.1 Density and Conductivity	109
		5.5.2.2 pH	109
		5.5.2.3 Viscosity	109
5.6		Conclusion	110
		References	111
<b>VI</b>		<b>Synthesis and Characterization Studies of Malonic Acid-Based Ternary Deep Eutectic Solvents</b>	
6		Malonic acid-based Ternary Deep Eutectic Solvents (TDES)	115
6.1		Introduction	115

6.2	Preparation of Malonic acid- Glucose- Glutamine (MA-GLU-GLUT) TDES	115
6.3	Preparation of Malonic acid- Fructose- Glutamine (MA-FRU-GLUT) TDES	116
6.4	Preparation of Malonic acid- Glucose- Glycine (MA-GLU-GLY) TDES	116
6.5	Preparation of Malonic acid- Fructose- Glycine (MA-FRU-GLY) TDES	116
6.6	Preparation of Malonic acid- Glucose- Histidine (MA-GLU-HIS) TDES	117
6.7	Preparation of Malonic acid- Fructose- Histidine (MA-FRU-HIS) TDES	117
6.8	Results and Discussion	117
6.8.1	Characterization of Malonic Acid- Glucose-Glutamine TDES	117
6.8.1.1	Density and Conductivity	117
6.8.1.2	pH	118
6.8.1.3	Viscosity	118
6.8.1.4	FTIR spectrum of MA-GLU-GLUT TDES	118
6.8.2	Characterization of Malonic Acid- Fructose-Glutamine TDES	119
6.8.2.1	Density and Conductivity	119
6.8.2.2	pH	120
6.8.2.3	Viscosity	120
6.8.2.4	FTIR spectrum of MA-FRU-GLUT TDES	120
6.8.3	Characterization of Malonic Acid- Glucose-Glycine TDES	120
6.8.3.1	Density and Conductivity	120
6.8.3.2	pH	121
6.8.3.3	Viscosity	121
6.8.3.4	FTIR spectrum of MA-GLU-GLY TDES	121
6.8.4	Characterization of Malonic Acid- Fructose-Glycine TDES	122

	6.8.4.1	Density and Conductivity	122
	6.8.4.2	pH	122
	6.8.4.3	Viscosity	123
	6.8.4.4	FTIR spectrum of MA-FRU-GLY TDES	123
6.8.5		Characterization of Malonic Acid- Glucose-Histidine TDES	123
	6.8.5.1	Density and Conductivity	123
	6.8.5.2	pH	124
	6.8.5.3	Viscosity	124
	6.8.5.4	FTIR spectrum of MA-GLU-HIS TDES	124
6.8.6		Characterization of Malonic Acid- Fructose-Histidine TDES	125
	6.8.6.1	Density and Conductivity	125
	6.8.6.2	pH	125
	6.8.6.3	Viscosity	125
	6.8.6.4	FTIR spectrum of MA-FRU-HIS TDES	126
6.9		Conclusion	126
		References	127

## VII

### **Synthesis and Characterization Studies of Zinc Chloride- Based Ternary Deep Eutectic Solvents**

7.		Zinc chloride-based Ternary Deep Eutectic Solvents (TDES)	139
7.1		Introduction	139
7.2		Preparation of Zinc chloride- Glucose- Glutamine (ZC-GLU-GLUT) TDES	139
7.3		Preparation of Zinc chloride- Fructose- Glutamine (ZC-FRU-GLUT) TDES	139
7.4		Preparation of Zinc chloride- Glucose- Glycine (ZC-GLU-GLY) TDES	140
7.5		Preparation of Zinc chloride- Fructose- Glycine (ZC-FRU-GLY) TDES	140
7.6		Preparation of Zinc chloride- Glucose- Histidine (ZC-GLU-HIS) TDES	140

7.7	Preparation of Zinc chloride- Fructose- Histidine (ZC-FRU-HIS) TDES	141
7.8	Results and Discussion	141
7.8.1	Characterization of Zinc Chloride- Glucose-Glutamine TDES	141
7.8.1.1	Density and Conductivity	141
7.8.1.2	pH	141
7.8.1.3	Viscosity	142
7.8.1.4	FTIR spectrum of ZC-GLU-GLUT TDES	142
7.8.2	Characterization of Zinc Chloride- Fructose-Glutamine TDES	142
7.8.2.1	Density and Conductivity	142
7.8.2.2	pH	142
7.8.2.3	Viscosity	143
7.8.2.4	FTIR spectrum of ZC-FRU-GLUT TDES	143
7.8.3	Characterization of Zinc Chloride- Glucose-Glycine TDES	143
7.8.3.1	Density and Conductivity	143
7.8.3.2	pH	143
7.8.3.3	Viscosity	144
7.8.3.4	FTIR spectrum of ZC-GLU-GLY TDES	144
7.8.4	Characterization of Zinc Chloride- Fructose-Glycine TDES	144
7.8.4.1	Density and Conductivity	144
7.8.4.2	pH	145
7.8.4.3	Viscosity	145
7.8.4.4	FTIR spectrum of ZC-FRU-GLY TDES	145
7.8.5	Characterization of Zinc Chloride- Glucose-Histidine TDES	146
7.8.5.1	Density and Conductivity	146
7.8.5.2	pH	146
7.8.5.3	Viscosity	146
7.8.5.4	FTIR spectrum of ZC-GLU-HIS TDES	146

7.8.6	Characterization of Zinc Chloride- Fructose-Histidine TDES	147
7.8.6.1	Density and Conductivity	147
7.8.6.2	pH	147
7.8.6.3	Viscosity	147
7.8.6.4	FTIR spectrum of ZC-FRU-HIS TDES	147
7.9	Conclusion	148
	References	149

## **VIII**

### **Synthesis and Characterization Studies of Manganese Chloride-Based Ternary Deep Eutectic Solvents**

8	Manganese chloride-based Ternary Deep Eutectic Solvents (TDES)	161
8.1	Introduction	161
8.2	Preparation of Manganese Chloride- Glucose-Glutamine (MC-GLU-GLUT) TDES	161
8.3	Preparation of Manganese Chloride- Fructose-Glutamine (MC-FRU-GLUT) TDES	161
8.4	Preparation of Manganese Chloride- Glucose-Glycine (MC-GLU-GLY) TDES	162
8.5	Preparation of Manganese Chloride- Fructose-Glycine (MC-FRU-GLY) TDES	162
8.6	Preparation of Manganese Chloride- Glucose-Histidine (MC-GLU-HIS) TDES	162
8.7	Preparation of Manganese Chloride- Fructose-Histidine (MC-FRU-HIS) TDES	163
8.8	Results and discussion	163
8.8.1	Characterization of Manganese Chloride- Glucose-Glutamine TDES	163
8.8.1.1	Density and Conductivity	163
8.8.1.2	pH	163
8.8.1.3	Viscosity	164



	8.8.1.4	FTIR spectrum of MC-GLU-GLUT TDES	164
8.8.2		Characterization of Manganese Chloride- Fructose-Glutamine TDES	164
	8.8.2.1	Density and Conductivity	164
	8.8.2.2	pH	164
	8.8.2.3	Viscosity	165
	8.8.2.4	FTIR spectrum of MC-FRU-GLUT TDES	165
8.8.3		Characterization of Manganese Chloride- Glucose-Glycine TDES	165
	8.8.3.1	Density and Conductivity	165
	8.8.3.2	pH	165
	8.8.3.3	Viscosity	166
	8.8.3.4	FTIR spectrum of MC-GLU-GLY TDES	166
8.8.4		Characterization of Manganese Chloride- Fructose-Glycine TDES	166
	8.8.4.1	Density and Conductivity	166
	8.8.4.2	pH	166
	8.8.4.3	Viscosity	167
	8.8.4.4	FTIR spectrum of MC-FRU-GLY TDES	167
8.8.5		Characterization of Manganese Chloride- Glucose-Histidine TDES	167
	8.8.5.1	Density and Conductivity	167
	8.8.5.2	pH	167
	8.8.5.3	Viscosity	168
	8.8.5.4	FTIR spectrum of MC-GLU-HIS TDES	168
8.8.6		Characterization of Manganese Chloride- Fructose-Histidine TDES	168
	8.8.6.1	Density and Conductivity	168
	8.8.6.2	pH	169
	8.8.6.3	Viscosity	169
	8.8.6.4	FTIR spectrum of MC-FRU-HIS TDES	169
8.9		Conclusion	169
		References	170

**IX****Synthesis and characterization of copper, Silver, Cadmium and Mercury Nanoparticles in Binary Deep Eutectic Solvents**

9	Synthesis and characterization of Nanoparticles in Binary Deep Eutectic Solvents	181
9.1	Introduction	181
9.2	Synthesis of copper nanoparticles in Malonic acid-based binary deep eutectic solvents	182
9.3	Synthesis of silver nanoparticles in Malonic acid-based binary deep eutectic solvents	182
9.4	Synthesis of cadmium nanoparticles in Malonic acid-based binary deep eutectic solvents	183
9.5	Synthesis of mercury nanoparticles in Malonic acid-based binary deep eutectic solvents	183
9.6	Synthesis of copper nanoparticles in Zinc chloride-based binary deep eutectic solvents	183
9.7	Synthesis of silver nanoparticles in Zinc chloride-based binary deep eutectic solvents	184
9.8	Results and Discussion	184
9.8.1	Characterization studies of copper nanoparticles in malonic acid-based binary deep eutectic solvents	184
9.8.1.1	UV-Visible spectra of copper oxide nanoparticles	184
9.8.1.2	FTIR spectra of copper oxide nanoparticles	185

	9.8.1.3	XRD patterns of copper oxide nanoparticles	185
	9.8.1.4	Morphological analysis of copper oxide nanoparticles by SEM	186
	9.8.1.5	Energy Dispersive X-ray Analysis	187
9.8.2		Characterization studies of Silver nanoparticles in malonic acid-based binary deep eutectic solvents	187
	9.8.2.1	UV-Visible spectra of Silver oxide nanoparticles	187
	9.8.2.2	FTIR spectra of Silver oxide nanoparticles	188
	9.8.2.3	XRD patterns of Silver oxide nanoparticles	188
	9.8.2.4	Morphological analysis of Silver oxide nanoparticles by SEM	189
	9.8.2.5	Energy Dispersive X-ray Analysis	189
9.8.3		Characterization studies of Cadmium nanoparticles in malonic acid-based binary deep eutectic solvents	190
	9.8.3.1	UV-Visible spectra of Cadmium sulfide nanoparticles	190
	9.8.3.2	FTIR spectra of Cadmium sulfide nanoparticles	190
	9.8.3.3	Morphological analysis of Cadmium sulfide nanoparticles by SEM	190
9.8.4		Characterization studies of Mercury nanoparticles in malonic acid-based binary deep eutectic solvents	191
	9.8.4.1	UV-Visible spectra of Mercury sulfide nanoparticles	191
	9.8.4.2	FTIR spectra of Mercury sulfide nanoparticles	191
	9.8.4.3	Morphological analysis of Mercury sulfide nanoparticles by SEM	191

9.8.5	Characterization studies of copper nanoparticles in Zinc chloride-based binary deep eutectic solvents	192
9.8.5.1	UV-Visible spectra of copper oxide nanoparticles	192
9.8.5.2	FTIR spectra of copper oxide nanoparticles	192
9.8.5.3	XRD patterns of copper oxide nanoparticles	193
9.8.5.4	Morphological analysis of copper oxide nanoparticles by SEM	193
9.8.5.5	Energy Dispersive X-ray Analysis	194
9.8.6	Characterization studies of Silver nanoparticles in Zinc chloride-based binary deep eutectic solvents	194
9.8.6.1	UV-Visible spectra of Silver oxide nanoparticles	194
9.8.6.2	FTIR spectra of Silver oxide nanoparticles	195
9.8.6.3	XRD patterns of Silver oxide nanoparticles	195
9.8.6.4	Morphological analysis of Silver oxide nanoparticles by SEM	195
9.8.6.5	Energy Dispersive X-ray Analysis	196
9.9	Conclusion	196
	References	197

## X

### **Synthesis and characterization of Copper and Silver Nanoparticles in Ternary Deep Eutectic Solvents**

10	Synthesis and characterization of nanoparticles using Ternary Deep Eutectic Solvents	217
10.1	Introduction	217
10.2	Synthesis of copper nanoparticles in Malonic acid-sugar-amino acids based ternary deep eutectic solvents	217

10.3	Synthesis of silver nanoparticles in Malonic acid-sugar-amino acids based ternary deep eutectic solvents	218
10.4	Synthesis of silver nanoparticles in Zinc chloride-sugar-amino acids based ternary deep eutectic solvents	218
10.5	Synthesis of copper nanoparticles in Manganese chloride-sugar-amino acids based ternary deep eutectic solvents	219
10.6	Results and discussion	219
10.6.1	Characterization studies of copper nanoparticles in malonic acid-sugar-amino acids based ternary deep eutectic solvents	219
10.6.1.1	UV-Visible spectra of copper oxide nanoparticles	219
10.6.1.2	FTIR spectra of copper oxide nanoparticles	220
10.6.1.3	XRD patterns of copper oxide nanoparticles	220
10.6.1.4	Morphological analysis of copper oxide nanoparticles by SEM	221
10.6.1.5	Energy Dispersive X-ray Analysis	222
10.6.2	Characterization studies of silver nanoparticles in malonic acid-sugar-amino acids based ternary deep eutectic solvents	223
10.6.2.1	UV-Visible spectra of silver oxide nanoparticles	223
10.6.2.2	FTIR spectra of silver oxide nanoparticles	223
10.6.2.3	XRD patterns of silver oxide nanoparticles	223
10.6.2.4	Morphological analysis of silver oxide nanoparticles by SEM	224
10.6.2.5	Energy Dispersive X-ray Analysis	224

10.6.3	Characterization studies of Silver nanoparticles in Zinc chloride -sugar-amino acids based ternary deep eutectic solvents	225
10.6.3.1	UV-Visible spectra of Silver oxide nanoparticles	225
10.6.3.2	FTIR spectra of Silver oxide nanoparticles	225
10.6.3.3	XRD patterns of Silver oxide nanoparticles	225
10.6.3.4	Morphological analysis of Silver oxide nanoparticles by SEM	226
10.6.3.5	Energy Dispersive X-ray Analysis	227
10.6.4	Characterization studies of Copper nanoparticles in Manganese chloride-sugar-amino acids based ternary deep eutectic solvents	228
10.6.4.1	UV-Visible spectra of Copper oxide nanoparticles	228
10.6.4.2	FTIR spectra of Copper oxide nanoparticles	228
10.6.4.3	XRD patterns of Copper oxide nanoparticles	229
10.6.4.4	Morphological analysis of Copper oxide nanoparticles by SEM	230
10.6.4.5	Energy Dispersive X-ray Analysis	230
10.7	Conclusion	231
	References	232
<b>XI</b>	<b>Antimicrobial studies of some synthesized nanoparticles</b>	
11	Antimicrobial studies of some nanoparticles	251
11.1	Introduction	251
11.2	Antibacterial studies of copper nanoparticles	251
11.2.1	Growth of bacterial media	251

11.2.2	Preparation of dried filter paper discs	252
11.2.3	Antimicrobial assay	252
11.3	Antifungal studies of Silver Nanoparticles	253
11.3.1	Growth of fungal media	253
11.3.2	Preparation of dried filter paper discs	254
11.3.3	Antimicrobial assay	254
11.4	Conclusion	255
	References	256

## **XII**

### **Conclusion**

12.1	Summary and conclusion	263
12.2	Future perceptive of the work	264
	List of articles published as in the UGC listed Scopus indexed peer-reviewed journals	267
	List of papers presented in the international conferences	268

## LIST OF TABLES

<b>Table no.</b>	<b>Name of the table</b>	<b>Page no.</b>
1.1	Comparison of ionic liquids with Deep Eutectic Solvents	16
2.1	Chemicals used for the investigation	69
2.2	Prepared BDES	71
2.3	Prepared TDES	72
11.1	Comparison of antibacterial activity of copper nanoparticles obtained using Malonic Acid-Glucose (MA-GLU) and Malonic Acid-Fructose (MA-FRU) sample solutions with a standard solution, Chloramphenicol (Std)	259
11.2	Table 11.2. Comparison of antifungal activity of silver nanoparticles obtained using Malonic Acid-Glucose-Glutamine (MA-GLU-GLUT) and Malonic Acid-Fructose-Glutamine (MA-FRU-GLUT) sample solutions with a standard solution, Fluconazole (Std).	259



## LIST OF FIGURES

<b>Figure no.</b>	<b>Name of the figure</b>	<b>Page no.</b>
3.1.1	pH as a function against T of MA-GLU BDES	88
3.1.2	Viscosity of MA-GLU BDES At Different Temperatures	88
3.1.3	FTIR spectrum of MA-GLU BDES	89
3.2.1	pH as a function against T of MA-FRU BDES	89
3.2.2	Viscosity of MA-FRU BDES At Different Temperatures	90
3.2.3	FTIR spectrum of MA-FRU BDES	90
3.3.1	pH as a function against T of MA-GCL BDES	91
3.3.2	Viscosity of MA-GCL BDES At Different Temperatures	91
3.3.3	FTIR spectrum of MA-GCL BDES	92
4.1.1	pH as a function against T of ZC-GLU BDES	101
4.1.2	Viscosity of ZC-GLU BDES At Different Temperatures	101
4.1.3	FTIR spectrum of ZC-GLU BDES	102
4.2.1	pH as a function against T of ZC-FRU BDES	102
4.2.2	Viscosity of ZC-FRU BDES At Different Temperatures	103
4.2.3	FTIR spectrum of ZC-FRU BDES	103
4.3.1	pH as a function against T of ZC-LA BDES	104
4.3.2	Viscosity of ZC-LA BDES At Different Temperatures	104
4.3.3	FTIR spectrum of ZC-LA BDES	105
5.1.1	pH as a function against T of MC-GLU BDES	112
5.1.2	Viscosity of MC-GLU BDES At Different Temperatures	112
5.2.1	pH as a function against T of MC-FRU BDES	113
5.2.2	Viscosity of MC-FRU BDES At Different Temperatures	113
6.1.1	pH as a function against T of MA-GLU-GLUT TDES	129
6.1.2	Viscosity of MA-GLU-GLUT TDES At Different Temperatures	129
6.1.3	FTIR spectrum of MA-GLU-GLUT TDES	130
6.2.1	pH as a function against T of MA-FRU-GLUT TDES	130
6.2.2	Viscosity of MA-FRU-GLUT TDES At Different Temperatures	131
6.2.3	FTIR spectrum of MA-FRU-GLUT TDES	131
6.3.1	pH as a function against T of MA-GLU-GLY TDES	132

6.3.2	Viscosity of MA-GLU-GLY TDES At Different Temperatures	132
6.3.3	FTIR spectrum of MA-GLU-GLY TDES	133
6.4.1	pH as a function against T of MA-FRU-GLY TDES	133
6.4.2	Viscosity of MA-FRU-GLY TDES At Different Temperatures	134
6.4.3	FTIR spectrum of MA-FRU-GLY TDES	134
6.5.1	pH as a function against T of MA-GLU-HIS TDES	135
6.5.2	Viscosity of MA-GLU-HIS TDES At Different Temperatures	135
6.5.3	FTIR spectrum of MA-GLU-HIS TDES	136
6.6.1	pH as a function against T of MA-FRU-HIS TDES	136
6.6.2	Viscosity of MA-FRU-HIS TDES At Different Temperatures	137
6.6.3	FTIR spectrum of MA-FRU-HIS TDES	137
7.1.1	pH as a function against T of ZC-GLU-GLUT TDES	151
7.1.2	Viscosity of ZC-GLU-GLUT TDES At Different Temperatures	151
7.1.3	FTIR spectrum of ZC-GLU-GLUT TDES	152
7.2.1	pH as a function against T of ZC-FRU-GLUT TDES	152
7.2.2	Viscosity of ZC-FRU-GLUT TDES At Different Temperatures	153
7.2.3	FTIR spectrum of ZC-FRU-GLUT TDES	153
7.3.1	pH as a function against T of ZC-GLU-GLY TDES	154
7.3.2	Viscosity of ZC-GLU-GLY TDES At Different Temperatures	154
7.3.3	FTIR spectrum of ZC-GLU-GLY TDES	155
7.4.1	pH as a function against T of ZC-FRU-GLY TDES	155
7.4.2	Viscosity of ZC-FRU-GLY TDES At Different Temperatures	156
7.4.3	FTIR spectrum of ZC-FRU-GLY TDES	156
7.5.1	pH as a function against T of ZC-GLU-HIS TDES	157
7.5.2	Viscosity of ZC-GLU-HIS TDES At Different Temperatures	157
7.5.3	FTIR spectrum of ZC-GLU-HIS TDES	158
7.6.1	pH as a function against T of ZC-FRU-HIS TDES	158
7.6.2	Viscosity of ZC-FRU-HIS TDES At Different Temperatures	159
7.6.3	FTIR spectrum of ZC-FRU-HIS TDES	159
8.1.1	pH as a function against T of MC-GLU-GLUT TDES	171
8.1.2	Viscosity of MC-GLU-GLUT TDES At Different Temperatures	171
8.1.3	FTIR spectrum of MC-GLU-GLUT TDES	172
8.2.1	pH as a function against T of MC-FRU-GLUT TDES	172

8.2.2	Viscosity of MC-FRU-GLUT TDES At Different Temperatures	173
8.2.3	FTIR spectrum of MC-FRU-GLUT TDES	173
8.3.1	pH as a function against T of MC-GLU-GLY TDES	174
8.3.2	Viscosity of MC-GLU-GLY TDES At Different Temperatures	174
8.3.3	FTIR spectrum of MC-GLU-GLY TDES	175
8.4.1	pH as a function against T of MC-FRU-GLY TDES	175
8.4.2	Viscosity of MC-FRU-GLY TDES At Different Temperatures	176
8.4.3	FTIR spectrum of MC-FRU-GLY TDES	176
8.5.1	pH as a function against T of MC-GLU-HIS TDES	177
8.5.2	Viscosity of MC-GLU-HIS TDES At Different Temperatures	177
8.5.3	FTIR spectrum of MC-GLU-HIS TDES	178
8.6.1	pH as a function against T of MC-FRU-HIS TDES	178
8.6.2	Viscosity of MC-FRU-HIS TDES At Different Temperatures	179
8.6.3	FTIR spectrum of MC-FRU-HIS TDES	179
9.1.1	UV-Visible spectra of copper oxide nanoparticles obtained using (a) Malonic acid - Glucose BDES (b) Malonic acid – Fructose BDES	201
9.1.1 c	UV-Visible spectra of copper oxide nanoparticles obtained using Malonic acid - Glycerol BDES	201
9.1.2	FTIR spectra of copper oxide nanoparticles obtained using (a) Malonic acid - Glucose BDES (b) Malonic acid – Fructose BDES	202
9.1.3	XRD patterns of copper oxide nanoparticles obtained using (a) Malonic acid Glucose BDES and (b) Malonic acid-Fructose BDES	202
9.1.4	SEM images of copper oxide nanoparticles obtained using (a) Malonic acid Glucose BDES and (b) Malonic acid – Fructose BDES	203
9.1.5	EDAX Spectra of copper oxide nanoparticles obtained using (a) Malonic acid –Glucose BDES and (b) Malonic acid – Fructose BDES	203
9.2.1	UV-Visible spectra of silver oxide nanoparticles obtained using (a) Malonic - Glucose BDES (b) Malonic acid – Fructose BDES	204
9.2.2	FTIR spectra of silver oxide nanoparticles obtained using (a) Malonic - Glucose BDES (b) Malonic acid – Fructose BDES	204
9.2.3	XRD patterns of silver oxide nanoparticles obtained using (a) Malonic - Glucose BDES (b) Malonic acid – Fructose BDES	205

9.2.4	SEM images of silver oxide nanoparticles obtained using (a) Malonic - Glucose BDES (b) Malonic acid – Fructose BDES	205
9.2.5	EDAX spectra of silver oxide nanoparticles obtained using (a) Malonic - Glucose BDES (b) Malonic acid – Fructose BDES	206
9.3.1	UV-Visible spectra of Cadmium sulfide nanoparticles obtained using (a) Malonic - Glucose BDES (b) Malonic acid – Fructose BDES	207
9.3.2	FTIR spectra of Cadmium sulfide nanoparticles obtained using (a) Malonic - Glucose BDES (b) Malonic acid – Fructose BDES	207
9.3.3	SEM images of Cadmium sulfide nanoparticles obtained using (a) Malonic - Glucose BDES (b) Malonic acid – Fructose BDES	208
9.4.1	UV-Visible spectra of Mercury sulfide nanoparticles obtained using (a) Malonic - Glucose BDES (b) Malonic acid – Fructose BDES	208
9.4.2	FTIR spectra of Mercury sulfide nanoparticles obtained using (a) Malonic - Glucose BDES (b) Malonic acid – Fructose BDES	209
9.4.3	SEM images of Mercury sulfide nanoparticles obtained using (a) Malonic - Glucose BDES (b) Malonic acid – Fructose BDES	209
9.5.1	UV-Visible spectra of copper nanoparticles obtained using (a) Zinc chloride - Glucose BDES (b) Zinc chloride – Fructose BDES	210
9.5.2	FTIR spectra of copper nanoparticles obtained using (a) Zinc chloride - Glucose BDES (b) Zinc chloride – Fructose BDES	210
9.5.3	XRD patterns of copper nanoparticles obtained using (a) Zinc chloride - Glucose BDES (b) Zinc chloride – Fructose BDES	211
9.5.4	SEM images of copper nanoparticles obtained using (a) Zinc chloride - Glucose BDES (b) Zinc chloride – Fructose BDES	211
9.5.5	EDAX spectra of copper nanoparticles obtained using (a) Zinc chloride - Glucose BDES (b) Zinc chloride – Fructose BDES	212
9.6.1	UV-Visible spectra of silver nanoparticles obtained using (a) Zinc chloride - Glucose BDES (b) Zinc chloride – Fructose BDES	213
9.6.2	FTIR spectra of silver nanoparticles obtained using (a) Zinc chloride - Glucose BDES (b) Zinc chloride – Fructose BDES	213
9.6.3	XRD patterns of silver nanoparticles obtained using (a) Zinc chloride - Glucose BDES (b) Zinc chloride – Fructose BDES	214

9.6.4	SEM images of silver nanoparticles obtained using (a) Zinc chloride - Glucose BDES (b) Zinc chloride – Fructose BDES	214
9.6.5	EDAX spectra of silver nanoparticles obtained using (a) Zinc chloride - Glucose BDES (b) Zinc chloride – Fructose BDES	215
10.1.1	UV-Visible spectra of copper oxide nanoparticles obtained using (a) Malonic acid - Glucose – Glycine (MA – GLU - GLY) TDES (b) Malonic acid – Fructose- Glycine (MA – FRU - GLY) TDES (c) Malonic acid – Glucose – Histidine (MA – GLU - HIS) TDES (d) Malonic acid – Fructose- Histidine (MA -FRU – HIS) TDES	236
10.1.2	FTIR spectra of copper oxide nanoparticles obtained using (a) Malonic acid - Glucose – Glycine (MA – GLU - GLY) TDES (b) Malonic acid – Fructose - Glycine (MA – FRU - GLY) TDES (c) Malonic acid – Glucose – Histidine (MA – GLU - HIS) TDES (d) Malonic acid – Fructose - Histidine (MA -FRU – HIS) TDES	236
10.1.3	10.1.3. XRD patterns of copper oxide nanoparticles obtained using (a) Malonic acid - Glucose – Glycine (MA – GLU - GLY) TDES (b) Malonic acid – Fructose- Glycine (MA – FRU - GLY) TDES (c) Malonic acid – Glucose – Histidine (MA – GLU - HIS) TDES (d) Malonic acid – Fructose- Histidine (MA -FRU – HIS) TDES	237
10.1.4.1	SEM images of copper oxide nanoparticles obtained using (a), (b) Malonic acid - Glucose – Glycine (MA – GLU - GLY) TDES (c), (d) Malonic acid – Fructose- Glycine (MA – FRU - GLY) TDES	237
10.1.4.2	SEM images of copper oxide nanoparticles obtained using (e), (f) Malonic acid – Glucose – Histidine (MA – GLU - HIS) TDES (g), (h) Malonic acid – Fructose- Histidine (MA -FRU – HIS) TDES	238
10.1.5	EDAX spectra of copper oxide nanoparticles obtained using (a) Malonic acid - Glucose – Glycine (MA – GLU - GLY) TDES (b) Malonic acid – Fructose- Glycine (MA – FRU - GLY) TDES (c) Malonic acid – Glucose – Histidine (MA – GLU - HIS) TDES (d) Malonic acid – Fructose- Histidine (MA -FRU – HIS) TDES	238
10.2.1	UV-Visible spectra of silver oxide nanoparticles obtained using (a) Malonic acid - Glucose – Glutamine (MA – GLU - GLUT) TDES (b) Malonic acid – Fructose- Glutamine (MA – FRU - GLUT) TDES	239

10.2.2	FTIR spectra of silver oxide nanoparticles obtained using	239
	(a) Malonic acid - Glucose – Glutamine (MA – GLU - GLUT) TDES	
	(b) Malonic acid – Fructose- Glutamine (MA – FRU - GLUT) TDES	
10.2.3	XRD patterns of silver oxide nanoparticles obtained using (a) Malonic acid - Glucose – Glutamine (MA – GLU - GLUT) TDES (b) Malonic acid – Fructose- Glutamine (MA – FRU - GLUT) TDES	240
10.2.4	SEM images of silver oxide nanoparticles obtained using (a), (b) Malonic acid - Glucose – Glutamine (MA – GLU - GLUT) TDES (c), (d) Malonic acid – Fructose- Glutamine (MA – FRU - GLUT) TDES	240
10.2.5	EDAX spectra of silver oxide nanoparticles obtained using (a) Malonic acid – Fructose- Glutamine (MA – FRU - GLUT) TDES (b) Malonic acid - Glucose – Glutamine (MA – GLU - GLUT) TDES	241
10.3.1	UV-Visible spectra of silver oxide nanoparticles obtained using (a) Zinc chloride - Glucose – Glycine (ZC – GLU - GLY) TDES (b) Zinc chloride – Fructose- Glycine (ZC – FRU - GLY) TDES (c) Zinc chloride – Glucose – Glutamine (ZC – GLU - GLUT) TDES (d) Zinc chloride – Fructose- Glutamine (ZC -FRU – GLUT) TDES (e) Zinc chloride – Glucose – Histidine (ZC – GLU - HIS) TDES (f) Zinc chloride – Fructose- Histidine (ZC -FRU – HIS) TDES	242
10.3.2	FTIR spectra of silver oxide nanoparticles obtained using (a) Zinc chloride - Glucose – Glycine (ZC – GLU - GLY) TDES (b) Zinc chloride – Fructose- Glycine (ZC – FRU - GLY) TDES (c) Zinc chloride – Glucose – Glutamine (ZC – GLU - GLUT) TDES (d) Zinc chloride – Fructose- Glutamine (ZC -FRU – GLUT) TDES (e) Zinc chloride – Glucose – Histidine (ZC – GLU - HIS) TDES (f) Zinc chloride – Fructose- Histidine (ZC -FRU – HIS) TDES	242
10.3.3	XRD patterns of silver oxide nanoparticles obtained using (a) Zinc chloride - Glucose – Glycine (ZC – GLU - GLY) TDES (b) Zinc chloride – Fructose- Glycine (ZC – FRU - GLY) TDES (c) Zinc chloride – Glucose – Glutamine (ZC – GLU - GLUT) TDES (d) Zinc chloride – Fructose- Glutamine (ZC -FRU – GLUT) TDES (e) Zinc chloride – Glucose – Histidine (ZC – GLU - HIS) TDES (f) Zinc chloride – Fructose- Histidine (ZC -FRU – HIS) TDES	243

10.3.4.1	SEM images of silver oxide nanoparticles obtained using	243
	(a) (b) Zinc chloride - Glucose – Glycine (ZC – GLU - GLY) TDES	
	(c) (d) Zinc chloride – Fructose- Glycine (ZC – FRU - GLY) TDES	
10.3.4.2	SEM images of silver oxide nanoparticles obtained using	244
	(a) (b) Zinc chloride - Glucose - Glutamine (ZC-GLU - GLUT) TDES	
	(c) (d) Zinc chloride – Fructose - Glutamine (ZC-FRU - GLUT)TDES	
10.3.4.3	SEM images of silver oxide nanoparticles obtained using	244
	(a) (b) Zinc chloride - Glucose – Histidine (ZC – GLU - HIS) TDES	
	(c) (d) Zinc chloride – Fructose- Histidine (ZC – FRU - HIS) TDES	
10.3.5	EDAX spectra of silver oxide nanoparticles obtained using	245
	(a) Zinc chloride - Glucose – Glycine (ZC – GLU - GLY) TDES	
	(b) Zinc chloride – Fructose- Glycine (ZC – FRU - GLY) TDES	
	(c) Zinc chloride – Glucose – Glutamine (ZC – GLU - GLUT) TDES	
	(d) Zinc chloride – Fructose- Glutamine (ZC -FRU – GLUT) TDES (e)	
	Zinc chloride – Glucose – Histidine (ZC – GLU - HIS) TDES	
	(f) Zinc chloride – Fructose- Histidine (ZC -FRU – HIS) TDES	
10.4.1	UV spectra of copper oxide nanoparticles obtained using	246
	(a) Manganese chloride - Glucose - Glycine (MC-GLU - GLY) TDES	
	(b) Manganese chloride - Fructose- Glycine (MC - FRU - GLY)TDES	
	(c) Manganese chloride -Glucose-Glutamine (MC-GLU-GLUT) TDES	
	(d) Manganese chloride-Fructose- Glutamine (MC-FRU-GLUT) TDES	
	(e) Manganese chloride - Glucose - Histidine (MC - GLU - HIS) TDES	
10.4.2	FTIR spectra of copper oxide nanoparticles obtained using	246
	(a) Manganese chloride - Glucose - Glycine (MC - GLU - GLY) TDES	
	(b) Manganese chloride - Fructose- Glycine (MC – FRU - GLY) TDES	
	(c) Manganese chloride-Glucose - Glutamine (MC-GLU-GLUT)TDES	
	(d) Manganese chloride -Fructose- Glutamine (MC-FRU-GLUT)TDES	
	(e) Manganese chloride -Glucose - Histidine (MC - GLU - HIS) TDES	

10.4.3	XRD Patterns of copper oxide nanoparticles obtained using	247
	(a) Manganese chloride - Glucose - Glycine (MC - GLU - GLY) TDES	
	(b) Manganese chloride - Fructose- Glycine (MC – FRU - GLY) TDES	
	(c)Manganese chloride- Glucose- Glutamine (MC-GLU-GLUT) TDES	
	(d) Manganese chloride- Fructose-Glutamine (MC-FRU- GLUT)TDES	
	(e) Manganese chloride - Glucose - Histidine (MC- GLU - HIS) TDES	
10.4.4.1	SEM images of copper oxide nanoparticles obtained using	247
	(a) (b) Manganese chloride-Glucose - Glycine (MC-GLU-GLY) TDES	
	(c) (d) Manganese chloride- Fructose- Glycine (MC-FRU-GLY) TDES	
10.4.4.2	SEM images of copper oxide nanoparticles obtained using	248
	(a) (b) Manganese chloride-Glucose-Glutamine (MC-GLU-GLUT)	
	TDES (c) (d) Manganese chloride - Fructose- Glutamine (MC - FRU -	
	GLUT) TDES	
10.4.4.3	SEM images of copper oxide nanoparticles obtained using (a) (b)	248
	Manganese chloride - Glucose - Histidine (MC – GLU - HIS) TDES	
10.4.5	EDAX spectra of copper oxide nanoparticles obtained using	249
	(a) Manganese chloride - Glucose - Glycine (MC - GLU - GLY) TDES	
	(b) Manganese chloride - Fructose- Glycine (MC - FRU - GLY) TDES	
	(c) Manganese chloride-Glucose- Glutamine (MC-GLU-GLUT) TDES	
	(d) Manganese chloride- Fructose-Glutamine (MC-FRU- GLUT)TDES	
	(e) Manganese chloride - Glucose- Histidine (MC - GLU - HIS) TDES	
11.1.1	Images of the zone of inhibition at various concentrations of copper	260
	nanoparticles obtained using MA-GLU	
11.1.2	Images of the zone of inhibition at various concentrations of copper	260
	nanoparticles obtained using MA-FRU	
11.2.1	Images of the zone of inhibition at various concentrations of silver	261
	nanoparticles obtained using MA-GLU-GLUT	
11.2.2	Images of the zone of inhibition at various concentrations of silver	261
	nanoparticles obtained using MA-FRU-GLUT	



# 1. INTRODUCTION

---

## 1.1. GENERAL INTRODUCTION TO DEEP EUTECTIC SOLVENTS

Since the potential for new chemical technology was recognized two decades ago, research into ionic liquids (ILs) has exploded. During the previous two decennia, ionic liquids (ILs) have a noticeable effect, particularly in the fields of catalysis, electrochemistry, material chemistry, and new for the pre-treatment of biomes<sup>[1-3]</sup>. At the onset of this investigation, researchers mostly concentrated on the development of ionic liquids by blending metal salts, chiefly Zinc, Aluminium, Tin, and Iron chlorides, with quaternary ammonium salts. Although both salts have very high melting points, their decent blending provided the production of a liquid phase known as eutectic mixtures are usually characterized by a large depression of freezing point, probably higher than 150°C. After the introduction of the interpretation of green chemistry at the beginning of the 1990s, the inquiry for metal-free ionic liquids (ILs) has developed of spreading significance<sup>[4]</sup>.

The ionic liquids (IL) play a noteworthy role recently in chemical applications because of their recognized physicochemical properties such as low toxicity, indistinct vapor pressure, high solubility, and their existence in the liquid state<sup>[5-7]</sup> over a wide range of temperatures. Due to these reasons ionic liquids are commonly used as solvents in chemical laboratories and for industrial processes such as CO<sub>2</sub> capture<sup>[8-10]</sup>, extraction<sup>[9]</sup> and biomedical applications<sup>[9]</sup> battery development<sup>[11-12]</sup>, electrochemical applications<sup>[13]</sup> and biocatalysts<sup>[14-15]</sup>, organic synthesis<sup>[16]</sup>, material synthesis<sup>[17]</sup>. In this chapter, enormous works were carried to the improvement of Ionic Liquids by adding an organic cation (normally imidazolium-based cations) with a huge kind of anions, the most frequent ones being Cl<sub>2</sub>, BF<sub>4</sub>, PF<sub>6</sub>. From that point in time, ionic liquids have developed

as innovative types of promising solvents. The chance to change chemically the cationic moiety in a mixture with a large choice of anions offers researchers a wide range of ionic liquids showing various physical properties such as melting point, solubility, viscosity, density, conductivity, and refractivity. For example, Seddon and co-workers have reported that 1018 different ionic liquids can be theoretically produced in 2009. Among them, 250 ionic liquids were already commercialized <sup>[18]</sup>. Due to their low vapour pressure and high boiling point, they are eco-friendly and thus ionic liquids (ILs) were accepted as green solvents.

Many reports mentioned the harmful toxicity and the poor biodegradability of most ILs as reported by Romero et.al <sup>[19]</sup>. ILs with very high purity are mandatory since impurities even in little amounts change their physical properties. In addition, their synthesis is fair to be eco-friendly since it generally requires many salts and solvents to exchange the anions completely. Unfortunately, these drawbacks altogether with the high price of common ILs, slow down their industrial materialization. Thus, new concepts are now strongly desired to develop these systems in a more balanced way.

Qinghua Zhang et al. reported that to surmount the high price and toxicity of ILs, an invention of solvent, named Deep Eutectic Solvents (DES) <sup>[20]</sup>, have emerged at the early stage of this century. Production of these DESs can be obtained by simple mixing of two safe components (cheap, renewable, and biodegradable), which has the capability of forming a eutectic mixture. One of the most common components used for the formation of these DESs is choline chloride (ChCl). Choline chloride is a very cheap, biodegradable, and non-toxic quaternary ammonium salt that can be either extracted from biomass or readily synthesized from fossil reserves (million metric tons) through a very high atom economy process. ChCl can form a DES quickly when combined with safe hydrogen bond donors like urea, renewable carboxylic acids (e.g., oxalic, citric,

succinic, or amino acids), or renewable polyols (e.g., glycerol, polysaccharides). Although most of DESs are made from ChCl as an ionic species, DESs cannot be considered as ILs due to two reasons. Firstly, DESs are not fully composed of ionic species and secondly, can also be obtained from non-ionic species.

When compared with the usual ionic liquids, deep eutectic solvents obtained from ChCl draw together many advantages as listed below.

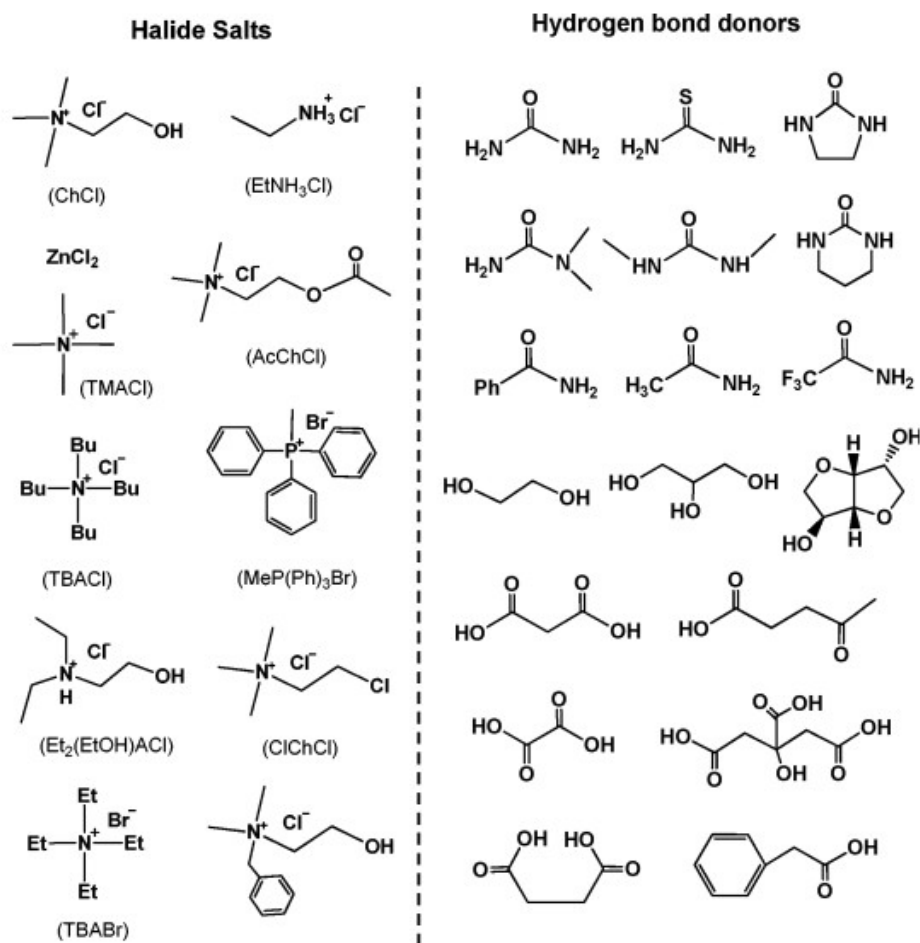
1. Cheap
2. Chemical inertness with water (i.e., safe, and easy storage)
3. Easy to synthesize since DESs are obtained by simply mixing two components, thus overcoming all problems of purification and waste disposal generally encountered with ILs.
4. Most of them are biodegradable <sup>[21]</sup>, biocompatible <sup>[22]</sup> and non-toxic <sup>[23]</sup>, reinforcing the greenness of these media <sup>[24]</sup> as reported by Y. Yu et al., K. D Weaver et al., F. Ilegan, et al., D. Reinhardt.

Cooper et al. <sup>[25]</sup> first announced another sort of solvothermal combination in which ILs were utilized as both the solvent and the structure-directing agent (SDA) in the blend of zeolites. This approach has been named ionothermal synthesis and, since this original work, has gotten perhaps the most broadly utilized synthetic strategies among the zeolite area. Curiously, it was likewise reached out to the preparation of not just other open-system structures metal–natural systems, covalent–natural structures or polymer–natural systems among others—yet in addition periodic mesoporous silicas and organosilica. While perceiving the enormous concepts in this theme, the focal point of this audit won't be on the utilization of ILs helped synthetic measures for the readiness of open-system structures, on the grounds that there are now excellent reviews and books that cover most of the new advances here <sup>[26]</sup>.

DESs have physico-chemical properties that are extremely similar to those of typical ILs (density, viscosity, refractive index, conductivity, surface tension, chemical inertness, etc.). For this reason, DESs derived from ChCl are named “biocompatible” or “renewable” ionic liquids in a few studies. Due to their low environmental path and attractive price, DESs have now become of rising interest both at intellectual and manufacturing levels. The number of publications dedicated to the use of DESs is now rapidly growing in the present literature and further indicating the magnetism of these media.

## **1.2. DEEP EUTECTIC SOLVENTS-DEFINITION**

A Deep Eutectic Solvent is commonly a combination of two or three cheap and safe components which can blend with each other, through hydrogen bond interactions, to form a eutectic mixture. The prepared DES is characterized by a melting point lower than that of the individual component. Generally, DESs are characterized by a huge depression of freezing point and are liquid at temperatures lower than 150°C. Most of them are liquids between room temperature and 70°C. In most cases, mixing of a quaternary ammonium salt with a metal salts or a hydrogen bond donor (HBD) that can form a complex with the halide anion of the quaternary ammonium salts a DES is obtained. Large, nonsymmetric ions with low lattice energy and thus low melting points are found in DESs. A quaternary ammonium salt is normally complexed with a metal salt or a hydrogen bond donor (HBD) to prepare DES. The decrease in the melting point of the mixture compared to the melting points of the individual components is due to charge delocalization caused by hydrogen bonding between, for example, a halide ion and the hydrogen-donor moiety. Scheme1 summarizes the different quaternary ammonium salts that are broadly used in combination with various HBDs in the formation of DESs.



**Scheme 1: Typical structures of the halide salts and hydrogen bond donors used for DES syntheses**

In 2007, Abbott and co-workers defined DESs using the general formula  $R_1 R_2 R_3 R_4 N^+ X^- Y^-$  [27].

Type1: DES  $Y = MCl_x$ ,  $M = Zn, Sn, Fe, Al, Ga$ ,

Type2: DES  $Y = MCl_x \cdot yH_2O$ ,  $M = Cr, Co, Cu, Ni, Fe$

Type3: DES  $Y = RZ$  with  $Z = -CONH_2, -COOH, -OH$

The same group also defined a fourth type of DES which is composed of metal chlorides (e.g.,  $ZnCl_2$ ) mixed with different HBDs such as urea, ethylene glycol, acetamide or hexanediol (Type 4 DES).

Recently, deep eutectic solvents (DES) have emerged as the alternatives for ionic liquids at room temperature. Deep eutectic solvents commonly indicate a mixture of a

halide salt and a hydrogen bond donor (HBD) to give a liquid below 100°C. The amazing qualities such as acceptance to humidity, non-combustible due to irrelevant vapour pressure, stability at high temperature, cheap, non-hazardous, reusable and recyclable [28] natures of DES make them replace ionic liquids.

### **1.3. PHYSICOCHEMICAL PROPERTIES OF DEEP EUTECTIC SOLVENTS**

DESs are chemically modified solvents since they can be planned by properly combining various quaternary ammonium salts (e.g., ChCl) with different hydrogen bond donors (HBD). Hence, task-specific DESs with different physicochemical properties such as freezing point, viscosity, conductivity, and pH, among others, can be identified. Due to their potential applications, many works have been committed to the physicochemical characterization of DESs.

#### **1.3.1 Freezing point ( $T_f$ )**

We know DESs are formed by mixing two solids capable of generating a new liquid phase by self-combination through hydrogen bonds. This new phase is generally characterized by a lower freezing point than that of individual components. For example, when ChCl and urea are mixed in a molar ratio of 1:2, the freezing point of the eutectic mixture is 12°C, which is considerably lower than that of ChCl and urea (melting point of ChCl and urea are 302 and 133°C, respectively). The significant depression of the freezing point shows from an interaction between the halide anion and the hydrogen bond donor component, here urea. For all reported DESs, their freezing points are below 150°C. In general, DESs with a freezing point lower than 50°C are more attractive since they can be used as economical and eco-friendly solvents in many fields.

#### **1.3.2. Density**

The density is one of the most vital physical properties of solvents. In general densities of DESs are calculated by means of a specific gravity meter. Most of DESs

show higher densities than water. For instance, type IV ZnCl<sub>2</sub>-HBD eutectic mixtures have densities higher than 1.3 g cm<sup>-3</sup>. Among them, density of ZnCl<sub>2</sub>-urea (1:3.5) and ZnCl<sub>2</sub>-acetamide (1:4) are different (1.63 and 1.36 g cm<sup>-3</sup>, respectively). This significant difference in density might be attributed to a different molecular group or packing of the DES. Note that densities of both DESs are higher than those of pure HBDs (acetamide: 1.16 and urea: 1.32g cm<sup>-3</sup>). This phenomenon may be explained by the hole theory. Like imidazolium-based ILs, DESs are composed of holes or empty vacancies. When ZnCl<sub>2</sub> was mixed with urea, for instance, the average hole radius was decreased, resulting in a slight increase of the DES density as compared to that of urea<sup>[27]</sup>.

### 1.3.3. Viscosity

Like most of the ILs, the viscosity of DESs is a significant topic that needs to be concerned. Except for the ChCl-ethylene glycol (EG) eutectic mixture, most of the DESs exhibit relatively high viscosities (>100cP) at room temperature. The high viscosity of DESs is often accepted to the presence of an extensive hydrogen bond system between each component, which results in lower mobility of free species within the DES. The large ion size and very small void volume of most DESs but also other forces such as electrostatic or Vander Waals interaction may contribute to the high viscosity of DES. Owing to their potential applications as green media, the development of DESs with low viscosities is highly enviable. In general, viscosities of eutectic mixtures are mainly exaggerated by the chemical nature of the DES components (type of the ammonium salts and HBDs, organic salt/HBD molar ratio, etc.), the temperature, and the water content. As discussed above, the viscosity of DES is also dependent on the free volume. Hence, the hole theory can also be used to design DESs with low viscosities. For example, the use of small cations or fluorinated hydrogen-bond donors can lead to the formation of DES with low viscosity<sup>[29]</sup>.

#### 1.3.4. Ionic conductivity

Due to their comparatively high viscosities, most of DESs show poor ionic /conductivities (lower than  $2 \text{ mS cm}^{-1}$  at room temperature). Conductivities of DESs generally increase noticeably as the temperature increases due to a decrease in the DES viscosity. Hence, the Arrhenius-like equation can also be used to calculate the conductivity behaviour of DESs. Taking into explanation the changes of the organic salt/HBD molar ratio greatly impact the viscosities of DES, this factor also radically influences the conductivities of DESs <sup>[30]</sup>.

#### 1.3.5 Acidity or Alkalinity

The Hammett function has been broadly used to calculate the acidity and basicity of non-aqueous solvents by determining the ionization ratio of indicators in a system. For a basic solution, the Hammett function shows the affinity of the solution to attracting protons. When weak acids are selected as indicators, the Hammett function H is defined by the following equation.

$$H^+ = pK (HI) + \log([I^-] / [HI] )$$

Where  $pK (HI)$  is the thermodynamic ionization constant of the indicator in water,  $[I^-]$  and  $[HI]$  represent the molar concentrations of anionic and neutral forms of the indicator respectively. A medium with a large  $H^+$  value has strong basicity. Note that when the system contains 1-3wt% of water, the H values decreases somewhat due to partial solvation of basic sites <sup>[31]</sup>.

#### 1.4. BINARY DEEP EUTECTIC SOLVENTS (BDES)

Deep eutectic solvents are eutectic mixtures of Lewis or Bronsted acids and bases that can contain a wide range of anionic and cationic species <sup>[32]</sup>. They are categorized as ionic solvents with unique properties. The combination of two compounds forms a eutectic with a melting point that is much lower than any of the individual components <sup>[33]</sup>.



A 1:2 mole ratio of choline chloride and urea created one of the most important deep eutectic phenomena ever observed. The resulting mixture has a melting point of 12 °C (much lower than choline chloride's melting point of 302 °C or urea's melting point of 133 °C), making it liquid at room temperature [34].

The first generation of eutectic solvents is composed of quaternary ammonium salts coupled with hydrogen bond donors including amines and carboxylic acids [35].

#### 1.4.1 Types of Deep Eutectic Solvents:

Eutectic solvents are divided into four categories:

<b>Types of DES</b>	<b>Components</b>
<b>Type I</b>	Quaternary ammonium salt + metal chloride
<b>Type II</b>	Quaternary ammonium salt + metal chloride hydrate
<b>Type III</b>	Quaternary ammonium salt + hydrogen bond donor
<b>Type IV</b>	Metal chloride hydrate + hydrogen bond donor

DES has a low density and can be liquid at a wide range of temperatures, up to -50 °C in some cases [36]. DESs are much less costly to manufacture and are often biodegradable. As a result, DES can be used as a solvent that is safe, efficient, simple, and inexpensive [37]. A Binary deep eutectic solvent (BDES) is a fluid made up of two inexpensive and harmless components that can self-associate, usually by hydrogen bond interactions, to form a eutectic mixture with a melting point lower than the melting point of each component individually as reported by Zhang et al [20].

For the first time, binary and ternary deep eutectic solvent (DES) mixtures based on choline chloride, ethylene glycol, oxalic acid, urea, and fructose were used as a medium for electropolymerized of poly(methylene blue) (PMB) on glassy carbon electrodes (GCEs)

and GCEs changed with multiwalled carbon nanotubes (MWCNTs) as reported by Lucía Abad-Gil et al<sup>[38]</sup>.

The use of DESs and NADESs in biofuel <sup>[39,40–42]</sup> and bio-oil extraction <sup>[43,44]</sup>, as reaction media or extractive factors <sup>[45]</sup>, and as media to control intermolecular interactions <sup>[46]</sup> as one of broad lists of applications <sup>[20,47,48]</sup>.

### **1.5. TERNARY DEEP EUTECTIC SOLVENTS (TDES)**

The combination of three components forms ternary deep eutectic solvents. Yu-Ting Liu et.al. prepared and reported that Imidazolium halides, zinc halides, and amides were used to generate a set of room-temperature ternary deep eutectic solvents (TDESs). In the sequence, the [BMIM]Cl–ZnCl<sub>2</sub>–acetamide (1:1:1) system has the lowest freezing point (-60 °C) and density <sup>[49]</sup>. Deep eutectic solvents (DESs) can be used as designer media with a wide range of physical, chemical, electrochemical, and spectroscopic properties <sup>[50]</sup>.

TDES is more thermally stable than BDES and has a larger free volume, making it potentially beneficial for high-temperature sorption applications. Because of its environmentally benign preparation procedure, the TDES is predicted to be capable of large-scale industrial applications <sup>[51]</sup>.

Ternary deep eutectic solvents (DESs) were designed to facilitate quick and high-solid biomass pretreatment as well as the production of concentrated sugar hydrolysate reported by Chen et al <sup>[52]</sup>. TDES loses less weight than BDES as the temperature rises, indicating that it is more thermally stable. Because of its lower viscosity and higher conductivity, as well as its low freezing points, TDES is suitable for enhancing polar reactions. Furthermore, since TDESs based on zinc halides have a Lewis acidic centre, they can be used as both a catalyst and a dye <sup>[49]</sup>.

Two series of liquids at room temperature, choline chloride–urea–glycerol and choline chloride–malic acid–glycerol, were synthesized in different molar ratios and their properties were investigated by Mohammed A.Khadhom and associates <sup>[53]</sup>.

Yu-hui Chi et.al. reported as the proportions of lignin and hemicellulose removed was 88.39 per cent and 84.38 per cent, respectively, under optimal conditions (DES ratio of 1: 1: 1.5, 120°C, 4 h), with enzymatic intake reaching 59.3 per cent in the subsequent enzymatic saccharification with a short period (5 days) and low enzyme load (30 FPU g<sup>-1</sup>) <sup>[54]</sup>. TDESs with the best composition is made from choline chloride, oxalic acid, and ethylene glycol (n/n/n, 1/1/3). Water-TDESs (50 vol per cent TDES in water-TDESs) prepared by Weiyang Tang et al., was used as solvents in a heating phase (60°C) for 30 minutes at a solid/liquid ratio of 1:10 g/mL to extract flavonoids <sup>[55]</sup>.

## **1.6. ZINC CHLORIDE-BASED DEEP EUTECTIC SOLVENTS**

In 2015 Fatemeh S.Ghareh Bagh and associates reported Deep mixture solvents (DESs) have gained interest due to their melting temperatures, viscosities, electrical conductivities, refractive indices, likewise as an electrical window over a good vary of temperatures, The ammonium-based deep mixture solvents possessed lower melting temperatures, lower viscosities and higher electrical conductivities as compared to phosphonium-based ones. The deep mixture solvents made from B complex chloride and metal (II) chloride at a mole magnitude relation of 1:1 possessed high conductivities, 574-4779 $\mu$ S cm<sup>-1</sup>, comparatively low viscosities, 0.8278-0.2842 Pa-s, and wide electrochemical window, 3.74 V among the studied temperature vary <sup>[56]</sup>.

ZnCl<sub>2</sub>: Acetamide DES (in 1:4 molar proportion) keeps up its fluid-structure till temperatures as low as -16 °C <sup>[57]</sup> accordingly giving a wide scope of temperature whereby it can be utilized as a solvent. The freezing point of ZnCl<sub>2</sub> is 293°C, that of acetamide is

81°C, while the DES shaped out of these in the salt: H-bond bond factor molar proportion of 1: 4 is pretty much as low as- 16°C <sup>[58]</sup> as reported by Tripti Kumari & co-workers.

The use of a DES containing zinc chloride and choline chloride as a non-volatile solvent and catalyst for one-step heterogeneous production of acetylated chitin nanocrystals is reported. This type of DES acts as better catalysis of the functional reaction. The thermal stability of Chitin Nano Crystals decreased after being treated by Choline Chloride/ZnCl<sub>2</sub> and showed less expenditure and toxicity as reported by Shu Hong et.al <sup>[59]</sup>.

Lian. H reported that the incorporation of Zn improved the stability even at various temperatures and upgraded lignin's reactivity towards phenol-formaldehyde resin arrangement <sup>[60]</sup>. DES containing Choline chloride (ChCl) and Zinc chloride (ZnCl<sub>2</sub>) is widely used as a Lewis acid catalyst and reaction medium for a variety of reactions, including Diels–Alder reactions <sup>[61]</sup>, Fischer indole annulation <sup>[62]</sup>, esterification of long-chain carboxylic acid <sup>[63]</sup>, O-acetylation of cellulose and monosaccharides <sup>[64]</sup>, and car protection <sup>[65]</sup>.

Patil et al. <sup>[66]</sup> examined the performance of the most used Lewis-acid type DES ChCl-ZnCl<sub>2</sub> as a catalyst and solvent in the synthesis of primary amides from aldehydes and nitriles. The use of DES in the reactions generated green and atom efficient synthesis by reducing waste and toxic material, according to the authors.

A deep eutectic solvent based on choline chloride–zinc chloride is a green and effective reaction medium for the [2+3] cycloaddition reaction of organic nitriles with sodium azide to yield 5-substituted 1H-tetrazoles <sup>[67]</sup>.

Yu-Ting Liu and associates reported that a series of novel room-temperature ternary deep eutectic solvents (TDES) were successfully prepared using imidazolium ionic liquids, zinc halides, and amides. TDES is ideal for enhancing polar reactions due to its lower viscosity and higher conductivity, in addition to its low freezing points. Furthermore, the

presence of a Lewis acidic core in TDESs based on zinc halides allows them to be used as both a catalyst and a dye [68].

By replacing  $\text{AlCl}_3$  with more stable metal halides such as  $\text{ZnCl}_2$  to form eutectic derived ionic liquids, the moisture sensitivity of these systems can be reduced somewhat [69]. DESs based on choline chloride and zinc chloride was first introduced by Abbott et al. as low-cost, readily available substitutes to ILs in synthesis. Diels–Alder cycloaddition, Fischer indole annulation, and polymerizations have all been successfully carried out with these  $\text{ChCl-ZnCl}_2$  Lewis acidic solvents [70,71].

Since starch is soluble in choline chloride: oxalic acid and choline chloride:  $\text{ZnCl}_2$ , these DESs could be used as a solvent for chemical changes of starch as reported by Biswas et al [72].

The presence of metal salts such as  $\text{ZnCl}_2$  in Types I, II, and IV DESs gives them a Lewis acidic character.  $\text{ChCl-ZnCl}_2$  (1:3) had several advantages, including low toxicity, low cost, and ease of handling. It could also be reused up to five times without losing its catalytic activity as reported by Ayşe Ezgi Ünlü et. al [73].

In Friedel-Crafts acylation reactions, Tran et al. used  $\text{ChCl-ZnCl}_2$  as a catalyst and a green solvent. Under microwave irradiation, they achieved high regio- and chemo-selectivity in reactions involving acid anhydrides and the catalyst  $\text{ChCl-ZnCl}_2$  (1:3 molar ratio) [74].

### **1.7. MALONIC ACID-BASED DEEP EUTECTIC SOLVENTS**

A deep eutectic solvent (DES) made from choline chloride and malonic acid was made quickly and cheaply. In a one-pot, the four-component reaction of amines, aldehydes, 1, 3-dicarbonyl compounds, and nitromethane, was used as a dual catalyst and reaction medium for the synthesis of functionalized pyrroles [75].

Some ChCl with Carboxylic-acid-based DESs has also been reported to undergo chemical reactions such as esterification between DES components. As a result, it was discovered that a number of DESs containing ChCl and carboxylic acids (lactic acid, glutaric acid, glycolic acid, malic acid, malonic acid, oxalic acid, and levulinic acid) undergo an esterification reaction between the hydroxyl group of choline chloride and the carboxylic acid [76].

The efficiency of two DESs - choline chloride-malonic acid of molar ratios 1:1 and 1:0.5 - in enhancing oil recovery was investigated for the first time by Iman Al-Wahaibi et al [77]. Gunny et al investigated the use of the DES-cellulase mechanism to hydrolyze lignocellulose from rice husk. The DES is comprised of choline chloride and a hydrogen-bond donor molecule (glycerol, ethylene glycol, or malonic acid) [78].

### **1.8. MANGANESE BASED DEEP EUTECTIC SOLVENTS**

Five novel manganese (II)-based DESs were successfully synthesized by Koon-Kee Kow et al and they reported that the  $\text{MnCl}_2 \cdot 4\text{H}_2\text{O}$  acetamide DES has the lowest freezing point (27.5 °C), the highest thermal stability (193 °C point of dehydration), the lowest viscosity ( $\eta = 112.8$  cP), and the highest conductivity (0.12723 mS/cm [79]).

Mesoporous alpha-manganese dioxide ( $\text{MnO}_2$ ) was synthesized by Xiaochen Lai et al., using a 1:7 molar ratio of manganese (II)-based deep eutectic solvent (DES) of  $\text{MnCl}_2 \cdot 4\text{H}_2\text{O}$  and acetamide. The DES can be used as both a solvent and a reducing agent. Congo red (CR) was removed from aqueous solutions using as-prepared samples that were characterised and used as absorbents [80].

### **1.9. SUGAR-BASED DEEP EUTECTIC SOLVENTS**

The glucose-based novel DESs have the potential to be used for a variety of industrial applications, including food processing and separation, pharmaceutical applications, and chemical reaction mediums as reported by Adeeb Hayyan [81].

Two DESs d-glucose: choline chloride: water (GCH) and d-glucose: citric acid: water (GCiH) has been characterized by Fernando Bergua et al.,<sup>[82]</sup> and the used techniques to analyze both the supramolecular structure and the role of water and to calculate the diffusion coefficients.

For the first time, deep eutectic solvents (DESs) made NMR up of natural compounds like choline chloride (ChCl) and sugars were proposed as NH<sub>3</sub> absorbents by Zi –Liang Liu et al. The absorption of NH<sub>3</sub> in DESs exhibits non-ideal behaviour due to the abundance of hydroxyl groups that allow strong hydrogen-bond interaction with NH<sub>3</sub>, and the NH<sub>3</sub> capacities show a small decrease as temperatures rise. The absorption of NH<sub>3</sub> in ChCl + sugar DESs also exhibits strong selectivity over other components in industrial tail gas (e.g., N<sub>2</sub>, H<sub>2</sub>, and CO<sub>2</sub>), as well as reversibility<sup>[83]</sup>.

Ionic liquids are used in a unique technique to separate sugars from combinations of fructose and glucose in a liquid phase or a solid mixture containing the fructose and glucose patented by AlNashef et al.,<sup>[84]</sup>.

Deep eutectic solvents (DES) containing chiral hydrogen-bonded donors derived from biomass, glucose, and fructose, as well as the hydrogen bond acceptor tetrabutylammonium chloride ([TBA]Cl) can be used as solvents in (CPL) Circularly polarized light-emitting materials<sup>[85]</sup>. The magnitude of induced CPL is influenced by the polarity of the DES and the anomeric form of the monosaccharide, according to results from the glucose DES.

## **1.10. SIGNIFICANCE OF DEEP EUTECTIC SOLVENTS**

Deep eutectic solvents (DESs) are a novel class of solvents that potentially overcome the major problems of traditional ILs, such as high toxicity, non-biodegradability, complex synthesis that necessitates purification, and expensive starting material costs<sup>[86]</sup>. DESs are made by blending two safe components (cheap, renewable,

and biodegradable) into a eutectic mixture. Deep Eutectic Solvents (DESs), also known in the literature as Deep Eutectic Ionic Liquids (DEILs), Low Melting Mixtures (LMMs), Low Transition Temperature Mixtures (LTTMs), or Natural Deep Eutectic Solvents (NADES). According to the literature, at least two components are required to synthesize the desired DES: i) a hydrogen-bond donor (HBD), and ii) a hydrogen-bond acceptor (HBA) [87]. The hydrogen bond donor causes a weaker anion/cation coupling, allowing the DES to melt at low temperatures.

### 1.11. COMPARISON OF IONIC LIQUIDS WITH DEEP EUTECTIC SOLVENTS

As compared to ionic liquids, Deep Eutectic Solvents has many advantages [87],

- i) low cost,
- ii) chemical inertness with water,
- iii) simple to create (because DESs are made by just mixing two components, bypassing the purification and waste disposal issues that typical ILs have), and
- iv) biodegradable, biocompatible, and non-toxic, strengthening the greenness of these media.

**Table 1.1 Comparison of Ionic liquids with Deep Eutectic solvents**

Ionic Liquids	Deep Eutectic Solvents
Low melting point ionic compounds	Low melting eutectic mixture of compounds
Not always environmentally friendly, can be toxic	Biodegradable and nontoxic starting materials
Solution conductivity-moderate to high	Highly conductive
Expensive: recycling is critical	Cheaper than ILs



## 1.12. APPLICATIONS OF DEEP EUTECTIC SOLVENTS

Matthijs et al. investigated the environmental effects of DES in electroplating applications based on choline chloride and ethylene glycol <sup>[88]</sup>. Nanocellulose materials have developed as a fascinating new class of nanomaterials. This is owing to its environmental benefits, which include renewable resource production, biodegradability, biocompatibility, and high potential availability reported by Angeles et al <sup>[89]</sup>.

Since DESs are less expensive than conventional ILs and are considerably easier to create in large batches, DES-based procedures in the metal polishing and metal extraction industries are being scaled up and commercialized <sup>[90]</sup>. Metal processing research has been classified into three broad categories: metal electrodeposition, metal electropolishing, metal extraction, and metal oxide processing <sup>[32]</sup>.

In suitable DES systems, the replacement of ecologically harmful metal coatings, the deposition of novel alloys and semiconductors, and new coating technologies for the deposition of corrosion-resistant metals such as Ti, Al, and W <sup>(91-93)</sup> are all possible.

Zn, <sup>(94, 95, 96)</sup> Sn, Cu, <sup>(97, 98)</sup> Ni, <sup>(99)</sup> Ag, <sup>(100)</sup> Cr, <sup>(101)</sup> Al, <sup>(102)</sup> Co, <sup>(103)</sup> are among the metal reduction processes investigated in DESs and reported. Addition reactions, cyclization reactions, replacement reactions, multicomponent reactions, condensation reactions, oxidation reactions, and reducing reactions are among the organic reactions studied in DES as reported by Peng Liu in a review <sup>[104]</sup>.

When compared to a conventional solvent, a betaine-based DES with glycerol (molar ratio 1:2) was shown to be the most effective for extracting phenolic chemicals <sup>[105]</sup>. DES was used as a novel solvent and catalyst in a typical organic synthesis method, mainly including halogenation reaction, Diels-Alder reaction, Knoevenagel reaction, Henry reaction, Perkin reaction, Paal-Knorr reaction, Biginelli reaction <sup>[106]</sup>.

### 1.12.1. APPLICATIONS OF DEEP EUTECTIC SOLVENTS IN NANOTECHNOLOGY

Ali Abo- Hamed et al., reported that due to the unique qualities as novel green solvents, effective dispersants, and large-scale media for chemical and electrochemical production of sophisticated functional nanomaterials, deep eutectic solvents (DESs) have recently piqued attention in a variety of sectors, including nanotechnology [107].

DESs are used to synthesize and fabricate a variety of nanomaterials, including zeolite analogues [25], carbon nanomaterials [108, 109], micro-and nanostructured semiconductors [110-112], and DNA nanostructures [113].

As a result of their excellent chemical and physical features, DESs have shown to be adaptable media for nanoscale synthesis [114, 107]. Despite the ubiquitous influence of DESs, their involvement in the synthesis of noble metal nanoparticles, notably gold and silver nanoparticles, has received less attention [115].

DES has been utilized as a reaction medium for nanomaterial production and electrodeposition, as well as a nanoparticle dispersion medium. The most popular nanomaterials include carbon, metal oxide, and gold nanoparticles, inorganic (bio)nanomaterials, and metal (bio)organic framework materials as reported by Abo-Hamed [107].

Muzamil Khatri et.al. used an electrospinning process to construct Zein nanofibers from DES and achieved extremely hydrophilic Zein nanofibers without any post-treatment. Choline chloride (HBA) and Furfuryl alcohol (HBD) in a 1:2 ratio was utilized to make the DES needed for electrospinning [116].

The use of DESs as a solvent for the shape-controlled production of metal nanoparticles is an intriguing and growing application that could have a significant impact on the science of electrocatalysts. Without the use of any surfactants or seeds, gold

nanoparticles were produced to generate Au-based catalysts using a DES as the solvent [32,117]. DESs are a new type of reaction media for the synthesis of noble metal nanomaterials that holds a lot of promise. They have a lot of advantages that have been studied [118].

Due to the advantages of their small particle size, large specific surface area, reproducibility, environmentally friendly materials, and easy solid-liquid separation, literature has recently confirmed that the combination of DESs and magnetic nanoparticles (MNPs), such as Fe<sub>3</sub>O<sub>4</sub>-DES [119] and SiO<sub>2</sub>@Fe<sub>3</sub>O<sub>4</sub>-DES, has a broad application prospect in the magnetic solid-phase extraction method [120].

Ionic liquids (ILs) and Deep eutectic solvents (DESs) are being used in the development of nano-sorbents such as nanoparticles, nanogels, and nanofluids as good alternative solvents. In the extraction process, ILs and DESs are frequently utilised as carriers/modifiers/dispersers of nano-sorbents to improve adsorption capacity and selectivity [121].

Different metallic nanoparticles have been used by Ingrid Hagarová et.al., [122] to separate and pre-concentrate organic and inorganic analytes in a variety of environmental, biological, pharmacological, and dietary samples. Iron oxide magnetic nanoparticles are useful in a variety of fields, including chemistry, physics, and materials science [123]. In ChCl/EG or urea DES, Anicai et al. described the electrochemical synthesis of high-grade TiO<sub>2</sub> nanopowders, a nanomaterial that is widely employed in industrial applications such as solar cells, photocatalysis, chemical sensors, microelectronics, and electrochemistry [124]. For the manufacture of Fe<sub>3</sub>O<sub>4</sub> magnetic nanoparticles, a novel oxidative precipitation-combined ionothermal approach is reported [125]. The nanoparticles created were stable and had a higher catalytic efficiency for degrading organic contaminants in water treatment.

The presence of stable and uniform ZnO nanoparticles, with increased dispersion stability and catalytic efficacy, was demonstrated using an ionothermal precipitation technique in ChCl/EG <sup>[126]</sup>. Laser ablation targeting a silver metal blank immersed in the DES produced silver nanoparticle colloidal suspensions in a ChCl/urea eutectic mixture. The silver nanoparticles' luminous characteristics were found to be superior to those obtained in aqueous solutions <sup>[127]</sup>. Karimi et al. <sup>[128]</sup> examined the ternary role of DES as a medium for the synthesis of monetite nanoparticles in ChCl-EG eutectic mixture.

A.J. Exposito et.al.,<sup>[129]</sup> used a combination of ChCl and Urea as the reaction medium, as well as the high heat and mass transfer rate given by microreactors, to demonstrate for the first time fast continuous synthesis of Ceria nanoparticles under mild temperatures. For the development of more effective nanoparticle-based catalysts, deep eutectic solvents (DES) have been employed as sustainable media <sup>[130]</sup>. Bruna et al. investigated how the deposition of DES onto TiO<sub>2</sub> surfaces modifies the catalytic activity of TiO<sub>2</sub> in the photodecomposition of organic dyes. The DES consisting of choline chloride (ChCl) and maleic acid is used to make Spinel ferrites, phase-pure nanoparticles MFe<sub>2</sub>O<sub>4</sub> (M=Mg, Zn, Co, Ni) at temperatures significantly lower than the solid-phase reactions of the metal oxides. As a result, the approach lowers the total amount of energy required to make nanoparticles examined by Anika Soldner et.al <sup>[131]</sup>.

Surface modification of graphene oxide (GO) nanosheets with different functional groups have recently shown interest in using DESs <sup>[132]</sup>. Mehrabi et.al. predicted that surface functionalization of GO (and other carbon nanomaterials) using DESs based on choline chloride and urea will allow resynthesized Fe<sub>3</sub>O<sub>4</sub> nanoparticles to be conjugated onto GO nanosheets at various GO: Fe<sub>3</sub>O<sub>4</sub> ratios. Cojocar et.al. described the experiments using a choline chloride – glycerol deep eutectic solvent with pulse reversed current to synthesize silver nanoparticles (Ag NPs) at 25°C <sup>[133]</sup>.

Jakubowska. et.al., extracted metal oxide NPs from plant material via NADES <sup>[134]</sup>. The root accumulated larger cerium (IV) oxide NPs, but the radish leaves accumulated smaller ones. The titanium (IV) oxide NPs were agglomerated and found in tiny amounts in radish leaves, with most of them aggregating in the root.

### **1.13. METAL NANOPARTICLES**

Metallic nanoparticles have stimulated the interest of scientists for over a century, and they are now widely used in biological and engineering fields. Because of their enormous potential in nanotechnology, they have attracted a lot of attention. Even though the phrase is new, it has become widely employed in the development of more efficient technologies. Due to its applications in the fields of electronic storage systems <sup>[135]</sup>, biotechnology, <sup>[136]</sup> magnetic separation and preconcentration of target analytes, targeted drug delivery, <sup>[137,138]</sup> and vehicles for gene and drug delivery, nanotechnology has recently been adopted by industrial sectors <sup>[135,137-139]</sup>. In general, nanoparticles utilised in biotechnology have particle sizes ranging from 10 to 500 nm, seldom reaching 700 nm.

#### **1.13.1. Silver nanoparticles (Ag NPs)**

Silver nanoparticles are ranging with the size of 1–100 nm. While many are classified as "silver," due to the enormous ratio of surface to bulk silver atoms, some have a high amount of silver oxide. There is now an endeavour to include silver nanoparticles into a variety of medical products, such as bone cement, surgical instruments, surgical masks, and so on. Furthermore, it has been demonstrated that ionic silver can be used to cure wounds in the correct amounts. <sup>[140–142]</sup> They are usually made by reducing a silver salt in the presence of a colloidal stabiliser using a reducing agent like sodium borohydride. To develop silver nanoparticles, newer revolutionary ways include the use of d-glucose as reducing sugar and starch as a stabiliser, as well as ion implantation <sup>[143]</sup>. Furno et al. produced biomaterials by employing supercritical carbon dioxide to impregnate silicone

covered with silver oxide nanoparticles <sup>[144]</sup>. These new biomaterials were created with the goal of reducing antimicrobial infection.

In general, three different approaches have been used to synthesize silver nanoparticles, including physical, chemical, and biological processes <sup>[145]</sup>. Several efforts have been made in the recent decade to develop green synthesis processes that prevent hazardous consequences <sup>[146]</sup>. The most common approach for developing Ag-NPs is chemical reduction <sup>[147,148,149]</sup> by using reducing agents like poly-ethylene glycol block copolymers, sodium citrate, Tollen's reagent, Ascorbate, essential hydrogen, N, N-dimethyl formamide (DMF), and sodium borohydride (NaBH<sub>4</sub>) <sup>[149,150,151]</sup>. Silver nanoparticles (AgNPs) offer a lot of potential applications as antimicrobial agents, biomedical device coatings, drug delivery carriers, imaging probes, and diagnostic and optoelectronic platforms <sup>[152]</sup>.

Chemical synthesis of nanoparticles has the advantages of ease of manufacture, low cost, and high yield; nevertheless, chemical reducing agents are toxic to living organisms <sup>[153]</sup>. Abbasi et al. have published a full review of AgNPs synthesis methods, characteristics, and bio-application <sup>[154]</sup>. High electrical and thermal conductivity <sup>[155]</sup>, surface-enhanced Raman scattering <sup>[156]</sup>, catalytic activity <sup>[157]</sup>, and non-linear optical properties <sup>[158]</sup> are just a few of the physicochemical properties of AgNPs that have led to many of the innovative products and related technologies <sup>[159]</sup>. Even if well-established methodologies for the manufacture of metallic nanoparticles exist, simple synthesis approaches with fast reaction times and inexpensive costs must be investigated in order to create nanoparticles with enhanced antibacterial activity <sup>[160]</sup>. To optimise the synthesis of AgNPs derived using the chemical reduction approach, a Face Centered Central Composite Design (FCCCD) was used by Quiroz et.al <sup>[161]</sup>.

### 1.13.2. Copper nanoparticles (Cu NPs)

In recent years, the usage of copper (Cu) and Cu-based nanoparticles, which are based on abundant and inexpensive copper metal, has sparked a lot of attention, particularly in the field of catalysis. Cu NPs are particularly appealing due to copper's abundant natural resources and low cost, as well as the numerous practical and simple approaches to synthesize Cu-based nanomaterials <sup>[162]</sup>. Cu-based nanocatalysts offer a wide range of applications in nanotechnology, including catalytic organic transformations, electrocatalysis, and photocatalysis, due to their unique qualities and properties. Copper nanoparticles have two functions: (i) they operate as an antibacterial agent, though not as well as other metal nanoparticles, and (ii) they increase the porosity of the beads, making the scattered AgNPs in the beads more accessible to bacteria <sup>[163]</sup>. Cu nanoparticles are frequently coated with a capping substance to prevent oxidation and control crystal formation by lowering the surface energy of crystals <sup>[164]</sup>. Laser ablation, thermal degradation, chemical reduction, and polyol synthesis are some of the currently developed nanoparticle synthesis methods. Chemical reduction is commonly favoured among these procedures because it is simple, cost-effective, and efficient, and it can provide better size and size dispersion control <sup>[165]</sup>. The size management of Cu NPs, as well as the presence of a surface coating to prevent oxidation, are essential to obtain Cu NPs with excellent antibacterial capabilities. For industrial applications, a simple route producing oxide-free Cu NPs by thermal disintegration of a copper precursor has recently been reported by Adner et.al <sup>[166]</sup>.

On the other hand, the production of copper oxides at the nanoscale has a wide range of applications <sup>[167]</sup>. Transition metal oxides, particularly cupric oxide (CuO), have unique catalytic and photocatalytic characteristics <sup>[168]</sup>. Cu-NPs synthesised in polymer

media have various advantages over conventional agents, including simplicity of processing, solubility, low toxicity, and nanoparticle growth control <sup>[169]</sup>.

### **1.13.3. Cadmium nanoparticles (Cd NPs)**

Cadmium sulphide nanoparticles were chosen as a compound of interest because of its great stability, good physical, chemical, and structural qualities, and ease of synthesis and handling. CdS nanoparticles are commonly utilised for cancer detection and antibacterial treatment <sup>[170]</sup>. Gas phase reaction (with H<sub>2</sub>S or sulphur vapour), solvothermal technique, solution precipitation, microwave-assisted solution precipitation, and several other ways are used to synthesize CdS nanoparticles <sup>[171]</sup>. Cadmium sulphide (CdS) has captivated researchers' interest not only because of its excellent semiconductor optical and electrical capabilities but also because of its wide spectrum absorption range <sup>[172,173]</sup>. CdS has a bandgap of 2.4 eV and can absorb visible light when the semiconductor bandgap is small (i.e 3.0 eV) <sup>[174]</sup>. CdS nanoparticles have been employed in a variety of applications, including photocatalytic hydrogen production, solar batteries, and redox process <sup>[175-177]</sup>. CdS was chosen to generate NADH by transferring electrons to the coenzyme NAD<sup>+</sup>. To speed up the biocatalytic reaction, an efficient coenzyme self-circulation reaction was created by Chang et.al <sup>[178]</sup>. The ability of microbes to manufacture green Cd-containing nanocrystals has been attributed to their ability to oppose heavy metals via bioreduction and precipitation of soluble metallic ions, resulting in insoluble nanometric complexes <sup>[179]</sup>. Because of their smaller size, excellent optical fluorescence property, and ease of functionalization, the development of innovative cadmium-based quantum dots has significant potential in the treatment and identification of cancer as well as targeted drug delivery <sup>[180]</sup>. CdS is employed as a pigment in paints and engineered plastics because of its good thermal consistency and dirt repelling capabilities <sup>[181,182]</sup>. For its photochemical and catalytic characteristics CdS NPs can be utilised as an air-water cleaner as well as a



source of hydrogen <sup>[183]</sup>. CdS nanoparticles can be employed for both visualisation and medication distribution to soft tissues such as the retina and cornea <sup>[184,185]</sup>. Durga et.al. chose *Annona muricata* leaf extract to produce cadmium sulphide nanoparticles and attempted green synthesis, evaluation of structural and morphological properties, and analysis of microbial activity <sup>[186]</sup>.

#### **1.13.4. Mercury Nanoparticles (HgNPs)**

Mercury is the only metal element in nature that exists as a liquid at room temperature, posing a challenge for material scientists to investigate Hg nanoparticles <sup>[187]</sup>. Nanoparticles have features that differ from bulk materials, and they frequently lead to major technological applications <sup>[188-192]</sup>. For the synthesis of mercury metal nanoparticles, Harika et.al., used liquid mercury as the starting material, eliminating the need of reducing agents <sup>[193]</sup>. In aqueous solutions, mercury sulphide (HgS) nanoparticles (NPs) were generated by Kuno et.al., with water-soluble thiols as capping ligands <sup>[194]</sup>. Mazrui et.al. studied the development and fate of -HgS(s) nano produced in combination with marine dissolved organic matter collected from the North Atlantic Ocean, as well as low molecular weight thiols <sup>[195]</sup>. Chemical deposition <sup>[196]</sup>, solvothermal <sup>[197]</sup>, microwave heating <sup>[198]</sup>, photochemical <sup>[199]</sup>, wet chemical <sup>[200]</sup>, and electrochemical <sup>[201]</sup> are all well-established processes for the synthesis of Hg nanoparticles. Because of its uses as acoustic optical materials <sup>[202]</sup> and infrared sensing <sup>[203]</sup>, HgS has gotten increased attention. By using pulsed laser ablation on a pellet of mercuric sulphide (-HgS) stilled in distilled water, J.Mohammed et.al., succeeded in a simple and straightforward technique for preparing the meta-cinnabar phase of mercuric sulphide (-HgS)<sup>[204]</sup>. For the preparation of  $\beta$ -HgS nanocrystals, Xin xu. et. al. employed a solvent-based method, followed by sonication and nitrogen purging at room temperature <sup>[205]</sup>.



## **1.14. REVIEW OF LITERATURE**

### **1.14.1. Deep eutectic solvents –synthesis and characterization**

Ionic liquids (ILs) are green solvents that can be used in a variety of applications. However, their production via chemical reactions with waste or by-products is incompatible with the concept of green chemistry, and the purity issue and cost feasibility restrict their use in several large-scale industrial applications. DES is produced, when halide salts and hydrogen bond donors (such as alcohol or acid) combine, resulting in a combination having a lower freezing/melting point than the individual components <sup>[206]</sup>. In green chemistry and processing, DES is becoming increasingly essential <sup>[207, 208]</sup>. Extensive research is being carried out to investigate the properties of newly synthesized DES <sup>[209–211]</sup>. The traditional DES is a binary deep eutectic solvent made up of two single components (BDES). The addition of a third component to the ternary deep eutectic solvent (TDES) improved the designable property much more than the standard BDES. TDES has been synthesized and used in a variety of applications so far <sup>[212-214]</sup>. BDES were prepared by mixing the two components at a molar ratio of 1:1. By heating the binary mixture to 80°C with continuous stirring, clear liquids were obtained <sup>[215]</sup>. After cooling to room temperature, the binary mixture remains at a liquid state <sup>[216]</sup> and the evaporating method was employed in water as given by Dai et al. <sup>[217]</sup>. Their cost of production is less and used as safer solvents in several fields <sup>[218]</sup>. It is possible to create endeavor DESs with various physicochemical parameters, such as freezing point, viscosity, conductivity, and pH, among others.

### **1.14.2. Copper nanoparticles**

Metallic nanoparticles have a lot of potential because of their chemical, physical, and catalytic capabilities <sup>[219]</sup>. Copper nanoparticles are a type of colloidal transition metal nanoparticle that receives a lot of interest since they are employed as an advanced material

with electrical, optical, and thermal properties <sup>[220]</sup>. A chemical reduction is a popular approach for making copper nanoparticles because it is low-cost, high-yielding, and requires little equipment. It is simple, and the control of particle size and shape obtained under-regulated parameters may be shown <sup>[221]</sup>. The copper nanoparticles were made using a wet chemical reduction method as reported by Jain et.al <sup>[222]</sup>. Mustafa G, et al. reported the synthesis of monoclinic CuO nanoparticles that were characterized by XRD analysis <sup>[223]</sup>.

CuO nanoparticles can be manufactured in a variety of methods, and synthesis parameters such as technique, solvents, surfactants, starting precursors, and temperature are employed to regulate the form and size of desired nanoparticles, according to Suleiman M, et al <sup>[224]</sup>. Wongpisutpaisana N, et al. suggested that well-defined CuO nanoparticles are generated by a sonochemical synthesis with ultrasound help, with a reaction duration of up to 30 minutes and pyrolysis at 600-700 °C <sup>[225]</sup>. CuO nanoparticles with a rectangular form and a monoclinic structure were generated by an aqueous precipitation technique, according to Lange AS, et al <sup>[226]</sup>.

H. Zhu et al. suggested a wet chemical approach for the large-scale production of stable CuO nanofluids <sup>[227]</sup>. Mousa MK suggested a rapid, economical, and simple method of precipitation with temperature control at 65, 75, and 85 ° C. The size of nanoparticles reduces as the temperature increases <sup>[228]</sup>. The latest research reports on the new production of Copper and Copper oxide nanoparticles utilizing the chemical reduction approach, as well as their physicochemical characterization according to Karthik AD et.al <sup>[229]</sup>.

Copper materials are synthesized first and then oxidized to copper oxide. UV-visible spectroscopy, Fourier transform infrared spectroscopy (FTIR), X-ray diffraction measurements (XRD), and scanning electron microscopy (SEM) were used to characterize the nanoparticles, according to the researchers. S. Srivastava and co-workers reported the

chemical approach was used to synthesize cupric oxide (CuO) nanoparticles, which involved calcination at temperatures ranging from 300 to 400 ° C <sup>[230]</sup>. K. Phiwdanga et al. CuO nanoparticles were produced using a precipitation approach with different precursors such as copper nitrate (Cu (NO<sub>3</sub>)<sub>2</sub>) and copper chloride (CuCl<sub>2</sub>), and post-heating was used to compare the as-synthesized and after-calcination of CuO nanoparticles <sup>[231]</sup>. Thermal decomposition was used to generate spherical CuO nanoparticles with a mean diameter of 170 nm as reported by Darezereshki E, et al <sup>[232]</sup>. This process does not necessitate the use of organic solvents, costly raw materials, or sophisticated machinery. As a result, the given process to produce CuO nanoparticles from dilute CuSO<sub>4</sub> solution is better than the other methods. Cu nanoparticles (CuNPs) were made using a simple chemical reduction method at ambient temperature, with sodium borohydride and polyvinylpyrrolidone, the Cu<sup>2+</sup> ions were lowered and stabilized, respectively as reported by Aguilar et.al <sup>[233]</sup>. Chatterjee et al. proposed a straightforward approach for the manufacture of metallic copper nanoparticles with a size of 50-60 nm utilizing Cucl<sub>2</sub> as a reducing agent and gelatin as a stabilizer <sup>[234]</sup>. Copper nanoparticles were made by reducing aqueous copper chloride solution with NaBH<sub>4</sub> in non-ionic water-in-oil (w/o) microemulsions <sup>[235]</sup>. To generate copper nanoparticles, chemical methods such as chemical reduction, photochemical, electrochemical, and thermal decomposition are used, with the chemical reduction being the most used method for the creation of stable, colloidal dispersions in organic solvents <sup>[236]</sup>. Chemical reduction is the most practical way for fabricating nanoparticles out of all the methods. The chemical reduction process yielded a high yield of metallic nanoparticles. By manipulating the experimental conditions, this method is cost-effective, simple, and speedier, and it may produce a superior size distribution of nanoparticles <sup>[237]</sup>. Copper nanoparticles were generated by chemically reducing copper sulfate with sodium borohydride in water without the use of inert gas. During the synthesis process and during

storage, ascorbic acid was used as a protective agent to prevent the nascent Cu nanoparticles from oxidation. The use of polyethylene glycol served as a size controller as well as a capping agent. Under inert argon-purged conditions, copper nanoparticles were successfully produced by borohydride reduction of copper nitrate salt in a water/CH<sub>3</sub>CN mixed solvent. For the first time, Cu nanoparticles were generated in large-scale production by injecting CH<sub>3</sub>CN into the water and preventing oxidation throughout the nanoparticle preparation [238].

### **1.14.3. Silver nanoparticles**

Metal nanoparticles can be synthesized in a variety of ways, including physical and chemical processes. Even though physical methods can make nanoparticles, the literature is full of data on chemical approaches. The reduction of metal ions in solution is the most common chemical technique (chemical reduction method) [239]. The polyol technique [240] and the liquid-liquid method [241] are two chemical methods for the manufacture of silver nanoparticles that have been developed in recent years. Chemical reduction, on the other hand, is the most widely used method due to its simplicity. Examples of bottom-up methods include metal reduction, electrochemical processes, and decomposition. Silver nanoparticles are fascinating because of their unique features, which can be used in antibacterial applications, biosensor materials, composite fibres, cryogenic superconducting materials, cosmetics, and electronic components. Silver NPs have been synthesized and stabilized using a variety of physical and chemical processes [242, 243]. Chemical reduction with organic and inorganic reducing chemicals is the most frequent method for producing silver NPs. For the reduction of silver ions (Ag<sup>+</sup>) in aqueous or non-aqueous solutions, several reducing agents such as sodium citrate, ascorbate, sodium borohydride (NaBH<sub>4</sub>), elemental hydrogen, polyol process, Tollen's reagent, N, N-dimethylformamide (DMF), and poly (ethylene glycol)-block copolymers are utilized [244].

In nanoparticle synthesis, it is necessary to observe nanosilver content, size, shape, surface charge, crystal structure, surface chemistry, and surface change. Ojha et al. combined  $\text{AgNO}_3$  and citrate in a solution and added  $\text{NaOH}$  to it. Then, while stirring, an ice-cold  $\text{NaBH}_4$  solution was added [245]. The aqueous solution containing  $\text{AgNO}_3$  was made by Ajitha et al. with sodium citrate dihydrate as a stabilizer. Then, while vigorously stirring, a solution of sodium borohydride (a reducing agent) was added into the above solution all at once. The color of the solution was lightened [246]. Gebeyehu et al. used a simple polyol technique to make silver nanowire. Polyvinylpyrrolidone was utilized as a stabilizing and capping agent, along with sodium chloride and potassium bromide salts, ethylene glycol as a solvent and reducing agent, and silver nitrate as a silver precursor [247]. The reduction of silver nitrate with ethylene glycol in the presence of polyvinylpyrrolidone resulted in cubic silver nanoparticles (PVP). Ethylene glycol with hydroxyl groups serves as both a solvent and a reducing agent in the polyol process. The cubic form was developed using polyvinylpyrrolidone as a capping agent [248-250]. By adding a trace quantity of sodium sulfide ( $\text{Na}_2\text{S}$ ) or sodium hydrosulfide ( $\text{NaHS}$ ) to the traditional polyol synthesis, Siekkien et al. achieved a quicker approach to produce cubic silver nanoparticles. For the synthesis of NPs with various chemical compositions, sizes, and morphologies, as well as regulated disparities, the reduction agent is critical [251]. Sun et al. investigated how reaction circumstances, such as the ratio of PVP to silver nitrate, reaction temperature, and seeding conditions, may change the shape of silver nanostructures, ranging from nanoparticles to nanorods to long nanowires. They discovered that silver nanowires with diameters ranging from 30 to 40 nm and lengths up to 50 m could be synthesized on a huge scale [252]. For the manufacture of silver nanoprisms, Métraux and Mirkin used the chemical reduction process. They used a reagent mixture of  $\text{AgNO}_3 / \text{NaBH}_4 / \text{polyvinylpyrrolidone} / \text{trisodium citrate} / \text{H}_2\text{O}_2$  in an aqueous solution to make silver nanoprisms at room temperature [253].

Silver nanoparticles have attracted a lot of attention in recent years due to their good conductivity, chemical stability, use as catalysts <sup>[254]</sup> and applications in a variety of industries (e.g., medical sciences to prevent the HIV virus, food industries as anti-bacterial agents in food packaging <sup>[255]</sup>, anti-bacterial properties) <sup>[256]</sup>, as well as their unique electrical and optical properties <sup>[257, 258]</sup>. The antibacterial action of silver ions and silver nanoparticles is related to morphological and structural changes in the bacterial cell, according to research <sup>[259, 260]</sup>.

#### **1.14.4. Cadmium nanoparticles:**

Cadmium Sulfide Nanoparticles (CdS. nps) confirmed the bulk-sized material's distinct physical, chemical, and structural features. Cadmium Sulfide NPs are employed in everyday life because of their distinctive melting point, crystal arrangement, bandgap energy, optoelectronic absorption spectra, high stability, availability, and ease of manufacture and handling. The atomic distribution over the nanoparticle shell, in addition to the surface/volume ratio, has a significant effect on semiconductivity<sup>[261]</sup>.

Due to advantages in several areas, CdS NPs have been industrially developed. Chemical precipitation <sup>[262]</sup>, Chemical Vapor Deposition <sup>[263]</sup>, laser ablation <sup>[264]</sup>, physical evaporation <sup>[265]</sup>, template synthesis <sup>[266]</sup>, thermal evaporation <sup>[267]</sup>, hydrothermal synthesis <sup>[268]</sup>, pulsed laser deposition <sup>[269]</sup>, solvothermal <sup>[270]</sup>, and biosynthesis using bacteria, fungi, yeast, and plants <sup>[271]</sup> and Electrodeposition <sup>[272]</sup> have all been used to create nano-forms of CdS films or powder.

Chemical precipitation is commonly used since it requires ambient environmental conditions, simple lab equipment, and consistent findings, as opposed to other procedures that require extreme environmental conditions, sophisticated equipment, and are time-consuming. Limiting the reaction area with capping agents such as EDTA, long-chain alkyl xanthates, mercaptoacetic acid, phosphates, phosphine oxides, thioglycerol, thiols, and



thiourea<sup>[273]</sup> controls the stability and size of CdS NPs. Chemical precipitation of cadmium sulfide (CdS) nanoparticles was carried out using cadmium chloride (CdCl<sub>2</sub>), sodium sulfide (Na<sub>2</sub>S), and water as a solvent at temperatures ranging from 20 to 80 degrees Celsius<sup>[274]</sup>.

CdS NPs were formed by adding aqueous CdCl<sub>2</sub>, KOH, NH<sub>4</sub>NO<sub>3</sub>, and CS(NH<sub>2</sub>)<sub>2</sub> for 30 minutes at pH 10, temperature 80°C, and centrifugation at 6000 rpm for 1 hour<sup>[275]</sup>. Chemical precipitation of deionized aqueous CdCl<sub>2</sub> and thiourea solution with continuous stirring at 100 °C for 15 hours yielded CdS NPs. As a capping agent, ammonia was used by R.Gupta<sup>[276]</sup>. M.M.Kamble & co. developed Cadmium sulfide nanocrystals with oleylamine as the solvent, surfactant, and capping ligand by using the Hot Injection Method<sup>[277]</sup>.

#### **1.14.5. Mercury Nanoparticles**

Mercury is one of the few metal elements that may exist as liquids in nature under normal conditions, posing a challenge to material scientists to learn more about Hg nanoparticles (NPs)<sup>[278]</sup>. Nanoparticles have properties that differ from bulk materials, and they frequently lead to significant technological applications<sup>[279-283]</sup>. Alireza et al. proposed an innovative processing method for manufacturing HgO nanoparticles by solid-state thermal decomposition of mercury (II) acetate nanostructures generated by sublimation at 150 °C for 2 hours<sup>[284]</sup>. Using ultrasonication under ambient conditions, V.K.Harika et al. proposed a simple synthetic technique for producing very stable crystalline mercury nanoparticles supported on solid carbon sources such as reduced graphene oxide, graphene, graphite oxide, graphite, and others<sup>[285]</sup>. Avik. J.G generated oxidized mercury nanoparticles using two methods i.e., vapor-phase condensation and aqueous nebulization using three basic chemicals like mercury (II) bromide, mercury (II) chloride, and mercury (II) oxide<sup>[286]</sup>. Synthesizing nano-sized β-HgS particles in a practical and simple manner remains a

difficulty. A lot of established methods such as chemical deposition <sup>[287]</sup>, photochemical <sup>[288]</sup>, wet chemical <sup>[289]</sup>, and electrochemical <sup>[290]</sup> have been used for the synthesis of Hg nanoparticles. At room temperature, nanocrystals are synthesized via sonication and nitrogen purging by Xin Xiu et.al. Surfactants and stabilizing ligands were not employed in the analyses of the NPs to avoid changing their chemical and toxicological behavior <sup>[291]</sup>. For the first time, Mercury Cadmium Telluride (MCT) nanoparticles are synthesized by R.R. Arnepelli using the Solvothermal technique. In the Teflon-Stainless-Steel autoclave, Mercury, Cadmium, and Tellurium in compound/elemental form were added to Ethylenediamine (solvent) together with a reducing agent <sup>[292]</sup>.

A new type of base fluid known as Deep Eutectic Solvents (DESs) is proposed in this work, which is generated by mixing solid substances that turn liquid under specified conditions, offering another option to utilizing traditional organic solvents. At room temperature, many of these combinations are liquids. Since their discovery, these deep eutectic solvents have been the subject of significant research. Because of sharing many characteristics and properties with ionic liquids (e.g., similar conductivities, polarities, viscosities, densities, surface tensions, refractive indexes, chemical inertness, etc.) deep eutectic solvents (DESs) are now commonly recognized as a new family of Ionic liquids (IL) substitutes. They are typically affordable due to the comparatively inexpensive components and their straightforward synthesis, which produces little waste and requires no additional purifying procedures. In addition, the components of DESs are frequently biodegradable and non-toxic.

The first part of this research focused on the synthesis of six novel Binary DESs using Malonic acid (MA), Zinc chloride (ZC) with Glucose (GLU), Fructose (FRU), Lactic acid (LA), and Glycerol (GLY) followed by measuring the physical properties like Density, pH, Conductivity, Viscosity, and Fourier Transform Infra-Red absorptions.

The second part of this research focused on the synthesis of six novel Malonic acid-based ternary DESs, six Zinc chloride-based ternary DESs, six Manganese chloride (MC) based ternary DESs with sugars (Glucose and Fructose), and Amino acids (Glutamine, Histidine, and Glycine). These solvents are also measured by physical properties like Density, pH, Conductivity, Viscosity, and Fourier Transform Infrared absorptions.

Nanoscale structures have sparked a lot of interest in the research world, making them a good intermediate between large size and atomic/molecular formations. The third part of the research deals with the synthesis of nanoparticles (NPs) like Copper, Cadmium, Mercury, and silver using the above synthesized Malonic acid with Glucose and Fructose binary DESs. This research is continued by the synthesis of Copper and Silver Nanoparticles using Zinc chloride with Glucose and Fructose binary DESs. They were prepared via chemical reduction and co-precipitation method and the synthesized nanoparticles were characterized by Scanning Electron Microscopy (SEM), Ultraviolet Spectroscopy (UV), and Fourier Transform Infrared absorptions (FTIR), X-Ray Diffraction Pattern (XRD), and Energy Dispersive X-ray Analysis (EDAX) techniques.

The next part of the work focused on the synthesis of Nanoparticles like Copper and silver nanoparticles using the above synthesized ternary DESs. They were prepared via chemical reduction and co-precipitation method and the synthesized nanoparticles were characterized by the techniques followed for the binary DESs based nanoparticles.

The final part of the research deals with the application of Copper Nanoparticles in Malonic acid based binary DESs to determine the anti-microbial activity by using the Disc Diffusion method.



### **1.15. AIM, SCOPE, AND OBJECTIVES OF THE PRESENT WORK**

The aim of the present study is to develop an eco-friendly a better alternative solvent. It should be cheap, harmless, bio-degradable and it should be highly stable even at high temperatures. The work proposes a new form of base liquid known as Deep Eutectic Solvents (DESs) as a viable replacement for conventional base fluid due to their unique solvent properties. Using the newly developed DESs, metal nanoparticles are synthesized and to study the antimicrobial activities.

The objectives of the present work are

- To use an efficient method to develop DESs
- To find the cost-effective, cheaper, and low-cost method.
- To synthesize less toxic, most usable metal nanoparticles.
- To find any one application of the synthesized nanoparticles.

The implication of this study was the preparation of newer Malonic acid (MA), Zinc chloride (ZC), Manganese chloride (MC) based BDES, and TDES. The physicochemical parameters such as viscosity, conductivity, pH, density were measured for the prepared BDESs and TDESs. To find out whether they depict the nature, characteristics, and features of DES to substitute as the common solvents.

The peak of this research was the synthesis of metal nanoparticles like Copper, Cadmium, Mercury, Silver using chemical reduction methods in presence of deep eutectic solvents which were eliminating surfactants or seeds for the preparation of nanomaterials and also by achieving less toxic, bio-degradable, fewer by-products. Then, the study was extended to characterize the nanoparticles by Scanning Electron Microscopy (SEM), Ultraviolet Spectroscopy (UV), Fourier Transform Infrared absorptions (FTIR), X-Ray Diffraction patterns (XRD), and Energy Dispersive X-ray Analysis (EDAX) techniques. We have studied the antimicrobial activities of some nanoparticles.

Chapter 1 deals with the introduction about the deep eutectic solvents and their applications, metal nanoparticles and their applications, also include a literature review.

Chapter 2 explains the experimental procedures and the instrumentations for the study.

Chapter 3 explains the preparation, characterization studies of Malonic acid-based binary Deep Eutectic Solvents.

Chapter 4 explains the preparation, characterization studies of Zinc chloride-based binary Deep Eutectic Solvents.

Chapter 5 explains the preparation, characterization studies of Malonic acid-based ternary Deep Eutectic Solvents.

Chapter 6 explains the preparation, characterization studies of Zinc chloride-based ternary Deep Eutectic Solvents.

Chapter 7 explains the preparation, characterization studies of Manganese chloride-based binary Deep Eutectic Solvents.

Chapter 8 deals with the synthesis of copper, silver, cadmium, and mercury nanoparticles in binary deep eutectic solvents and the characterization studies of the nanoparticles.

Chapter 9 deals with the synthesis of copper and silver nanoparticles in ternary deep eutectic solvents and the characterization studies of the nanoparticles.

Chapter 10 explains the antimicrobial studies of some nanoparticles.

Chapter 11 highlights the summary and conclusion of the investigations of the present study.

## REFERENCES

- [1]. J.P. Hallett and T. Welton, *Chem. Rev.*, 2011, 111, 3 08-3 76; P. Wasserscheid and W. Keim, *Angew. Chem., Int, Ed.*, 2000, 39,3772-3789; (b) H. Wang, G. Gurau and R.D. Rogers, *Chem. Soc.Rev.*, 2012, 41,1 19-1 37.
- [2]. D. A. Walsh, K. R. J. Lovelock and P. Licence, *Chem. Soc. Rev.*, 2010,39,418 -4194; *Electrodeposition from Ionic Liquids*, ed. F. Endres, D. MacFarlane and A. Abbott, Wiley-VCH,2008.
- [3]. (a) J. Dupont and J.D. Scholten, *Chem. Soc. Rev.*, 2010, 39, 1780-1804; (b) J. L. Bideau, L. Viau and A. Vioux, *Chem. Soc. Rev.*, 2011,40, 907-92.
- [4]. R. Rogers, K. Seddon, and S. Volkov, *Green Industrial Applications of Ionic Liquids*, ed. Springer, 2003.
- [5] P. Wasserschild, T. Welton, *Ionic Liquids in Synthesis*, Wiley-VCH, Weinheim, 2003  
<https://doi.org/10.1021/op0340210>.
- [6] M. A. Kareem, F. S. Mjalli, M.A. Hashim, I. M. Alnashef, Phosphonium-based ionic liquids analogues and their physical properties, *J. Chem. Eng. Data* 55 (2010) 4632 – 4637.  
<https://doi.org/10.1021/je100104v>.
- [7] J. Sun, M. Forsyth, D. R. Mac Farlene, Room-temperature molten salts based on the quaternary ammonium ion, *J. Phys. Chem. B* 102 (1998) 8858 –8864.  
<https://doi.org/10.1021/jp981159p>.
- [8] S. J. Zhang, Y. H. Chen, R. X. F. Ren, et al., Solubility of CO<sub>2</sub> in sulfonate ionic liquids at high pressure, *J. Chem. Eng. Data* 50 (2005) 230 – 233.  
<https://doi.org/10.1021/je0497193>.
- [9] A. Paiva, R. Craveiro, I. Aroso, et al., Natural deep eutectic solvents-solvents for the 21st century, *ACS Sust. Chem. Eng.* 2 (2014) 1063– 1071.  
<https://doi.org/10.1021/sc500096j>.

- [10] C. M. Wang, X. Y. Luo, X. Zhu, et al., The strategies for improving carbon dioxide chemisorption by functionalized ionic liquids, *RSC Adv.* 3 (2013) 15518 – 15527. <https://doi.org/10.1039/c3ra42366b>.
- [11] M. A. Navarra, J. Manzi, L. Lombardo, S. Panero, B. Scrosati, Ionic liquid-based membranes as electrolytes for advanced lithium polymer batteries, *Chem- Sus Chem* 4 (2011) 125 – 130. <https://doi.org/10.1002/cssc.201000254>.
- [12] X. Ge, C.D. Gu, Y. Lu, X.L. Wang, J.P. Tu, A Versatile protocol for the ionothermal synthesis of nanostructured nickel compounds as energy storage materials from a choline chloride-based ionic liquid, *J. Mater. Chem. A* 1 (2013) 13454 – 13461. <https://doi.org/10.1039/C3TA13303F>.
- [13] M. Hayyan, F. S. Mjalli, M. A. Hashim, I. M. Alnashef, X. M. Tan, Electrochemical reduction of dioxygen in bis (trifluoromethylsulfonyl) imide based Ionic liquids, *J. Electroanal. Chem.* 657 (2011) 150 – 157. doi: 10.1016/j.jelechem.2011.04.008.
- [14] P. D. de Maña, Z. Maugeri, Ionic liquids in biotransformations: from proof-of-concept to emerging deep-eutectic-solvents, *Curr. Opin. Chem. Biol.* 15 (2011) 220 – 225. DOI: 10.1016/j.cbpa.2010.11.008.
- [15] N. V. Plechkova, K. R. Seddon, Applications of ionic liquids in the chemical industry, *Chem. Soc. Rev.* 37 (2008) 123 – 150. <https://doi:10.1039/B006677J>.
- [16] C. Rub, B. König, Low melting mixtures in organic synthesis-an alternative to ionic liquids, *Green Chem.* 14 (2012) 2969 – 2982. <https://doi.org/10.1039/C2GC36005E>.
- [17] X. Ge, C.D. Gu, X. L. Wang, J. P. Tu, Endowing manganese oxide with fast adsorption ability through controlling the manganese carbonate precursor assembled in ionic liquid, *J. Colloid Interface Sci.* 438 (2015) 149 – 158. <https://doi.org/10.1016/j.jcis.2014.09.029>.
- [18]. (a) M. J. Earle, S. P. Kaydare and K.R. Seddon, *Org. Lett.*, 2004,6,707-710; (b) Q.zhang, S. Zhang, S. Zhang and Y. Deng, *Green Chem.*, 2011, 13 , 2619-2637.



- [19]. (a) A. Romero, A. Santos, J. Tojo and A. Rodriguez, *J. Hazard. Mater.*, 2008, 268-273; (b) N. V. Plechkova and K. R. Seddo, *Chem. Soc. Rev.*, 2008, 37, 123-10.
- [20]. Qinghua Zhang, Karine De Oliveira Vigier, Sebastien Royer and Francois Jerome, Deep Eutectic solvents: synthesis, properties and applications, *Chem. Soc. Rev.* 2012, DOI:10.1039/c2cs3178a.
- [21]. Y. Yu, X. Lu, Q. Zhou, K. Dong, H. Yao and S. Zhang, *Chem-Eur. J.*, 2008, 14, 11174-11182.
- [22]. K. D. Weaver, H.J. Kim, J. Sun, D. R. MacFarlane and G. D. Elliott, *Green Chem.*, 2010, 12, 07-13.
- [23]. F. Ilegan, D. Ott, D. Kralish, C. Reil, A. Palmberger and B. König, *Green chem.*, 2009, 11, 1948-1954.
- [24]. D. Reinhardt, F. Ilegan, D. Kralisch, B. König and D. Kralish, *Green chem.*, 2008, 10, 1170-1181.
- [25]. E. R. Cooper, C. D. Andrews, P. S. Wheatley, P. B. Webb, P. Wormald and R. E. Morris, Ionic liquids and eutectic mixtures as solvent and template in synthesis of zeolite analogues, *Nature*, 2004, 430, 1012–1016.
- [26]. Daniel Carriazo, Mari´a Concepcio´n Serrano, Mari´a Concepcio´n Gutie´rrez, Mari´a Luisa Ferrer and Francisco del Monte, Deep-eutectic solvents playing multiple roles in the synthesis of polymers and related materials, *Chem. Soc. Rev.*, 2012, 41, 4996–5014 DOI: 10.1039/c2cs15353j.
- [27]. A. P. Abbott, J. C. Barron, K. S. Ryder and D. Wilson, *Chem-Eur. J.*, 2007, 13, 649-661.
- [28] M. Francisco, A. van den Bruinhorst, M. C. Kroon, Low-Temperature-Temperature Mixtures (LTTMs): a new generation of designer solvents, *Angew. Chem. Int. Ed.* 52 (2013) 3074 – 3085. <https://doi.org/10.1002/anie.201207548>.

- [29]. A. P. Abbott, G. Capper and S. Gray, *ChemPhysChem*, 2006, 7, 803-806.
- [30]. A. P. Abbott, D. Boopathy, G. Capper, D. L. Davies and R. K. Rasheed, *J. Am. Chem. Soc.*, 2004, 126, 9142-9147.
- [31]. W. Li, Z. Zhang, B. Han, S. Hu, J. Song, Y. Xie and X. Zhou, *Green Chem.*, 2008, 10, 1142-114.
- [32] Emma L. Smith; Andrew P. Abbott; Karl S. Ryder (2014). "Deep Eutectic Solvents (DESs) and their applications". *Chemical Reviews*. 114 (21): 11060–11082. doi:10.1021/cr300162p. PMID 25300631.
- [33] "Deep Eutectic Solvents" (PDF). *kuleuven.be*. The University of Leicester. Retrieved 17 June 2014.
- [34] Andrew P. Abbott; Glen Capper; David L. Davies; Raymond K. Rasheed; Vasuki Tambyrajah (2003). "Novel solvent properties of choline chloride/urea mixtures". *Chem. Commun.* 0 (1): 70–71. doi:10.1039/B210714G.
- [35] Andrew Abbott; John Barron; Karl Ryder; David Wilson (2007). "Eutectic-Based Ionic Liquids with Metal-Containing Anions and Cations". *Chem. Eur. J.* 13 (22): 6495–6501. doi:10.1002/chem.200601738.
- [36] Mukhtar A. Kareem; Farouq S. Mjalli; Mohd Ali Hashim; Inas M. AlNashef (2010). "Phosphonium-Based Ionic Liquids Analogues and Their Physical Properties". *Journal of Chemical & Engineering Data*. 55 (11): 4632–4637. doi:10.1021/je100104v.
- [37] Clarke, Coby J.; Tu, Wei-Chien; Levers, Oliver; Bröhl, Andreas; Hallett, Jason P. (2018-01-24). "Green and Sustainable Solvents in Chemical Processes". *Chemical Reviews*. 118(2): 747–800. DOI: 10.1021/acs.chem rev.7b00571.
- [38] Lucía Abad-Gil; "Binary and ternary deep eutectic solvent mixtures: Influence on methylene blue electropolymerization"; *Electrochemistry Communications* Volume 124, March 2021, 106967.

- [39] Xu, G.; Ding, J.; Han, R.; Dong, J.; Ni, Y. Enhancing cellulose accessibility of corn stover by deep eutectic solvent pretreatment for butanol fermentation. *Bioresour. Technol.* 2016, 203, 364–369.
- [40] Xia, S.; Baker, G.A.; Li, H.; Ravular, S.; Zhao, H. Aqueous ionic liquids and deep eutectic solvents for cellulosic biomass pretreatment and saccharification. *RSC Adv.* 2014, 4, 10586–10596.
- [41] Procentese, A.; Raganati, F.; Olivieri, G.; Elena, M.; Rehmann, L.; Marzocchella, A. Low-Energy biomass pretreatment with deep eutectic solvents for bio-butanol production. *Bioresour. Technol.* 2017, 243, 464–473.
- [42] Zhang, C.W.; Xia, S.Q.; Ma, P.S. Facile pretreatment of lignocellulosic biomass using deep eutectic solvents. *Bioresour. Technol.* 2016, 219, 1–5.
- [43] Alhassan, Y.; Pali, H.S.; Kumar, N.; Bugaje, I.M. Co-Liquefaction of whole *Jatropha curcas* seed and glycerol using deep eutectic solvents as catalysts. *Energy* 2017, 138, 48–59.
- [44] Alhassan, Y.; Kumar, N.; Bugaje, I.M. Hydrothermal liquefaction of de-oiled *Jatropha curcas* cake using deep eutectic solvents (DESS) as catalysts and co-solvents. *Bioresour. Technol.* 2016, 199, 375–381.
- [45] Cao, Q.; Li, J.; Xia, Y.; Li, W.; Luo, S.; Ma, C.; Liu, S. Green extraction of six phenolic compounds from rattan (*calamoideae faberii*) with deep eutectic solvent by a homogenate-assisted vacuum-cavitation method. *Molecules* 2019, 24, 113.
- [46] Dwan, J.; Durant, D.; Ghandi, K.; Warsaw, V.; Heidelberg, S.B. Nuclear magnetic resonance spectroscopic studies of the trihexyl (tetradecyl) phosphonium chloride ionic liquid mixtures with water. *Cent. Eur. J.Chem.* 2008, 6, 347–358.
- [47] Lan, D.; Wang, X.; Zhou, P.; Hollmann, F.; Wang, Y. Deep eutectic solvents as performance additives in biphasic reactions. *RSC Adv.* 2017, 7, 40367–40370.

- [48] Tang, B.; Park, H.E.; Row, K.H. Simultaneous extraction of flavonoids from *chamaecyparis obtusa* using deep eutectic solvents as additives of conventional extractions solvents.
- [49] Yu-TingLiu et.al. Synthesis and characterization of novel ternary deep eutectic solvents, *Chinese Chemical Letters* Volume 25, Issue 1, January 2014, pp 104-106.
- [50] Parker J. Smith, Crystal B. Arroyo, Felipe Lopez Hernandez; Ternary Deep Eutectic Solvent behavior of Water and Urea–Choline Chloride Mixtures; *J. Phys. Chem. B* 2019, 123, 25, pp 5302–5306
- [51] Jing Wang and Sheila N. Baker; Pyrrolidinium salt-based binary and ternary deep eutectic solvents: green preparations and physiochemical property characterizations; *De Gruyter; Green Process Synth* 2018; 7: 353–359
- [52] ZhuChen, William A. Jacoby, Caixia Wan; Ternary deep eutectic solvents for effective biomass deconstruction at high solids and low enzyme loading; *Bioresource Technology* Volume 279, May 2019, Pages 281-286.
- [53] Mohammed A. Kadhom, Studying Two Series of Ternary Deep Eutectic Solvents (Choline Chloride–Urea–Glycerol) and (Choline Chloride–Malic Acid–Glycerol), Synthesis and Characterizations; *Arabian journal for science and engineering*;42, pages1579–1589(2017)
- [54] Yu-hui Chi et al. New ternary deep eutectic solvents for effective wheat straw deconstruction into its high-value utilization under near-neutral conditions; *Royal Society of Chemistry; Green chemistry*; Issue 24,2020
- [55] Weiyang Tang.et al.; Evaluating ternary deep eutectic solvents as novel media for extraction of flavonoids from *Ginkgo biloba*; *Tylor & Francis online; Separation Science and Technology*; Volume 52, 2017-Issue 1

- [56]. Fatemeh Sm Ghareh Bagh, Kavehshahbaz, Farouq S. Mjallli, Mohd A. Hashim, Inas M. AINashef; Zinc (II) chloride-based deep eutectic solvents for application as electrolytes: preparation and characterization *Journal of Molecular Liquids*, 2015.
- [57]. Zhang, Q., Vigier, K., Se´bastien Royer, S., Jerome, F. (2012). Deep eutectic solvents: syntheses, properties and applications. In *Chem. Soc. Rev.* Vol: 41 pp. (7108–7146).
- [58]. Tripti Kumari, Ritika Chauhana, Neha Sharmaa, Kohinoor Kaurb, Aparna Krishnamurthy, Priya Pandey, Shivangi Aggarwal. (2016). Zinc Chloride as Acetamide based Deep Eutectic Solvent. *DU Journal of Undergraduate Research and Innovation* Volume 2, Issue 1 pp 203- 210.
- [59] Shu Hong et.al., Choline chloride-zinc chloride deep eutectic solvent-mediated preparation of partial O-acetylation of chitin nanocrystal in one-step reaction. *Carbohydrate Polymers*, Sep 15; volume 220 pp 211-218, (2019) DOI: 10.1016/j.carbpol.2019.05.075.
- [60] Lian, H. Hong, S. Carranza, A. Mota-Morales, J. D. Pojman, J. A., Processing of lignin in urea–zinc chloride deep-eutectic solvent and its use as a filler in a phenol-formaldehyde resin.; *RSC Adv.*,2015, 5, 28778-28785 (2016) DOI: 10.1039/C4RA16734A
- [61] Abbott A.P., Capper G., Davies D.L., Rasheed R.K., Tambyrajah V., Quaternary ammonium zinc-or tin-containing ionic liquids: water insensitive, recyclable catalysts for Diels–Alder reactions. *Green Chem.*, 2002, 4, 24-26.
- [62] Morales R.C., Tambyrajah V., Jenkins P.R., Davies D.L., Abbott A.P., The regiospecific Fischer indole reaction in choline chloride·2ZnCl<sub>2</sub> with product isolation by direct sublimation from the ionic liquid. *Chem. Commun.*, 2004, 2, 158-159.
- [63] Sunitha S., Kanjilal S., Reddy P.S., Prasad R.B.N., Liquid-liquid biphasic synthesis of long-chain wax esters using the Lewis acidic ionic liquid choline chloride-ZnCl<sub>2</sub> *Tetrahedron Lett.*, 2007, 48, 6962-6965.

- [64] Abbott A.P., Bell T.J., Handa S., Stoddart B., O-Acetylation of cellulose and monosaccharides using a zinc-based ionic liquid. *Green Chem.*, 2005, 7, 705-707.
- [65] Duan Z., Gu Y., Deng Y., Green and moisture-stable Lewis acidic ionic liquids (choline chloride: ZnCl<sub>2</sub>) catalyzed the protection of carbonyls at room temperature under solvent-free conditions. *Catal. Commun.*, 2006, 7, 651-656.
- [66] Patil U.B., Singh A.S., Nagarkar J.M., Choline chloride-based eutectic solvent: an efficient and reusable solvent system for the synthesis of primary amides from aldehydes and from nitriles. *RSC Adv.*, 2014, 4, 1102-1106.
- [67] Swapnil A. Padvi et.al., Choline chloride–ZnCl<sub>2</sub>: Recyclable and efficient deep eutectic solvent for the [2+3] cycloaddition reaction of organic nitriles with sodium azide; *An International Journal for Rapid Communication of Synthetic Organic Chemistry*; Vol 47; Issue 8; pp 779-787.
- [68] Yu-Ting Liu, Yan-A Chen, Yan-Jun Xing; Synthesis and characterization of novel ternary deep eutectic solvents[J]. *Chin. Chem. Lett.*, 2014,25(01): 104-106
- [69] Lin, Y.-F.; Sun, I. W. *Electrochim. Acta* 1999, 44, 277
- [70] Morales, R. C.; Tambyrajah, V.; Jenkins, P. R.; Davies, D. L.; Abbott, A. *Chem. Commun.* 2004, 158
- [71] Abbott, A. P.; Capper, G.; Davies, D. L.; Rasheed, R.; Tambyrajah, V. *Green Chem.* 2002, 4, 24
- [72] Biswas, A.; Shogren, R. L.; Stevenson, D. G.; Willett, J. L.; Bhowmik, P. K. *Carbohydr. Polym.* 2006, 66, 546
- [73] Ayşe Ezgi Ünlü et.al., Use of deep eutectic solvents as a catalyst: A mini-review, *Green Process Synth* 2019; 8: 355–372

- [74] Tran P.H., Nguyen H.T., Hansen P.E., Le T.N., An efficient and green method for regio-and chemo-selective Friedel–Crafts acylations using a deep eutectic solvent ([CholineCl] [ZnCl<sub>2</sub>] 3). *RSC Adv.*, 2016, 6, 37031-37038.
- [75] Hai-Chuan-Hu, Deep eutectic solvent based on choline chloride and malonic acid as an efficient and reusable catalytic system for one-pot synthesis of functionalized pyrroles, *RSC Advances*, Issue 10,2015.
- [76] Kroon, M.C.; Binnemans, K. Degradation of deep-eutectic solvents based on choline chloride and carboxylic acids. *ACS Sustain. Chem. Eng.* 2019, 7, 11521–11528.
- [77] Iman Al-Wahaibi et al., The novel use of malonic acid-based deep eutectic solvents for enhancing heavy oil recovery; *International Journal of Oil, Gas and Coal Technology*, 2019 Vol.20 No.1, pp.31 – 54; DOI: 10.1504/IJOGCT.2019.096493.
- [78] Gunny, A. A. N.; Arbain, D.; Nashef, E. M.; Jamal, P.; *Bioresour. Technol.* 2015, 181, 297.
- [79] Koon Kee Kow et al., Novel manganese (II)-based deep eutectic solvents: Synthesis and physical properties analysis; *CCL* 26(10)2015; DOI: 10.1016/j.ccllet.2015.05.049
- [80] Xiaochen Lai et.al., Synthesis of mesoporous  $\alpha$ -MnO<sub>2</sub> in manganese (II)-based deep eutectic solvent and their application in the absorption of Congo red; *Separation Science and Technology*; Vol 54,2019,8, pp 1269-1277.
- [81] Adeeb Hayyan et al., Glucose-based deep eutectic solvents: Physical properties; *Journal of Molecular Liquids*; Volume 178, February 2013, Pages 137-141; <https://doi.org/10.1016/j.molliq.2012.11.025>
- [82] Fernando Bergua et al., Structure and properties of two glucose-based deep eutectic systems; *Food Chemistry*; Volume 336; 2021, 127717; <https://doi.org/10.1016/j.foodchem.2020.127717>

- [83] Zi –Liang Liu et al., Sugar-based natural deep eutectic solvents as potential absorbents for NH<sub>3</sub> capture at elevated temperatures and reduced pressures; *Journal of Molecular Liquids*; Vol 317, 2020, 113992.
- [84] I.M. AlNashef et al., Method for separating Glucose and Fructose, US patent, 0283093A1,2009
- [85] Liam Vanden Elzen et.al., Monosaccharide-Based Deep Eutectic Solvents for Developing Circularly Polarized Luminescent Materials; *ACS Sustainable Chem.Engg.*2019,7, pp 16690-16697
- [86] Rajiv Kohli, Chapter 16 - Applications of Ionic Liquids in Removal of Surface Contaminants; *Developments in Surface Contamination and Cleaning: Applications of Cleaning Techniques*; Vol 11 2019, pp 619-680.
- [87] Aydin K.Sunol, Tiziana Fornari, in handbook of solvents ( 3rd edition), Chapter 20- Substitution of solvents by safer products; *ChemTec Publishing*, Vol 2, Use, Health and Environment,2019, pp 1455-1634.
- [88] Haerens, K.; Matthijs, E.; Chmielarz, A.; Van der Bruggen, B. J. *Environ. Manage.* 2009, 90, 3245
- [89] Angeles et al., Chapter 5 - Nanocellulose for Industrial Use: Cellulose Nanofibers (CNF), Cellulose Nanocrystals (CNC), and Bacterial Cellulose (BC); *Handbook of Nanomaterials for Industrial Applications; Micro and Nano Technologies*;2018, pp 74-126
- [90] Smith, E. L.; Fullarton, C.; Harris, R. C.; Saleem, S.; Abbott, A. P.; Ryder, K. S. *Trans. Inst. Met. Finish.* 2010, 88, 285
- [91] Abbott, A. P.; Barron, J. C.; Elhadi, M.; Frisch, G.; Gurman, S. J.; Hillman, A. R.; Smith, E. L.; Mohamoud, M. A.; Ryder, K. S. *ECS Trans.* 2009, 16, 47
- [92] Abbott, A. P.; McKenzie, K. J. *Phys. Chem. Chem. Phys.* 2006, 8, 4265
- [93] Abbott, A. P.; Ryder, K. S.; Konig, U. *Trans. Inst. Met. Finish.* 2008, 86, 196



- [94] Abbott, A. P.; Barron, J. C.; Ryder, K. S. *Trans. Inst. Met. Finish.* 2009, 87, 201
- [95] Abbott, A. P.; Barron, J. C.; Frisch, G.; Ryder, K. S.; Silva, A. F. *Electrochim. Acta* 2011, 56, 5272
- [96] Abbott, A. P.; McKenzie, K. J. *Phys. Chem. Chem. Phys.* 2006, 8, 4265
- [97] Abbott, A. P.; El Taib, K.; Frisch, G.; McKenzie, K. J.; Ryder, K. S. *Phys. Chem. Chem. Phys.* 2009, 11, 4269.
- [98] Popescu, A. M.; Cojocaru, A.; Donath, C.; Constantin, V. *Chem. Res. Chin. Univ.* 2013, 29, 991
- [99] Abbott, A. P.; El Ttaib, K.; Ryder, K. S.; Smith, E. L. *Trans. Inst. Met. Finish.* 2008, 86, 234
- [100] Abbott, A. P.; El Ttaib, K.; Frisch, G.; Ryder, K. S.; Weston, D. *Phys. Chem. Chem. Phys.* 2012, 14, 2443
- [101] Abbott, A. P.; Capper, G.; Davies, D. L.; Rasheed, R. K. *Chem.—Eur. J.* 2004, 10, 3769
- [102] Abood, H. M. A.; Abbott, A. P.; Ballantyne, A. D.; Ryder, K. S. *Chem. Commun.* 2011, 47, 3523
- [103] Gomez, E.; Cojocaru, P.; Magagnin, L.; Valles, E. J. *Electro anal. Chem.* 2011, 658, 18
- [104] Peng Liu et.al., Recent advances in the application of deep eutectic solvents as sustainable media as well as catalysts in organic reactions; *RSC Adv*; Issue 60,2015,5, pp 48675-48704.
- [105] Chiara Fanali et al., Application of deep eutectic solvents for the extraction of phenolic compounds from extra-virgin olive oil; *National Library of Medicine; Electrophoresis*; 2020 Oct;41(20):1752-1759.

- [106] Wang Ailing et al., Deep Eutectic Solvents to Organic Synthesis; Progress in Chemistry, 2014, Vol.26, Issue 5, pp 784-795.
- [107] Ali Abo-Hamed et.al., Potential applications of deep eutectic solvents in nanotechnology; Chem.Engg., Journal; 2015; 273; pp 551-567.
- [108] Carriazo D, et.al. Resorcinol-based deep eutectic solvents as both carbonaceous precursors and templating agents in the synthesis of hierarchically porous carbon monoliths. Chem. Mater. 2010, 22, 6146–6152.
- [109] Chakrabarti MH, et al., One-pot electrochemical gram-scale synthesis of graphene using deep eutectic solvents and acetonitrile. Chem. Eng. J. 2015, 274, 213–223.
- [110] Querejeta-Fernández A, et al., Unknown aspects of self-assembly of PbS microscale superstructures. ACS Nano. 2015, 6, 3800–3812.
- [111] Liu W, et.al., Synthesis of monoclinic structured BiVO<sub>4</sub> spindle microtubes in deep eutectic solvent and their application for dye degradation. J. Hazard. Mater. 2010, 181, 1102–1108.
- [112] Dong J. et.al. Growth of ZnO nanostructures with controllable morphology using a facile green antisolvent method. J. Phys. Chem. C 2010, 114, 8867–8872.
- [113] Gallego I, et.al., Folding and imaging of DNA nanostructures in anhydrous and hydrated deep-eutectic solvents. Angew. Chem., Int. Ed. 2015, 54, 6765–6769.
- [114] Wagle DV, et.al., Deep eutectic solvents: sustainable media for nanoscale and functional materials. Acc. Chem. Res. 2014, 47, 2299–2308.
- [115] Ma Z, Yu JH, Dai S. Preparation of inorganic materials using ionic liquids. Adv. Mater. 2010, 22, 261–285.
- [116] Muzamil Khatri et al., Ze in nanofibers via deep eutectic solvent electrospinning: tunable morphology with super hydrophilic properties; Scientific Reports 10, 15307, 2020.

- [117] Liao, H.G.; Jiang, Y.-X.; Zhou, Z.-Y.; Chen, S.-P.; Sun, S.-G. *Angew. Chem.* 2008, 120, 9240
- [118] Jae-Seung Lee; Deep eutectic solvents as versatile media for the synthesis of noble metal nanomaterials; De Gruyter; *Nanotechnology Rev*;6,3, 2017.
- [119] Liu, Q., Huang, X., and Liang, P.; Preconcentration of copper and lead using deep eutectic solvent modified magnetic nanoparticles and determination by inductively coupled plasma optical emission spectrometry. *Atomic Spectrosc.* 41, 2020; pp 36–42. DOI: 10.46770/AS.2020.01.005
- [120] Majidi, S. M., and Hadjmohammadi, M. R.; Alcohol-based deep eutectic solvent as a carrier of SiO<sub>2</sub>@Fe<sub>3</sub>O<sub>4</sub> for the development of magnetic dispersive micro-solid-phase extraction method: application for the preconcentration and determination of morin in apple and grape juices, diluted and acidic extract of dried onion and green tea infusion samples. *J. Sep. Sci.* 42, 2019; pp 2842–2850. DOI: 10.1002/jssc.201900234
- [121] Lirong Nie et al., Rethinking the Applications of Ionic Liquids and Deep Eutectic Solvents in Innovative Nano-Sorbents; *Front.Chem.*Apr.2021.
- [122] Ingrid Hagarova et.al., Application of Metallic Nanoparticles and Their Hybrids as Innovative Sorbents for Separation and Pre-concentration of Trace Elements by Dispersive Micro-Solid Phase Extraction: A Minireview; *Front.Chem.*May 2021.
- [123] N.Azizi et.al., *Sci.Iranica C*; Greener synthesis of magnetic nanoparticles in an aqueous deep eutectic solvent; 23(6), 2016, pp 2750-2755.
- [124] L. Anicai, et.al, Electrochemical synthesis of nanosized TiO<sub>2</sub> nanopowder involving choline chloride-based ionic liquids, *Mat. Sci. Eng. B* 199,2015, pp 87-95.
- [125] F. Chen, S. Xie, X. Huang, X. Qiu, Ionothermal synthesis of Fe<sub>3</sub>O<sub>4</sub>magnetic nanoparticles as efficient heterogeneous Fenton-like catalysts for degradation of organic pollutants with H<sub>2</sub>O<sub>2</sub>, *J. Haz. Mater.* 322 (2017) 152-162.

- [126] T. Cun, C. Dong, Q. Huang, Ionothermal precipitation of highly dispersive ZnO nanoparticles with improved photocatalytic performance, *Appl. Surface Sci.* 384 (2016) 73-82.
- [127] D.O. Oseguera-Galindo, R. Machorro-Mejia, Silver nanoparticles synthesized by laser ablation confined in urea choline chloride deep eutectic solvent, *Colloids Interface Sci, Commun.* 12 (2016) 1-4.
- [128] M. Karimi, M.R. Ramsheh, et.al., One-step and low-temperature synthesis of monetite nanoparticles in an all-in-one system (reactant, solvent, and template) based on calcium chloride-choline chloride deep eutectic medium, *Ceramics International* 43 (2017) 2046-2050.
- [129] Antonio Jose et.al., Fast Synthesis of CeO<sub>2</sub> Nanoparticles in a Continuous Microreactor Using Deep Eutectic Reline as Solvent; *ACS Sustainable Chem.Engg.*2020,8,49, pp18297-18302.
- [130] Bruna et.al., TiO<sub>2</sub> nanoparticles coated with deep eutectic solvents: characterization and effect on photodegradation of organic dyes; *RSC, New J. Chem.*, 3,2019,43, pp 1415-1423.
- [131] Anika Soldner, Julia Zach et.al., Preparation of Magnesium, Cobalt and Nickel Ferrite Nanoparticles from Metal Oxides using Deep Eutectic Solvents; *PUB MED NLM*, 2016;22 (37):13108-13.
- [132] Mehrabi, Novin; Abdul Haq, Umar Faruq; Reza, M. Toufiq; Aich, Nirupam (2020): Using Deep Eutectic Solvent for Conjugation of Fe<sub>3</sub>O<sub>4</sub> Nanoparticles onto Graphene Oxide for Water Pollutant Removal. *ChemRxiv. Preprint.*  
<https://doi.org/10.26434/chemrxiv.12089658.v1>

- [133] A. Cojocaru, O. Brincoveanu et.al., Electrochemical preparation of Ag nanoparticles involving choline chloride – glycerol deep eutectic solvents; Bulgarian Chemical Communications, Volume 49 Special Issue C (pp. 194– 204) 2017
- [134] Jakubowska M, Ruzik L et.al., Application of Natural Deep Eutectic Solvents for the metal nanoparticles extraction from plant tissue; Analytical Biochemistry, 2021, 617:114117
- [135] Kang YS, Risbud S, Rabolt JF, Stroeve P. Synthesis and characterization of nanometer-size Fe<sub>3</sub>O<sub>4</sub> and  $\gamma$ -Fe<sub>2</sub>O<sub>3</sub> Particles. Chem Mater. 1996; 8:2209–11.
- [136] Pankhurst QA, J Connolly, Jones SK, Dobson J. Applications of magnetic nanoparticles in biomedicine. J Phys D Appl. Phys. 2003;36: R167.
- [137] Dobson J. Gene therapy progress and prospects: magnetic nanoparticle-based gene delivery. Gene Ther. 2006; 13:283–7. [PubMed]
- [138] Rudge S, Peterson C, Vesely C, Koda J, Stevens S, Catterall L. Adsorption, and desorption of chemotherapeutic drugs from a magnetically targeted carrier (MTC) J Control Release. 2001; 74:335–40. [PubMed]
- [139] Appenzeller T. The man who dared to think small. Science. 1991; 254:1300.
- [140] Qin Y. Silver-containing alginate fibers and dressings. Int Wound J. 2005; 2:172–6. [PMC free article]
- [141] Atiyeh BS, Costagliola M, Hayek SN, Dibo SA. Effect of silver on burn wound infection control and healing: a review of the literature. Burns. 2007; 33:139–48. [PubMed]
- [142] Lansdown AB. Silver in health care: antimicrobial effects and safety in use. Curr Probl Dermatol. 2006; 33:17–34. [PubMed]
- [143] Stepanov AL, Popok VN, Hole DE. Formation of Metallic Nanoparticles in Silicate Glass through Ion Implantation. Glass Phy Chem. 2002; 28:90–5.

- [144] Elechiguerra JL, Burt JL, Morones JR, Camacho-Bragado A, Gao X, Lara HH, et al. Interaction of silver nanoparticles with HIV-1. *J Nanobiotechnology*. 2005; 3:6.
- [145] Shabir Ahmad, Sidra Munir, Nadia Zeb; Green nanotechnology: a review on green synthesis of silver nanoparticles - an ecofriendly approach; *Int J Nanomedicine*. 2019 Jul 10; 14:5087-5107. DOI: 10.2147/IJN.S200254.
- [146] Muhammad Rafique, Iqra Sadaf, M Shahid Rafique, M Bilal Tahir, A review on green synthesis of silver nanoparticles and their applications; *Artif Cells Nanomed Biotechnol*. 2017 Nov; 45(7):1272-1291. DOI: 10.1080/21691401.2016.1241792.
- [147] Chitsazi MR, Korbekandi H, Asghari G, Bahri Najafi R, Badii A, Iravani S. 2016. Synthesis of silver nanoparticles using methanol and dichloromethane extracts of *Pulicariagnaphalodes* (Vent.) Boiss. aerial parts. *Artifl cells, Nanomed Biotechnol*. 44:328–333.
- [148] Wang H, Qiao X, Chen J, Wang X, Ding S. 2005. Mechanisms of PVP in the preparation of silver nanoparticles. *Mater Chem Phys*. 94:449–453.
- [149] Guzmán MG, Dille J, Godet S. 2009. Synthesis of silver nanoparticles by chemical reduction method and their antibacterial activity. *Int J Chem Biol Eng*. 2:104–111.
- [150] Tran QH, Le AT. 2013. Silver nanoparticles: synthesis, properties, toxicology, applications, and perspectives. *Adv Nat Sci Nanosci Nanotechnol*. 4:033001.
- [151] Chou CW, Hsu SH, Wang PH. 2008. Biostability and biocompatibility of poly(ether)urethane containing gold or silver nanoparticles in a porcine model. *J Biomed Mater Res A*. 84:785–794. [PubMed]
- [152] Sang-Hun Lee 1, Bong-Hyun Jun; Silver Nanoparticles: Synthesis and Application for Nanomedicine; *Int J Mol Sci*. 2019 Feb 17;20(4):865. DOI: 10.3390/ijms20040865.
- [153] Gurunathan S., Han J.W., Kim E.S., Park J.H., Kim J.H. Reduction of graphene oxide by resveratrol: A novel and simple biological method for the synthesis of an effective

anticancer nanotherapeutic molecule. *Int. J. Nanomed.* 2015; 10:2951–2969. DOI: 10.2147/IJN.S79879.

[154] Ganaie S.U., Abbasi T., Abbasi S.A. Green synthesis of silver nanoparticles using an otherwise worthless weed mimosa (*Mimosa pudica*): Feasibility and process development toward shape/size control. *Part. Sci. Technol.* 2015; 33:638–644. DOI: 10.1080/02726351.2015.1016644.

[155] Alshehri, A. H., Jakubowska, M., Młozniak, A., Horaczek, M., Rudka, D., Free, C., et al. (2012). Enhanced electrical conductivity of silver nanoparticles for high-frequency electronic applications. *ACS Appl. Mater. Interfaces* 4, 7007–7010. DOI: 10.1021/am3022569.

[156] Nie, S., and Emory, S. R. (1997). Probing single molecules and single nanoparticles by surface-enhanced Raman scattering. *Science* 275, 1102–1106. DOI: 10.1126/science.275.5303.1102.

[157] Xu, R., Wang, D., Zhang, J., and Li, Y. (2006). The shape-dependent catalytic activity of silver nanoparticles for the oxidation of styrene. *Chem. Asian J.* 1, 888–893. DOI: 10.1002/asia.200600260.

[158] Kelly, K. L., Coronado, E., Zhao, L. L., and Schatz, G. C. (2003). The optical properties of metal nanoparticles: the influence of size, shape, and dielectric environment. *J. Phys. Chem. B.* 107, 668–677. DOI: 10.1021/jp026731y.

[159] Tran, Q. H., Nguyen, V. Q., and Le, A. T. (2013). Silver nanoparticles: synthesis, properties, toxicology, applications, and perspectives. *Adv. Nat. Sci.* 4, 20. DOI: 10.1088/2043-6262/4/3/033001.

[160] Ajitha B, Reddy YA, Reddy P. Enhanced antimicrobial activity of silver nanoparticles with controlled particle size by pH variation. *Powder Technol.* 2015; 269(3):110–7. <https://doi.org/10.1016/j.powtec.2014.08.049>.

- [161] Catalina Quintero-Quiroz, et al., Optimization of silver nanoparticle synthesis by chemical reduction and evaluation of its antimicrobial and toxic activity; *Biomaterials Research* volume 23, Article number: 27 (2019)
- [162] Manoj B. Gawande et al., Cu and Cu-Based Nanoparticles: Synthesis and Applications in Catalysis; *Chem. Rev.* 2016, 116, 6, 3722–3811; <https://doi.org/10.1021/acs.chemrev.5b00482>
- [163] Prateek Khare; Synthesis of phenolic precursor-based porous carbon beads in situ dispersed with copper–silver bimetal nanoparticles for antibacterial applications; 2014; *Journal of Colloid and Interface Science* 418:216–224 DOI: 10.1016/j.jcis.2013.12.026
- [164] Cushing, B.L., Kolesnichenko, V.L., O'Connor, C.J.: Recent advances in the liquid-phase syntheses of inorganic nanoparticles. *Chem. Rev.* 104, 3893–3946 (2004)
- [165] Dang, T.M.D., Le, T.T.T., Blanc, E.F., Dang, M.C.: Synthesis and optical properties of copper nanoparticles prepared by a chemical reduction method. *Adv. Nat. Sci. Nanosci. Nanotechnol.* 2, 15009–15012 (2011)
- [166] D. Adner, M. Korb, S. Schulze, M. Hietschold, and H. Lang, “A straightforward approach to oxide-free copper nanoparticles by thermal decomposition of a copper(I) precursor,” *Chemical Communications*, vol. 49, pp. 6855–6857, 2013.
- [167] R. K. Bortoleto-Bugs, T. Mazon, M. Tarozzo Biasoli, A. Pavani Filho, J. Willibrordus Swart, and M. Roque Bugs, “Understanding the formation of the self-assembly of colloidal copper nanoparticles by a surfactant: a molecular velcro,” *Journal of Nanomaterials*, vol. 2013, Article ID 802174, 8 pages, 2013.
- [168] S. P. Meshram, P. V. Adhyapak, U. P. Mulik, and D. P. Amalnerkar, “Facile synthesis of CuO nanomorphs and their morphology dependent sunlight driven photocatalytic properties,” *Chemical Engineering Journal*, vol. 204-205, pp. 158–168, 2012.



- [169] M. S. Usman, N. A. Ibrahim, K. Shameli, N. Zainuddin, and W. M. Z. W. Yunus, "Copper nanoparticles mediated by chitosan: synthesis and characterization via chemical methods," *Molecules*, vol. 17, no. 12, pp. 14928–14936, 2012.
- [170] Jiang W, Singhal A, Zheng J, Wang C, Chan CW, Optimizing the Synthesis of Red-to Near-IR-Emitting CdS-Capped CdTe<sub>1-x</sub> Alloyed Quantum Dots for Biomedical Imaging. *Chem Mater* 2006; 18: 4845--4854.
- [171] Claudia Martínez-Alonso, Carlos A. Rodríguez-Castañeda, Paola Moreno-Romero, C. Selene Coria-Monroy, Hailin Hu, "Cadmium Sulfide Nanoparticles Synthesized by Microwave Heating for Hybrid Solar Cell Applications", *International Journal of Photoenergy*, vol. 2014, Article ID 453747, 11 pages, 2014. <https://doi.org/10.1155/2014/453747>
- [172] F. Chen, R. Zhou, L. Yang, M. Shi, G. Wu, M. Wang and H. Chen, *J. Phys. Chem. C*, 2008, 112, 13457–13462.
- [173] Y. Huang, F. Sun, T. Wu, Q. Wu, Z. Huang, H. Su, and Z. Zhang, *J. Solid State Chem.*, 2011, 184, 644.
- [174] M. R. Gholipour, C. T. Dinh, F. Beland, and T. O. Do, *Nanoscale*, 2015, 7, 8187–8203 RSC.
- [175] W. Wei, P. Q. Sun and Z. Li, *Sci. Adv.*, 2018, 4, 9253–9260.
- [176] M. Mollavali, C. Falamaki and S. Rohani, *Int. J. Hydrogen Energy*, 2018, 43(19), 9259–9278.
- [177] K. A. Brown, D. F. Harris, and M. B. Wilker, *Science*, 2016, 352, 447–451
- [178] Zhaoyu Chang; Cadmium sulfide net framework nanoparticles for photo-catalyzed cell redox; *RSC Adv.*, 2020, 10, 37820-37825; DOI: 10.1039/D0RA08235J
- [179] K. B. Narayanan and N. Sakthivel, "Biological synthesis of metal nanoparticles by microbes," *Advances in Colloid and Interface Science*, vol. 156, no. 1–2, pp. 1–13, 2010.

- [180] B. A. Rzigalinski and J. S. Strobl, "Cadmium-containing nanoparticles: perspectives on pharmacology and toxicology of quantum dots," *Toxicology and Applied Pharmacology*, vol. 238, no. 3, pp. 280–288, 2009.
- [181] Acharya KP. Photocurrent spectroscopy of CdS/plastic, CdS/glass, and ZnTe/GaAs hetero-pairs formed with pulsed laser deposition. Doctoral dissertation, Bowling Green State University, USA; 2009.
- [182] Zhu H, Jiang R, Xiao L, Chang Y, Guan Y, Li X, et al. Photocatalytic decolorization and degradation of Congo Red on innovative cross-linked chitosan/nano-CdS composite catalyst under visible light irradiation. *J Hazardous Mater* 2009; 169:933-40.
- [183] Song X, Yao W, Zhang B, Wu Y. Application of Pt/CdS for the photocatalytic flue gas desulfurization. *Int J Photoenergy* 2012;1-5. <http://dx.doi.org/10.1155/2012/684735>
- [184] El-Kemary M, El-Shamy H, Mosaad MM. The role of capping agent on the interaction of cadmium sulfide nanoparticles with flufenamic acid drug. *Mater Chem Phys* 2009; 118:81-5.
- [185] Kozhevnikova NS, Vorokh AS. Preparation of stable colloidal solution of cadmium sulfide CdS using ethylenediaminetetraacetic acid. *Russian J Gen Chem* 2010; 80:391-4.
- [186] Bokka Durga, Shaik Raziya,, Santoshi G Rajamahanti, Boddeti Govindh, Korimella Vijaya Raju, Nowduri Annapurna; Synthesis and Characterization of Cadmium Sulphide nanoparticles Using Annona Muricata Leaf Extract as Reducing/Capping Agent; DOI:10.7598/cst2016.1291 *Chemical Science Transactions*; 2016, 5(4), 1035-1041
- [187] J. D. Blum *Nat. Chem.*, 2013, 5, 1066.
- [188] J. Jeevanandam , A. Barhoum , Y. S. Chan , A. Dufresne and M. K. Danquah , *Beilstein J. Nanotechnol.*, 2018, 9 , 1050 —1074.
- [189] W. Lin *Chem. Rev.*, 2015, 115, 10407 —10409.

- [190] K. Watanabe, D. Menzel, N. Nilius and H. J. Freund, *Chem. Rev.*, 2006, 106, 4301—4320.
- [191] F. J. Heiligtag and M. Niederberger, *Mater. Today*, 2013, 16, 262—271.
- [192] C. Wang and D. Astruc, *Prog. Mater. Sci.*, 2018, 94, 306—383.
- [193] Villa Krishna Harika, Tirupathi Rao Penki, Sustainable existence of solid mercury (Hg) nanoparticles at room temperature and their applications; *Chemical science*; Issue 9, 2021
- [194] Jumpei Kuno, Tsuyoshi Kawai, and Takuya Nakashima; The effect of surface ligands on the optical activity of mercury sulfide nanoparticles; *J. Nanoscale*; Issue 32, 2017
- [195] Nashaat M. Mazrui, Emily Seelen, Cecil K. King'onde; The precipitation, growth and stability of mercury sulfide nanoparticles formed in the presence of marine dissolved organic matter; *Environmental science: Processes and Impacts*; Issue 4; 2018
- [196] Kale, S. S., Lokhande, C. D., “Preparation and Characterization of HgS Films by Chemical Deposition.” *Mater. Chem. Phys.*, 1999, 59, 242-246.
- [197] Qin, A., Fang, Y., Zhao, W., Liu, H., Su, C., “Directionally Dendritic Growth of Metal Chalcogenide Crystals via Mild Template-free Solvothermal Method.” *J. Cryst. Growth.*, 2005, 283, 230-241.
- [198] Ding, T., Zhu, J., “Microwave Heating Synthesis of HgS and PbS Nanocrystals in Ethanol Solvent.” *Mater. Sci. Eng.*, 2003, 100, 307-313.
- [199] Ren, T., Xu, S., Zhao, W., Zhu, J., “A Surfactant-Assisted Photochemical Route to Single-Crystalline HgS Nanotubes.” *J. Photochem. Photobiol.*, 2005, 173, 93- 98.
- [200] Mahapatra, A., K., Dash, A., K., “alpha-HgS Nanocrystals: synthesis, structure and optical properties.” *Physica*, 2006, 35, 9-15.
- [201] Patel, B. K., Rath, S., Sarangi, S. N., Sahu, S. N., “HgS Nanoparticles: Structure and Optical Properties.” *Appl. Phys.*, 2007, 86, 447-450.

- [202] Sapriel, J., “Cinnabar ( $\alpha$  HgS), a promising acoustic optical material.” *Appl. Phys. Lett.*, 1971, 19, 533-535.
- [203] Higginson, K. A., Kuno, M., Bonevich, J., Qadri, S. B., Yousuf, M., Mattoussi, H., “Synthesis and Characterization of Colloidal  $\beta$ -HgS Quantum Dots.” *J. Phys. Chem.*, 2002, 106, 9982-9985.
- [204] N. Jassim Mohammed and H. Fakher Dagher; Synthesis and Characterization of Mercuric Sulfide Nanoparticles Thin Films by Pulsed Laser Ablation (PLA) in Distilled Water (DW). *IJMSE*, 2020, Vol. 17, No. 3, DOI: 10.22068/ijmse.17.3.11
- [205] Xin Xu, Elizabeth R. Carraway, Sonication-Assisted Synthesis of  $\beta$ -Mercuric Sulphide Nanoparticles, *Nanomaterials and Nanotechnology*, 2012, <https://doi.org/10.5772/55823>
- [206] Jing Wang and Sheila N. Baker; Pyrrolidinium salt-based binary and ternary deep eutectic solvents: green preparations and physiochemical property characterizations; *De Gruyter, Green Process Synth* 2018; 7: 353–359
- [207]. Kumar V, Nigam KDP. *Green Process Synth.* 2012, 1, 79–107.
- [208] Durand E, Lecomte J, Villeneuve P. *Biochimie* 2016, 120, 119–123.
- [209] Taysun MB, Sert E, Atalay FS. *J. Mol. Liq.* 2016, 223, 845–852.
- [210] Martins MA, Paveglio GC, Munchen TS, Meyer AR, Moreira DN, Rodrigues LV, Frizzo CP, Zanatta N, Bonacorso HG, Melo PA. *J. Mol. Liq.* 2016, 223, 934–938.
- [211] Craveiro R, Aroso I, Flammia V, Carvalho T, Viciosa M, Dionísio M, Barreiros S, Reis R, Duarte ARC, Paiva A. *J. Mol. Liq.* 2016, 215, 534–540.
- [212] Sze LL, Pandey S, Ravula S, Pandey S, Zhao H, Baker GA, Baker SN. *ACS Sust. Chem. Eng.* 2014, 2, 2117–2123.
- [213] Chemat F, Anjum H, Shariff AM, Kumar P, Murugesan T. *J. Mol. Liq.* 2016, 218, 301–308.

- [214] Liu YT, Chen YA, Xing YJ. *Chin. Chem. Lett.* 2014, 25, 104–106.
- [215] Abbott, A. P., Boopathy, D., Capper, G., Davies, D. L., and Rasheed, R. K. (2004). Deep eutectic solvents formed between choline chloride and carboxylic acids: versatile alternatives to ionic liquids. *J. Am. Chem. Soc.* 126, 9142–9147. DOI: 10.1021/ja048266j.
- [216] Abbott AP, Harris RC, Ryder KS, D’Agostino C, Gladden LF, Mantle MD. *Green Chem.* 2011, 13, 82–90.
- [217] Y.T. Dai, J. van Spronsen, G.J. Witkamp, R. Verpoorte, Y.H. Choi, *Anal. Chim. Acta* 766 (2013) 61–68.
- [218] Q.H. Zhang, K. De Oliveira Vigier, S. Royer, F. Jérôme, *Chem. Soc. Rev.* 41 (2012) 7108–7146.
- [219] T.M.D. Dang, T.T.T. Le, M.C. Fribourg-Blanc Dang, Synthesis and optical properties of copper nanoparticles prepared by a chemical reduction method, *Adv. Nat. Sci. Nanosci. Nanotechnol.* 2 (2011) 015009–015015.
- [220] V.L. Colvin, M.C. Schlamp, A.P. Alivisatos, Light-emitting diodes made from cadmium selenide nanocrystals and a semiconducting polymer, *Nature* 370 (1994) 354–357.
- [221] Q. Liu, R.L. Yu, G.Z. Qiu, Z. Fang, A.L. Chen, Z.W. Zhao, Optimization of separation processing of copper and iron of dump bioleaching solution by Lix 984 in indexing copper mine, *Trans. Nonferrous Met. Soc. China* 18 (2008) 1258–1261.
- [222] Shikha Jain, Ankita Jain, Vijay Devra; Copper nanoparticles catalyzed oxidation of threonine by peroxomonosulfate, *Journal of Saudi Chemical Society* (2017),21, 803-810.
- [223] Mustafa G, Tahir H, Sultan M, Akhtar N (2013) Synthesis and characterization of cupric oxide (CuO) nanoparticles and their application for the removal of dyes12: 6650-6660.

- [224] Suleiman M, Mousa M, Hussein A, Hammouti B, Hadda TB, et al. (2013) Copper (II)-Oxide nanostructures: synthesis, characterizations, and their applications-review. *J Mater Environ Sci* 4: 792-797.
- [225] Wongpisutpaisan N, Charoonsuk P, Vittayakorn N, Pecharapa W (2011) Sonochemical synthesis and characterization of copper oxide nanoparticles. *Energy Procedia* 9: 404-409.
- [226] Lanje AS, Sharma SJ, Pode RB, Ningthoujam RS (2010) Synthesis and optical characterization of copper oxide nanoparticles. *Adv Appl Sci Res* 1:36-40.
- [227] Zhu H, Han D, Meng Z, Wu D, Zhang C (2011) Preparation and thermal conductivity of CuO nanofluid via a wet chemical method. *Nanoscale Res Lett* 6: 181.
- [228] Mousa MK (2015) Wastewater disinfection by synthesized copper oxide nanoparticles stabilized with surfactant. *J Mater Environ Sci* 6: 1924-1937.
- [229] Karthik AD, Kannappan G (2013) Synthesis of copper precursor, copper and its oxide nanoparticles by green chemical reduction method and its antimicrobial activity. *J Appl. Pharm Sci* 3: 016-021.
- [230] Srivastava S, Kumar M, Agrawal A, Dwivedi SK (2013) Synthesis and characterization of copper oxide nanoparticles. *IOSR J Appl. Phys* 5: 61-65.
- [231] Phiwdang K, Suphankij S, Mekprasart W, Pecharapa W (2013) Synthesis of CuO nanoparticles by precipitation method using different precursors. *Energy Procedia* 34: 740-745
- [232] Darezereshki E, Bakhtiari F (2011) A novel technique to synthesis of tenorite (CuO) nanoparticles from low concentration CuSO<sub>4</sub> solution. *J Min Metall B Metall* 47: 73-78.
- [233] M.S.Aguilar R.Esparza G.Rosas, Synthesis of Cu nanoparticles by chemical reduction method, *Transactions of Nonferrous Metals Society of China*, Volume 29, Issue 7, 2019, pp 1510-1515

- [234] Chatterjee, A.K., Sarkar, R.K., Chattopadhyay, A.P., Aich, P., Chakraborty, R. & Basu, T. (2012). A simple robust method for synthesis of metallic copper nanoparticles of high antibacterial potency against E. coli. *Nanotechnology*, 23(8), 85103-85113.
- [235] Qi, L., Ma, J., Shen, J. (1997). Synthesis of Copper Nanoparticles in Nonionic Water-in-Oil Microemulsions, *Journal of Colloid and Interface Science*, 186 (2), 498-500.
- [236] H.R.Ghorbani, Chemical synthesis of copper nanoparticles,2014, *Oriental Journal of Chemistry*, Volume 30,2
- [237] Thi. M. D. D., Thi, T. T. L., Eric, F. B. and Mau, C. D., “Synthesis and optical properties of copper nanoparticles prepared by a chemical reduction method” *Adv. Nat. Sci. Nanosci. Nanotechnol*, 2, 6(2011).
- [238] Yoshizumi Kusumoto, Manickavachagam Muruganandham, Simple new synthesis of copper nanoparticles in water/acetonitrile mixed solvent and their characterization, *Materials Letters* 63(23), DOI: 10.1016/j.matlet.2009.06.037.
- [239] Chou K-S, Ren C-Y. Synthesis of nanosized silver particles by chemical reduction method. *Materials Chemistry and Physics*. 2000; 64:241-6.
- [240] Taguchi A, Fujii S, Ichimura T, Verma P, Inouye Y, Kawata S. Oxygen-assisted shape control in polyol synthesis of silver nanocrystals. *Chemical Physics Letters*. 2008; 462:92-5.
- [241] Cai M, Chen J, Zhou J. Reduction, and morphology of silver nanoparticles via a liquid-liquid method. *Applied surface science*. 2004; 226:422-6.
- [242] Senapati S. Ph.D. Thesis. India: University of Pune; 2005. Biosynthesis and immobilization of nanoparticles and their applications; pp. 1–57.
- [243] Klaus-Joerger T, Joerger R, Olsson E, Granqvist CG. Bacteria as workers in the living factory: metal-accumulating bacteria and their potential for materials science. *Trends Biotechnol*. 2001; 19:15–20.

- [244] S. Iravani, H. Korbekandi, S.V. Mirmohammadi, B. Zolfaghari, Synthesis of silver nanoparticles: chemical, physical, and biological methods, *Res Pharm Sci.* 2014; 9(6): 385–406.
- [245] Ojha AK, Forster S, Kumar S, Vats S, Negi S, Fischer I. Synthesis of well-dispersed silver nanorods of different aspect ratios and their antimicrobial properties against gram-positive and negative bacterial strains. *Journal of Nanobiotechnology.* 2013;11(42):1-7
- [246] Ajitha B, Reddy YAK, Reddy PS. Influence of synthesis temperature on growth of silver nanorods. *International Journal of Engineering Science.* 2014;3(5):144-148
- [247] Gebeyehu MB, Chala TF, Chang S-Y, Wu C-M, Lee J-Y. Synthesis, and highly effective purification of silver nanowires to enhance transmittance at low sheet resistance with simple polyol and scalable selective precipitation method. *RSC Advances.* 2017; 7:16139-16148
- [248] Im SH, Lee YT, Wiley B, Xia Y. Large-scale synthesis of silver nanocubes: The role of HCl in promoting cube perfection and monodispersity. *Angewandte Chemie International edition.* 2005; 44:2154-2157
- [249] Sun Y, Xia Y. Shape-controlled synthesis of gold and silver nanoparticles. *Science.* 2002a;298(5601):2176-2179
- [250] Tao A, Sinsersuksakul P, Yang PD. Polyhedral silver nanocrystals with distinct scattering signatures. *Angewandte Chemie International Edition.* 2006;45(28):4597-4601
- [251] Siekkinen AR, McLellan JM, Chen J, Xia Y. Rapid synthesis of small silver nanocubes by mediating polyol reduction with a trace amount of sodium sulfide or sodium hydrosulfide. *Chemical Physics Letters.* 2006; 432:491-496
- [252] Sun Y, Yin Y, Mayers BT, Herricks T, Xia Y. Uniform silver nanowires synthesis by reducing AgNO<sub>3</sub> with ethylene glycol in the presence of seeds and poly (vinyl pyrrolidone). *Chemistry of Materials.* 2002;14(11):4736-4745



- [253] Me'traux GS, Mirkin CA. Rapid thermal synthesis of silver nanoprisms with chemically tailorable thickness. *Advanced Materials*. 2005;17(4):412-415.
- [254] S. Hussain, A.K. Pal Incorporation of nanocrystalline silver on carbon nanotubes by electrodeposition technique *Mater. Lett.*, 62 (2008), pp. 1874-1877
- [255] A. Ahmad, P. Mukherjee, S. Senapati, D. Mandal, M. Islam Khan, R. Kumar, M. Sastry Extracellular biosynthesis of silver nanoparticles using the fungus *Fusarium oxysporum* *Colloids Surf., B*, 28 (2003), pp. 313-318
- [256] W.R. Hill Pillsbury, DM: *Argyria: The Pharmacology of Silver*, Baltimore Md. Williams & Wilkins Co (1939), pp. 128-132
- [257] J.T. Lue A review characterization and physical property studies of metallic nanoparticles *Phys. Chem. Solids*, 62 (2001), pp. 1599-1612
- [258] M. Rai, A. Yadav, A. Gade Silver nanoparticles as a new generation of antimicrobials *Biotechnol. Adv.*, 27 (2009), pp. 76-83
- [259] A. Henglein Small-particle research: physicochemical properties of extremely small colloidal metal and semiconductor particles *Chem. Rev.*, 89 (1989), pp. 1861-1873
- [260] W.K. Jung, H.C. Koo, K.W. Kim, S. Shin, S.H. Kim, Y.H. Park Antibacterial activity and mechanism of action of the silver ion in *Staphylococcus aureus* and *Escherichia coli* *Appl. Environ. Microbiol.*, 24 (2008), pp. 2171-2178, 10.1128/AEM.02001-07
- [261] Jamakala O, Rani AU. Mitigating role of zinc and iron against cadmium-induced toxicity in liver and kidney of the male albino rat: a study with reference to metallothionein quantification. *Int J Pharm Pharm Sci* 2014; 6:411-7.
- [262] Bandaranayake RJ, Wen GW, Lin JY, Jiang HX, Sorensen CM. Structural phase behavior in II-VI semiconductor nanoparticles. *Appl Phys Lett* 1995; 67:831-3.

- [263] Dneprovskii V, Zhukov E, Karavanskii V, Poborchii V, Salamatina I. Nonlinear optical properties of semiconductor quantum wires. *Superlattices Microstruct* 1998; 23:1217-21.
- [264] Anikin KV, Melnik NN, Simakin AV, Shafeev GA, Voronov VV, Vitukhnovsky AG. Formation of ZnSe and CdS quantum dots via laser ablation in liquids. *Chem Phys Lett* 2002; 366:357-60.
- [265] Pan A, Yang H, Liu R, Yu R, Zou B, Wang Z. Color-tunable photoluminescence of alloyed CdS<sub>x</sub>Se<sub>1-x</sub> nanobelts. *J Am Chem Soc* 2005; 127:15692-3.
- [266] Chakravarti SK, Kumar V, Kumar S. Galvanic fabrication of CdS microstructures using nuclear track filter membranes. *J Mater Sci* 2005; 40:503-4.
- [267] Yu LM, Zhu CC, Fan XH, Qi LJ, Yan W. CdS/SiO<sub>2</sub> nanowire arrays and CdS nanobelt synthesized by thermal evaporation. *J Zhejiang Univ Sci A* 2006; 7:1956-60.
- [268] Xiao J, Peng T, Dai K, Zan L, Peng Z. Hydrothermal synthesis, characterization and its photoactivity of CdS/Rectorite nanocomposites. *J Solid State Chem* 2007; 180:3188-95.
- [269] Mahdavi SM, Irajizad A, Azarian A, Tilaki RM. Optical and structural properties of copper doped CdS thin films prepared by pulsed laser deposition. *Scientia Iranica* 2008; 15:360-5.
- [270] Thongtem T, Phuruangrat A, Thongtem S. Solvothermal synthesis of CdS nanowires templated by polyethylene glycol. *Ceramics Int* 2009; 35:2817-22.
- [271] Pandian SR, Deepak V, Kalishwaralal K, Gurunathan S. Biologically synthesized fluorescent CdS NPs encapsulated by PHB. *Enzyme Microb Technol* 2011; 48:319-25.
- [272] Mammadov MN, Aliyev AS, Elrouby M. Electrodeposition of cadmium sulfide. *Int J Thin Film Sci-Tech* 2012; 1:43-53.

- [273] Girginer B, Galli G, Chiellini E, Bicak N. Preparation of stable CdS nanoparticles in aqueous medium and their hydrogen generation efficiencies in the photolysis of water. *Int J Hydrog. Energy* 2009; 34:1176-84.
- [274] R Aruna Devi, M Latha, S Velumani, Goldie Oza, P Reyes-Figueroa, M Rohini, I G Becerril-Juarez, Jae-Hyeong Lee, Junsin Yi, Synthesis and Characterization of Cadmium Sulfide Nanoparticles by Chemical Precipitation Method, *J Nanosci Nanotechnol.* 2015 Nov;15 (11):8434-9. DOI: 10.1166/jnn.2015.11472.
- [275] Rodriguez Fragoso P, Reyes Esparza J, Leon Buitimea A, Rodriguez Fragoso L. Synthesis, characterization, and toxicological evaluation of maltodextrin capped cadmium sulfide nanoparticles in human cell lines and chicken embryos. *J. Nanobiotech* 2012; 10:47.
- [276] Rajnish Gupta, Cadmium nanoparticles and its toxicity *Journal of Critical Reviews* (6), Issue 5, 2019
- [277] Mahesh M Kamble, Sachin R Rondiya, Bharat R Bade, Kiran B Kore, et.al., Optical, structural, and morphological study of CdS nanoparticles: role of sulfur source, *Nanomaterials, and Energy*, (9),1, June 2020, pp. 72-81  
<https://doi.org/10.1680/jnaen.19.00041>
- [278] J. D. Blum, *Nat. Chem.*, 2013, 5, 1066.
- [279] J. Jeevanandam, A. Barhoum, Y. S. Chan, A. Dufresne and M. K. Danquah, *Beilstein J. Nanotechnol.*, 2018, 9, 1050–1074
- [280] W. Lin, *Chem. Rev.*, 2015, 115, 10407–10409.
- [281] K. Watanabe, D. Menzel, N. Nilius and H. J. Freund, *Chem. Rev.*, 2006, 106, 4301–4320
- [282] F. J. Heiligtag and M. Niederberger, *Mater. Today*, 2013, 16, 262–271
- [283] C. Wang and D. Astruc, *Prog. Mater. Sci.*, 2018, 94, 306–383

- [284] Alireza Mohadesia, Mehdi Ranjbar, S.M.Hosseinpour-Mashkanic, Solvent-free synthesis of mercury oxide nanoparticles by a simple thermal decomposition method, *Superlattices and Microstructures*, 66, February 2014, Pages 48-53
- [285] Villa Krishna Harika, Tirupathi Rao Penki, Boddapati Loukya, Atanu Samanta, et al., Sustainable existence of solid mercury (Hg) nanoparticles at room temperature and their applications, *RSC, Chem. Sci.*, 2021, 12, 3226-3238, DOI: 10.1039/D0SC06139
- [286] Avik J. Ghoshdastidar, Janani Ramamurthy, Maxwell Morissette & Parisa A. Ariya, Development of methodology to generate, measure, and characterize the chemical composition of oxidized mercury nanoparticles, *Analytical and Bioanalytical Chemistry*, 412, pp 691–702 (2020)
- [287] Kale, SS, Lokhande, CD (1999) Preparation and Characterization of HgS Films by Chemical Deposition. *Mater. Chem. Phys.* 59: 242–246.
- [288] Ren, T, Xu, S, Zhao, W, Zhu, J (2005) A Surfactant-Assisted Photochemical Route to Single-Crystalline HgS Nanotubes. *J. Photochem. Photobiol. A* 173: 93–98.
- [289] Mahapatra, AK, Dash, AK (2006)  $\alpha$ -HgS Nanocrystals: Synthesis, Structure and Optical Properties. *Physica E.* 35: 9–15.
- [290] Patel, BK, Rath, S, Sarangi, SN, Sahu, SN (2007) HgS Nanoparticles: Structure and Optical Properties. *Appl. Phys. A* 86, 447–450.
- [291] Xin Xu, Elizabeth R. Carraway, Sonication-Assisted Synthesis of  $\beta$ -Mercuric Sulphide Nanoparticles, *Nanomaterials and Nanotechnology*, 2012, <https://doi.org/10.5772/55823>
- [292] Ranga Rao Arnepalli, Viresh Dutta, Synthesis of Mercury Cadmium Telluride Nanoparticles by Solvothermal Method, Online proceedings, Cambridge University Press, February 2011

## 2. MATERIALS AND METHODS

---

### 2.1 Materials

All the reagent grade chemicals used for this investigation such as Malonic acid, Zinc chloride, Manganese chloride, D-glucose, D-fructose, Glycerol, Lactic acid, Glycine, Histidine, Glutamine, Copper nitrate trihydrate, Cupric chloride, Copper sulfate pentahydrate, Copper acetate, Hydrazine hydrate, Silver nitrate, Sodium hydroxide, Cadmium chloride, Mercuric chloride, Yellow Ammonium Sulfide, Sodium borohydride and methanol were purchased from Sigma – Aldrich, India and used as received without any further purifications. The deionized water used for this investigation was completely free from ions.

**Table: 2.1 Chemicals used for the investigation**

S.No.	Chemical components	Molecular formula	Molecular weight (g/mol)
1.	Malonic acid	$C_3H_4O_4$	180.156
2.	Zinc chloride	$ZnCl_2$	136.286
3.	Manganese chloride	$MnCl_2$	125.844
4.	D-Glucose	$C_6H_{12}O_6$	180.156
5.	D-Fructose	$C_6H_{12}O_6$	180.156
6.	Glycerol	$C_3H_8O_3$	92.09382
7.	Lactic Acid	$C_3H_6O_3$	90.08
8.	L-Glycine	$C_2H_5NO_2$	75.067
9.	L-Histidine	$C_6H_9N_3O_2$	155.1546
10.	L-Glutamine	$C_5H_{10}N_2O_3$	146.14
11.	Copper (II) nitrate trihydrate	$Cu(NO_3)_2 \cdot 3H_2O$	241.60

S.No.	Chemical components	Molecular formula	Molecular weight (g/mol)
12.	Copper (II) chloride dihydrate	$\text{CuCl}_2 \cdot 2\text{H}_2\text{O}$	170.48
13.	Copper sulfate pentahydrate	$\text{CuSO}_4 \cdot 5\text{H}_2\text{O}$	249.69
14.	Copper (II) acetate monohydrate	$\text{Cu}(\text{COOCH}_3)_2 \cdot \text{H}_2\text{O}$	199.65
15.	Hydrazine hydrate	$\text{H}_6\text{N}_2\text{O}$	50.061
16.	Silver nitrate	$\text{AgNO}_3$	169.87
17.	Sodium hydroxide	$\text{NaOH}$	39.997
18.	Cadmium chloride dehydrate	$\text{CaCl}_2 \cdot 2\text{H}_2\text{O}$	147.01
19.	Mercuric chloride	$\text{HgCl}_2$	271.52
20.	Yellow Ammonium Sulfide	$(\text{NH}_4)_2\text{S}$	68.14
21.	Sodium borohydride	$\text{NaBH}_4$	37.84
22.	Methanol	$\text{CH}_3\text{OH}$	32.04

## 2. 2 Experimental methods

### 2.2.1 General Preparation of Binary Deep Eutectic Solvents (BDES)

Nine types of Binary DESs were prepared from a 1:1 mole ratio of the two components is given in table 2.2. The 1:1 mole ratio of respective substances for the preparation of these nine DESs was decided using the plot of a freezing point versus the percent composition of the above mixtures. The evaporating method was employed in water as reported by Dai et al. <sup>[1]</sup>. The 1:1 mole ratio of the components was taken,

dissolved in double distilled water and excess water was removed by heating until the weight of the components remains constant. The mixtures were kept in a desiccator containing anhydrous CaCl<sub>2</sub> for about two weeks and as there was no turbidity appeared during this period. Then the DESs were subjected for the measurement of physical properties such as density, pH, conductivity, and viscosity. The H- bonded interactions between the components were characterized by FTIR.

**Table: 2.2. Prepared BDESs**

S.No.	Type of DES	Component-1	Component-2	Mole ratio
1.		Malonic Acid	Glucose	1:1
2.		Malonic Acid	Fructose	1:1
3.		Malonic Acid	Glycerol	1:1
4.	Type – IV	Zinc Chloride	Glucose	1:1
5.	Type – IV	Zinc Chloride	Fructose	1:1
6.	Type – IV	Zinc Chloride	Lactic acid	1:1
7.	Type – IV	Manganese chloride	Glucose	1:1
8.	Type – IV	Manganese chloride	Fructose	1:1
9.	Type – IV	Manganese chloride	Citric acid	1:1

### 2.2.2 General Preparation of Ternary Deep Eutectic Solvents (TDES)

Eighteen types of Ternary DESs were prepared from a 1:1:1 mole ratio of the components is given in Table 2.3. The 1:1:1 mole ratio of respective substances for all the preparation of these DESs was decided using the plot of a freezing point versus the percent composition of the above mixtures. The evaporating method was employed in water as reported by Dai et al. <sup>[1]</sup>. The components at a 1:1:1 mole ratio was taken, dissolved in double distilled water and excess water was removed by heating until the weight of the

components remains constant. The mixtures were kept in a desiccator containing anhydrous CaCl<sub>2</sub> for about two weeks and as there was no turbidity appeared during this period. Then the DESs were subjected for the measurement of physical properties such as density, pH, conductivity, and viscosity. The H- bonded interactions between the components were characterized by FTIR.

**Table: 2.3. Prepared TDESs**

S. No.	Type of DES	Component-1	Component-2	Component-3	Mole ratio
1.		Malonic Acid	Glucose	Glycine	1:1:1
2.		Malonic Acid	Glucose	Glutamine	1:1:1
3.		Malonic Acid	Glucose	Histidine	1:1:1
4.		Malonic Acid	Fructose	Glycine	1:1:1
5.		Malonic Acid	Fructose	Glutamine	1:1:1
6.		Malonic Acid	Fructose	Histidine	1:1:1
7.	Type - IV	Zinc chloride	Glucose	Glycine	1:1:1
8.	Type - IV	Zinc chloride	Glucose	Glutamine	1:1:1
9.	Type - IV	Zinc chloride	Glucose	Histidine	1:1:1
10.	Type - IV	Zinc chloride	Fructose	Glycine	1:1:1
11.	Type - IV	Zinc chloride	Fructose	Glutamine	1:1:1
12.	Type - IV	Zinc chloride	Fructose	Histidine	1:1:1
13.	Type - IV	Manganese chloride	Glucose	Glycine	1:1:1
14.	Type - IV	Manganese chloride	Glucose	Glutamine	1:1:1
15.	Type - IV	Manganese chloride	Glucose	Histidine	1:1:1
16.	Type - IV	Manganese chloride	Fructose	Glycine	1:1:1



S. No.	Type of DES	Component-1	Component-2	Component-3	Mole ratio
17.	Type - IV	Manganese chloride	Fructose	Glutamine	1:1:1
18.	Type - IV	Manganese chloride	Fructose	Histidine	1:1:1

### 2.2.3. General procedure for the synthesis of nanoparticles

Nanoparticles were synthesized by various methods, including physical method, chemical reduction method, and biological method. We had followed the chemical reduction method for the synthesis of nanoparticles using various reducing agents such as hydrazine hydrate, sodium borohydride, yellow ammonium sulfide, and sodium hydroxide was used as a stabilizing agent. Then the nanoparticles were washed with deionized water followed by methanol.

#### 2.2.3.1 Synthesis of copper nanoparticles

Nanoparticles were obtained by putting 10 ml of 0.01M Copper salts (such as Copper nitrate trihydrate, Copper (II) chloride dehydrate, Copper sulfate pentahydrate, Copper (II) acetate monohydrate) with BDES /TDES in a beaker and stirring for 30 minutes at 1200 RPM with a magnetic stirrer. During vigorous stirring, 0.01 M Hydrazine Hydrate (about 8-10 ml) was slowly introduced into the mixture, followed by 20 ml of 1 M sodium hydroxide <sup>[2]</sup>. The copper oxide nanoparticles were ultra-centrifuged, and then washed with deionized water followed by methanol, and finally dried.

#### 2.2.3.2 Synthesis of silver nanoparticles

In a beaker, 10 ml of 0.01M silver nitrate was mixed with 15 ml of BDES/ TDES and agitated at 1200 RPM for 30 minutes using a magnetic stirrer. During vigorous stirring, 0.01 M hydrazine hydrate/ sodium borohydride (about 8-10 ml) was added drop by drop, followed by 20 ml of 1 M sodium hydroxide <sup>[3]</sup>. The silver oxide nanoparticles were ultra-centrifuged, then washed in deionized water followed by methanol, and dried <sup>[4]</sup>.

### **2.2.3.3 Synthesis of cadmium and mercury nanoparticles**

Cadmium and mercury nanoparticles were synthesized in two binary deep eutectic solvents: MA-GLU & MA-FRU. Cadmium nanoparticles were synthesized by combining cadmium chloride with MA-GLU DES, and MA-FRU DES in two different beakers. Similarly, Mercury nanoparticles were made by combining mercury chloride with MA-GLU DES and MA-FRU DES separately. They were stirred for 30 minutes using a magnetic stirrer at 1200 RPM after mixing. 0.01 M Yellow Ammonium Sulfide (about 8-10ml) was added drop by drop in all beakers with vigorous shaking. The metal sulfide nanoparticles precipitate was ultra-centrifuged, then washed with deionized water followed by methanol, and dried.

### **2.2.4. Instrumentations used for the characterization of deep eutectic solvents and nanoparticles**

#### **2.2.4.1 pH meter**

A pH meter measures the movement of hydrogen ions in water-based solutions and displays the acidity or alkalinity as pH. pH is an important feature that has a lot of consequences for designing and controlling industrial-scale applications. The pH of these DESs at different temperatures was measured using the digital pH meter of ELICO make model no LI120 using the combined electrode CL- 51B.

#### **2.2.4.2 Viscometer**

The digital viscometer is a new digital instrument for measuring liquid viscosity capacity and absolute viscosity. The digital display rotational viscometer of Labman WENSAR make model LMDV 60 was employed to measure the viscosities of the DESs at different temperatures. In various applications, such as grease, painting, pharmaceuticals, and adhesives, it is commonly used to determine and measure liquid viscosity.

#### **2.2.4.3 Conductivity meter**

The Systronics Conductivity Meter 304 was used to measure the conductivities of the newly prepared DESs. Digital Conductivity Meters are reliable and accurate test instruments for the measurement of Conductivity of aqueous solutions.

#### **2.2.4.4 Density calculation**

The mass was measured by the known volume of the prepared DESs using a digital weighing balance. The densities were measured at room temperature using a standard 5 ml specific gravity bottle. Then the density was calculated using the formula as follows:

$$\text{Density} = \frac{\text{Mass}}{\text{Volume}}$$

#### **2.2.4.5 Fourier Transform Infrared spectroscopy**

Fourier-transform infrared spectroscopy (FTIR) is a technique for obtaining infrared frequencies of absorption or emission of solid, liquid, or gas. FTIR spectrum was recorded using a Shimadzu FTIR-8900 spectrometer between 4000 and 400  $\text{cm}^{-1}$ . FTIR is a very versatile tool for the functional group characterization of solvents and nanoparticles [5]. FTIR spectrum consists of absorption peaks that correspond to the frequencies of vibration between the bonds of atoms in the nanoparticles.

#### **2.2.4.6 Ultraviolet-Visible spectroscopy**

UV-Visible spectroscopy (UV-Vis) analyses the extinction (scatter + absorption) of light passing through a substance. UV-Vis is a great tool for discovering, characterizing, and investigating nanomaterials because nanoparticles have unique optical properties that are sensitive to size, shape, concentration, aggregation state, and refractive index near the nanoparticle surface. The preliminary investigation of nanoparticles was done by Perkin - Elmer make Lambda 35 UV-Visible Spectrophotometer range from 190 nm to 1100 nm.

#### **2.2.4.7 Scanning Electron Microscopy**

One of the most extensively used tools for the characterization of nanomaterials and nanostructures is the scanning electron microscope (SEM). The signals generated by electron-sample interactions disclose information about the surface morphology (texture) of the sample, as well as its particle size <sup>[6]</sup>. The morphology of nanoparticles was examined in their natural state under a range of conditions including very high-water vapor pressure up to 3000 Pa using Carl Zeiss made model EVO 18 Scanning Electron Microscope.

#### **2.2.4.8 X-Ray Diffractometer**

The analytical technique of X-ray diffraction (XRD) is based on the diffraction of X-rays by matter, particularly crystalline materials. As a more ordered material is studied, X-ray diffraction is elastic scattering (without loss of photon energy) that results in increasing interference <sup>[7]</sup>. The XRD pattern of nanoparticles was recorded on PANalytical made model X'pert3 powder X-ray diffractometer.

#### **2.2.4.9 Energy Dispersive X-ray Analysis**

EDAX works on the principle of generating X-rays from a specimen using an electron beam. The features and type of the elements contained in the sample are used to generate the X-rays <sup>[8]</sup>. The Energy Dispersive X-Ray Analysis of nanoparticles was recorded on EDAX Inc., USA made TEAM EDS model. From this, the elemental composition and the purity of the nanoparticles were known.

#### **2.2.5 Disc diffusion method**

The antimicrobial activity of some of the nanoparticles was determined by the disc diffusion method as reported by NCCLS (1993) <sup>[9]</sup> and Awoyinka. et al., (2007) <sup>[10]</sup>. The antibiogram was created using samples by the disc diffusion method. 30 mL of Nutrient agar (NA) medium were poured into Petri plates. With the use of a micropipette, the test organism was inoculated on a solidified agar plate, spread out, and left to dry for 10

minutes. Bacteria from a broth culture were injected on the surfaces of the medium. The entire surface of the Nutrient agar plates is equally inoculated with a sterile cotton swab soaked in a standardized microorganism's test mixture. In a Roux bottle, a loop containing each of the bacteria was suspended in around 10ml of physiological saline to maintain living tissues. Then these were traced onto the appropriate culture slants and incubated for 24 hours at 37°C. When growth was observed after the incubation period, the tubes were stored at 2-8° C until used.

The basic culture medium used for the growth of fungi is Potato Dextrose Agar (PDA-Himedia). In 1000 mL distilled water, dissolve 28.0 g of PDA-Himedia, boil, mix them completely. Then it was autoclaved at 15 lbs, 121°C for 15 minutes to sterilize using tartaric acid. After that, it was poured into sterile Petri plates. In a Roux bottle, a loop containing each of the bacteria was suspended in around 10ml of physiological saline to maintain living tissues. Then these were traced onto the appropriate culture slants and incubated for 48 hours at 25°C. When growth was observed after the incubation period, the tubes were stored at 2-8° C until used.

## References

- [1] Y.T. Dai, J. van Spronsen, G.J. Witkamp, R. Verpoorte, Y.H. Choi, *Anal. Chim. Acta* 766 (2013) 61–68.
- [2] Md.Abdulla-Al-Mamum, Yoshihumi Kusumoto, Manickavachagam Muruganandham, *Materials Letters* 63(23), (2009) 2007 - 2009.
- [3] Fang J, Zhang C, Mu R. The study of deposited silver particulate films by simple method for efficient SERS. *Chem Phys Lett.* 401:271–275, (2005).
- [4] S. Iravani, H. Korbekandi, S.V. Mirmohammadi,<sup>3</sup> and B. Zolfaghari, Synthesis of silver nanoparticles: chemical, physical and biological methods, *Res Pharm Sci.* Nov-Dec; 9(6): 385–406, (2014).
- [5] Biosynthesized Nanomaterials; Karina Torres-Rivero, Antonio Florido, in *Comprehensive Analytical Chemistry*, 2021
- [6] Sagadevan S, Koteeswari P (2015) Analysis of Structure, Surface Morphology, Optical and Electrical Properties of Copper Nanoparticles. *J Nanomed Res* 2(5): 00040.
- [7] Khadija El Bourakadi, Abou el Kacem Qaiss, Characterization techniques for hybrid nanocomposites based on cellulose nanocrystals /nanofibrils and nanoparticles in Cellulose; *Nanocrystal/Nanoparticles Hybrid Nanocomposites*, 2021.
- [8] Nidhi Raval, Rakesh K. Tekade; Importance of Physicochemical Characterization of Nanoparticles in Pharmaceutical Product Development; *Basic Fundamentals of Drug Delivery*, 2019.
- [9] NCCLS- National Committee for Clinical Laboratory Standards for antimicrobial disc susceptibility tests. PA: NCCLS Publications 25; (1993).
- [10] Awoyinka O.A, Balogun I.O, Ogunnowo A.A, Phytochemical screening and its in-vitro bioactivity of *cnidoscolusa conitifolius* (Euphorbiaceae), *Journal of Medicinal Plants Research* vol.1(3) pp.063-065 (2007)

### **3. Malonic acid Based Binary Deep Eutectic Solvents (BDES)**

---

#### **3.1. Introduction**

A deep eutectic solvent (DES) based on choline chloride and malonic acid was easily made at a cheap cost and with high purity <sup>[1]</sup>. This eco-friendly solvent could be recycled and reused three times without losing effectiveness <sup>[1]</sup>. We had prepared 3 types of Malonic acid-based binary deep eutectic solvents by combining Malonic acid with Glucose, Fructose and Glycerol separately. We had followed the evaporation method <sup>[2]</sup> as reported by Dai et.al, to prepare the BDESs. Then the BDESs were subjected to measure physical properties such as Density, pH, Conductivity, Viscosity, and the hydrogen-bonded interactions between the chemicals taken for the preparation of binary deep eutectic solvents.

#### **3.2. Preparation of Malonic acid- Glucose (MA-GLU) BDES**

The 1:1 mole ratio of Malonic acid and Glucose were taken in a beaker for the preparation of BDES, which was dissolved in water. Then excess water was allowed to evaporate by heating until the weight of the components remains constant <sup>[2]</sup>. Then the beaker was kept in a desiccator containing anhydrous calcium chloride for about two weeks to remove the water molecules if any were present and there was no turbidity formed during this period, then the prepared MA-GLU BDES was subjected to measure the physical properties.

#### **3.3. Preparation of Malonic acid- Fructose (MA-FRU) BDES**

The 1:1 mole ratio of Malonic acid and Fructose were taken in a beaker for the preparation of BDES which was dissolved in water. Then excess water was allowed to evaporate by heating until the weight of the components remains constant <sup>[2]</sup>. Then the beaker was kept in a desiccator containing anhydrous calcium chloride for about two weeks

to remove the water molecules if any were present and there was no turbidity formed during this period, then the prepared MA-FRU BDES was subjected to measure the physical properties.

### **3.4. Preparation of Malonic acid- Glycerol (MA-GCL) BDES**

For the preparation of MA-GCL BDES, a 1:1 mole ratio of malonic acid and glycerol was taken in a beaker, which was dissolved in water. Then it was allowed to evaporate the excess water molecules until the weight of the components remains constant [2]. The beaker was then placed in a desiccator with anhydrous calcium chloride for around two weeks to reduce any excess moisture particles and ensure that no turbidity appeared during this time. The generated MA-GCL BDES was then submitted to physical property measurements.

## **3.5. Results and Discussion**

### **3.5.1 Characterization of Malonic Acid- Glucose BDES**

#### **3.5.1.1 Density and Conductivity**

Density is an important property of any liquid. The density of the DESs was calculated at room temperature using a standard Pycnometer. By taking 5 ml of MA-GLU BDES, the mass was measured and the density of MA-GLU BDES was calculated as follows.

$$\text{Density} = \frac{\text{Mass}}{\text{Volume}}$$

The density of MA-GLU BDES is calculated as 1.018 g/cm<sup>3</sup>.

The conductivity of the prepared MA-GLU BDES was measured at room temperature by Systronics Conductivity Meter. The conductivity of BDES is highly affected by its viscosity and ion concentration [4, 5]. The conductivity decreases as viscosity of BDES increases [3, 5]. It is measured as 0.0012 mS/cm.



### 3.5.1.2 pH

The pH is an important physical parameter that has a considerable impact on chemical reactions. The influence of temperature on the pH of newly generated BDESs was investigated in this study. Fig.3.1.1 shows the effect of temperature on pH of MA-GLU BDES. The H-bonded interactions of malonic acid with the hydrogen bond donor, glucose, decrease as the temperature rises<sup>[6]</sup>. As a result, an increase in the number of free malonic acid molecules at higher temperatures could be the reason of an increase in acidic character of MA-GLU.

### 3.5.1.3 Viscosity

The interaction of molecules in a liquid mixture is reflected in viscosity<sup>[4]</sup>. The lower the viscosity of DES, the better it may be employed as a solvent<sup>[3]</sup>. Fig.3.1.2 shows the viscosity as a function of temperature for MA-GLU BDES. The viscosity of MA-GLU reduces as the temperature rises.

### 3.5.1.4 FTIR spectral analysis of MA-GLU

The FTIR spectrum of MA-GLU BDES is shown in fig.3.1.3. The broad peak at  $3440.64\text{cm}^{-1}$  revealed the presence of H-bonded alcoholic O–H groups<sup>[3]</sup>, the peaks at  $2978.53\text{ cm}^{-1}$  and  $2938.58\text{ cm}^{-1}$  in this spectrum are due to  $>\text{CH}_2$  stretching vibrations<sup>[7]</sup> of malonic acid and glucose. The broad peaks noticed between  $2500$  and  $3000\text{ cm}^{-1}$  showed the presence of H-bonded carboxylic O–H groups of Malonic acid<sup>[7]</sup>. The carboxylic C=O stretching in Malonic acid, the aldehydic C=O stretching in glucose are also involved in intramolecular H-bond formations, seen as a broad peak at  $1717\text{ cm}^{-1}$ <sup>[3, 7-9]</sup>. The O–H deformations of MA-GLU BDES are observed at  $1425.28\text{ cm}^{-1}$ <sup>[7, 10]</sup>. Further the peaks found at  $1300\text{ cm}^{-1}$  are assigned to C–O stretching of carboxylic groups of malonic acid<sup>[7]</sup>. The C–O stretching of alcoholic OH groups are observed at  $1013.59\text{ cm}^{-1}$  in MA-GLU

BDES <sup>[3]</sup>. The >CH<sub>2</sub> rocking and O–H out of plane bending vibrations of glucose are seen around 770 and 650 cm<sup>-1</sup> respectively <sup>[10]</sup>.

### 3.5.2 Characterization of Malonic Acid- Fructose BDES

#### 3.5.2.1 Density and Conductivity

The density of the DESs was calculated at room temperature using a standard Pycnometer. By taking 5 ml of MA-FRU BDES, the mass was measured, and the density of MA-FRU BDES was calculated as follows.

$$\text{Density} = \frac{\text{Mass}}{\text{Volume}}$$

The density of MA-FRU BDES is calculated as 1.127 g/cm<sup>3</sup>.

The conductivity of the prepared MA-FRU BDES was measured at room temperature by Systronics Conductivity Meter. The conductivity of BDES is highly affected by its viscosity and ion concentration <sup>[3, 4]</sup>. The conductivity decreases as the viscosity of BDES increases <sup>[3, 5]</sup>. It is measured as 0.0024 mS/cm.

#### 3.5.2.2 pH

Fig.3.2.1 shows the effect of temperature on pH of MA-FRU BDES. The H-bonded interactions of malonic acid with the hydrogen bond donor, fructose, decrease as the temperature rises <sup>[6]</sup>. As a result, an increase in the number of free malonic acid molecules at higher temperatures could be the reason for an increase in the acidic character of MA-FRU.

#### 3.5.2.3 Viscosity

Fig.3.2.2 shows the viscosity as a function of temperature for MA-FRU BDES. The viscosity of MA-FRU reduces as the temperature rises. The less viscous DES is, the better it may be used as a solvent <sup>[4]</sup>.

### 3.5.2.4 FTIR spectral analysis of MA-FRU

The FTIR spectrum of MA-FRU BDES is shown in fig.3.2.3. The broad peak at  $3443.36\text{cm}^{-1}$  is due to the presence of H-bonded alcoholic O–H groups [3], the peaks at  $2978.95\text{cm}^{-1}$  and  $2940.30\text{cm}^{-1}$  in this spectrum are due to  $>\text{CH}_2$  stretching vibrations [7] of malonic acid and fructose. The strong, broad peaks noticed between  $2500$  and  $3000\text{cm}^{-1}$  showed the presence of H-bonded carboxylic O–H groups of Malonic acid [7]. The O–H deformations of MA-FRU BDES are observed at  $1426.74\text{cm}^{-1}$  [7, 10]. Further the peaks found at  $1300\text{cm}^{-1}$  are assigned to C–O stretching of carboxylic groups of malonic acid [7]. The C–O stretching of alcoholic OH groups is observed at  $1014.63\text{cm}^{-1}$  in MA-FRU BDES [3]. The  $>\text{CH}_2$  rocking and O–H out-of-plane bending vibrations of fructose are seen around  $778$  and  $650\text{cm}^{-1}$  respectively [10].

### 3.5.3 Characterization of Malonic Acid- Glycerol (MA-GCL) BDES

#### 3.5.3.1 Density and Conductivity

The density of the MA-GCL BDESs was calculated at room temperature using a standard Pycnometer. The density of MA-GCL BDES was calculated after measuring the mass of 5 ml of MA-GCL BDES as follows.

$$\text{Density} = \frac{\text{Mass}}{\text{Volume}}$$

The density of MA-GCL BDES is calculated as  $1.252\text{g/cm}^3$ .

At room temperature, the conductivity of the developed MA-GCL BDES was measured using a Systronics Conductivity Meter. The viscosity and ion concentration of BDES have a significant impact on its conductivity [3, 4]. As the viscosity of BDES increases, the conductivity reduces [3, 5] hence the very high viscous BDES, MA-GCL has the lowest conductivity value of  $0.0002\text{mS/cm}$ .

### 3.5.3.2 pH

The effect of temperature on pH of MA-GCL BDES is shown in Fig.3.3.1. As the temperature rises, the H-bonded interactions of malonic acid decrease with the hydrogen bond donor, glycerol [6]. As a result, at higher temperatures, an increase in the number of free malonic acid molecules could be the reason for an increase in the acidic character of MA-GCL BDES.

### 3.5.3.3 Viscosity

Fig.3.3.2 shows the viscosity as a function of temperature for MA-GCL BDES. The viscosity of MA-GCL reduces as the temperature rises. The less viscous DES is, the better it may be used as a solvent [4]. High viscous DES is not ideal since it has limits [3, 11]. The application of DES with a high viscosity needs a higher temperature [3], which could reduce the viscosity of a particular DES [11]. MA-GCL BDES has high viscosity of 16111 mPa.s at room temperature. So, it is not suitable for applications at a temperature below 100°C.

### 3.5.3.4 FTIR spectral analysis of MA-GCL

The FTIR spectrum of MA-GCL BDES is shown in fig.3.3.3. The broad peak at 3500  $\text{cm}^{-1}$  is due to the presence of H-bonded alcoholic O–H groups [3], the peak at 2960.44  $\text{cm}^{-1}$  is due to  $> \text{CH}_2$  stretching vibrations [7] of malonic acid and fructose. The C = O stretching vibrations are seen as a broad peak in 1754.43  $\text{cm}^{-1}$ [3]. The O – H deformations of MA-GCL BDES are observed at 1411.22  $\text{cm}^{-1}$  [7, 10]. Further, the peaks found at 1342.55  $\text{cm}^{-1}$  are assigned to the C – O stretching of carboxylic groups of malonic acid [7]. The C – O stretching of alcoholic OH groups is observed at 1049.03  $\text{cm}^{-1}$  in MA-GCL BDES [3]. The  $>\text{CH}_2$  rocking and O –H out-of-plane bending vibrations of glycerol are seen around 787.89 and 652.27  $\text{cm}^{-1}$  respectively [10].

### **3.6 Conclusion**

The innovative MA-GLU, MA-FRU, and MA-GCL were successfully prepared at room temperature. The acidic nature of these BDESs reduces viscosity significantly below 100°C, and their conductivity makes them ideal solvents for supporting polar reactions as well as industrial uses. The high viscosity of MA-GCL BDES significantly below 100°C and low conductivity make it not suitable for solvent for supporting polar reactions as well as industrial uses.

## References

- [1]. Hai-Chuan Hu, Yu-Heng Liu, Bao-Le Li, Zhen-Shui Cui and Zhan-Hui Zhang; Deep eutectic solvent based on choline chloride and malonic acid as an efficient and reusable catalytic system for one-pot synthesis of functionalized pyrroles; *RSC Adv.*, 5, 7720-7728 (2015)
- [2]. Y.T. Dai, J. van Spronsen, G.J. Witkamp, R. Verpoorte, Y.H. Choi, Natural deep eutectic solvents as new potential media for green technology, *Anal. Chim. Acta* 766 (2013) 61 – 68. 1. <https://doi.org/10.1016/j.aca.2012.12.019>
- [3]. Koon-Kee Kow, Kamaliah Sirat, Novel manganese (II)-based deep eutectic solvents: Synthesis and physical properties analysis, *Chinese Chemical Letters*, 26 10 (2015) 1311 –1314. <https://doi.org/10.1016/j.ccllet.2015.05.049>.
- [4]. W. J. Guo, Y. C. Hou, S. H. Ren, S. D. Tian, W. Z. Wu, Formation of deep eutectic solvents by phenols and choline chloride and their physical properties, *J. Chem. Eng. Data* 58 (2013) 866 – 872. <https://doi.org/10.1021/je300997v>
- [5]. Q. H. Zhang, K. De Oliveira Vigier, S. Royer, F. Jérôme, Deep eutectic solvents: syntheses, properties, and applications, *Chem. Soc. Rev.* 41 (2012) 7108 – 7146. <https://doi.10.1039/C2CS35178A>
- [6]. Andrea Skulcova, Albert Russ, Michal Jablonsky, JozefSima, “pH of eutectic solvents,” *BioResources* 13(3), (2018) 5042 - 5051. <https://doi.10.15376/biores.13.3.5042-5051>
- [7]. Donlad L. Pavia, Gary M. Lampman, George S. Kriz, *Introduction to Spectroscopy*, 3rd Edition, BROOKS/COLE, Thomson Learning, USA, 2001.
- [8]. P.G. Ramesh, D. Ilangeswaran, Thermal and physical properties of L-Lysine based deep eutectic solvents, *International Journal of Advanced Scientific Research and Management*, Special Issue 4, 2019 (ICAMA-18), 100 – 104.

[9]. P.G. Ramesh, D. Ilangeswaran, Thermal and physical properties of some deep eutectic solvents, Springer Nature Switzerland AG 2019, Springer Proceedings in Materials: (ICON 2019), 2019, 1–8, [https://doi.org/10.1007/978-3-030-25135-2\\_4](https://doi.org/10.1007/978-3-030-25135-2_4)

[10]. B.D. Mistry, A Handbook of Spectroscopic Data, Oxford Book Company, India, 2009.

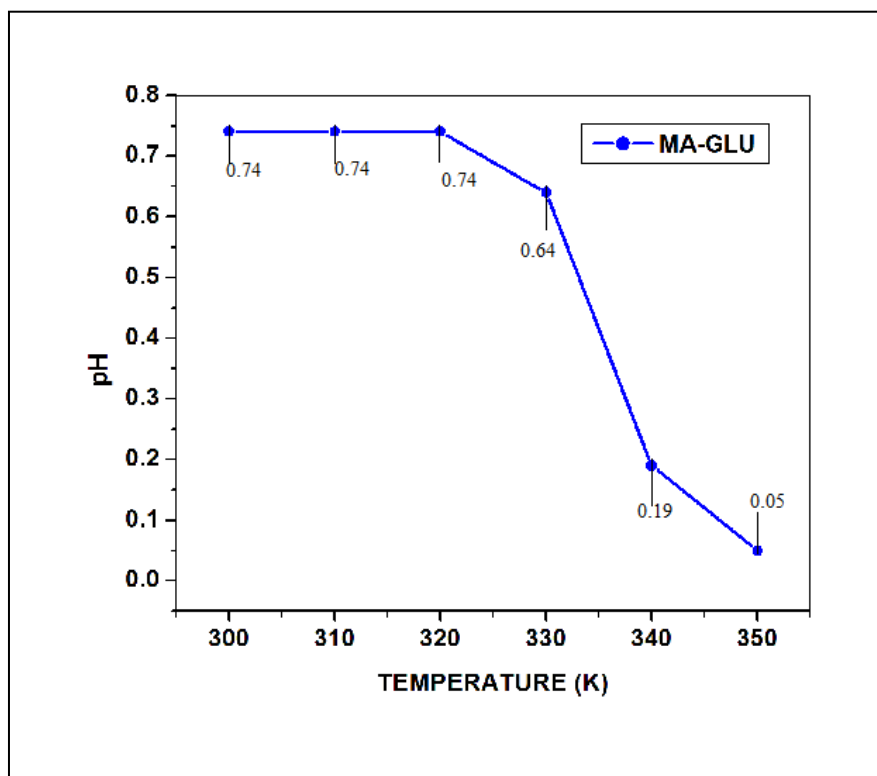


Figure 3.1.1 pH as a function against T of MA-GLU BDES

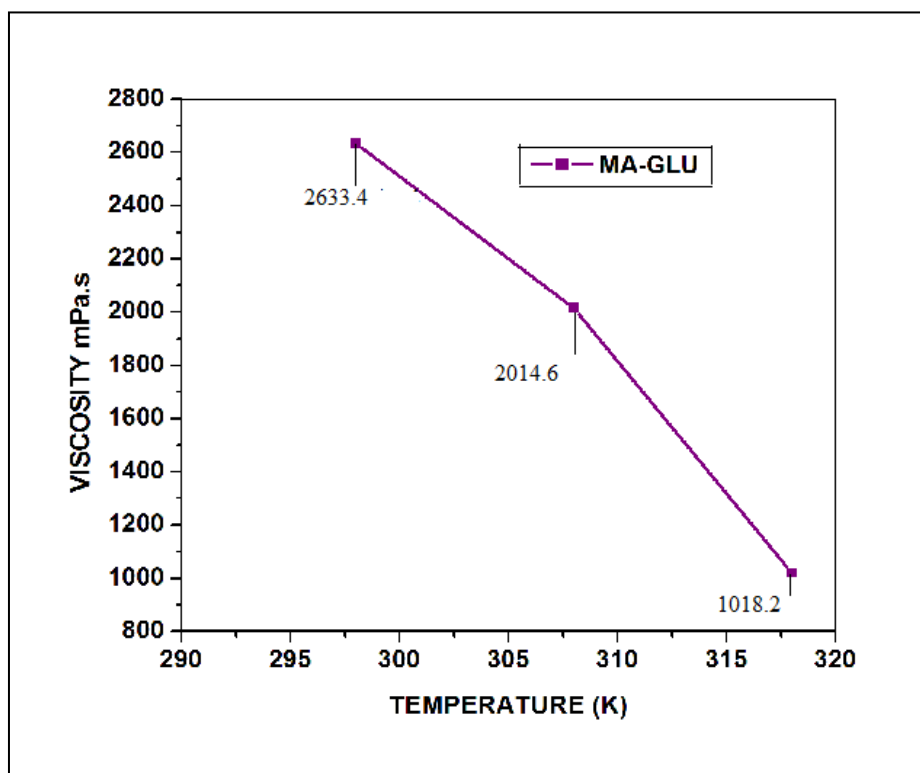


Figure 3.1.2 Viscosity of MA-GLU BDES at Different Temperatures



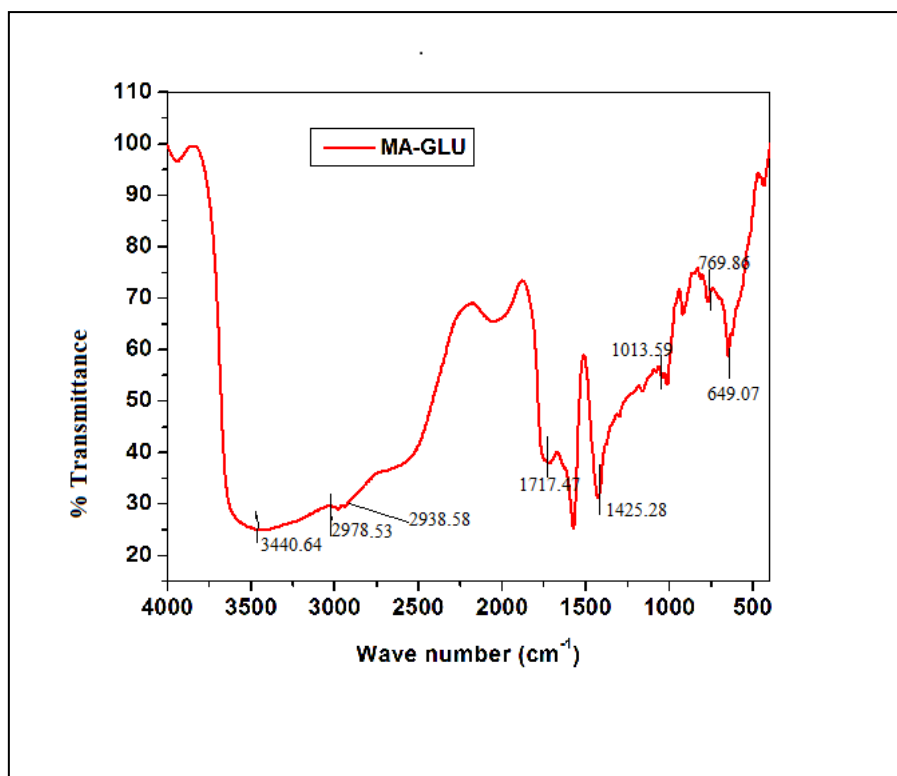


Figure 3.1.3 FTIR spectrum of MA-GLU BDES

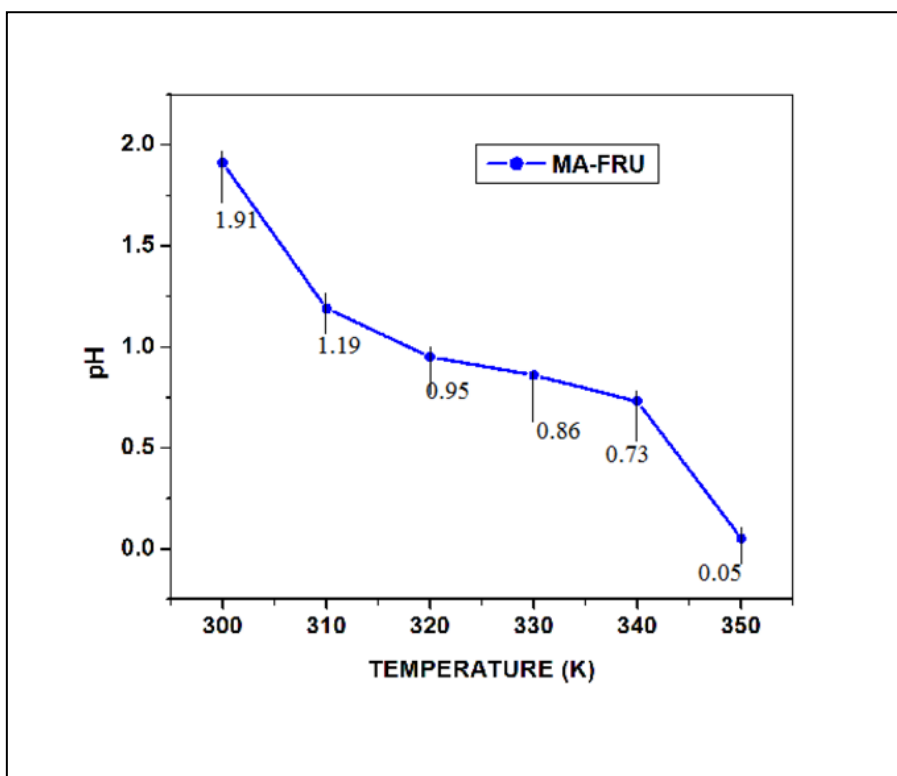


Figure 3.2.1 pH as a function against the temperature of MA-FRU BDES

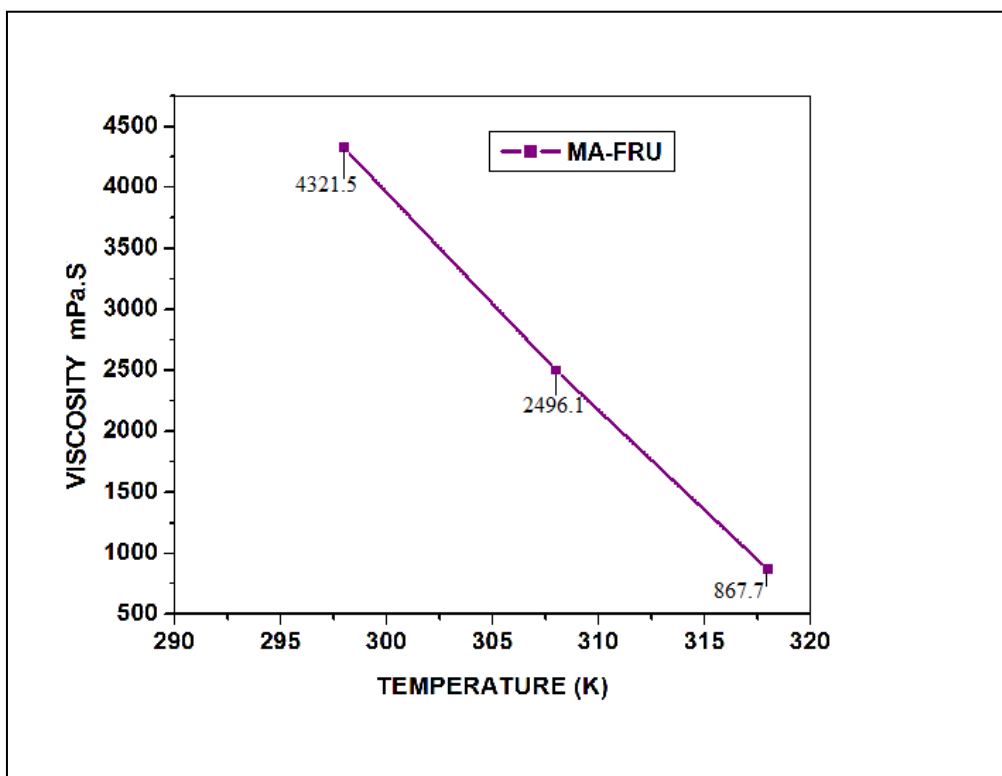


Figure 3.2.2 Viscosity of MA-FRU BDES at different temperatures

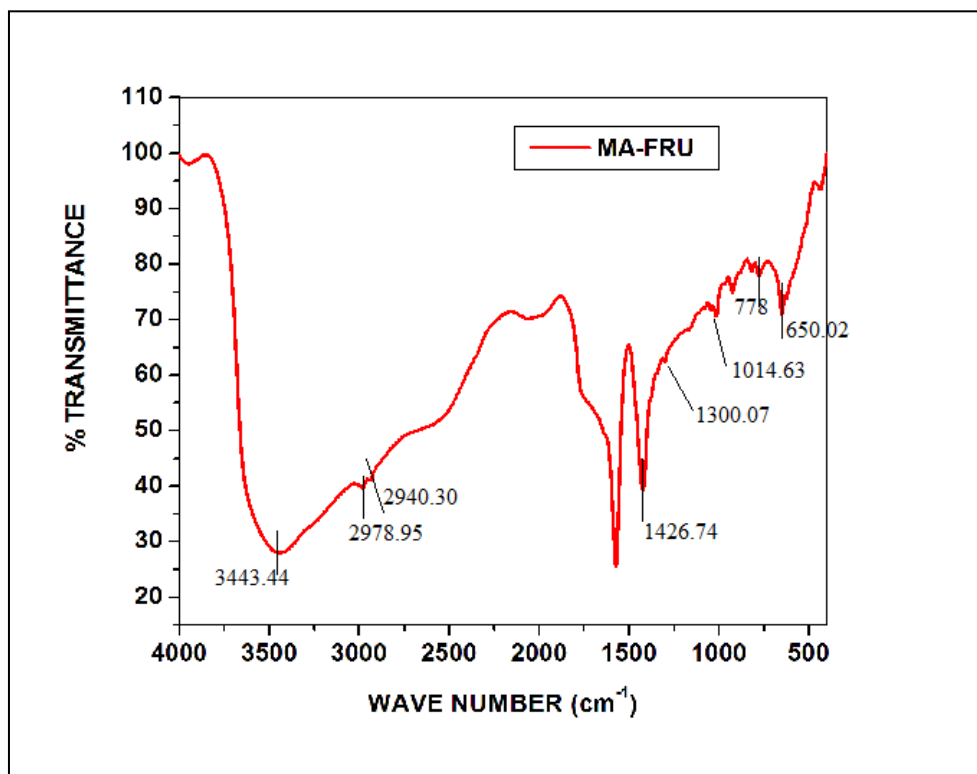


Figure 3.2.3 FTIR spectrum of MA-FRU BDES

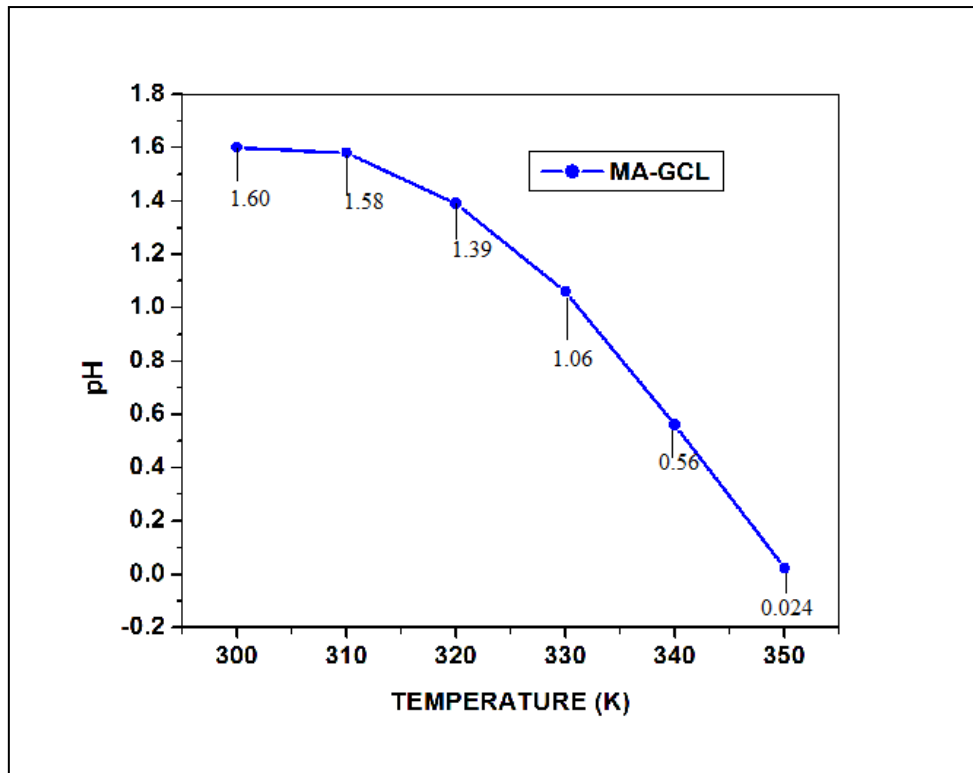


Figure 3.3.1 pH as a function against temperature of MA-GCL BDES

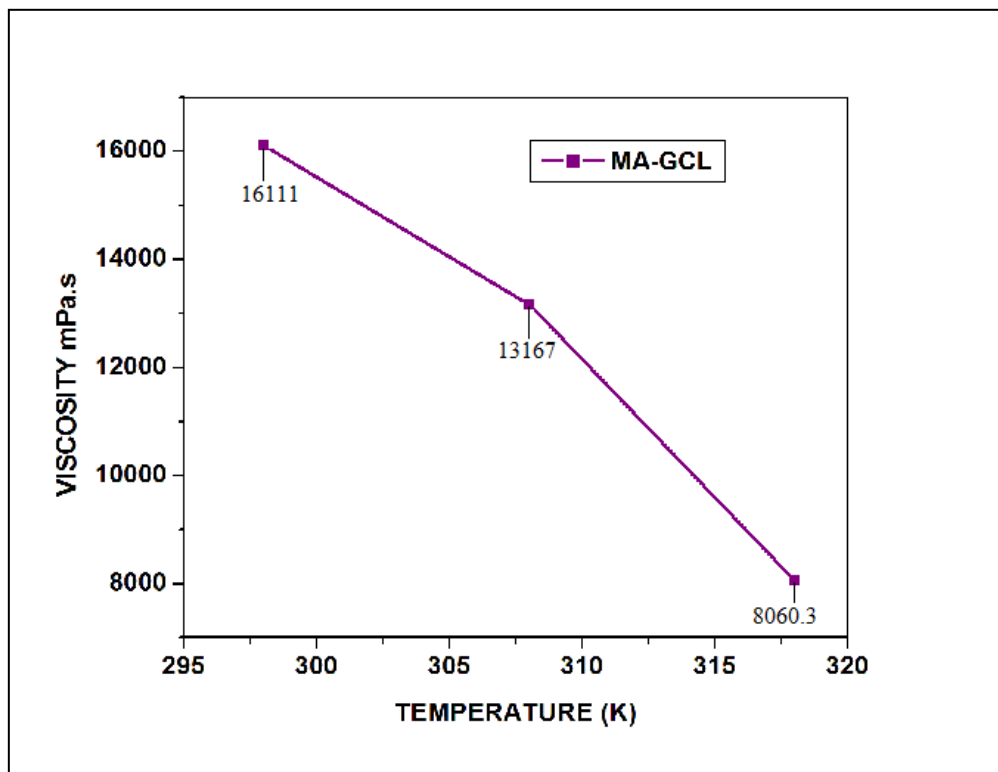
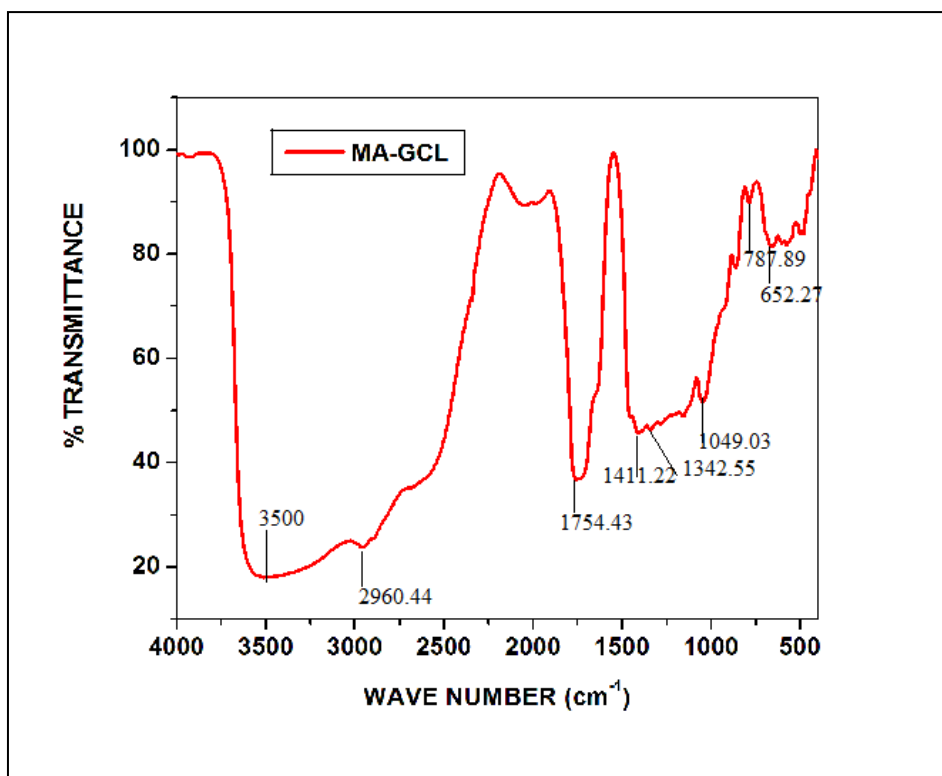


Figure 3.3.2 Viscosity of MA-GCL BDES at different temperatures



**Figure 3.3.3 FTIR spectrum of MA-GCL BDES**

## **4. Zinc chloride-based Binary Deep Eutectic Solvents**

---

### **4.1 Introduction**

Zinc (II) based metal chloride was used to make deep eutectic solvents (DESs). All the DESs that have been developed have good electrochemical characteristics. The DES electrochemical windows widen as the temperature rises. Different electrolysis techniques can use these DESs as electrolytes <sup>[1]</sup>. Abbott et al. were the first to introduce DESs based on choline chloride and zinc chloride as low-cost, readily available alternatives to ILs in synthesis <sup>[2]</sup>.

By mixing Zinc chloride with Glucose, Fructose, and Lactic acid separately, we were able to make three different forms of binary deep eutectic solvents. To make the BDESs, we used the evaporation method as reported by Dai. et.al <sup>[3]</sup>. The BDESs were then tested for physical properties like density, pH, conductivity, and viscosity. The FTIR spectra were used to find the hydrogen-bonded interactions amongst the compounds.

### **4.2. Preparation of Zinc chloride- Glucose (ZC-GLU) BDES**

For the preparation of BDES, a 1:1 mole ratio of zinc chloride and glucose was placed in a beaker, dissolved in water. The excess water molecules were allowed to evaporate by heating until the weight of the composition remains constant <sup>[3]</sup>. The synthesized ZC-GLU BDES was then placed in a desiccator containing anhydrous calcium chloride for around two weeks to eliminate any remaining water molecules and to ensure that no turbidity formed during this time. Then the prepared BDES was subjected to measure their physical properties.

### **4.3. Preparation of Zinc chloride- Fructose (ZC-FRU) BDES**

For the manufacture of BDES, a 1:1 mole ratio of zinc chloride and fructose was put in a beaker containing water to dissolve. The excess water molecules were allowed to

evaporate by heating until the weight of the composition remains constant <sup>[3]</sup>. The produced ZC-FRU BDES was then stored in a desiccator containing anhydrous calcium chloride for around two weeks to eliminate water molecules and to ensure that no turbidity formed during this time. Then the prepared BDES was subjected to measure their physical properties.

#### **4.4. Preparation of Zinc chloride- Lactic Acid (ZC-LA) BDES**

For the manufacture of BDES, a 1:1 mole ratio of zinc chloride and lactic acid was taken in a beaker, dissolved in water. The excess water molecules were allowed to evaporate by heating until the weight of the composition remains constant <sup>[3]</sup>. The newly developed ZC-LA BDES was then stored in a desiccator containing anhydrous calcium chloride for around two weeks to eliminate any remaining water molecules and to ensure that no turbidity formed during this time. Then the prepared BDES was subjected to measure their physical properties.

#### **4.5. Results and Discussion**

##### **4.5.1 Characterization of Zinc chloride- Glucose BDES**

###### **4.5.1.1 Density and Conductivity**

The density of a liquid is one of its most important properties. The densities of ionic liquids and DES are subjected to a great deal of uncertainty. The conductivity of newly generated Zinc chloride-based BDESs with hydrogen bond donors like Glucose is 0.06 mS/cm and the density is calculated by measuring its mass of volume 5 ml as 1.002 g/cm<sup>3</sup>. The viscosity and ion concentration of DES have a significant impact on its conductivity [4, 5].

###### **4.5.1.2 pH**

The pH is an important physical parameter that considerably impacts chemical reactions. The pH levels dropped as the temperature goes up. The influence of temperature

on the pH of freshly generated DESs was investigated in this study for ZC-GLU BDES, as shown in Fig.4.1.1. At room temperature (299 K), the DESs had an acidic pH, which reduces as the temperature rises <sup>[6]</sup>. The rise in acidic nature at higher temperatures could be due to an increase in the number of free zinc chloride molecules.

#### **4.5.1.3 Viscosity**

The interaction of molecules in a liquid mixture is indicated in the viscosity <sup>[7]</sup>. The lower the viscosity, the better the BDES as a solvent can be employed <sup>[3, 4]</sup>. Because of its limits, DES with higher viscosity is not recommended <sup>[3, 4]</sup>. The application of DES with a high viscosity necessitates a higher temperature <sup>[4]</sup> so that the viscosity of a particular DES can be reduced <sup>[8]</sup>. As a result, the viscosity of the prepared DESs is measured at various temperatures to determine their appropriate application. The viscosity of ZC-GLU was plotted Vs temperature in Fig.4.1.2. The viscosity of this solution reduces dramatically as the temperature rises.

#### **4.5.1.4 FTIR spectral analysis of ZC-GLU**

The broad peak found near  $3433.24\text{cm}^{-1}$  revealed the presence of H bonded alcoholic O – H groups, as shown in the FTIR spectra of ZC-GLU BDES <sup>[4]</sup> in Fig. 4.1.3. The CH<sub>2</sub> stretching vibrations of glucose create the peak at  $2939.39\text{cm}^{-1}$  in this spectrum <sup>[9]</sup>. They form strong intramolecular H bond interactions with Zn<sup>2+</sup> ions. The O – H deformations in DESs are measured at  $1422\text{cm}^{-1}$ <sup>[9, 10]</sup>, while the O – H out-of-plane bending vibration of glucose is measured at  $650\text{cm}^{-1}$ <sup>[10]</sup>. Metal interacting O – H deformations are responsible for the various peaks observed near  $800\text{cm}^{-1}$  <sup>[11]</sup>. These findings showed that zinc chloride and glucose can coexist due to H-bonded interactions.

## **4.5.2 Characterization of Zinc chloride- Fructose BDES**

### **4.5.2.1 Density and Conductivity**

One of the most significant qualities of a liquid is its density. ZC-FRU BDES has a conductivity of 0.012 mS/cm and a density of 1.125 g/cm<sup>3</sup>. The conductivity of DES is significantly affected by its viscosity and ion concentration [4, 5].

### **4.5.2.2 pH**

The pH is a critical physical parameter that influences chemical processes significantly. As the temperature was increased, the pH levels decreased. For ZC-FRU BDES, the effect of temperature on the pH of freshly formed DESs was examined, as shown in Fig.4.2.1. The DESs had an acidic pH at room temperature (299 K), which decreases as the temperature rises [6]. The increase in the number of free zinc chloride molecules at higher temperatures could be the cause of the acidic nature.

### **4.5.2.3 Viscosity**

The viscosity of a liquid mixture indicates the interaction of molecules [7]. The lower the viscosity, the more effectively BDES can be used as a solvent [3, 4]. Higher viscosity DES is not suggested due to its limitations [3, 4]. The use of DES with a high viscosity needs a higher temperature [4] to reduce the viscosity of a specific DES [8]. As a result, the viscosity of the prepared DESs is evaluated at different temperatures to determine their suitability for use. In Fig.4.2.2, the viscosity of ZC-FRU was plotted against temperature. As the temperature rises, the viscosity of this solution decreases considerably.

### **4.5.2.4 FTIR spectral analysis of ZC-FRU**

The existence of H bonded alcoholic O – H groups was shown by the broad peak of about 3438.54cm<sup>-1</sup>, as shown in the FTIR spectra of ZC-FRU BDES [4] in Fig. 4.2.3. The peaks at 2987.39 cm<sup>-1</sup> and 2931 cm<sup>-1</sup> in this spectrum are caused by the > CH<sub>2</sub> and CH<sub>3</sub> stretching vibrations of fructose [9]. With Zn<sup>2+</sup> ions, they create strong intramolecular H



bond connections. DESs have O – H deformations of  $1424.01\text{ cm}^{-1}$ <sup>[9, 10]</sup>, whereas fructose has an O – H out-of-plane bending vibration of  $650.37\text{ cm}^{-1}$ <sup>[10]</sup>. The multiple peaks detected near  $800\text{-}900\text{ cm}^{-1}$  are due to metal interacting O – H deformations <sup>[11]</sup>. Zinc chloride and fructose can coexist due to H-bonded interactions, according to these studies.

### **4.5.3 Characterization of Zinc chloride- Lactic Acid BDES**

#### **4.5.3.1 Density and Conductivity**

The density of a liquid is one of its most important characteristics. The conductivity of ZC-LA BDES is  $0.0046\text{ mS/cm}$ , and the density is  $1.325\text{ g/cm}^3$ . The viscosity and ion concentration of DES have a considerable impact on its conductivity <sup>[4, 5]</sup>. Because of its high viscosity, ZC-LA BDES has low conductivity.

#### **4.5.3.2 pH**

The pH is a critical physical parameter that considerably impacts chemical reactions. The pH levels dropped as the temperature was raised. The influence of temperature on the pH of freshly generated DESs in ZC-LA BDES was investigated, as shown in Fig.4. 3.1. At room temperature ( $299\text{ K}$ ), the DESs had an acidic pH, which lowers as the temperature rises <sup>[6]</sup>. The acidic character could be due to an increase in the quantity of free zinc chloride molecules at higher temperatures.

#### **4.5.3.3 Viscosity**

The interaction of molecules is indicated by the viscosity of a liquid mixture <sup>[7]</sup>. BDES can be utilized as a solvent more effectively with a lower viscosity <sup>[3, 4]</sup>. Due to its limits, higher viscosity DES is not encouraged <sup>[3, 4]</sup>. To reduce the viscosity of a certain DES <sup>[8]</sup>, a higher temperature <sup>[4]</sup> is required when using DES with a high viscosity. As a result, the viscosity of DES is measured at various temperatures to determine its appropriateness for application. The viscosity of ZC-LA was plotted against temperature in Fig.4.3.2. The viscosity of this solution reduces dramatically as the temperature rises.

Because of its high viscosity, zinc chloride is thought to have significant H-bond interactions with lactic acid.

#### 4.5.3.4 FTIR spectral analysis of ZC-LA

The broad peak of about  $3497.28\text{cm}^{-1}$  in the FTIR spectra of ZC-LA BDES <sup>[4]</sup> in Fig. 4.3.3 demonstrated the presence of H bonded alcoholic OH groups. The  $\text{CH}_3$  and  $>\text{CH}_2$  stretching vibration of lactic acid create the peak at  $2942\text{ cm}^{-1}$  in this spectrum <sup>[9]</sup>. Lactic acid has a carboxylic  $\text{C} = \text{O}$  stretching at  $1730.40\text{ cm}^{-1}$ <sup>[30]</sup>. They form strong intramolecular H bond interactions with  $\text{Zn}^{2+}$  ions. The O – H deformations of DESs are  $1455.72\text{ cm}^{-1}$ <sup>[9, 10]</sup>, whereas the O – H out-of-plane bending vibration of lactic acid is  $650\text{ cm}^{-1}$ <sup>[10]</sup>. The multiple peaks detected near  $811.01\text{ cm}^{-1}$  are due to metal interacting O – H deformations <sup>[11]</sup>. According to research, zinc chloride and lactic acid can coexist due to H-bonded interactions.

#### 4.6 Conclusion

The preparation of three types of novel room-temperature binary deep eutectic solvents based on zinc chloride was successful. DESs are ideal solvents for encouraging polar reactions as well as industrial applications due to their acidic character, significantly less viscosity below  $100^\circ\text{C}$ , and conductivity. Because of its high viscosity, ZC-LA BDES requires a high temperature and is difficult to utilize at room temperature.

## References

- [1]. Fatemeh Sm Ghareh Bagh, Kavehshahbaz, Farouq S. Mjalli, Mohd A. Hashim, Inas M. AlNashef; Zinc (II) chloride-based deep eutectic solvents for application as electrolytes: preparation and characterization *Journal of Molecular Liquids*, 2015.
- [2]. Deep Eutectic Solvents Formed between Choline Chloride and Carboxylic Acids: Versatile Alternatives to Ionic Liquids; Abbott, A. P.; Capper, G.; Davies, D. L.; Rasheed, R.; Tambyrajah, *J. Am. Chem. Soc.* 2004, 126, 29, 9142–9147
- [3]. Y. T. Dai, J. van Spronsen, G.J. Witkamp, R. Verpoorte, Y.H. Choi, Natural deep eutectic solvents as new potential media for green technology, *Anal. Chim. Acta* 766 (2013) 61 – 68. 1. <https://doi.org/10.1016/j.aca.2012.12.019>
- [4]. Koon-Kee Kow, Kamaliah Sirat, Novel manganese (II)-based deep eutectic solvents: Synthesis and physical properties analysis, *Chinese Chemical Letters*, 26 10 (2015) 1311 –1314. <https://doi.org/10.1016/j.ccllet.2015.05.049>.
- [5]. W. J. Guo, Y. C. Hou, S. H. Ren, S. D. Tian, W. Z. Wu, Formation of deep eutectic solvents by phenols and choline chloride and their physical properties, *J. Chem. Eng. Data* 58 (2013) 866 – 872. <https://doi.org/10.1021/je300997v>
- [6]. Andrea Skulcova, Albert Russ, Michal Jablonsky, JozefSima, “pH of eutectic solvents,” *BioResources* 13(3), (2018) 5042 - 5051. <https://doi.10.15376/biores.13.3.5042-5051>
- [7]. W. J. Guo, Y. C. Hou, S. H. Ren, S. D. Tian, W. Z. Wu, Formation of deep eutectic solvents by phenols and choline chloride and their physical properties, *J. Chem. Eng. Data* 58 (2013) 866 – 872. <https://doi.org/10.1021/je300997v>
- [8]. Hayyan, M., Mjalli, F. S., Hashim, M. A., & Alnashef, I. M. An investigation of the reaction between 1-butyl-3-methylimidazolium trifluoromethanesulfonate and superoxide

ion. Journal of Molecular Liquids, 181, 44-50. (2013)

<https://doi.org/10.1016/j.molliq.2013.02.001>

[9]. Donald L. Pavia, Gary M. Lampman, George S. Kriz, Introduction to Spectroscopy, 3rd Edition, BROOKS/COLE, Thomson Learning, USA, 2001.

[10]. B.D. Mistry, A Handbook of Spectroscopic Data, Oxford Book Company, India, 2009.

[11]. George Socrates, "Infrared and Raman Characteristic Group Frequencies Tables and Charts", Third Edition, JOHN WILEY & SONS, LTD, 2001, (Reprinted as Paperback January and October 2004), 324.

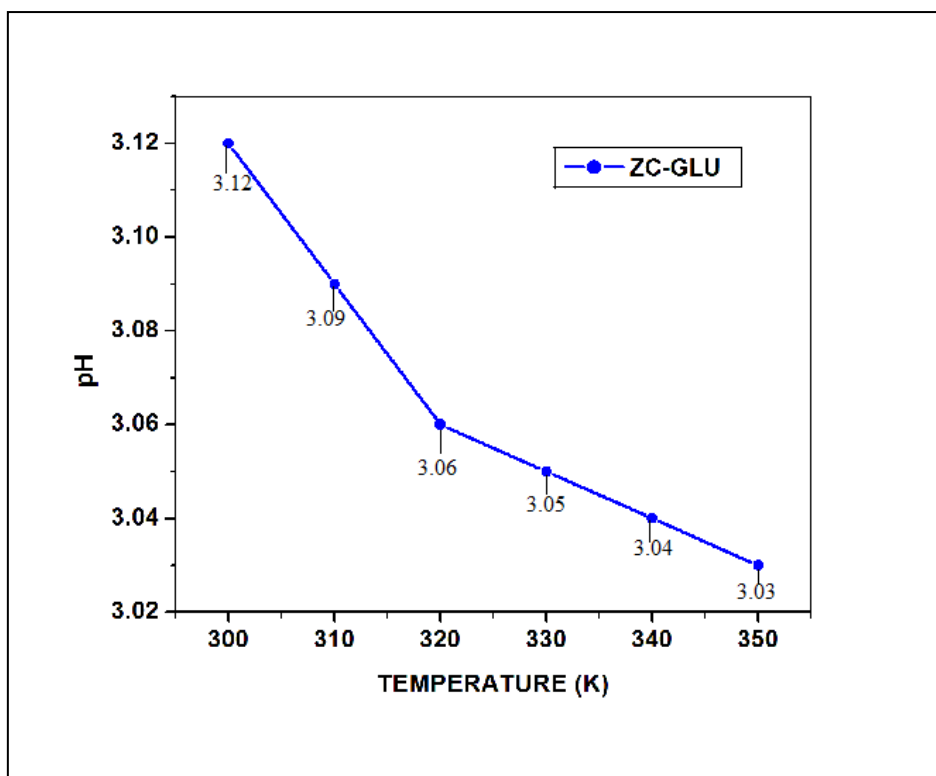


**Figure 4.1.1 pH as a function against T of ZC-GLU BDES**

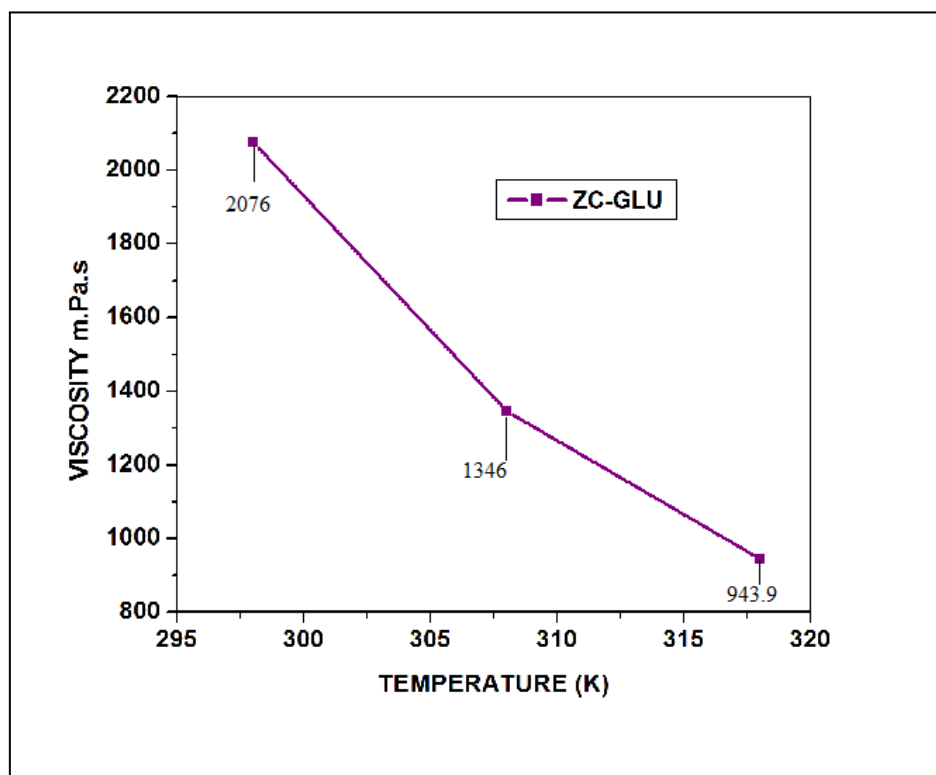


**Figure 4.1.2 Viscosity of ZC-GLU BDES at Different Temperatures**

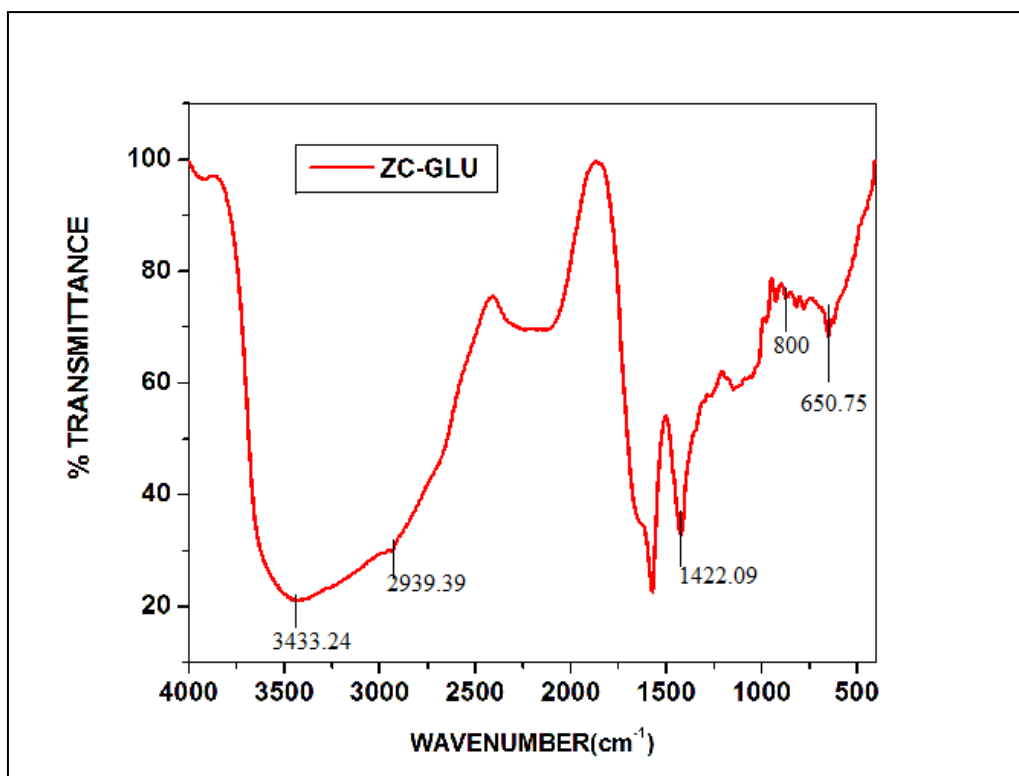


Figure 4.1.3 FTIR spectrum of ZC-GLU BDES

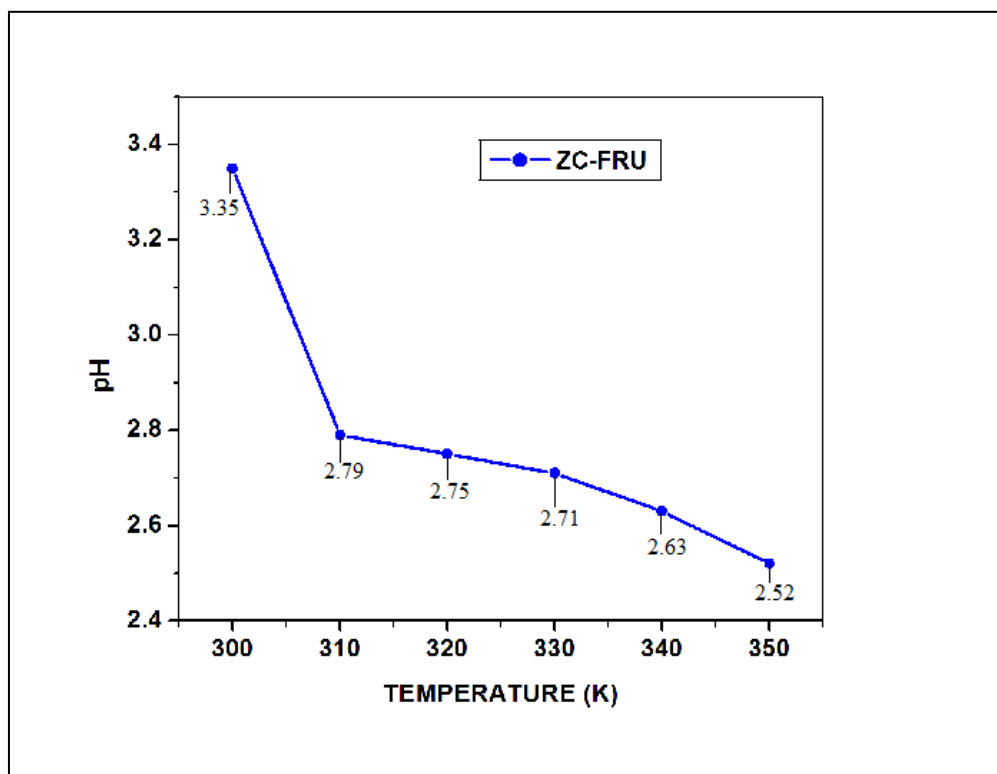


Figure 4.2.1 pH as a function against T of ZC-FRU BDES

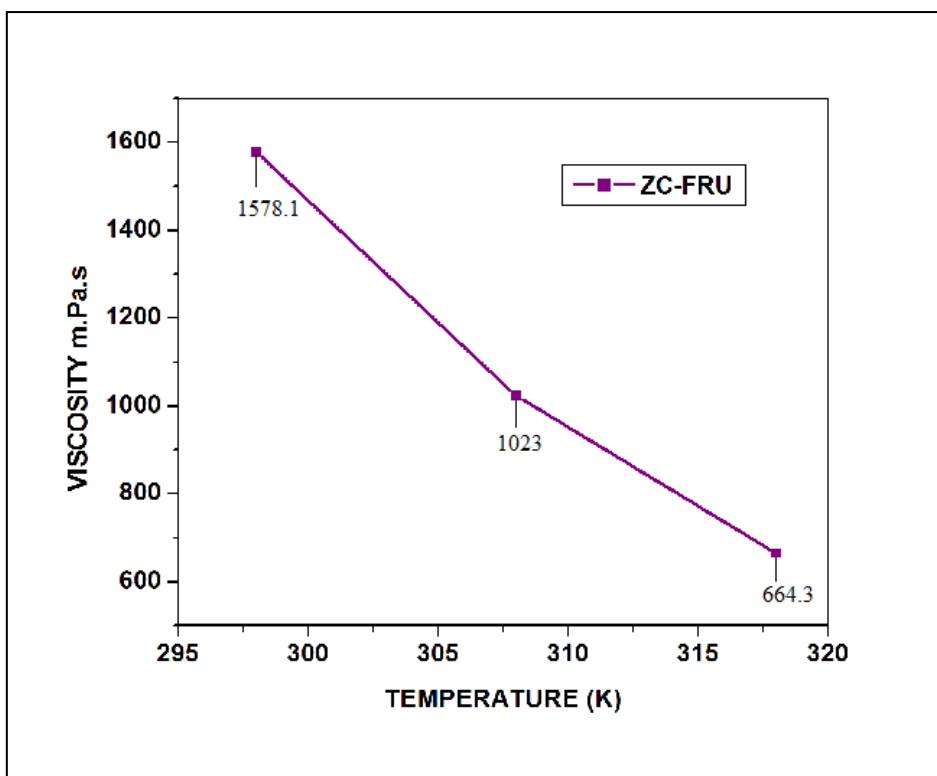


Figure 4.2.2. Viscosity of ZC-FRU BDES at Different Temperatures

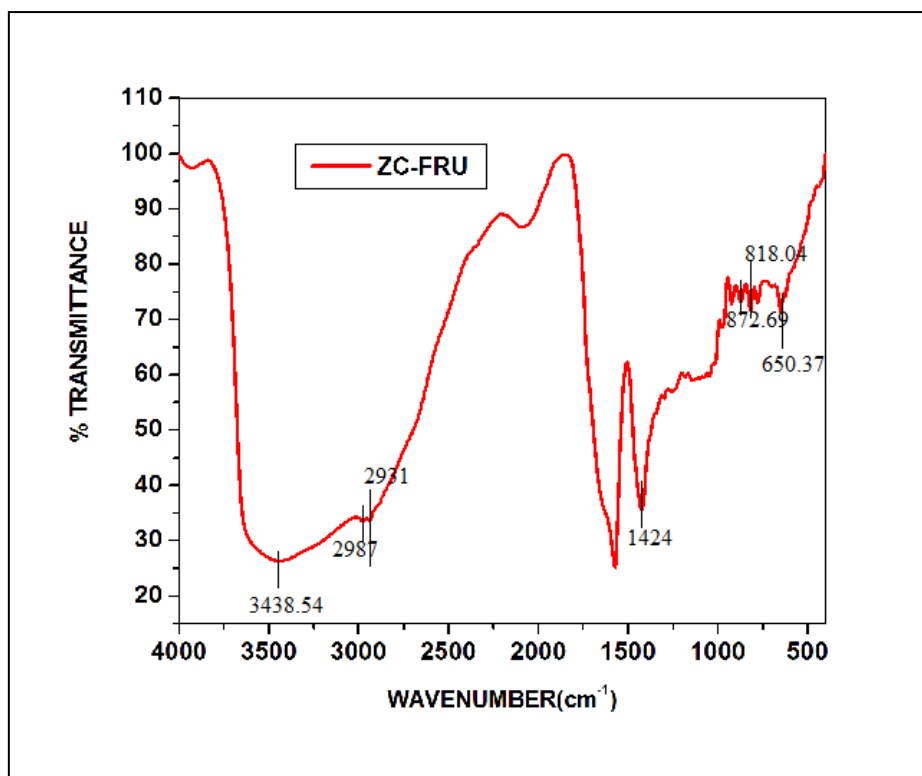
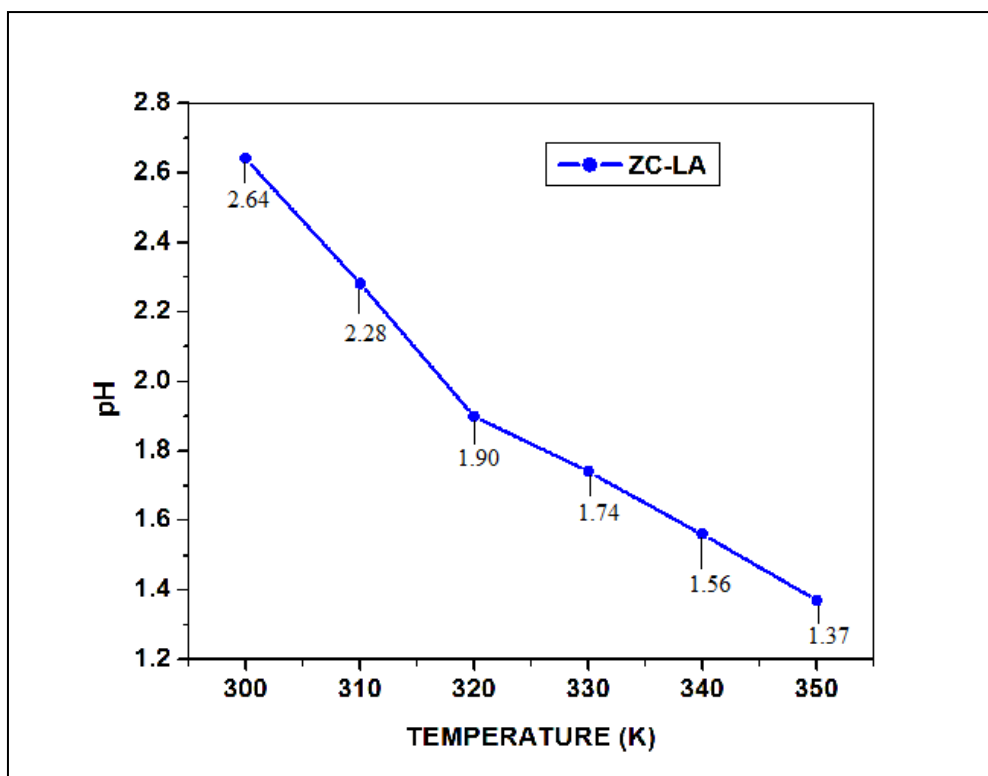
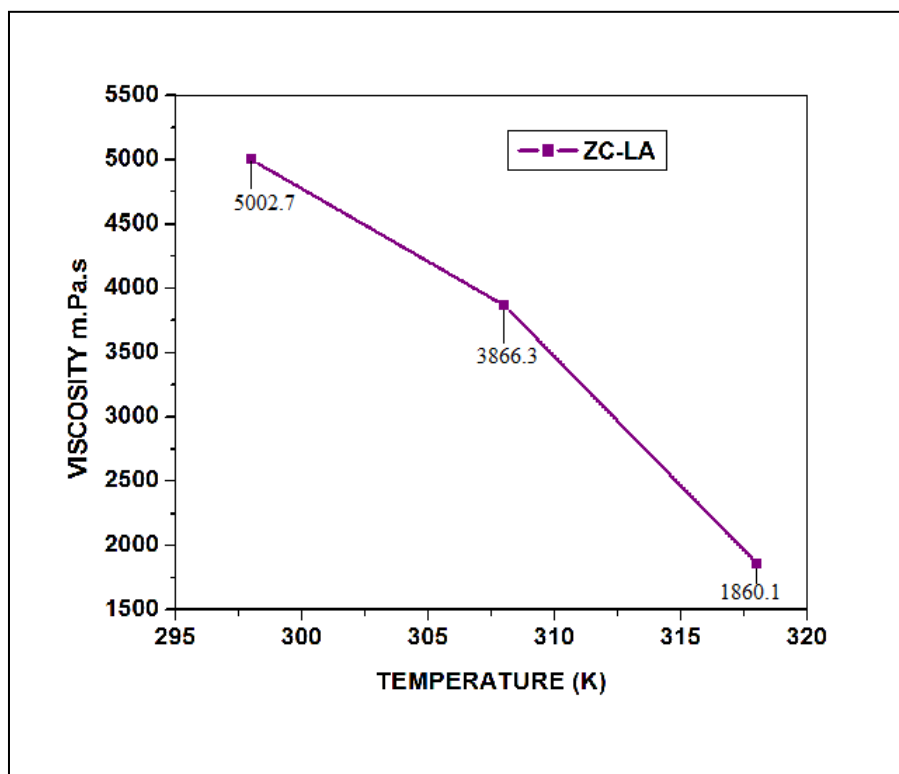


Figure 4.2.3 FTIR spectrum of ZC-FRU BDES



**Figure 4.3.1 pH as a function against T of ZC-LA BDES**



**Figure 4.3.2. Viscosity of ZC-LA BDES at Different Temperatures**



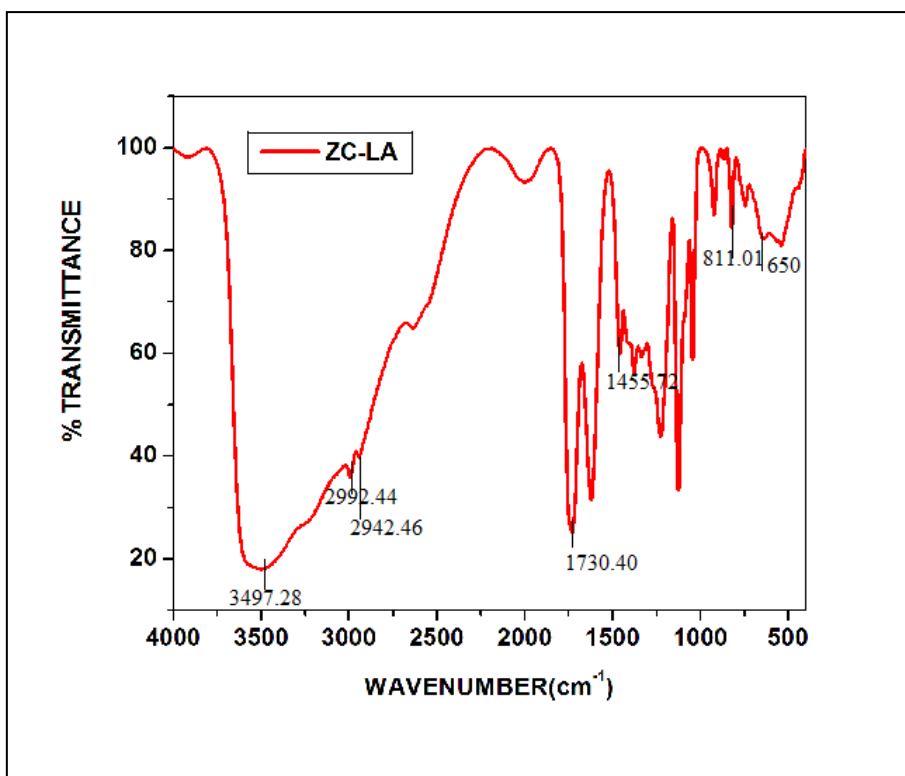


**Figure 4.3.3 FTIR spectrum of ZC-LA BDES**



## 5. Manganese chloride-based Binary Deep Eutectic Solvents

---

### 5.1 Introduction

The generation of metal-based eutectics from metal salts in combination with various hydrogen-bond donors (HBDs) is known as Type IV deep eutectic solvent (DES)<sup>[1]</sup>. The evaporation method was utilized to synthesize potential BDESs in this investigation. The successfully produced BDESs were characterized using physical properties like density, pH, viscosity, and conductivity studies. As revealed in this study, three novel manganese chloride-based BDESs were successfully synthesized.

### 5.2. Preparation of Manganese chloride- Glucose (MC-GLU) BDES

For the preparation of BDES, a 1:1 mole ratio of manganese chloride and glucose was placed in a beaker, dissolved in water. The mixture was allowed to evaporate by heating on a hot water bath until all the weight of components remains constant<sup>[2]</sup> so that excess water molecules are getting removed. The synthesized MC-GLU BDES was then placed in a desiccator containing anhydrous calcium chloride for around two weeks to eliminate any remaining water molecules and to ensure that no turbidity formed during this time. Then the prepared BDES was subjected to measure their physical properties.

### 5.3. Preparation of Manganese chloride- Fructose (MC-FRU) BDES

For the manufacture of BDES, a 1:1 mole ratio of manganese chloride and fructose was put in a beaker containing water to dissolve. The mixture was allowed to evaporate by heating on a hot water bath until all the weight of components remains constant<sup>[2]</sup> so that excess water molecules are getting removed. The produced MC-FRU BDES was then stored in a desiccator containing anhydrous calcium chloride for around two weeks to eliminate water molecules and to ensure that no turbidity formed during this time. Then the prepared BDES was subjected to measure their physical properties.

#### **5.4. Preparation of Manganese chloride- citric Acid (MC-CA) BDES**

For the manufacture of BDES, a 1:1 mole ratio of manganese chloride and citric acid was taken in a beaker, dissolved in water. The mixture was allowed to evaporate by heating on a hot water bath until all the weight of components remains constant <sup>[2]</sup> so that excess water molecules are getting removed. The newly developed MC-CA BDES was then stored in a desiccator containing anhydrous calcium chloride for around two weeks to eliminate any remaining water molecules. But the prepared BDES crystallized, and it was subjected to test the solubility in both aqueous and non-aqueous solvents. The crystals were dissolved in all the above-mentioned solvents, and it was confirmed that it was not stable.

#### **5.5. Results and Discussion**

##### **5.5.1 Characterization of Manganese chloride- Glucose (MC-GLU) BDES**

###### **5.5.1.1 Density and Conductivity**

The density of a liquid is one of its most important properties. The densities of ionic liquids and DES are subjected to a great deal of uncertainty. The conductivity of newly generated Manganese chloride-based BDESs with hydrogen bond donors like Glucose is 0.165 mS/cm and the density is calculated by measuring its mass of volume 5 ml as 1.123 g/cm<sup>3</sup>. The viscosity and ion concentration of DES have a significant impact on its conductivity <sup>[1, 3]</sup>.

###### **5.5.1.2 pH**

The pH is an important physical parameter that considerably impacts chemical reactions. The pH levels dropped as the temperature goes up. The influence of temperature on the pH of freshly generated DESs was investigated in this study for MC-GLU BDES, as shown in Fig.5.1.1. At room temperature (299 K), the DESs had an acidic pH, which reduces as the temperature rises <sup>[4]</sup>. The rise in acidic nature at higher temperatures could be due to an increase in the number of free manganese chloride molecules.

### **5.5.1.3 Viscosity**

The interaction of molecules in a liquid mixture is indicated in the viscosity <sup>[5]</sup>. The lower the viscosity, the better the BDES as a solvent can be employed <sup>[1, 2]</sup>. Because of its limits, DES with higher viscosity is not recommended <sup>[1, 2]</sup>. The application of DES with a high viscosity necessitates a higher temperature <sup>[1]</sup> so that the viscosity of a particular DES can be reduced <sup>[6]</sup>. As a result, the viscosity of the prepared DESs is measured at various temperatures to determine their appropriate application. The viscosity of MC-GLU was plotted Vs temperature in Fig.5.1.2. The viscosity of this solution reduces dramatically as the temperature rises.

## **5.5.2 Characterization of Manganese chloride- Fructose (MC-FRU) BDES**

### **5.5.2.1 Density and Conductivity**

One of the most significant qualities of a liquid is its density. MC-FRU BDES has a conductivity of 0.062 mS/cm and a density of 1.002 g/cm<sup>3</sup>. The conductivity of DES is significantly affected by its viscosity and ion concentration <sup>[1, 3]</sup>.

### **5.5.2.2 pH**

The pH is a critical physical parameter that influences chemical processes significantly. As the temperature was increased, the pH levels decreased. For MC-FRU BDES, the effect of temperature on the pH of freshly formed DESs was examined, as shown in Fig.5.2.1. The DESs had an acidic pH at room temperature (299 K), which decreases as the temperature rises <sup>[4]</sup>. The increase in the number of free zinc chloride molecules at higher temperatures could be the cause of the acidic nature.

### **5.5.2.3 Viscosity**

The viscosity of a liquid mixture indicates the interaction of molecules <sup>[5]</sup>. The lower the viscosity, the more effectively BDES can be used as a solvent <sup>[1, 2]</sup>. Higher viscosity DES is not suggested due to its limitations <sup>[1, 2]</sup>. The use of DES with a high

viscosity needs a higher temperature <sup>[3]</sup> to reduce the viscosity of a specific DES <sup>[6]</sup>. As a result, the viscosity of the prepared DESs is evaluated at different temperatures to determine their suitability for use. In Fig.5.2.2, the viscosity of MC-FRU was plotted against temperature. As the temperature rises, the viscosity of this solution decreases considerably.

## **5.6. Conclusion**

Three manganese chloride-based binary deep eutectic solvents were prepared. The physical properties such as density, pH, conductivity, and viscosity were measured for the prepared BDESs. The FTIR characterization of the BDESs was not studied. The MC-CA BDES crystallized, and it is not stable.

## References

- [1]. Koon-Kee Kow, Kamaliah Sirat, Novel manganese (II)-based deep eutectic solvents: Synthesis and physical properties analysis, *Chinese Chemical Letters*, 26 10 (2015) 1311–1314. <https://doi.org/10.1016/j.ccllet.2015.05.049>.
- [2]. Y.T. Dai, J. van Spronsen, G.J. Witkamp, R. Verpoorte, Y.H. Choi, Natural deep eutectic solvents as new potential media for green technology, *Anal. Chim. Acta* 766 (2013) 61 – 68. <https://doi.org/10.1016/j.aca.2012.12.019>
- [3]. W. J. Guo, Y. C. Hou, S. H. Ren, S. D. Tian, W. Z. Wu, Formation of deep eutectic solvents by phenols and choline chloride and their physical properties, *J. Chem. Eng. Data* 58 (2013) 866 – 872. <https://doi.org/10.1021/je300997v>
- [4]. Andrea Skulcova, Albert Russ, Michal Jablonsky, JozefSima, “pH of eutectic solvents,” *BioResources* 13(3), (2018) 5042 - 5051. <https://doi.10.15376/biores.13.3.5042-5051>
- [5]. W. J. Guo, Y. C. Hou, S. H. Ren, S. D. Tian, W. Z. Wu, Formation of deep eutectic solvents by phenols and choline chloride and their physical properties, *J. Chem. Eng. Data* 58 (2013) 866 – 872. <https://doi.org/10.1021/je300997v>
- [6]. Hayyan, M., Mjalli, F. S., Hashim, M. A., & Alnashef, I. M. An investigation of the reaction between 1-butyl-3-methylimidazolium trifluoromethanesulfonate and superoxide ion. *Journal of Molecular Liquids*, 181, 44-50. (2013) <https://doi.org/10.1016/j.molliq.2013.02.001>

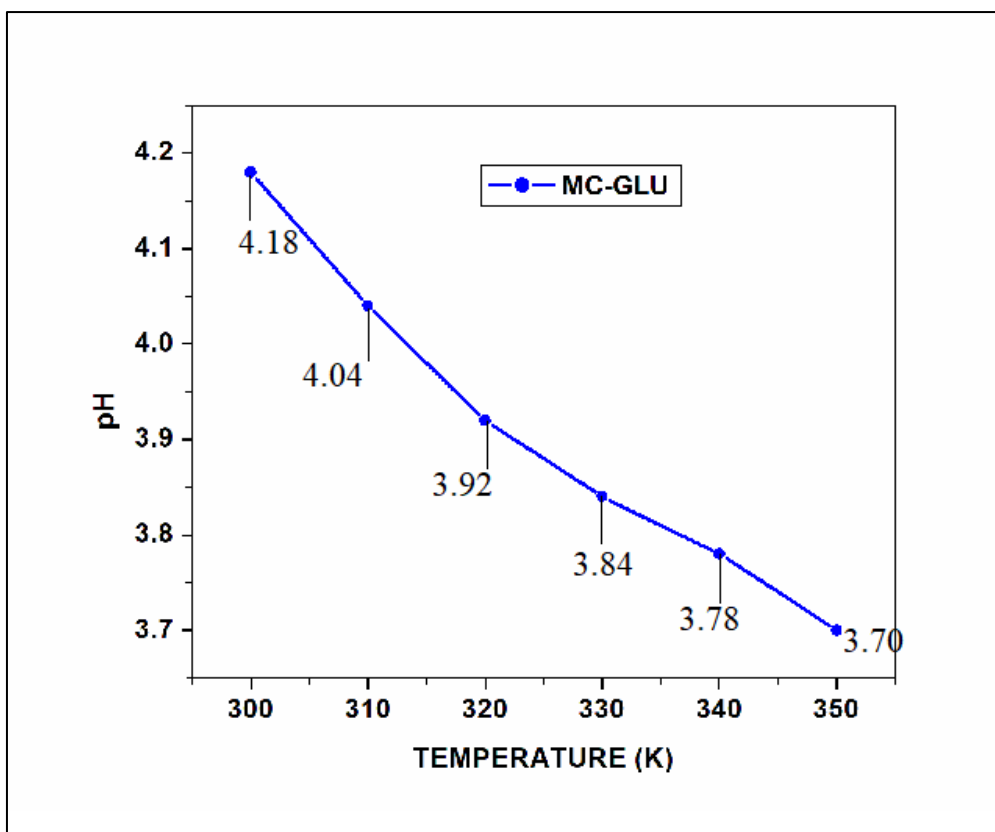


Figure 5.1.1 pH as a function against T of MC-GLU BDES

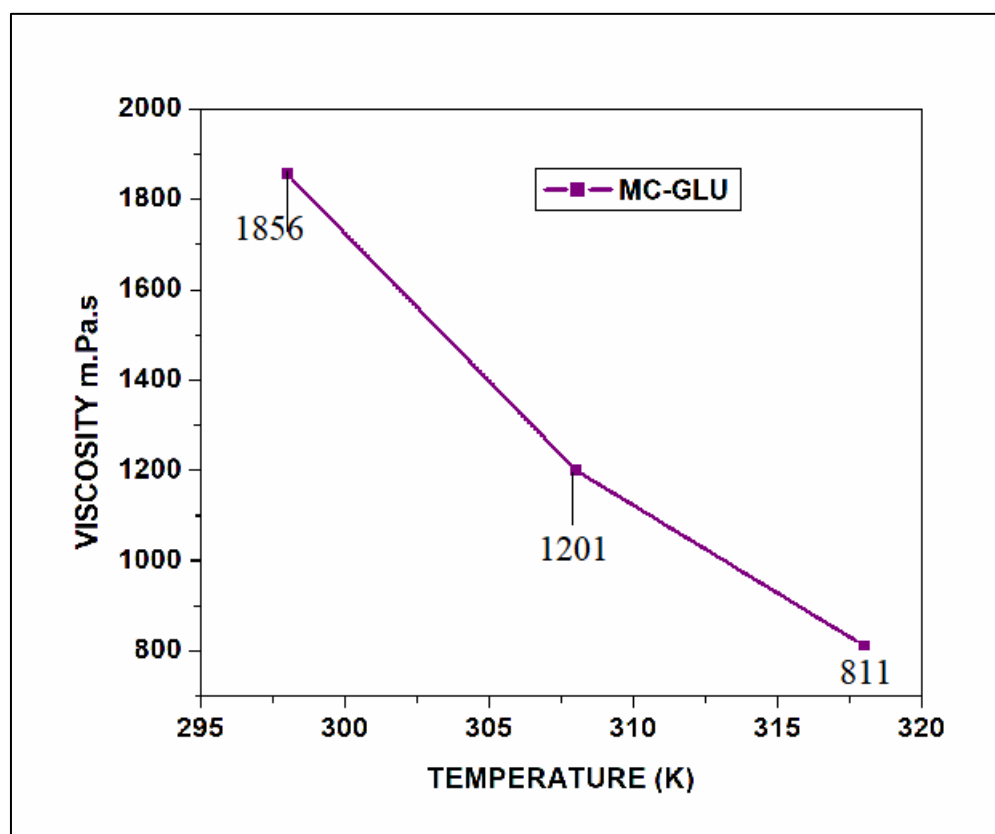


Figure 5.1.2 Viscosity of MC-GLU BDES at Different Temperatures



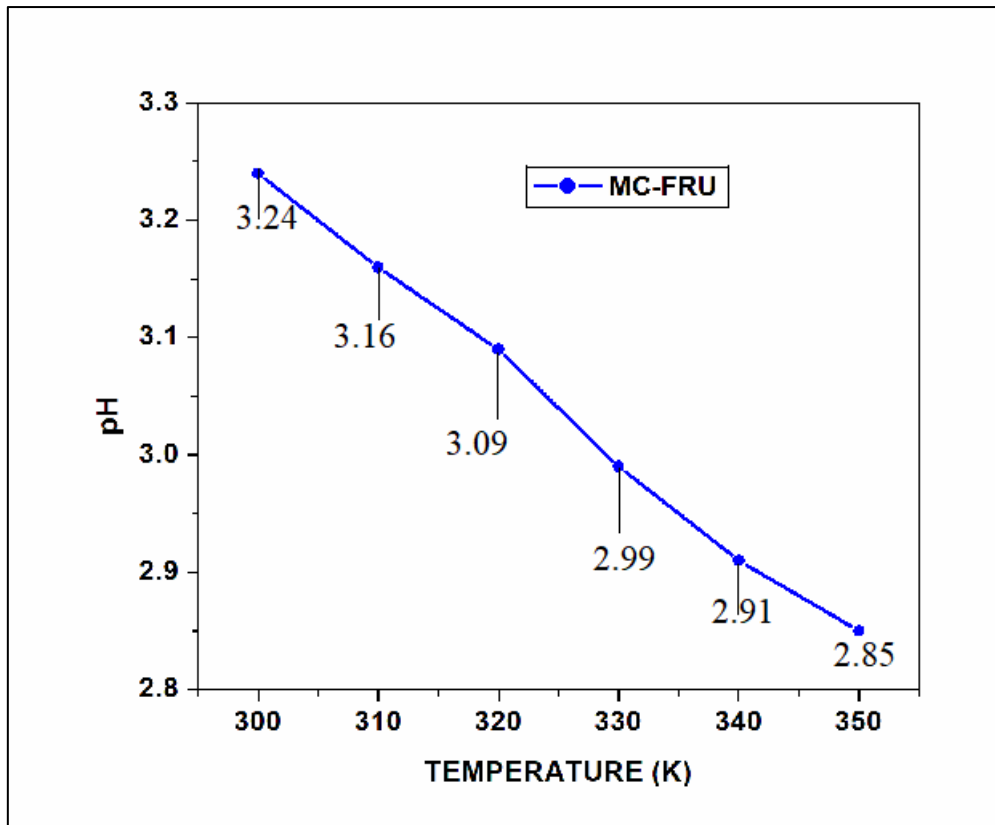


Figure 5.2.1 pH as a function against T of MC-FRU BDES

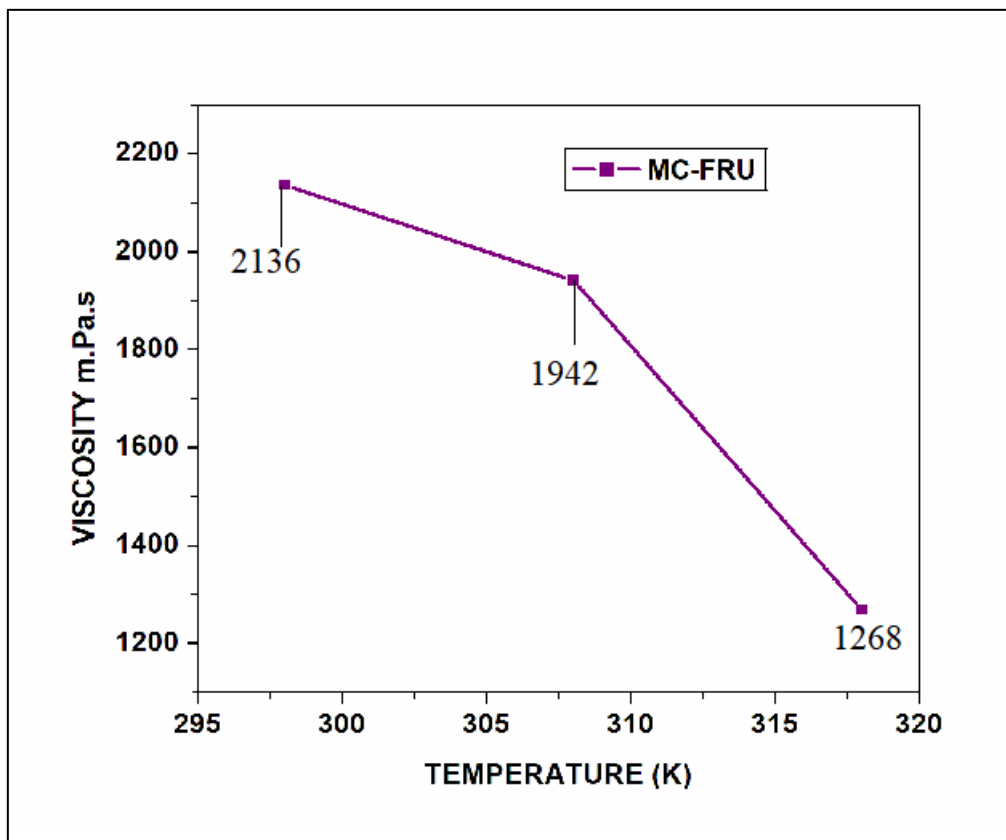


Figure 5.2.2 Viscosity of MC-FRU BDES at Different Temperatures



## 6. Malonic acid-based Ternary Deep Eutectic Solvents (TDES)

---

### 6.1 Introduction

The conventional DES is a binary deep eutectic solvent consisting of only two components (BDES). The designable property of the ternary deep eutectic solvent (TDES) was significantly improved when a third component was added. To date, TDES has been synthesized and employed in several applications <sup>[1-3]</sup>. Bengi Taysun et.al used choline chloride, citric acid, and glycerol to make a ternary deep eutectic solvent <sup>[4]</sup>. The effect of adding glycerol was studied using measurements of freezing point, density, viscosity, conductivity, and pH <sup>[4]</sup>. TDES is more thermally stable than BDES and has a greater free volume, making it a good potential for high-temperature absorption. The TDES is expected to be capable of large-scale industrial applications due to its environmentally friendly preparation technique <sup>[1]</sup>.

By mixing Malonic acid with Glucose/Fructose and amino acids such as Glutamine, Glycine, and Histidine separately, we were able to make six different types of Malonic acid-based ternary deep eutectic solvents. To make the TDESs, we used the evaporation method <sup>[5]</sup> described by Dai et al. The physical parameters of the TDESs were then measured, including density, pH, conductivity, and viscosity. The hydrogen-bonded interactions amongst the components used to make ternary deep eutectic solvents were characterized by FTIR.

### 6.2. Preparation of Malonic acid- Glucose- Glutamine (MA-GLU-GLUT) TDES

Malonic acid, glucose, and glutamine at a 1:1:1 mole ratio were dissolved in double-distilled water and allowed to evaporate the water in a water bath till the constant weight was attained <sup>[5]</sup>. The obtained mixtures were kept in desiccators containing anhydrous CaCl<sub>2</sub> for about two weeks. As no turbidity developed during this time, the ternary DESs

were subjected to measure physical properties such as density, pH, conductivity, and viscosity. The H-bonded interactions between the components were characterized using FTIR.

### **6.3. Preparation of Malonic acid- Fructose- Glutamine (MA-FRU-GLUT) TDES**

At a 1:1:1 mole ratio, malonic acid, fructose, and glutamine are dissolved in double distilled water and allowed to evaporate in a water bath until the weight of the components remains constant <sup>[5]</sup>. The ternary DESs were subjected to physical properties such as density, pH, conductivity, and viscosity. The H-bonded interactions between the components were characterized using FTIR after being kept in a desiccator containing anhydrous CaCl<sub>2</sub>, because no turbidity developed during this time.

### **6.4. Preparation of Malonic acid- Glucose- Glycine (MA-GLU-GLY) TDES**

Malonic acid, glucose, and glycine are dissolved in double distilled water at a 1:1:1 mole ratio and allowed to evaporate in a water bath until the constant weight of the components was attained <sup>[5]</sup>. After being stored in a desiccator containing anhydrous CaCl<sub>2</sub>, the ternary DESs were exposed to physical parameters such as density, pH, conductivity, and viscosity. The H-bonded interactions between the components were characterized using FTIR, because no turbidity occurred throughout this time.

### **6.5. Preparation of Malonic acid- Fructose- Glycine (MA-FRU-GLY) TDES**

Malonic acid, fructose, and glycine are dissolved in a 1:1:1 mole ratio in double-distilled water and evaporated in a water bath until the weight of the components remains constant <sup>[5]</sup>. The ternary DESs were exposed to physical properties such as density, pH, conductivity, and viscosity after being stored in a desiccator containing anhydrous CaCl<sub>2</sub>. The H-bonded interactions between the components were characterized using FTIR because no turbidity occurred during this time.

## **6.6. Preparation of Malonic acid- Glucose- Histidine (MA-GLU-HIS) TDES**

Malonic acid, glucose, and histidine are dissolved in a 1:1:1 mole ratio in double-distilled water and evaporated in a water bath until the weight of the components remains constant<sup>[5]</sup>. The ternary DESs were exposed to physical characteristics such as density, pH, conductivity, and viscosity after being stored in a desiccator containing anhydrous CaCl<sub>2</sub>. The H-bonded interactions between the components were characterized using FTIR because no turbidity occurred during this time.

## **6.7. Preparation of Malonic acid- Fructose- Histidine (MA-FRU-HIS) TDES**

In double distilled water, malonic acid, fructose, and histidine are dissolved in a 1:1:1 mole ratio and evaporated in a water bath until the weight of the components remains constant<sup>[5]</sup>. After being stored in a desiccator containing anhydrous CaCl<sub>2</sub>, the ternary DESs were exposed to physical parameters such as density, pH, conductivity, and viscosity. The H-bonded interactions between the components were studied using FTIR because no turbidity occurred during this period.

## **6.8. Results and Discussion**

### **6.8.1 Characterization of Malonic Acid-Glucose-Glutamine TDES**

#### **6.8.1.1 Density and Conductivity**

Density is one of the most essential physical properties of solvents. The densities of ionic liquids and DES are quite largely unexplored. When compared to water, TDESs have a larger density. At room temperature, MA-GLU-GLUT TDES has a density of 1.3624 g/cm<sup>3</sup>. The density of ionic liquids ranges from 1.0 to 1.6 g/cm<sup>3</sup> due to the influence of their ionic structure<sup>[6]</sup>. DESs are ionic liquid substitutes with densities that are like those of ionic liquids.

The conductivity of DES is influenced by its viscosity and ion concentration. At room temperature, the conductivity of MA-GLU-GLUT TDES is 4.7mS/cm. According to

certain literature assessments, the value is in the range of 0.1-14 mS/cm. As the temperature rises, the conductivity of the TDES rises due to a decrease in viscosity <sup>[7-9]</sup>.

### **6.8.1.2 pH**

The pH is a critical physical parameter that influences chemical processes significantly. Andrea Skulcova et al. <sup>[10]</sup> studied the effect of temperature on pH for a variety of DESs and discovered that as temperature rises, pH values decrease. This study investigated the effect of temperature on the pH of newly formed DESs. The hydrogen-bond donor has a considerable impact on the pH of the final product, according to the pH behavior analysis. The nature of the hydrogen bond donor determines the acidity of the mixture. The pH values of the solvent, MA-GLU-GLUT decrease somewhat as the temperature rises, as seen in Fig.6.1.1.

### **6.8.1.3 Viscosity**

The viscosity of a liquid mixture represents the attraction between molecules <sup>[11]</sup>. The viscosity of DES determines how well it may be used as a solvent. Because of its limitations, higher viscosity DES is not appropriate <sup>[12, 5]</sup>. When using DES with a high viscosity, a higher temperature is required <sup>[12]</sup>, which may reduce the viscosity of a particular DES <sup>[13]</sup>. DESs with strong hydrogen bonding in their structures had higher viscosity and surface tension <sup>[14]</sup>. As a result, the viscosity of the prepared MA-GLU-GLUT TDES was assessed at three different temperatures to determine their suitability for usage. As seen in Fig.6.1.2, increasing the temperature causes a gradual reduction in viscosity of the solvent.

### **6.8.1.4 FTIR spectrum of MA-GLU-GLUT TDES**

The FTIR spectrum of MA-GLU-GLUT TDES is shown in Fig.6.1.3. The peak noticed at  $3389\text{cm}^{-1}$  is due to N - H stretching. The broad peak at  $2620.80\text{cm}^{-1}$  is due to the intramolecular O - H stretching <sup>[15]</sup>. The peak at  $1667.83\text{cm}^{-1}$  is due to C = N stretching and

the peaks at  $1402.32\text{cm}^{-1}$  [15, 16] are due to O - H bending of the carboxylic acid of malonic acid. The peak observed at  $1287.75\text{cm}^{-1}$  is due to strong C - N stretching and the peaks observed between  $1200$  and  $1020\text{cm}^{-1}$  are due to C - OH stretching [12]. Furthermore, there are some peaks in the fingerprint region [17].

## **6.8.2 Characterization of Malonic Acid-Fructose-Glutamine TDES**

### **6.8.2.1 Density and Conductivity**

One of the most important physical features of solvents is density. The density of TDESs is higher than that of water. MA-FRU-GLUT TDES has a density of  $1.3192\text{g/cm}^3$  at room temperature. Due to the influence of their ionic structure, the density of ionic liquids ranges from  $1.0$  to  $1.6\text{ g/cm}^3$  [6]. Ionic liquid substitutes with densities similar to ionic liquids are known as DESs.

The viscosity and ion concentration of DES affect its conductivity. MA-FRU-GLUT TDES has a conductivity of  $4.9\text{mS/cm}$  at normal temperature. According to certain estimates in the literature, the value is between  $0.1$  and  $14\text{ mS/cm}$ . The conductivity of the TDES increases as the temperature rises due to a decrease in viscosity [7-9].

### **6.8.3.2 pH**

The pH is an important physical parameter that has a big influence on chemical processes. Andrea Skulcova et al. [10] studied the influence of temperature on pH for several DESs and discovered that as temperature raises, pH values decrease. This study investigated the effect of temperature on the pH of newly formed DESs. The hydrogen-bond donor has a substantial impact on the pH of the final product, according to the pH behavior analysis. The type of hydrogen bond donor determines the acidity of a combination. The pH values of MA-FRU-GLUT fall somewhat when the temperature rises, as seen in Fig.6.2.1.

### 6.8.2.3 Viscosity

The attraction between molecules is represented by the viscosity of a liquid mixture [11]. The viscosity of DES is what defines how effective it is as a solvent. Higher viscosity DES is not recommended due to its limitations [12, 5]. A greater temperature is necessary when utilizing DES with a high viscosity [12], which may lessen the viscosity of a particular DES [13]. The viscosity and surface tension of DESs with significant hydrogen bonding in their structures were higher [14]. As a result, the viscosity of MA-FRU-GLUT TDES was evaluated at three different temperatures to determine their appropriateness for use. As shown in Fig.6.2.2, increasing the temperature causes the solvent to gradually decrease its viscosity.

### 6.8.2.4 FTIR spectrum of MA-FRU-GLUT TDES

Figure 6.2.3 shows the FTIR spectrum of MA-FRU-GLUT TDES. The intermolecular O-H stretching of the alcoholic group causes a large peak at  $3435.76\text{cm}^{-1}$  [12]. The peaks at  $1667.33\text{cm}^{-1}$  and  $1422.45\text{cm}^{-1}$  [15, 16] are due to C = N stretching and O - H bending of the carboxylic acid of malonic acid, respectively. Strong C - N stretching causes the peak at  $1292.88\text{cm}^{-1}$  [12], while C - OH stretching causes the peaks between  $1100.59$  and  $1080.80\text{cm}^{-1}$  [12]. In addition, certain peaks can be found in the fingerprint region [17].

## 6.8.3 Characterization of Malonic Acid-Glucose-Glycine TDES

### 6.8.3.1 Density and Conductivity

Density is one of the most essential physical characteristics of solvents. TDESs have a density greater than that of water. At room temperature, MA-GLU-GLY TDES has a density of  $1.1792\text{g/cm}^3$ . Ionic liquids have a density of  $1.0$  to  $1.6\text{g/cm}^3$  due to the influence of their ionic structure [6]. DESs are ionic liquid substitutes with densities similar to ionic liquids.



The conductivity of DES is affected by its viscosity and ion concentration. At room temperature, MA-GLU-GLY TDES has a conductivity of 1.4mS/cm. The value is between 0.1 and 14 mS/cm, according to several estimations in the literature. Due to a decrease in viscosity, the conductivity of the TDES increases as the temperature rises [7-9].

### **6.8.3.2 pH**

The pH is an important physical parameter that has a big influence on chemical processes. Andrea Skulcova et al. [10] studied the influence of temperature on pH for a few DESs and discovered that as temperature raises, pH values decrease. This study looked into the effect of temperature on the pH of newly formed DESs. The hydrogen-bond donor has a substantial impact on the pH of the final product, according to the pH behavior analysis. The type of hydrogen bond donor determines the acidity of a combination. The pH values of MA-GLU-GLY fall somewhat when the temperature rises, as seen in Fig.6.3.1.

### **6.8.3.3 Viscosity**

The viscosity of a liquid mixture represents the attraction between molecules [11]. The viscosity of DES determines its ability to act as a solvent. Due to its limitations, higher viscosity DES is not advised [12, 5]. When using DES with a high viscosity, a higher temperature is required [12], which may reduce the viscosity of a particular DES [13]. DESs with strong hydrogen bonding in their structures had increased viscosity and surface tension [14]. As a result, the viscosity of MA-GLU-GLY TDES was measured at three different temperatures in order to determine its suitability for an application. The viscosity of solvent steadily decreases as the temperature rises, as illustrated in Fig.6.3.2.

### **6.8.3.4 FTIR spectrum of MA-GLU-GLY TDES**

Figure 6.3.3 shows the FTIR spectrum of MA-GLU-GLY TDES. The intermolecular O - H stretching of the alcoholic group causes a large peak at  $3458.27\text{cm}^{-1}$  [12]. The peak in  $1730.85\text{cm}^{-1}$  is due to the aldehydic stretching of glucose. The peaks at

1632.39 $\text{cm}^{-1}$  and 1414.53 $\text{cm}^{-1}$  [15, 16] are due to C = N stretching and O - H bending of the carboxylic acid of malonic acid, respectively. NO<sub>2</sub> stretching causes the peak at 1328.41 $\text{cm}^{-1}$  [12], while strong peaks between 1020-1200 $\text{cm}^{-1}$  are seen due to C - OH stretching [12]. In addition, certain peaks can be found in the fingerprint region [17].

## **6.8.4 Characterization of Malonic Acid-Fructose-Glycine TDES**

### **6.8.4.1 Density and Conductivity**

Density is one of the most essential physical characteristics of solvents. TDESs have a density greater than that of water. At room temperature, MA-FRU-GLY TDES has a density of 1.3564 $\text{g/cm}^3$ . Ionic liquids have a density of 1.0 to 1.6  $\text{g/cm}^3$  due to the influence of their ionic structure [6]. DESs are ionic liquid substitutes with densities similar to ionic liquids.

The conductivity of DES is affected by its viscosity and ion concentration. At room temperature, MA-FRU-GLY TDES has a conductivity of 2.5 $\text{mS/cm}$ . The value is between 0.1 and 14  $\text{mS/cm}$ , according to several estimations in the literature. Due to a decrease in viscosity, the conductivity of the TDES increases as the temperature rises [7-9].

### **6.8.4.2 pH**

The pH is an important physical parameter that has a big influence on chemical processes. Andrea Skulcova et al. [10] studied the influence of temperature on pH for several DESs and discovered that as temperature raises, pH values decrease. This study investigated the effect of temperature on the pH of newly formed DESs. The hydrogen-bond donor has a substantial impact on the pH of the final product, according to the pH behaviour analysis. The type of hydrogen bond donor determines the acidity of a combination. The pH values of MA-FRU-GLY fall somewhat when the temperature rises, as seen in Fig.6.4.1.

### 6.8.4.3 Viscosity

The viscosity of a liquid mixture represents the attraction between molecules <sup>[11]</sup>. The viscosity of DES determines its ability to act as a solvent. Due to its limitations, higher viscosity DES is not advised <sup>[12, 5]</sup>. When using DES with a high viscosity, a higher temperature is required <sup>[12]</sup>, which may reduce the viscosity of a particular DES <sup>[13]</sup>. DESs with strong hydrogen bonding in their structures had increased viscosity and surface tension <sup>[14]</sup>. As a result, the viscosity of MA-FRU-GLY TDES was measured at three different temperatures to determine its suitability for application. The viscosity of the solvent steadily decreases as the temperature rises, as illustrated in Fig.6.4.2.

### 6.8.4.4 FTIR spectrum of MA-FRU-GLY TDES

Figure 6.4.3 shows the FTIR spectrum of MA-FRU-GLY TDES. The intermolecular O - H stretching of the alcoholic group causes a large peak at  $3396.22\text{cm}^{-1}$  <sup>[12]</sup>. The peaks at  $1675.56\text{cm}^{-1}$  and  $1402.19\text{cm}^{-1}$  <sup>[15, 16]</sup> are due to C = N stretching and O - H bending of the carboxylic acid of malonic acid, respectively. The peak at  $1300.80\text{cm}^{-1}$  is due to NO<sub>2</sub> stretching. The strong peaks between  $1020\text{-}1200\text{cm}^{-1}$  are seen due to C - OH stretching <sup>[12]</sup>. In addition, certain peaks can be found in the fingerprint region <sup>[17]</sup>.

## 6.8.5 Characterization of Malonic Acid-Glucose-Histidine TDES

### 6.8.5.1 Density and Conductivity

Density is one of the most essential physical characteristics of solvents. TDESs have a density greater than that of water. At room temperature, MA-GLU-HIS TDES has a density of  $1.2456\text{g/cm}^3$ . Ionic liquids have a density of  $1.0$  to  $1.6\text{g/cm}^3$  due to the influence of their ionic structure <sup>[6]</sup>. DESs are ionic liquid substitutes with densities similar to ionic liquids.

The conductivity of DES is affected by its viscosity and ion concentration. At room temperature, MA-GLU-HIS TDES has a conductivity of  $0.56\text{mS/cm}$ . The value is between

0.1 and 14 mS/cm, according to several estimations in the literature. Due to a decrease in viscosity, the conductivity of the TDES increases as the temperature rises <sup>[7-9]</sup>.

### **6.8.5.2 pH**

The pH is an important physical parameter that has a big influence on chemical processes. Andrea Skulcova et al. <sup>[10]</sup> studied the influence of temperature on pH for a number of DESs and discovered that as temperature raises, pH values decrease. This study looked into the effect of temperature on the pH of newly formed DESs. The hydrogen-bond donor has a substantial impact on the pH of the final product, according to the pH behavior analysis. The type of hydrogen bond donor determines the acidity of a combination. The pH values of MA-GLU-HIS fall somewhat when the temperature rises, as seen in Fig.6.5.1.

### **6.8.5.3 Viscosity**

The viscosity of a liquid mixture represents the attraction between molecules <sup>[11]</sup>. The viscosity of DES determines its ability to act as a solvent. Due to its limitations, higher viscosity DES is not advised <sup>[12, 5]</sup>. When using DES with a high viscosity, a higher temperature is required <sup>[12]</sup>, which may reduce the viscosity of a particular DES <sup>[13]</sup>. DESs with strong hydrogen bonding in their structures had increased viscosity and surface tension <sup>[14]</sup>. As a result, the viscosity of MA-GLU-HIS TDES was measured at three different temperatures to determine its suitability for applications. The viscosity of the solvent steadily decreases as the temperature rises, as illustrated in Fig.6.5.2.

### **6.8.5.4 FTIR spectrum of MA-GLU-HIS TDES**

Figure 6.5.3 shows the FTIR spectrum of MA-GLU-HIS TDES. The intermolecular O – H stretching of the alcoholic group causes a large peak at  $3461.17\text{cm}^{-1}$  <sup>[12]</sup>. The peak at  $1733.85\text{cm}^{-1}$  is due to the aldehydic stretching of glucose. The peak at  $1632.84\text{cm}^{-1}$  <sup>[15, 16]</sup> is due to C = N stretching, NO<sub>2</sub> stretching causes the peak at  $1383.56\text{cm}^{-1}$  <sup>[12]</sup>, while strong

peaks between 1020-1200 $\text{cm}^{-1}$  are seen due to C - OH stretching <sup>[12]</sup>. In addition, certain peaks can be found in the fingerprint region <sup>[17]</sup>.

## **6.8.6 Characterization of Malonic Acid-Fructose-Histidine TDES**

### **6.8.6.1 Density and Conductivity**

One of the most important physical features of solvents is density. The density of TDESs is higher than that of water. MA-FRU-HIS TDES has a density of 1.2742 $\text{g}/\text{cm}^3$  at room temperature. Due to the influence of their ionic structure, the density of ionic liquids ranges from 1.0 to 1.6  $\text{g}/\text{cm}^3$  <sup>[6]</sup>. Ionic liquid substitutes with densities similar to ionic liquids are known as DESs.

The viscosity and ion concentration of DES affect its conductivity. MA-FRU-HIS TDES has a conductivity of 0.505 mS/cm at normal temperature. According to certain estimates in the literature, the value is between 0.1 and 14 mS/cm. The conductivity of the TDES increases as the temperature rises due to a decrease in viscosity <sup>[7-9]</sup>.

### **6.8.6.2 pH**

The pH is an important physical parameter that has a big influence on chemical processes. Andrea Skulcova et al. <sup>[10]</sup> studied the influence of temperature on pH for a number of DESs and discovered that as temperature raises, pH values decrease. This study looked into the effect of temperature on the pH of newly formed DESs. The hydrogen-bond donor has a substantial impact on the pH of the final product, according to the pH behavior analysis. The type of hydrogen bond donor determines the acidity of a combination. The pH values of MA-FRU-HIS fall somewhat when the temperature rises, as seen in Fig.6.6.1.

### **6.8.6.3 Viscosity**

The attraction between molecules is represented by the viscosity of a liquid mixture <sup>[11]</sup>. The viscosity of DES is what defines how effective it is as a solvent. Higher viscosity DES is not recommended due to its limitations <sup>[12, 5]</sup>. A greater temperature is necessary

when utilizing DES with a high viscosity <sup>[12]</sup>, which may lessen the viscosity of a particular DES <sup>[13]</sup>. The viscosity and surface tension of DESs with significant hydrogen bonding in their structures were higher <sup>[14]</sup>. As a result, the viscosity of MA-FRU-HIS TDES was evaluated at three different temperatures to determine their appropriateness for use. As shown in Fig.6.6.2, increasing the temperature causes the solvent to gradually decrease its viscosity.

#### **6.8.6.4 FTIR spectrum of MA-FRU-HIS TDES**

Figure 6.6.3 shows the FTIR spectrum of MA-FRU-HIS TDES. The intermolecular O - H stretching of the alcoholic group causes a large peak at  $3435.77\text{cm}^{-1}$  <sup>[12]</sup>. The strong peaks at  $2928.47\text{cm}^{-1}$  and  $1713\text{cm}^{-1}$  are due to carboxylic O - H stretching and the ketonic group of fructose respectively <sup>[12]</sup>. The peaks at  $1632\text{cm}^{-1}$  and  $1411.67\text{cm}^{-1}$  <sup>[15, 16]</sup> are due to C = N stretching and O - H bending of the carboxylic acid of malonic acid, respectively. Strong C - N stretching causes the peak at  $1272.02\text{cm}^{-1}$  <sup>[12]</sup>, while C-OH stretching of secondary alcoholic groups causes the peaks between 1200 and  $1020.80\text{cm}^{-1}$  <sup>[12]</sup>. In addition, certain peaks can be found in the fingerprint region <sup>[17]</sup>.

#### **6.9 Conclusion**

In this study, six types of malonic acid-based ternary deep eutectic solvents were prepared successfully. The physical properties were measured for all the solvents. The H-bonded interactions were also characterized by FTIR. The MA-based TDESs have appreciable conductivity as their viscosity went on decreasing when the temperature was increasing.

## References

- [1]. Jing Wang and Sheila N. Baker; Pyrrolidinium salt based binary and ternary deep eutectic solvents: green preparations and physiochemical property characterizations; De Gruyter, *Green Process Synth* 2018; 7: 353–359
- [2]. Kumar V, Nigam KDP., Process intensification in green synthesis; *Green Process Synth.* 2012, 1, 79–107.
- [3]. Durand E, Lecomte J, Villeneuve P. *Biochimie*; From green chemistry to nature: The versatile role of low transition temperature mixtures, 2016, 120, 119–123
- [4]. Taysun, M.B., Sert, E. & Atalay, F.S. Synthesis, characterization, and acid-catalyzed application of ternary deep eutectic solvent: effect of glycerol addition. *Braz. J. Chem. Eng.* (2021).
- [5]. Y.T. Dai, J. van Spronsen, G.J. Witkamp, R. Verpoorte, Y.H. Choi, Natural deep eutectic solvents as new potential media for green technology, *Anal. Chim. Acta* 766 (2013) 61 – 68.
- [6]. Q. Cao; X. Lu; X. Wu; Y. Guo; Xu, L.; Fang, W. Density, Viscosity, and Conductivity of Binary Mixtures of the Ionic Liquid N-(2-Hydroxyethyl) piperazinium Propionate with Water, Methanol, or Ethanol, *Journal of Chemical & Engineering Data* (2015) 60,3, 455-463.
- [7]. P. Wasserscheid and P. Welton eds., *Ionic Liquids in Synthesis*, Wiley-VCH Verlag, Weinheim, *Org. Proc. Res. Dev.* 2003, 7, 2, 223–224
- [8]. F. Endres, A. P. Abbott, D. R Mac Farlane eds., *Electrodeposition from Ionic liquids*, Wiley-VCH Verlag, Weinheim, 2008.
- [9]. A. P. Abbott, D. Boothby, G. Capper, D. L. Davies, R. Rasheed, Deep Eutectic Solvents Formed between Choline Chloride and Carboxylic Acids: Versatile Alternatives to Ionic Liquids, *J. Am. Chem. Soc.*, 126, 29, (2004). 9142–9147

- [10]. Andrea Skulcova, Albert Russ, Michal Jablonsky, JozefSima, “pH of eutectic solvents,” *BioResources* 13(3), (2018) 5042 - 5051.
- [12]. W.J. Guo, Y.C. Hou, S.H. Ren, S.D. Tian, W.Z. Wu, Formation of Deep Eutectic Solvents by Phenols and Choline Chloride and Their Physical Properties *J. Chem. Eng. Data* 58 (2013) 866–872.
- [13]. Koon-Kee Kow, Kamaliah Sirat. Novel manganese (II)-based deep eutectic solvents: Synthesis and physical properties analysis[J]. *Chinese Chemical Letters*, 26(10) (2015), 1311-1314.
- [14]. M. Hayyan, F.S. Mjalli, M.A. Hashim, I.M. Alnashef, An investigation of the reaction between 1-butyl-3-methylimidazolium trifluoromethanesulfonate and superoxide ion, *J. Mol. Liq.* 181 (2013) 44–50.
- [15]. Hosein Ghaed, Muhammad Ayoub, SuriatiSufian, Azmi Mohd Shariff, Bhajan Lal, The study on the temperature dependence of viscosity and surface tension of several Phosphonium-based deep eutectic solvents, *J.Mol. Liq*, 241,(2017), 500-510.
- [16]. Donald L. Pavia, Gary M. Lampman, George S. Kriz, *Introduction to Spectroscopy*, 3rd Edition, BROOKS/COLE, Thomson Learning, USA, 2001
- [17]. B.D. Mistry, *A Handbook of Spectroscopic Data*, Oxford Book Company, India, 2009.
- [18]. James Ashenhurst, *Infrared Spectroscopy: A Quick Primer On Interpreting Spectra* (2020)



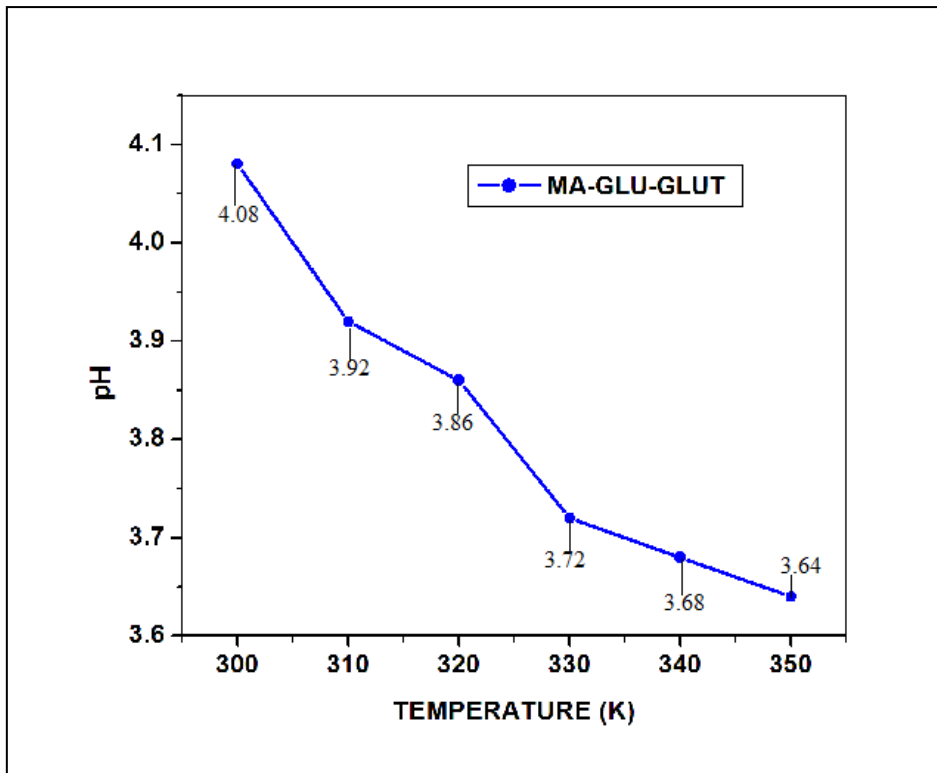


**Figure 6.1.1 pH as a function against T of MA-GLU-GLUT TDES**

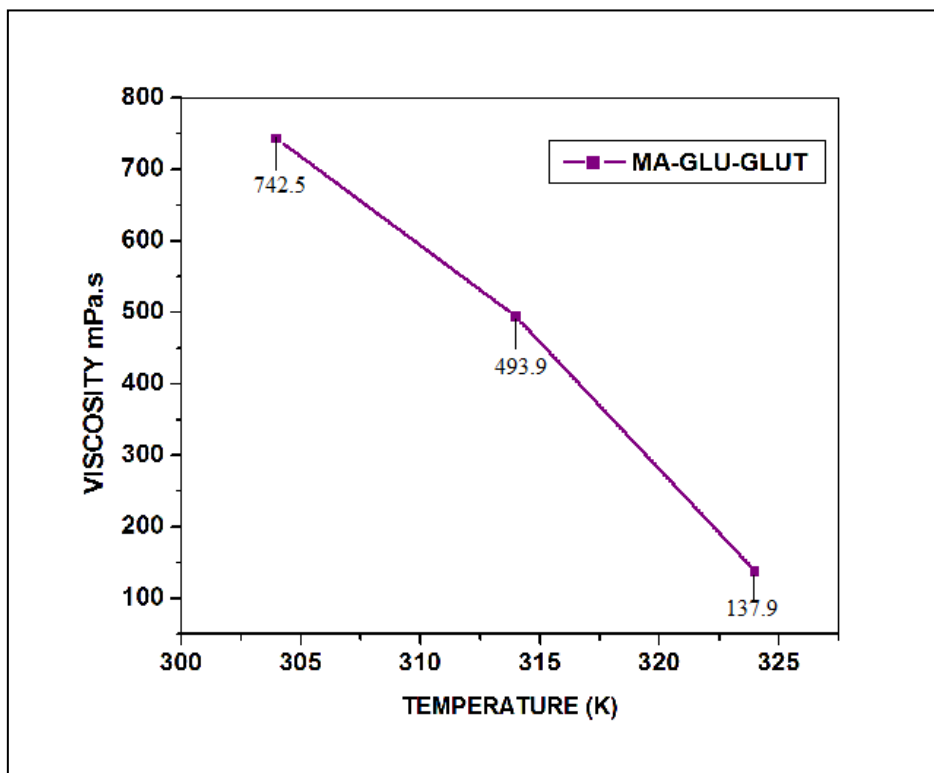


**Figure 6.1.2 Viscosity of MA-GLU-GLUT TDES At Different Temperatures**

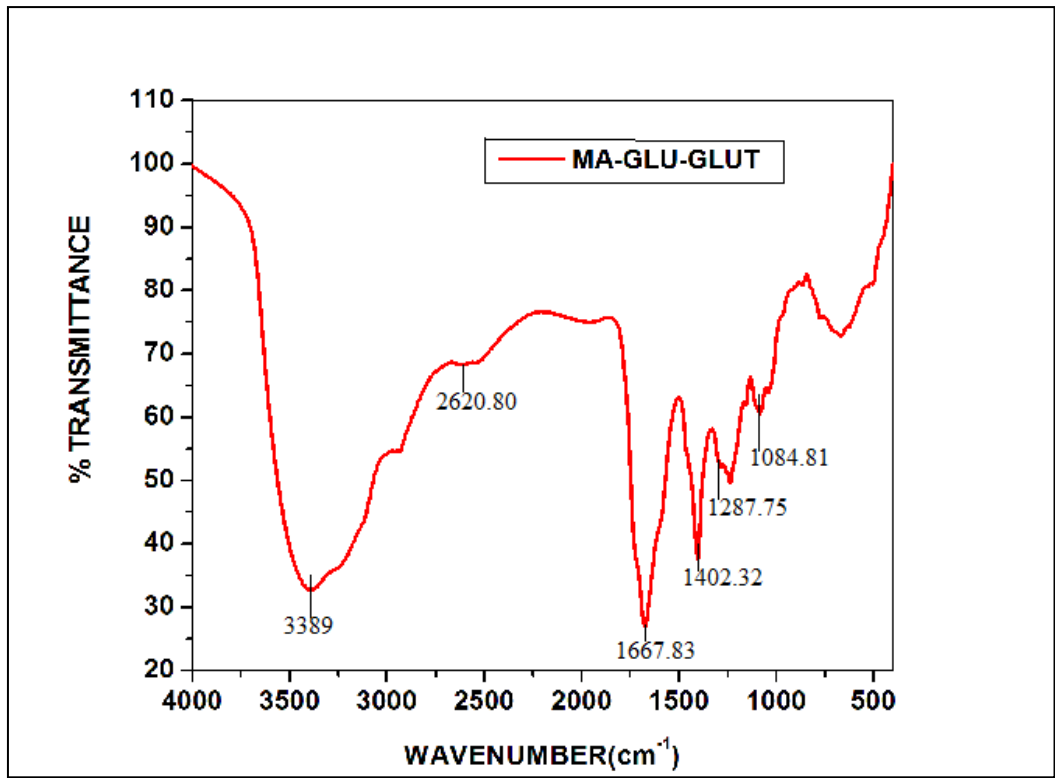


Figure 6.1.3 FTIR spectrum of MA-GLU-GLUT TDES

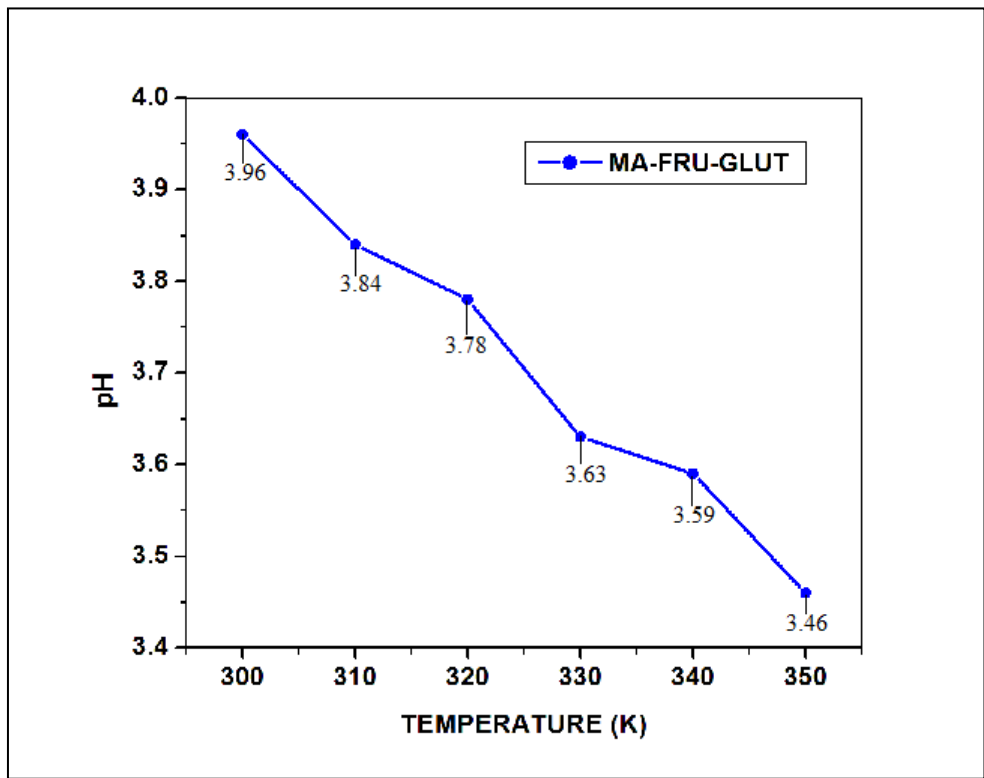


Figure 6.2.1 pH as a function against T of MA-FRU-GLUT TDES

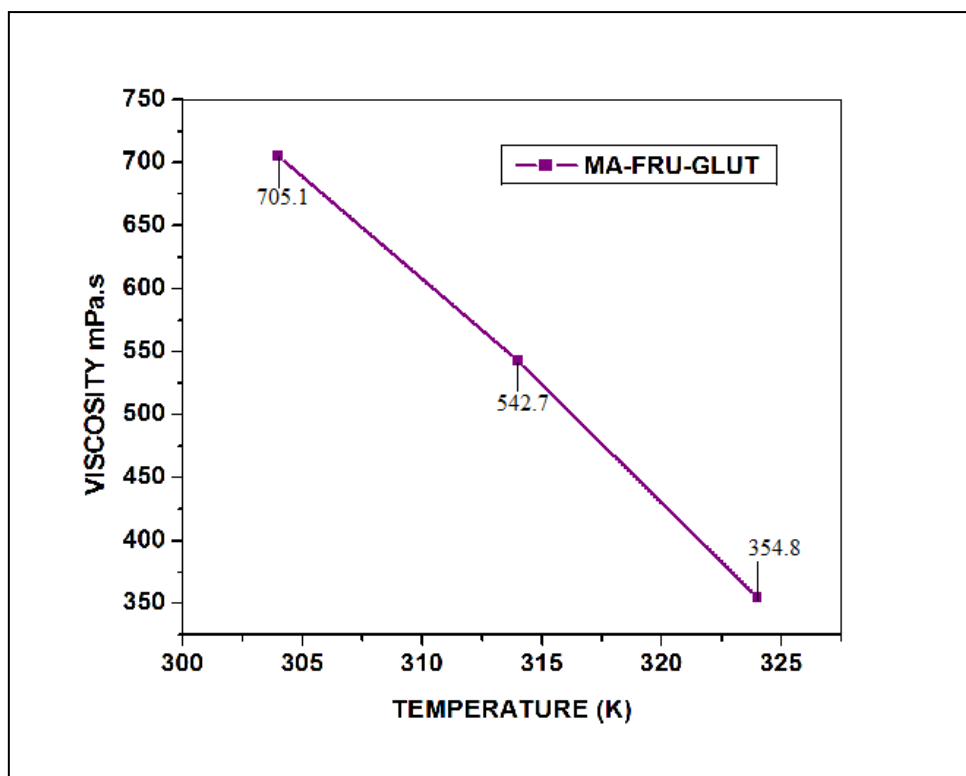


Figure 6.2.2 Viscosity of MA-FRU-GLUT TDES At Different Temperatures

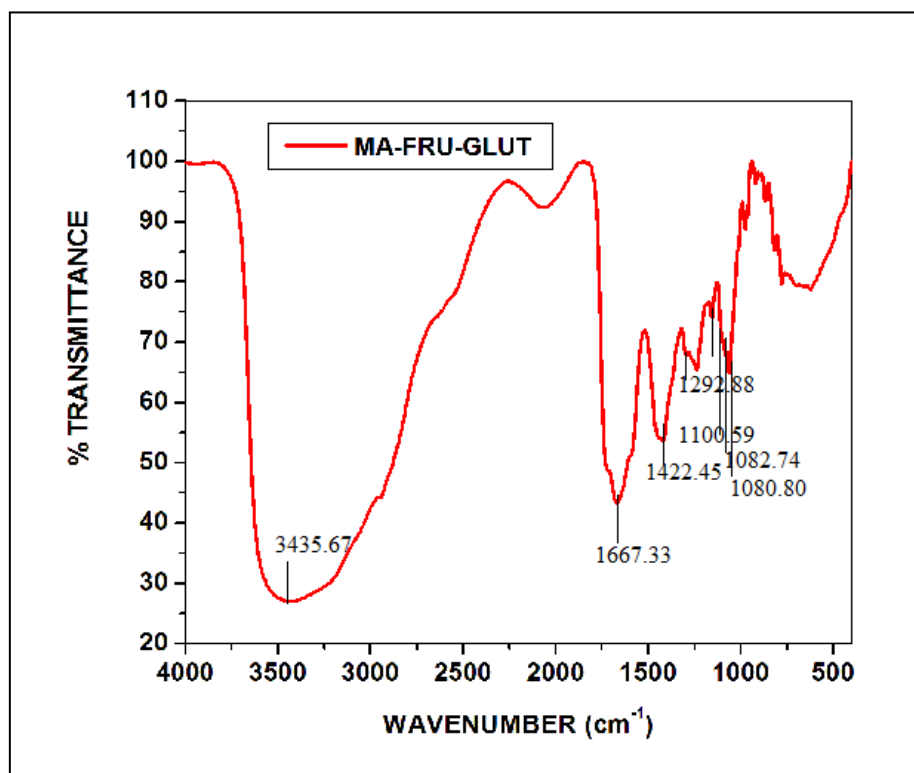


Figure 6.2.3 FTIR spectrum of MA-FRU-GLUT TDES

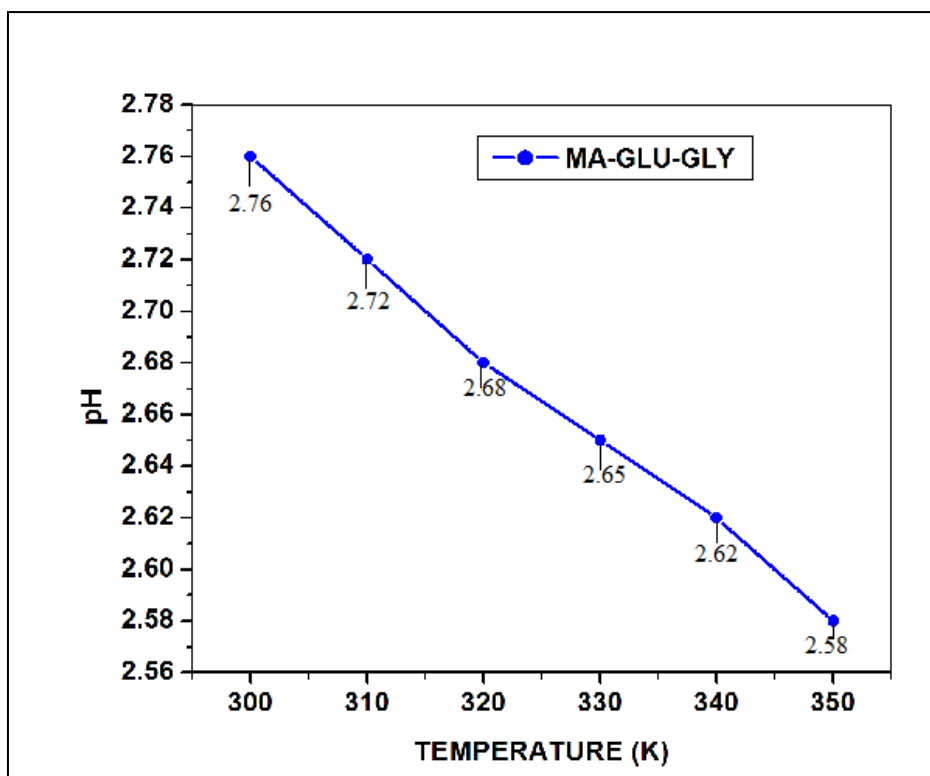


Figure 6.3.1 pH as a function against T of MA-GLU-GLY TDES

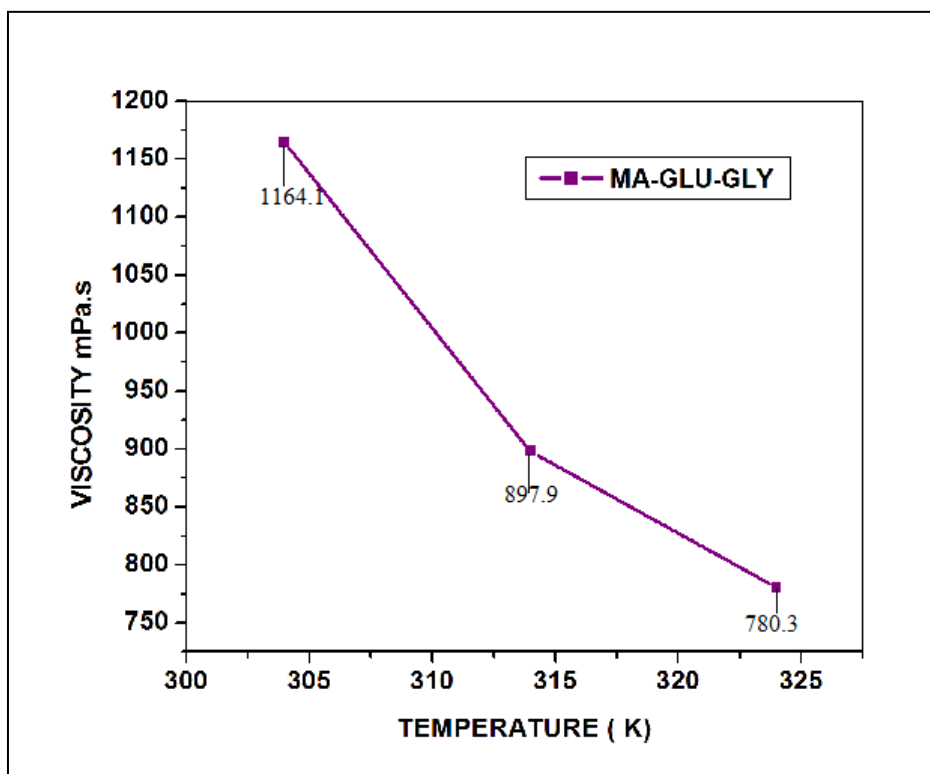


Figure 6.3.2 Viscosity of MA-GLU-GLY TDES At Different Temperatures

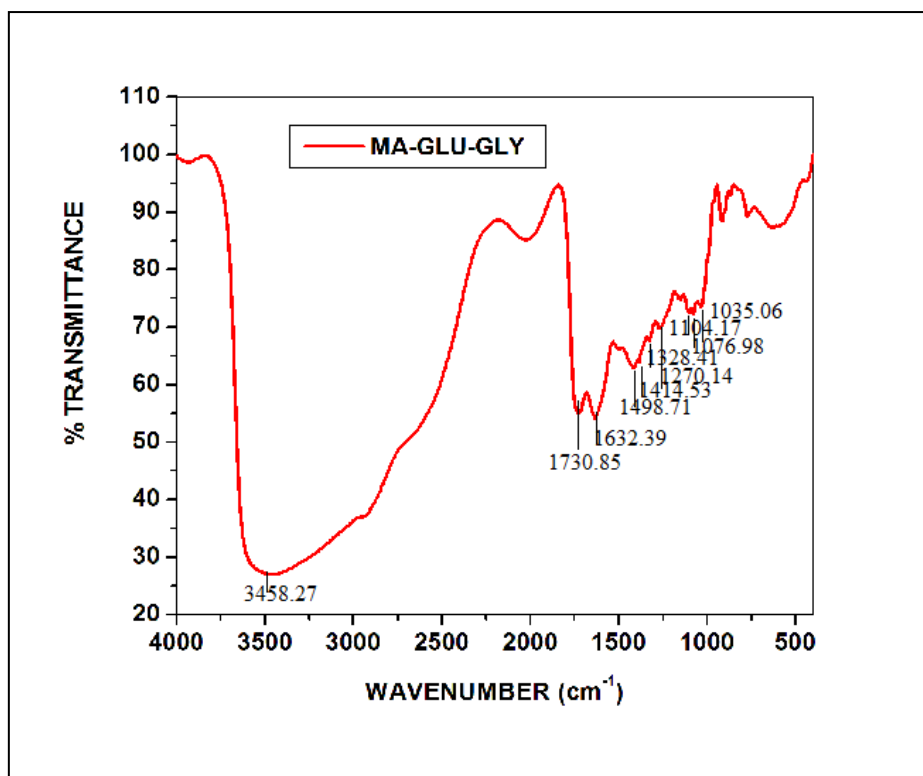


Figure 6.3.3 FTIR spectrum of MA-GLU-GLY TDES

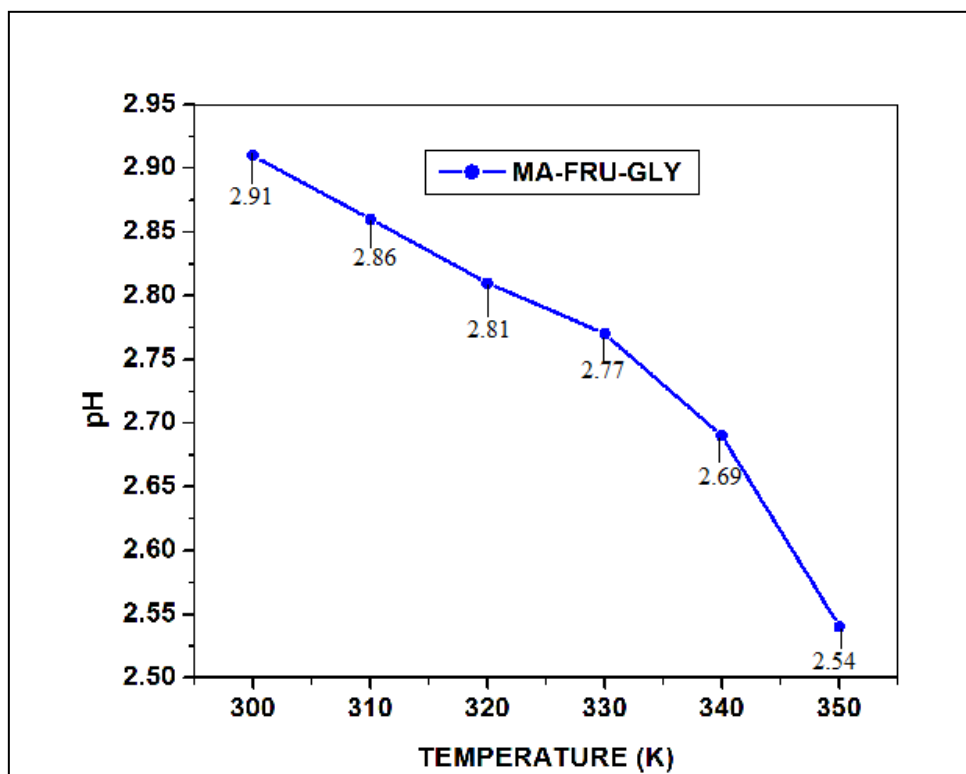


Figure 6.4.1 pH as a function against T of MA-FRU-GLY TDES

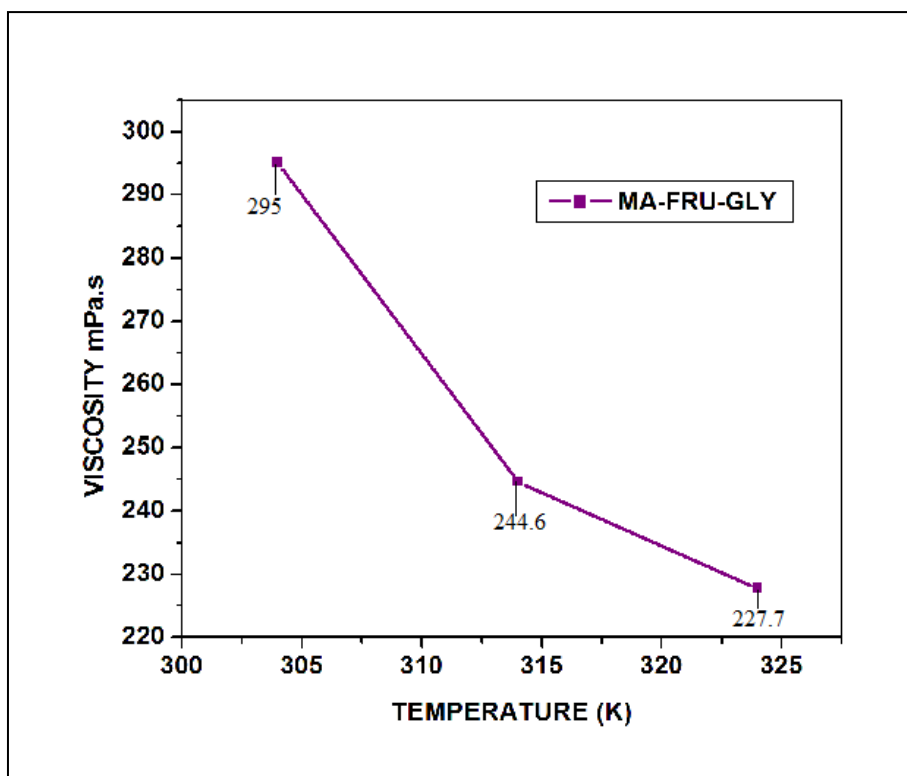


Figure 6.4.2 Viscosity of MA-FRU-GLY TDES at Different Temperatures

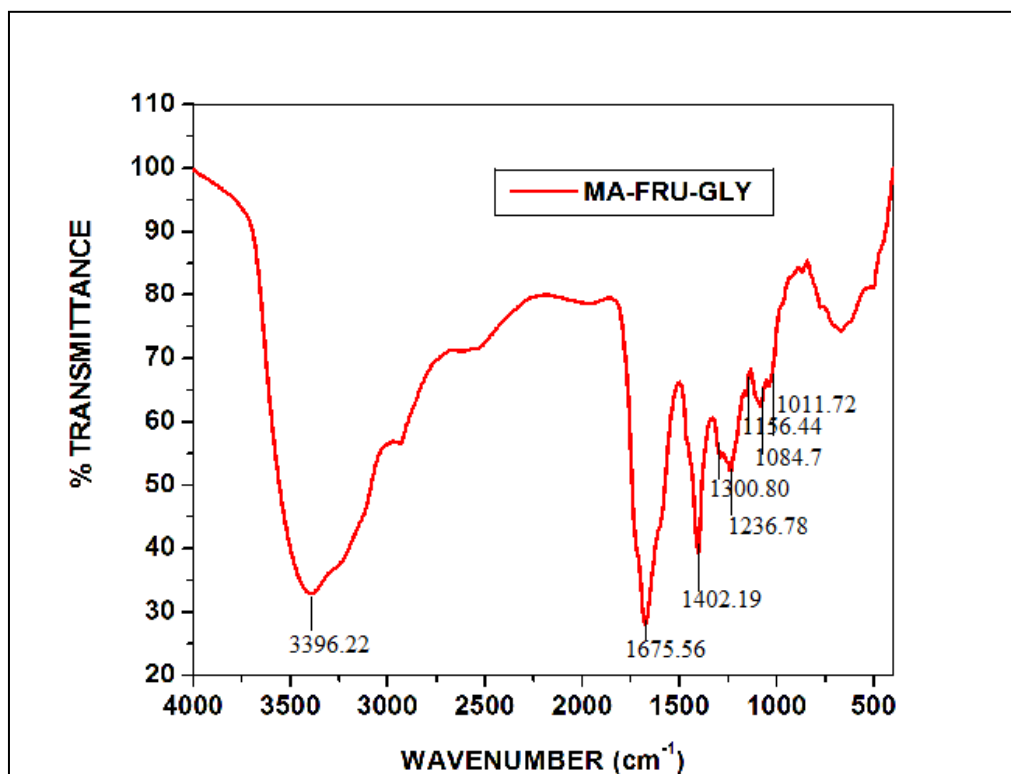


Figure 6.4.3 FTIR spectrum of MA-FRU-GLY TDES

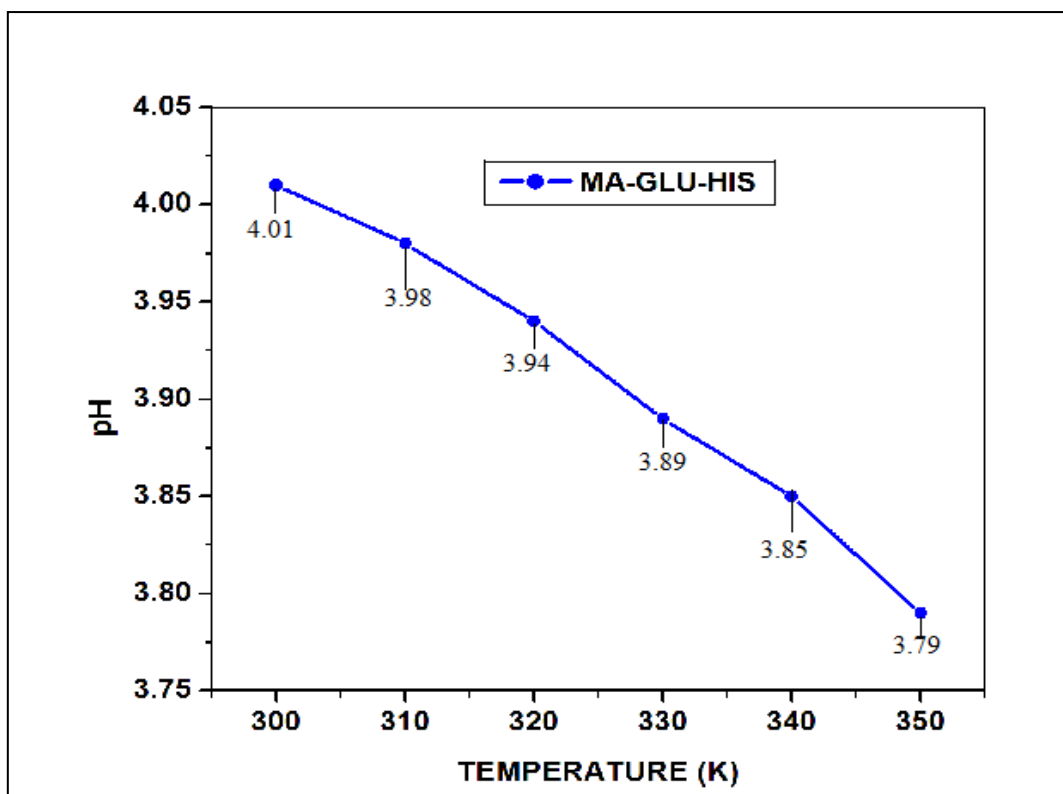


Figure 6.5.1 pH as a function against T of MA-GLU-HIS TDES

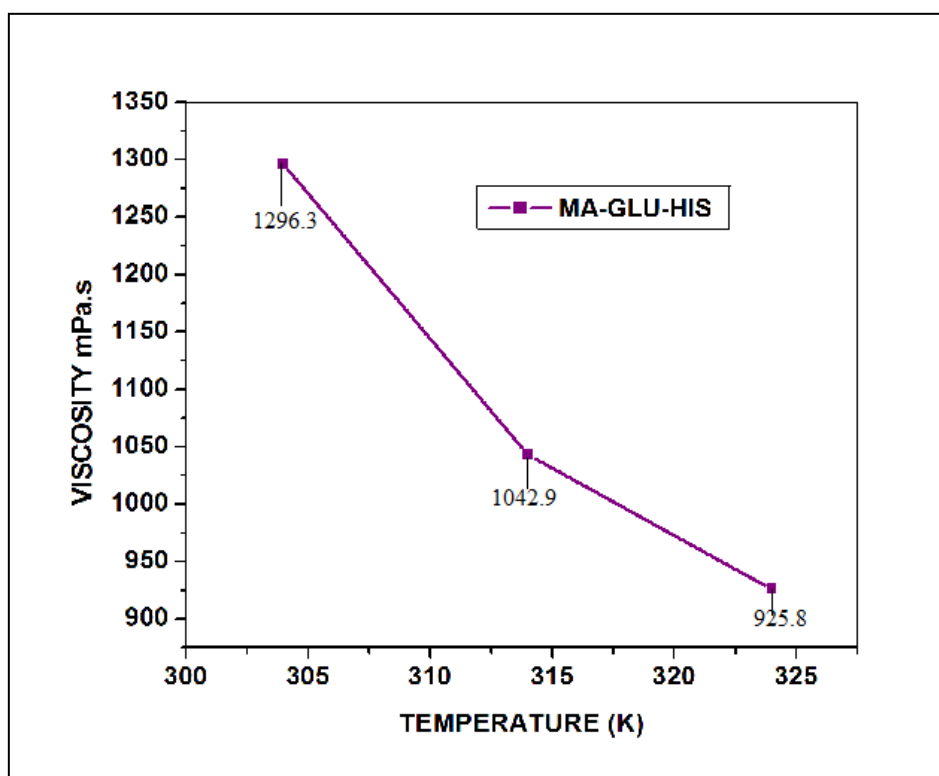


Figure 6.5.2 Viscosity of MA-GLU-HIS TDES at Different Temperatures

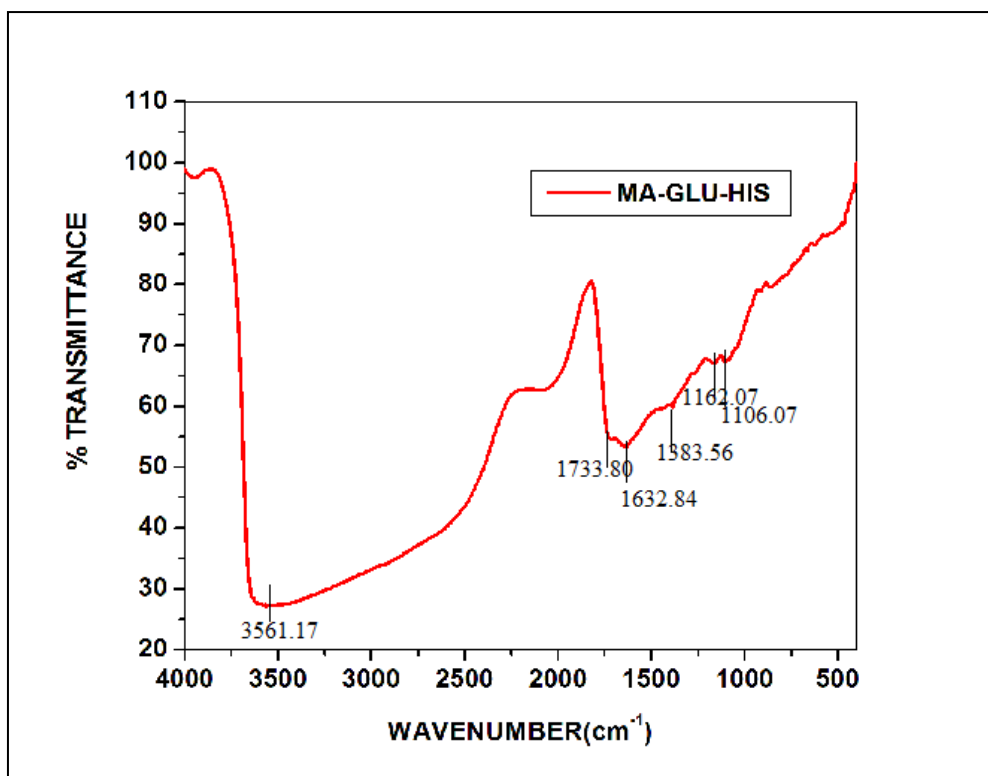


Figure 6.5.3 FTIR spectrum of MA-GLU-HIS TDES

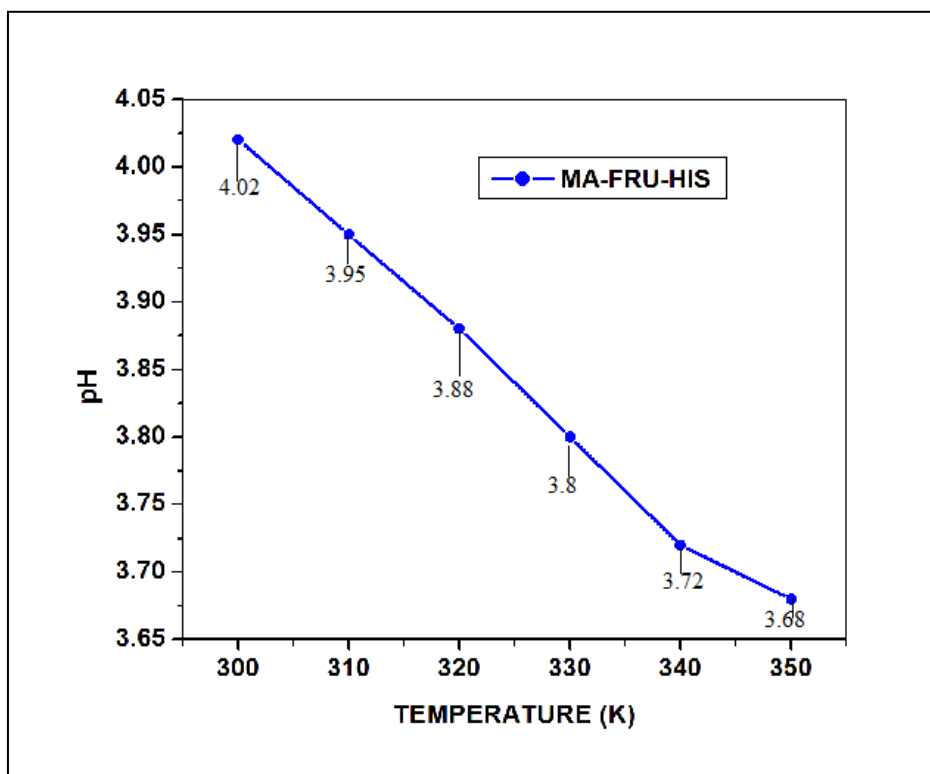


Figure 6.6.1 pH as a function against T of MA-FRU-HIS TDES



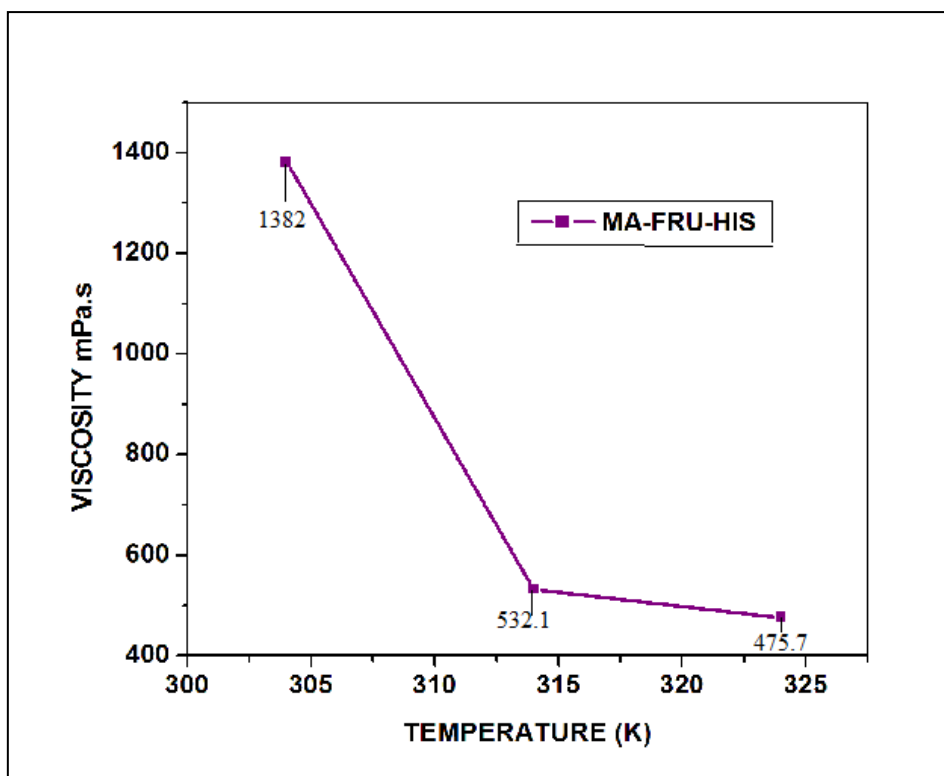


Figure 6.6.2 Viscosity of MA-FRU-HIS TDES at Different Temperatures

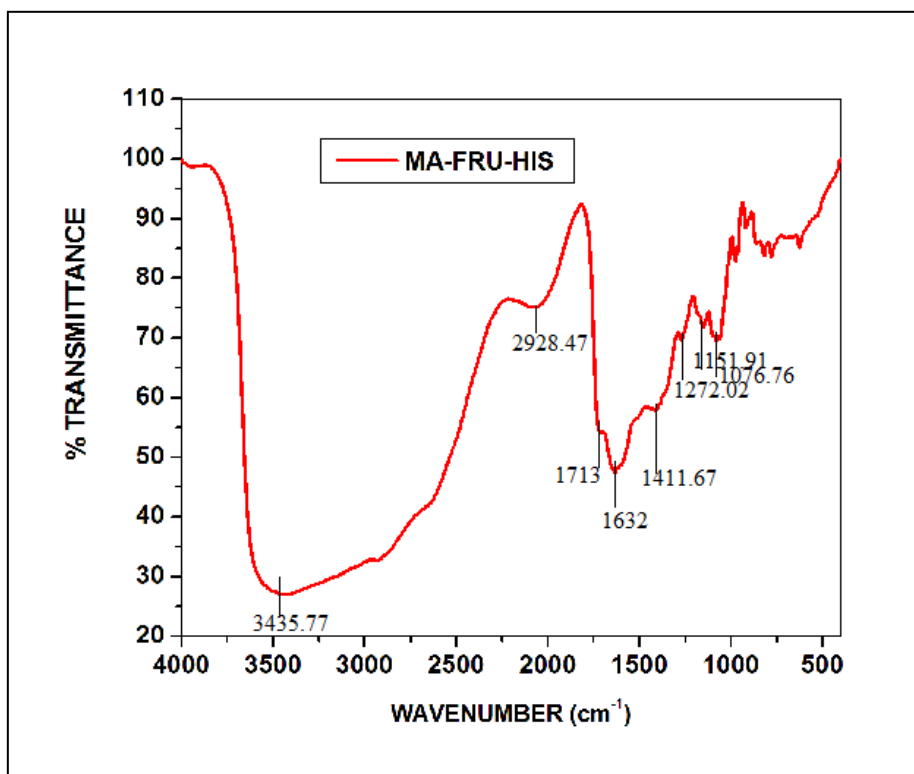


Figure 6.6.3 FTIR spectrum of MA-FRU-HIS TDES



## **7. Zinc chloride-based Ternary Deep Eutectic Solvents (TDES)**

---

### **7.1 Introduction**

When the concept of DES was first presented, it was defined as a eutectic mixture of two or more components. The melting point of the eutectic mixture was lower than the melting points of both separate components <sup>[1]</sup>. We investigated ternary deep eutectic solvents by blending zinc chloride, glucose/fructose and amino acids such as glutamine, histidine and glycine. TDESs are prepared by the evaporating method as reported by Dai, et.al. and then characterized by physical properties such as density, conductivity, pH, viscosity and FTIR.

### **7.2. Preparation of Zinc chloride- Glucose- Glutamine (ZC-GLU-GLUT) TDES**

At a 1:1:1 mole ratio, zinc chloride, glucose, and glutamine were dissolved in double distilled water and allowed to evaporate in a water bath until the weight of the components remains constant <sup>[2]</sup>. The mixture as a clear liquid was kept in a desiccator containing anhydrous CaCl<sub>2</sub> for about two weeks. As no turbidity developed during this time, the ternary DESs were subjected to physical property measurements such as density, pH, conductivity, and viscosity. The H-bonded interactions between the salts were characterized using FTIR.

### **7.3. Preparation of Zinc chloride- Fructose- Glutamine (ZC-FRU-GLUT) TDES**

At a 1:1:1 mole ratio, zinc chloride, fructose, and glutamine were dissolved in double distilled water and allowed to evaporate the water in a water bath until the weight of the components remains constant <sup>[2]</sup>. The mixtures were kept in a desiccator containing anhydrous CaCl<sub>2</sub> for about two weeks. There was no turbidity developed during this time, the ternary DESs were subjected to physical property measurements such as density, pH,

conductivity, and viscosity. The H-bonded interactions between the components were characterized using FTIR.

#### **7.4. Preparation of Zinc chloride- Glucose- Glycine (ZC-GLU-GLY) TDES**

Zinc chloride, glucose, and glycine were dissolved in double distilled water and evaporated at a 1:1:1 mole ratio in a water bath till the constant weight was attained <sup>[2]</sup>. The mixture as a clear liquid was kept in a desiccator containing anhydrous CaCl<sub>2</sub> for about two weeks. As no turbidity developed during this time, the ternary DESs were measured for physical properties such as density, pH, conductivity, viscosity. The H-bonded interactions between the components were characterized using FTIR.

#### **7.5. Preparation of Zinc chloride- Fructose- Glycine (ZC-FRU-GLY) TDES**

In a water bath, zinc chloride, fructose, and glycine at a 1:1:1 mole ratio were dissolved in double distilled water and allowed to evaporate till the constant weight was attained <sup>[2]</sup>. The mixture as a clear liquid was kept in a desiccator containing anhydrous CaCl<sub>2</sub> for about two weeks. As no turbidity developed during this time, the ternary DESs were measured for physical properties such as density, pH, conductivity, viscosity. The H-bonded interactions between the components were characterized using FTIR.

#### **7.6. Preparation of Zinc chloride- Glucose- Histidine (ZC-GLU-HIS) TDES**

Zinc chloride, glucose, and histidine are dissolved in double distilled water and evaporated at a 1:1:1 mole ratio in a water bath till the constant weight was attained <sup>[2]</sup>. The mixture as a clear liquid was kept in a desiccator containing anhydrous CaCl<sub>2</sub> for about two weeks. As no turbidity developed during this time, the ternary DESs were measured for physical properties such as density, pH, conductivity, viscosity. The H-bonded interactions between the components were characterized using FTIR.

## **7.7. Preparation of Zinc chloride- Fructose- Histidine (ZC-FRU-HIS) TDES**

In a water bath, zinc chloride, fructose, and histidine at a 1:1:1 mole ratio were dissolved in double distilled water and allowed to evaporate till the constant weight was attained <sup>[2]</sup>. The mixture as a clear liquid was kept in a desiccator containing anhydrous CaCl<sub>2</sub> for about two weeks. As no turbidity developed during this time, the ternary DESs were measured for physical properties such as density, pH, conductivity, viscosity. The H-bonded interactions between the components were characterized using FTIR.

## **7.8. Results and Discussion**

### **7.8.1 Characterization of Zinc chloride-Glucose-Glutamine TDES**

#### **7.8.1.1 Density and Conductivity**

The most significant property of any liquid is density. There is very little information about TDES densities. Because it is affected by ion concentration, the high viscous liquid will have low conductivity <sup>[3-6]</sup>. The density of ZC-GLU-GLUT TDES is 1.4292 g/cm<sup>3</sup> and its conductivity is 0.0531 mS/cm at normal temperature.

#### **7.8.1.2 pH**

The pH is a critical physical parameter that considerably impacts chemical reactions. Andrea Skulcova et al. <sup>[7]</sup> investigated the influence of temperature on pH for a range of DESs and discovered that pH values fell as the temperature rose. The influence of temperature on the pH of newly generated DESs was investigated in this work. According to a pH behaviour study, the hydrogen-bond donor has a significant impact on the pH of the final product. The acidity of the mixture is determined by the type of the hydrogen bond donor. As the temperature rises, the pH values of ZC-GLU-GLUT TDES decrease slightly, as seen in Fig.7.1.1.

### 7.8.1.3 Viscosity

The interaction between molecules in a liquid mixture is replicated by viscosity<sup>[8]</sup>. The lower the viscosity of DES, the better it may be employed as a solvent<sup>[9]</sup>. Fig. 7.1.2 shows the viscosity of ZC-GLU-GLUT TDES as a function of temperature. The viscosity reduces significantly as the temperature rises.

### 7.8.1.4 FTIR spectrum of ZC-GLU-GLUT TDES

Figure 7.1.3 shows the FTIR spectrum of ZC-GLU-GLUT TDES. The intermolecular O - H stretching of the alcoholic group causes the large peak at  $3411.87\text{cm}^{-1}$ <sup>[9]</sup> and the broad peak at  $2935.80\text{cm}^{-1}$  is due to the carboxylic O - H stretching<sup>[10]</sup>. The peak at  $1658.99\text{cm}^{-1}$  is due to amide C = O stretching and  $1401.61\text{cm}^{-1}$ <sup>[10, 11]</sup> is due to the C - H bending of the methyl group of glucose. The C - O stretching of the carboxylic acid of malonic acid is seen at  $1290.49\text{cm}^{-1}$ <sup>[11]</sup>, while C - OH stretching causes peaks between  $1100.39$  and  $1034.77\text{cm}^{-1}$ <sup>[11]</sup>.

## 7.8.2. Characterization of Zinc chloride-Fructose-Glutamine TDES

### 7.8.2.1 Density and Conductivity

The most significant property of any liquid is density. There is very little information about TDES densities. Because it is affected by ion concentration, the high viscous liquid will have low conductivity<sup>[3-6]</sup>. The density of ZC-FRU-GLUT TDES is  $1.3046\text{g/cm}^3$  and its conductivity is  $0.0132\text{mS/cm}$  at normal temperature.

### 7.8.2.2 pH

The pH is a critical physical parameter that considerably impacts chemical reactions. Andrea Skulcova et al.<sup>[7]</sup> investigated the influence of temperature on pH for a range of DESs and discovered that pH values fell as the temperature rose. The influence of temperature on the pH of newly generated DESs was investigated in this work. According to a pH behaviour study, the hydrogen-bond donor has a significant impact on the pH of

the final product. The acidity of the mixture is determined by the type of the hydrogen bond donor. As the temperature rises, the pH values of ZC-FRU-GLUT TDES decrease slightly, as seen in Fig.7.2.1.

### **7.8.2.3 Viscosity**

The interaction between molecules in a liquid mixture is replicated by viscosity <sup>[8]</sup>. The lower the viscosity of DES, the better it may be employed as a solvent <sup>[9]</sup>. Fig. 7.2.2 shows the viscosity of ZC-FRU-GLUT TDES as a function of temperature. The viscosity reduces significantly as the temperature rises.

### **7.8.2.4 FTIR spectrum of ZC-FRU-GLUT TDES**

Figure 7.2.3 shows the FTIR spectrum of ZC-FRU-GLUT TDES. The intermolecular O - H stretching of the alcoholic group causes the large peak at  $3404.30\text{cm}^{-1}$  <sup>[9]</sup> and the broad peak at  $2928.48\text{cm}^{-1}$  is due to the carboxylic O - H stretching <sup>[10]</sup>. The peak at  $1659.01\text{cm}^{-1}$  is due to amide C = O stretching and  $1402.05\text{cm}^{-1}$  <sup>[10, 11]</sup> is due to the C - H bending of the methyl group of glucose. The C - O stretching of the carboxylic acid of malonic acid is seen at  $1290.9\text{cm}^{-1}$  <sup>[11]</sup>, while C - OH stretching causes peaks between  $1151.8$  and  $1060.7\text{cm}^{-1}$  <sup>[11]</sup>.

## **7.8.3 Characterization of Zinc Chloride-Glucose-Glycine TDES**

### **7.8.3.1 Density and Conductivity**

The most significant property of any liquid is density. There is very little information about TDES densities. Because it is affected by ion concentration, the high viscous liquid will have low conductivity <sup>[3-6]</sup>. The density of ZC-GLU-GLY TDES is  $1.3498\text{ g/cm}^3$  and its conductivity is  $0.00145\text{ mS/cm}$  at normal temperature.

### **7.8.3.2 pH**

The pH is a critical physical parameter that considerably impacts chemical reactions. Andrea Skulcova et al. <sup>[7]</sup> investigated the influence of temperature on pH for a

range of DESs and discovered that pH values fell as the temperature rose. The influence of temperature on the pH of newly generated DESs was investigated in this work. According to a pH behaviour study, the hydrogen-bond donor has a significant impact on the pH of the final product. The acidity of the mixture is determined by the type of the hydrogen bond donor. As the temperature rises, the pH values of ZC-GLU-GLY TDES decrease slightly, as seen in Fig.7.3.1.

### **7.8.3.3 Viscosity**

The interaction between molecules in a liquid mixture is replicated by viscosity <sup>[8]</sup>. The lower the viscosity of DES, the better it may be employed as a solvent <sup>[9]</sup>. Fig. 7.3.2 shows the viscosity of ZC-GLU-GLY TDES as a function of temperature. The viscosity reduces significantly as the temperature rises.

### **7.8.3.4 FTIR spectrum of ZC-GLU-GLY TDES**

Figure 7.3.3 shows the FTIR spectrum of ZC-GLU-GLY TDES. The intermolecular O - H stretching of the alcoholic group causes the large peak at 3417.06  $\text{cm}^{-1}$ <sup>[9]</sup> and the broad peak at 2932.15 $\text{cm}^{-1}$  is due to the carboxylic O - H stretching <sup>[10]</sup>. The peak at 1633.91 $\text{cm}^{-1}$  is due to amide C = O stretching and the peaks at 1439.03 $\text{cm}^{-1}$ , 1410.66 $\text{cm}^{-1}$ <sup>[10, 11]</sup> are due to the C - H bending of the methyl group of glucose. The C - OH stretching causes peaks between 1099.32 and 1033.20 $\text{cm}^{-1}$ <sup>[11]</sup>.

## **7.8.4 Characterization of Zinc chloride-Fructose-Glycine TDES**

### **7.8.4.1 Density and Conductivity**

The most significant property of any liquid is density. There is very little information about TDES densities. Because it is affected by ion concentration, the high viscous liquid will have low conductivity <sup>[3-6]</sup>. The density of ZC-FRU-GLY TDES is 1.3054  $\text{g}/\text{cm}^3$  and its conductivity is 0.0043  $\text{mS}/\text{cm}$  at normal temperature.



#### **7.8.4.2 pH**

The pH is a critical physical parameter that considerably impacts chemical reactions. Andrea Skulcova et al. [7] investigated the influence of temperature on pH for a range of DESs and discovered that pH values fell as the temperature rose. The influence of temperature on the pH of newly generated DESs was investigated in this work. According to a pH behaviour study, the hydrogen-bond donor has a significant impact on the pH of the final product. The acidity of the mixture is determined by the type of the hydrogen bond donor. As the temperature rises, the pH values of ZC-FRU-GLY TDES decrease slightly, as seen in Fig.7.4.1.

#### **7.8.4.3 Viscosity**

The interaction between molecules in a liquid mixture is replicated by viscosity [8]. The lower the viscosity of DES, the better it may be employed as a solvent [9]. Fig. 7.4.2 shows the viscosity of ZC-FRU-GLY TDES as a function of temperature. The viscosity reduces significantly as the temperature rises.

#### **7.8.4.4 FTIR spectrum of ZC-FRU-GLY TDES**

Figure 7.4.3 shows the FTIR spectrum of ZC-FRU-GLY TDES. The intermolecular O - H stretching of the alcoholic group causes the large peak at  $3425.11\text{cm}^{-1}$ [9] and the broad peak at  $2928.48\text{cm}^{-1}$  is due to the carboxylic O - H stretching [10]. The peaks at  $1659.14\text{cm}^{-1}$  and  $1633.61\text{cm}^{-1}$  are due to amide C = O stretching and  $1401.96\text{cm}^{-1}$ [10, 11] is due to C - H bending of the methyl group of glucose. The C - O stretching of the carboxylic acid of malonic acid is seen at  $1291.55\text{cm}^{-1}$ [11], while C - OH stretching causes peaks between  $1152.38$  and  $1061.03\text{cm}^{-1}$ [11].

## **7.8.5 Characterization of Zinc Chloride-Glucose-Histidine TDES**

### **7.8.5.1 Density and Conductivity**

The most significant property of any liquid is density. There is very little information about TDES densities. Because it is affected by ion concentration, the high viscous liquid will have low conductivity<sup>[3-6]</sup>. The density of ZC-GLU-HIS TDES is 1.312 g/cm<sup>3</sup> and its conductivity is 0.004 mS/cm at normal temperature.

### **7.8.5.2 pH**

The pH is a critical physical parameter that considerably impacts chemical reactions. Andrea Skulcova et al.<sup>[7]</sup> investigated the influence of temperature on pH for a range of DESs and discovered that pH values fell as the temperature rose. The influence of temperature on the pH of newly generated DESs was investigated in this work. According to a pH behaviour study, the hydrogen-bond donor has a significant impact on the pH of the final product. The acidity of the mixture is determined by the type of the hydrogen bond donor. As the temperature rises, the pH values of ZC-GLU-HIS TDES decrease slightly, as seen in Fig.7.5.1.

### **7.8.5.3 Viscosity**

The interaction between molecules in a liquid mixture is replicated by viscosity<sup>[8]</sup>. The lower the viscosity of DES, the better it may be employed as a solvent<sup>[9]</sup>. Fig. 7.5.2 shows the viscosity of ZC-GLU-HIS TDES as a function of temperature. The viscosity reduces significantly as the temperature rises.

### **7.8.5.4 FTIR spectrum of ZC-GLU-HIS TDES**

Figure 7.5.3 shows the FTIR spectrum of ZC-GLU-HIS TDES. The intermolecular O - H stretching of the alcoholic group causes the large peak at 3385.87cm<sup>-1</sup><sup>[9]</sup> and the broad peak at 2927.6cm<sup>-1</sup> is due to the carboxylic O -H stretching<sup>[10]</sup>. The peak at 1630.24cm<sup>-1</sup> is due to amide C = O stretching and the peak at 1406.12cm<sup>-1</sup><sup>[10, 11]</sup> is due to the C - H

bending of the methyl group of glucose. The C - N stretching shows a peak at  $1195.8\text{cm}^{-1}$  and C - OH stretching causes the peak at  $1076.11\text{cm}^{-1}$ <sup>[11]</sup>.

## **7.8.6 Characterization of Zinc chloride-Fructose-Histidine TDES**

### **7.8.6.1 Density and Conductivity**

The most significant property of any liquid is density. There is very little information about TDES densities. Because it is affected by ion concentration, the high viscous liquid will have low conductivity<sup>[3-6]</sup>. The density of ZC-FRU-HIS TDES is  $1.2949\text{ g/cm}^3$  and its conductivity is  $0.0116\text{ mS/cm}$  at normal temperature.

### **7.8.6.2 pH**

The pH is a critical physical parameter that considerably impacts chemical reactions. Andrea Skulcova et al.<sup>[7]</sup> investigated the influence of temperature on pH for a range of DESs and discovered that pH values fell as the temperature rose. The influence of temperature on the pH of newly generated DESs was investigated in this work. According to a pH behaviour study, the hydrogen-bond donor has a significant impact on the pH of the final product. The acidity of the mixture is determined by the type of the hydrogen bond donor. As the temperature rises, the pH values of ZC-FRU-HIS TDES decrease slightly, as seen in Fig.7.6.1.

### **7.8.6.3 Viscosity**

The interaction between molecules in a liquid mixture is replicated by viscosity<sup>[8]</sup>. The lower the viscosity of DES, the better it may be employed as a solvent<sup>[9]</sup>. Fig. 7.6.2 shows the viscosity of ZC-FRU-HIS TDES as a function of temperature. The viscosity reduces significantly as the temperature rises.

### **7.8.6.4 FTIR spectrum of ZC-FRU-HIS TDES**

Figure 7.6.3 shows the FTIR spectrum of ZC-FRU-HIS TDES. The intermolecular O - H stretching of the alcoholic group causes the large peak at  $3399.68\text{cm}^{-1}$ <sup>[9]</sup> and the broad

peak at  $2937.88\text{cm}^{-1}$  is due to the carboxylic O - H stretching <sup>[10]</sup>. The peak at  $1631.25\text{cm}^{-1}$  is due to amide C = O stretching and  $1405.77\text{cm}^{-1}$ <sup>[10, 11]</sup> is due to the C - H bending of the methyl group of glucose. The C - O stretching of the carboxylic acid of malonic acid is seen at  $1287.27\text{cm}^{-1}$ <sup>[11]</sup>, while C - OH stretching causes peaks between  $1181.59$  and  $1058.79\text{cm}^{-1}$ <sup>[11]</sup>.

## **7.9. Conclusion**

Six types of zinc chloride-based ternary deep eutectic solvents were prepared. The physical parameters such as density, conductivity, pH, viscosity were studied. The hydrogen-bonded interactions between the components were also characterized.

## References

- [1]. Emma L. Smith, Andrew P. Abbot, and Karl S. Ryder, Deep Eutectic Solvents (DESs) and Their Applications, *Chem. Rev.* 2014, 114, 21, 11060–11082, <https://doi.org/10.1021/cr300162p>.
- [2]. Y.T. Dai, J. van Spronsen, G.J. Witkamp, R. Verpoorte, Y.H. Choi, Natural deep eutectic solvents as new potential media for green technology, *Anal. Chim. Acta* 766 (2013) 61 – 68.
- [3]. Q. Cao; X. Lu; X. Wu; Y. Guo; Xu, L.; Fang, W. Density, Viscosity, and Conductivity of Binary Mixtures of the Ionic Liquid N-(2-Hydroxyethyl) piperazinium Propionate with Water, Methanol, or Ethanol, *Journal of Chemical & Engineering Data* (2015) 60,3, 455-463.
- [4]. P. Wasserscheid and P. Welton eds., *Ionic Liquids in Synthesis*, Wiley-VCH Verlag, Weinheim, *Org. Proc. Res. Dev.* 2003, 7, 2, 223–224
- [5]. F. Endres, A. P. Abbott, D. R Mac Farlane eds., *Electrodeposition from Ionic liquids*, Wiley-VCH Verlag, Weinheim, 2008.
- [6]. A. P. Abbott, D. Boothby, G. Capper, D. L. Davies, R. Rasheed, Deep Eutectic Solvents Formed between Choline Chloride and Carboxylic Acids: Versatile Alternatives to Ionic Liquids, *J. Am. Chem. Soc.*, 126, 29, (2004). 9142–9147.
- [7]. Andrea Skulcova, Albert Russ, Michal Jablonsky, JozefSima, “pH of eutectic solvents,” *BioResources* 13(3), (2018) 5042 - 5051.
- [8]. W. J. Guo, Y. C. Hou, S. H. Ren, S. D. Tian, W. Z. Wu, Formation of deep eutectic solvents by phenols and choline chloride and their physical properties, *J. Chem. Eng. Data* 58 (2013) 866 – 872. <https://doi.org/10.1021/je300997v>

[9]. Koon-Kee Kow, Kamaliah Sirat, Novel manganese (II)-based deep eutectic solvents: Synthesis and physical properties analysis, *Chinese Chemical Letters*, 26 10 (2015) 1311–1314.

[10]. Donald L. Pavia, Gary M. Lampman, George S. Kriz, *Introduction to Spectroscopy*, 3rd Edition, BROOKS/COLE, Thomson Learning, USA, 2001

[11]. B.D. Mistry, *A Handbook of Spectroscopic Data*, Oxford Book Company, India, 2009.

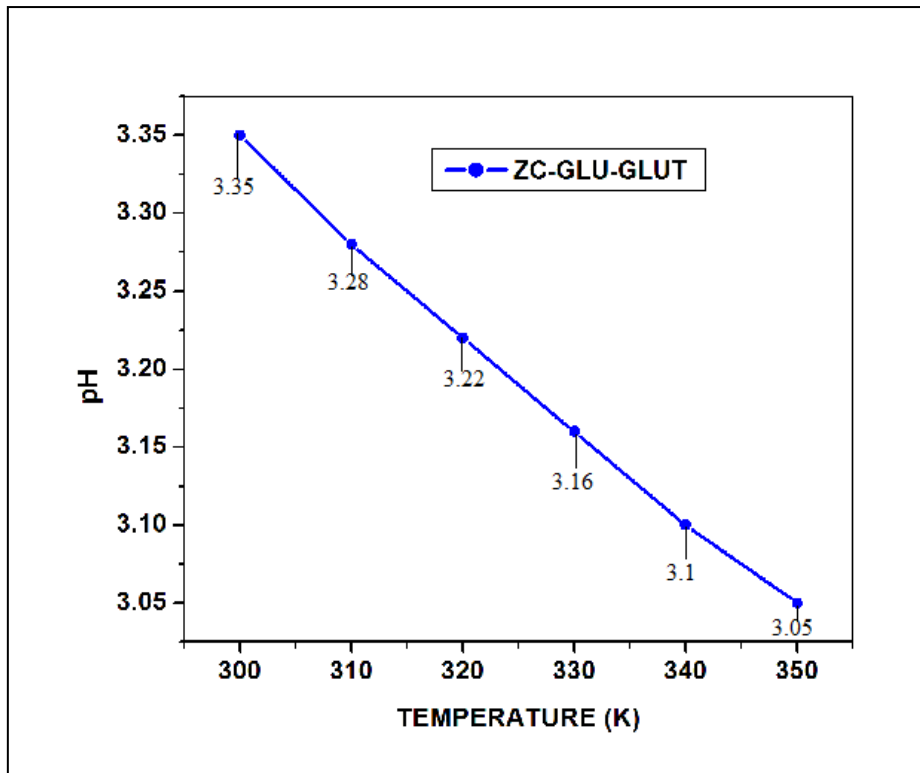


Figure 7.1.1 pH as a function against T of ZC-GLU-GLUT TDES

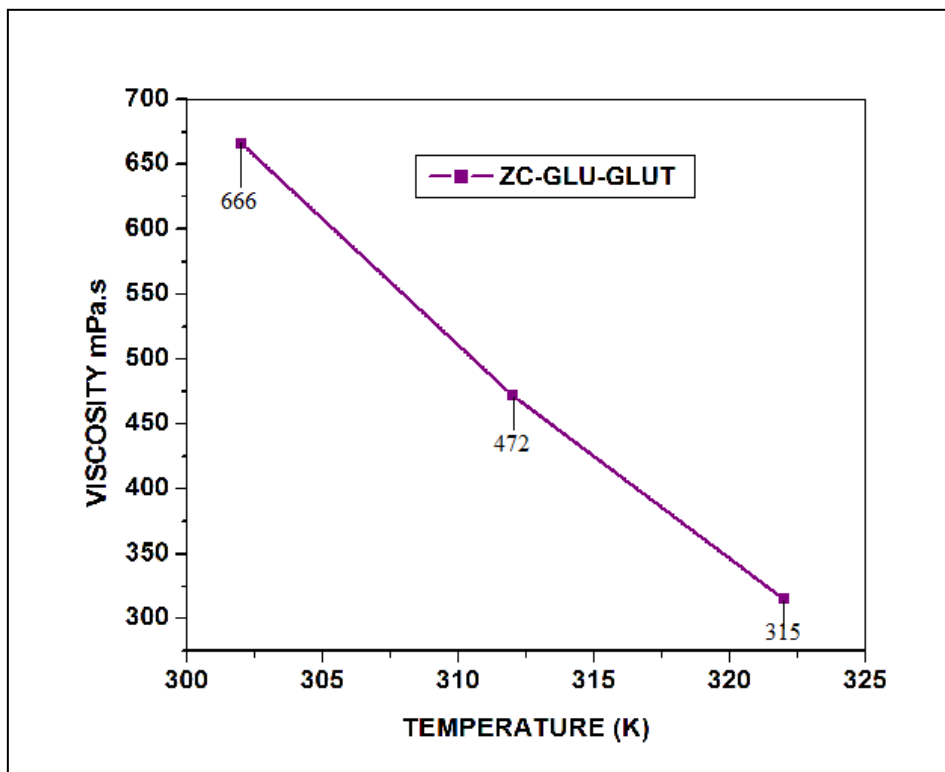


Figure 7.1.2 Viscosity of ZC-GLU-GLUT TDES at Different Temperature

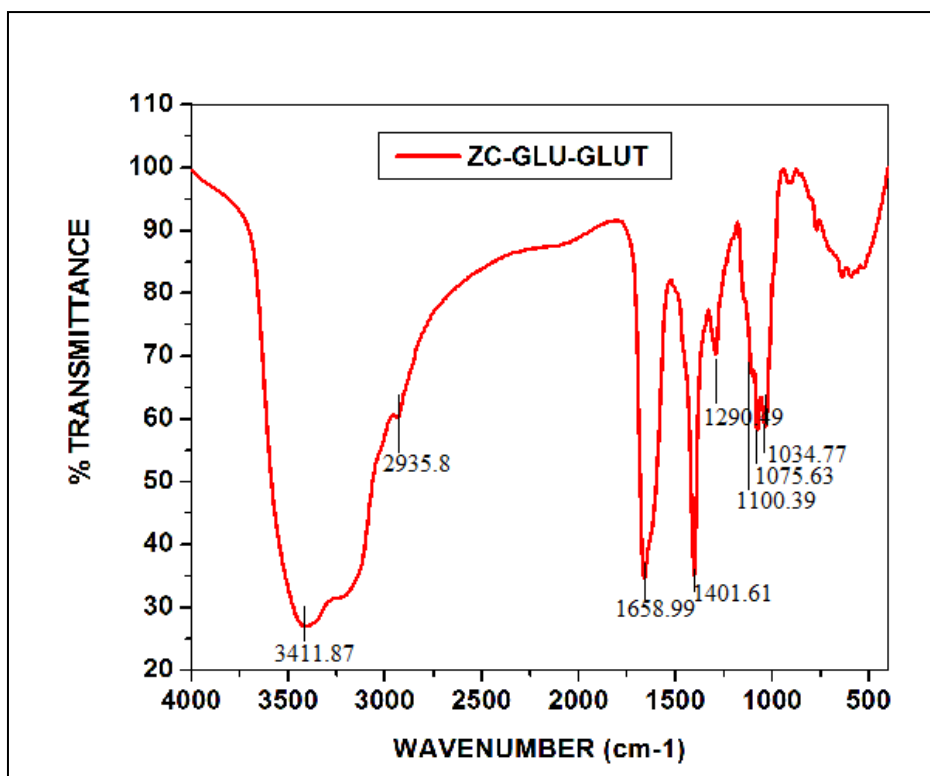


Figure 7.1.3 FTIR spectrum of ZC-GLU-GLUT TDES

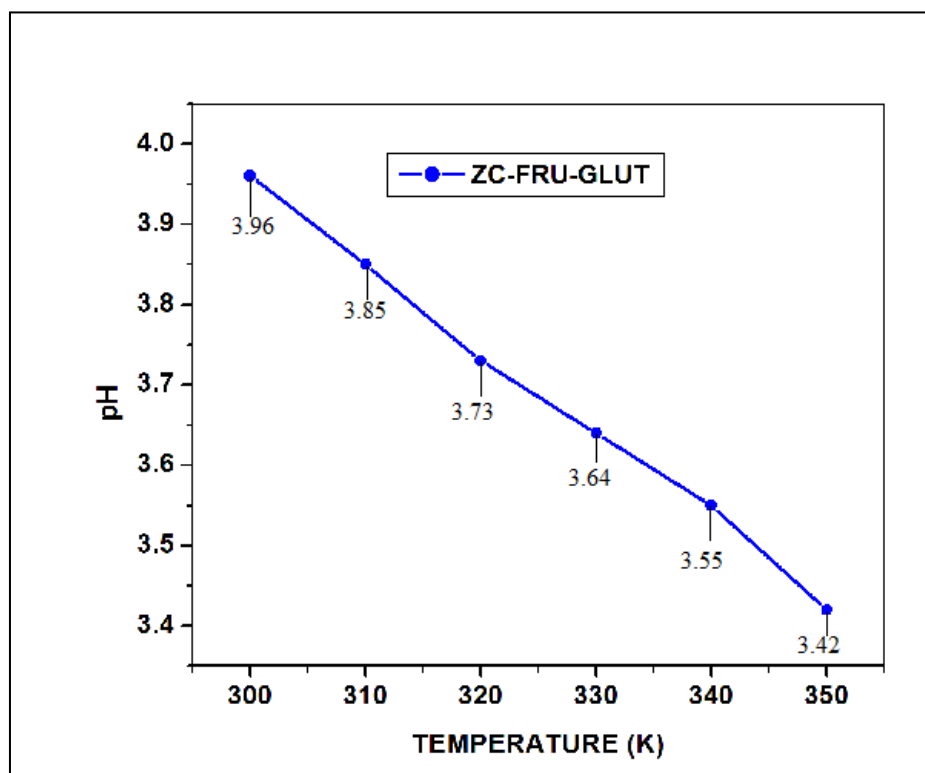


Figure 7.2.1 pH as a function against T of ZC-FRU-GLUT TDES



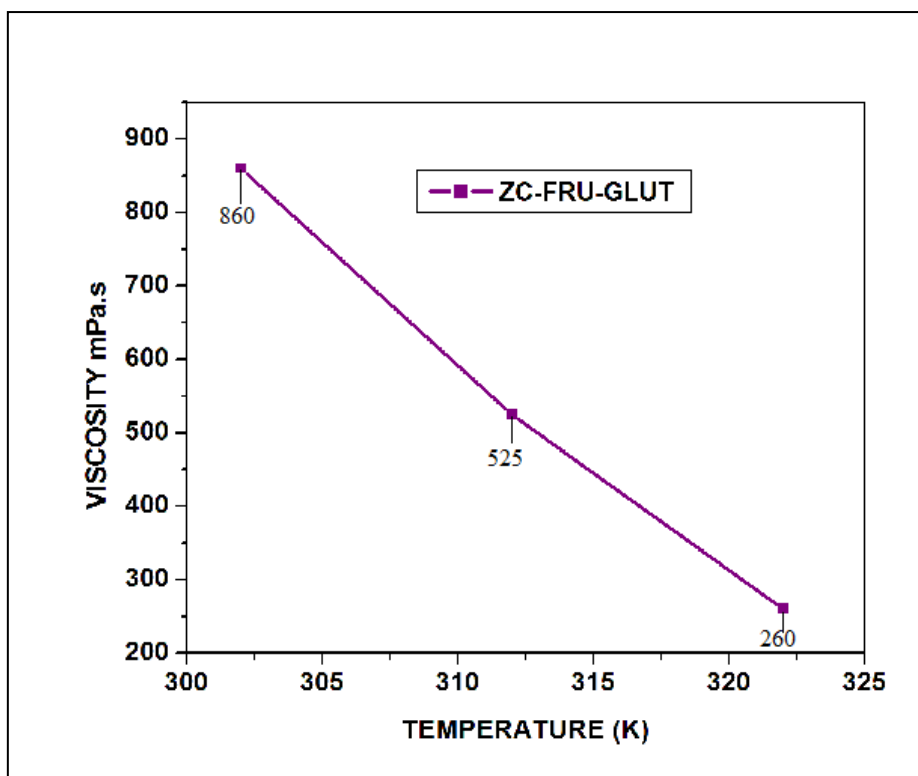


Figure 7.2.2 Viscosity of ZC-FRU-GLUT TDES at Different Temperatures

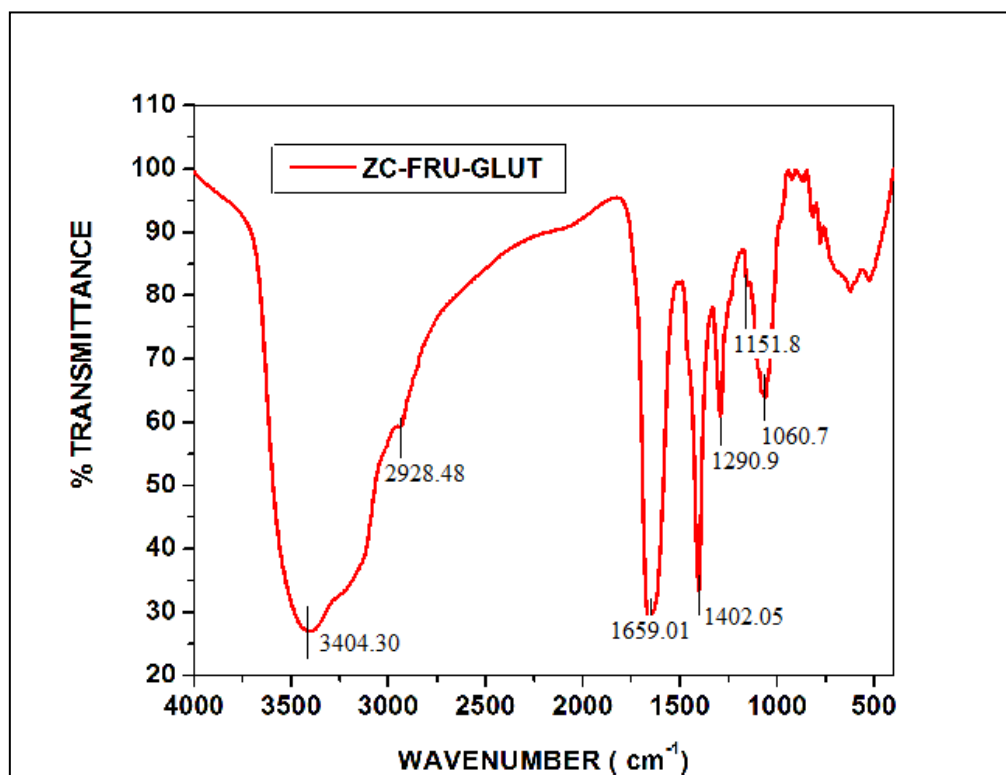


Figure 7.2.3 FTIR spectrum of ZC-FRU-GLUT TDES

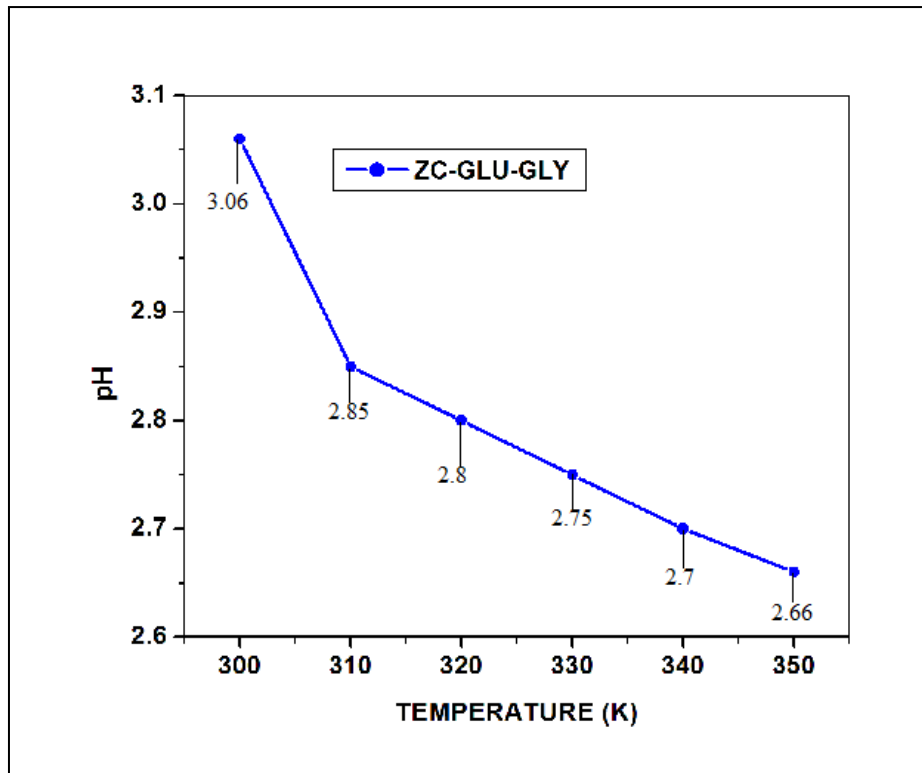


Figure 7.3.1 pH as a function against T of ZC-GLU-GLY TDES

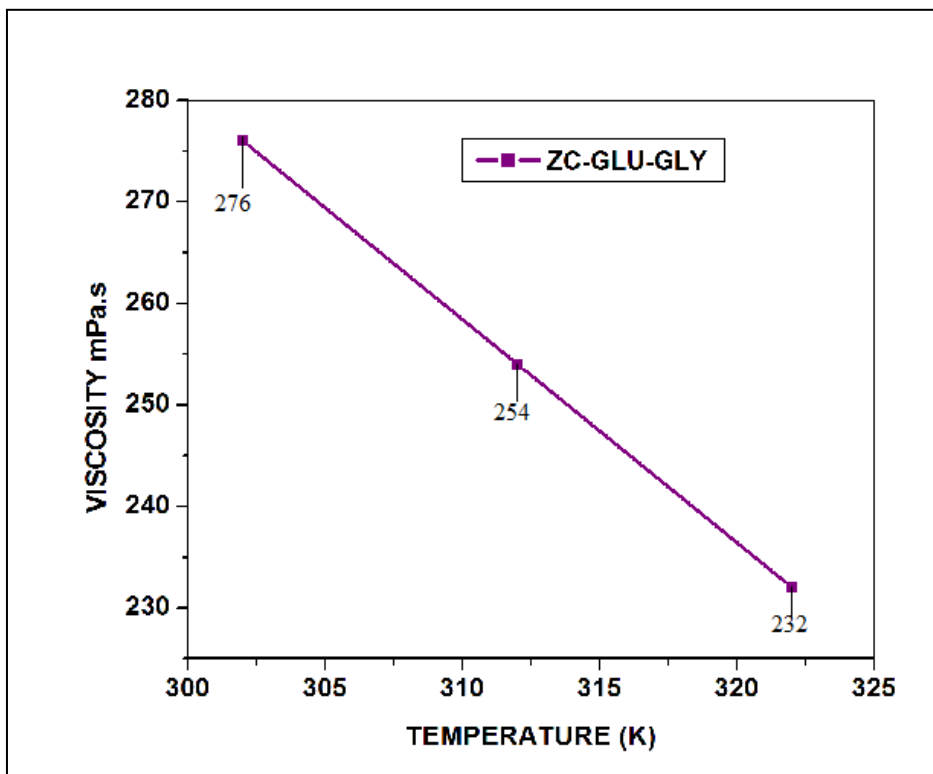


Figure 7.3.2 Viscosity of ZC-GLU-GLY TDES at Different Temperatures

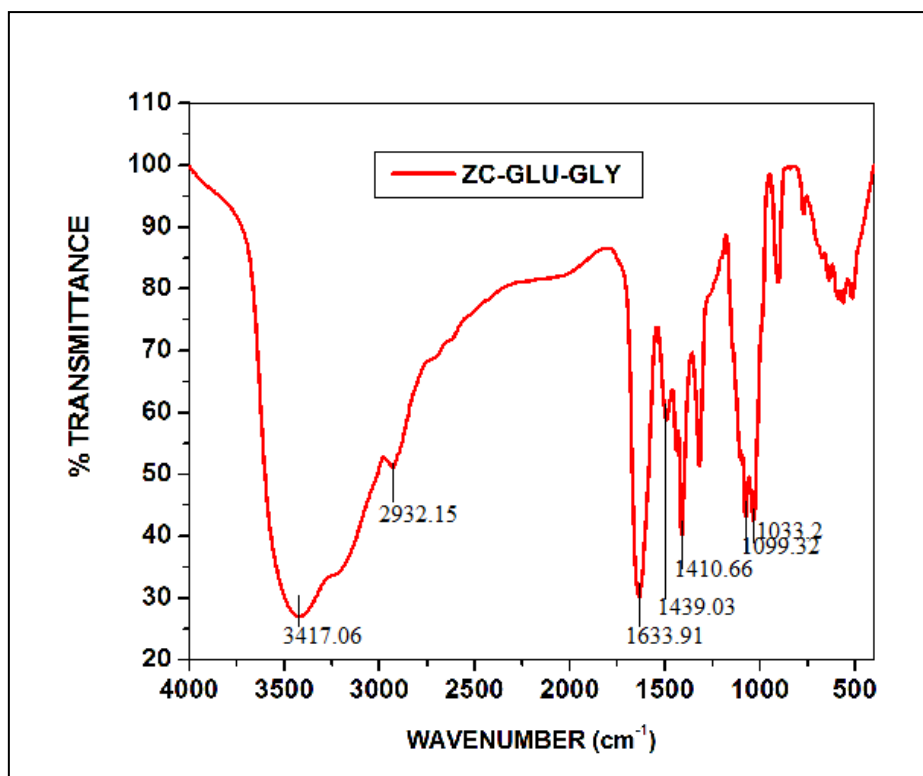


Figure 7.3.3 FTIR spectrum of ZC-GLU-GLY TDES

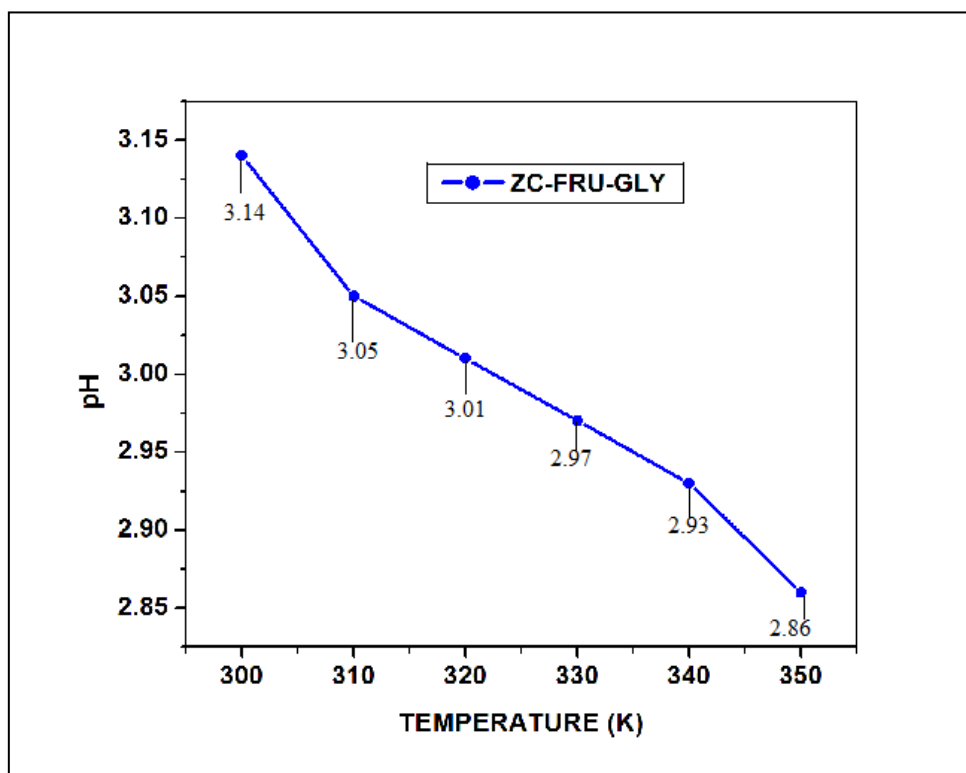


Figure 7.4.1 pH as a function against T of ZC-FRU-GLY TDES

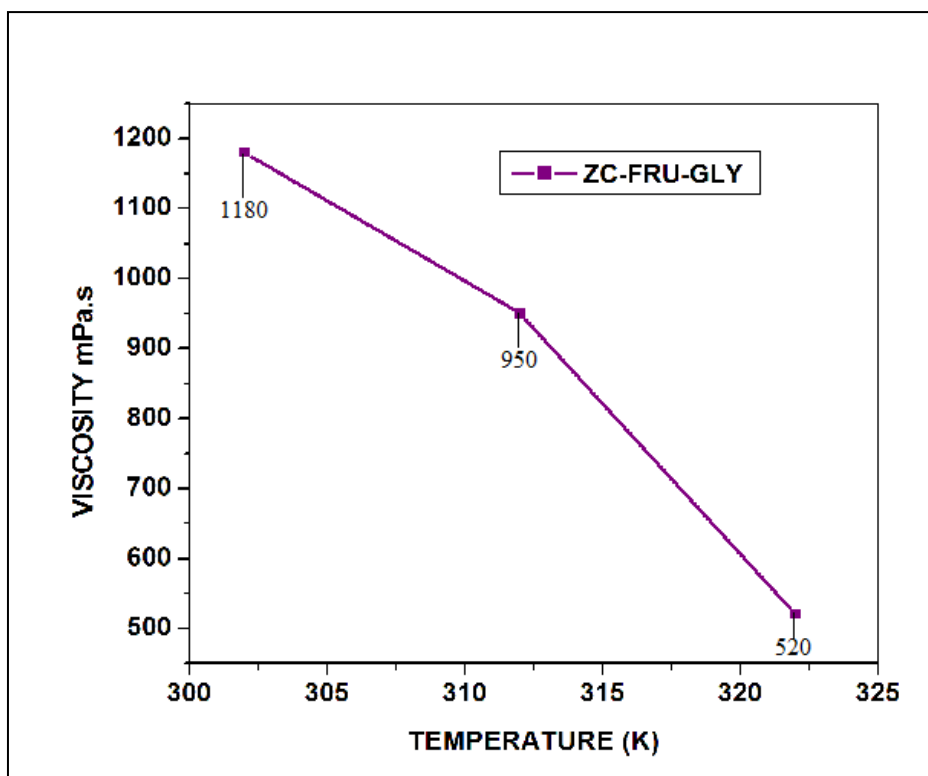


Figure 7.4.2. Viscosity of ZC-FRU-GLY TDES at Different Temperatures

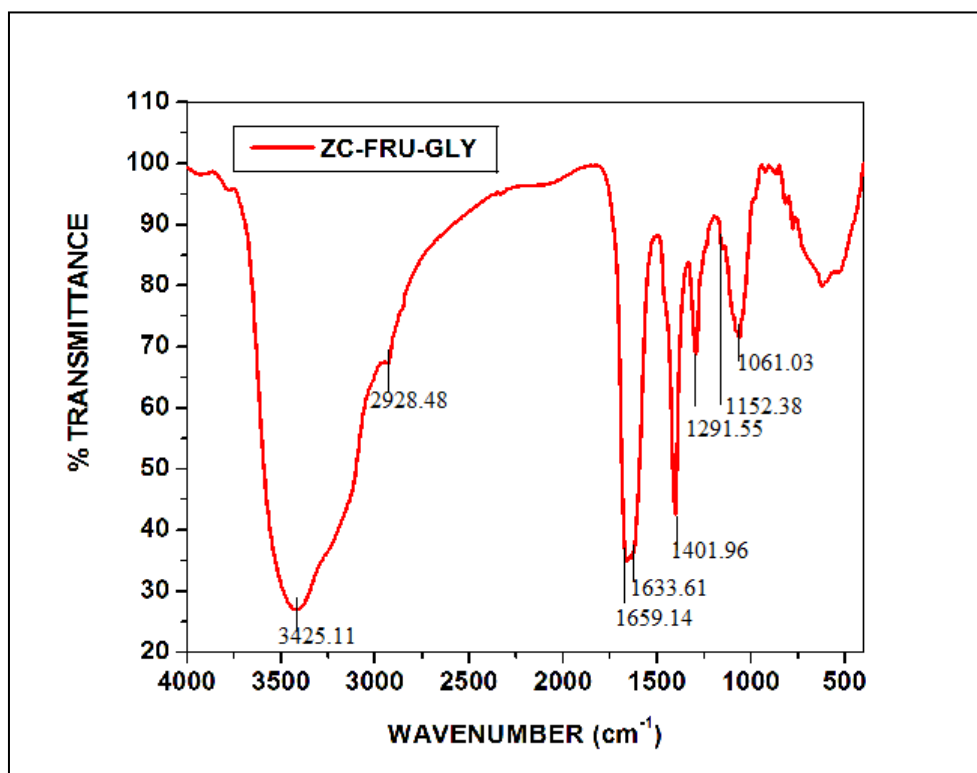


Figure 7.4.3 FTIR spectrum of ZC-FRU-GLY TDES

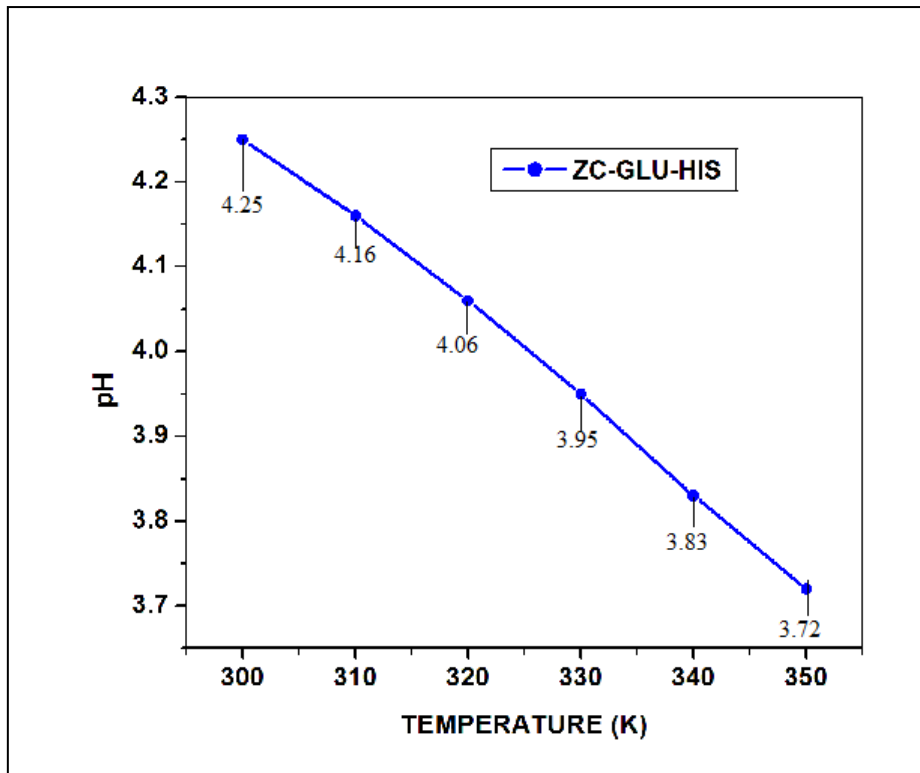


Figure 7.5.1 pH as a function against T of ZC-GLU-HIS TDES

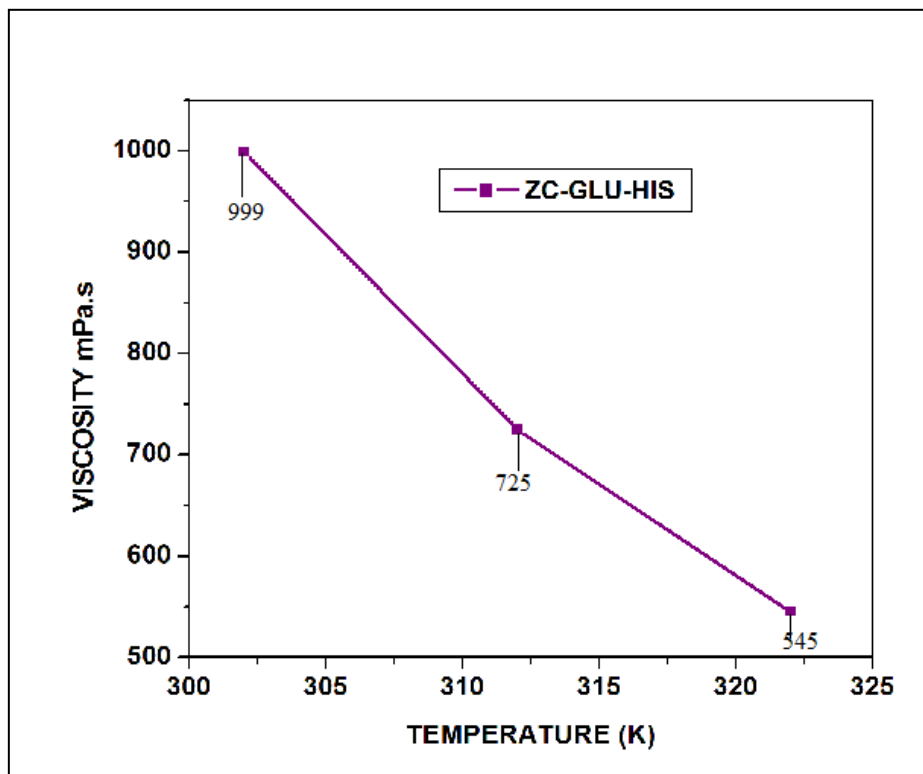


Figure 7.5.2 Viscosity of ZC-GLU-HIS TDES at Different Temperatures

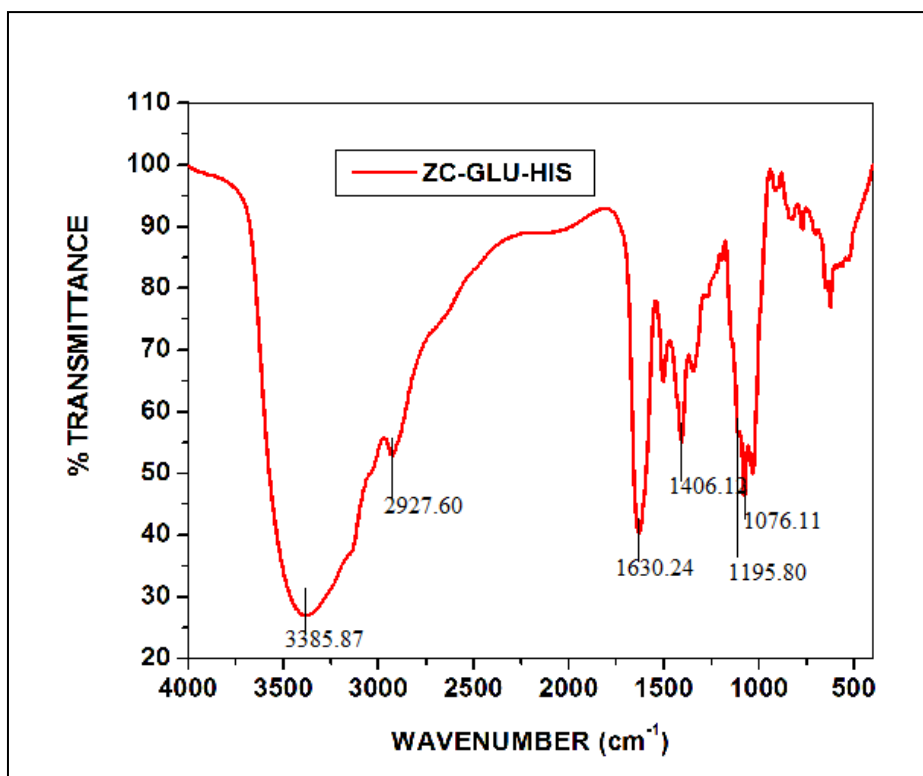


Figure 7.5.3 FTIR spectrum of ZC-GLU-HIS TDES

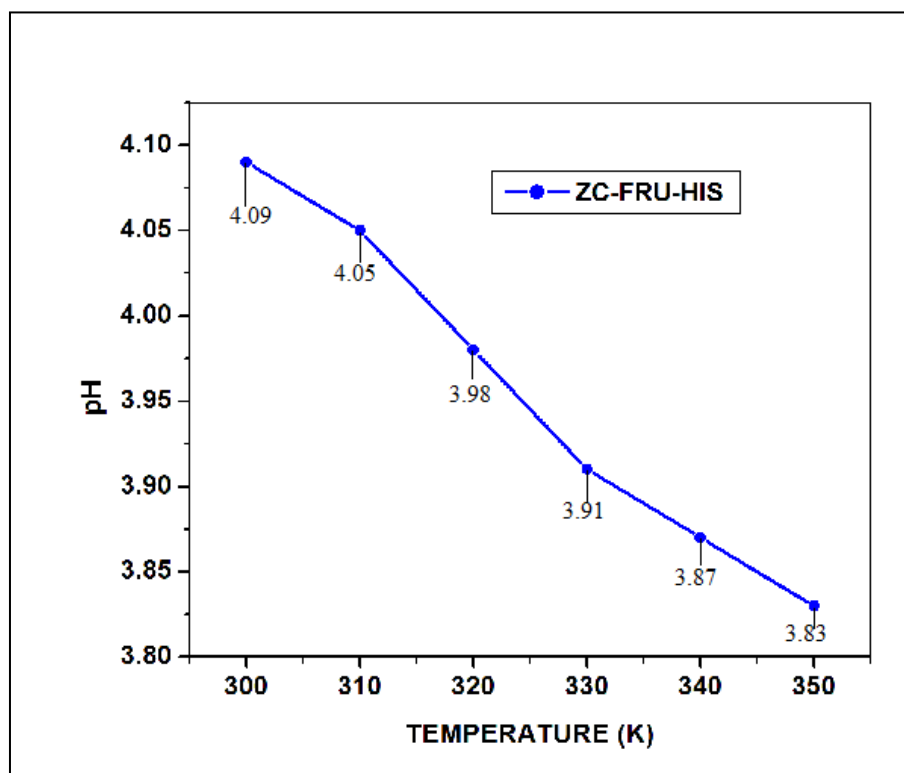


Figure 7.6.1 pH as a function against T of ZC-FRU-HIS TDES

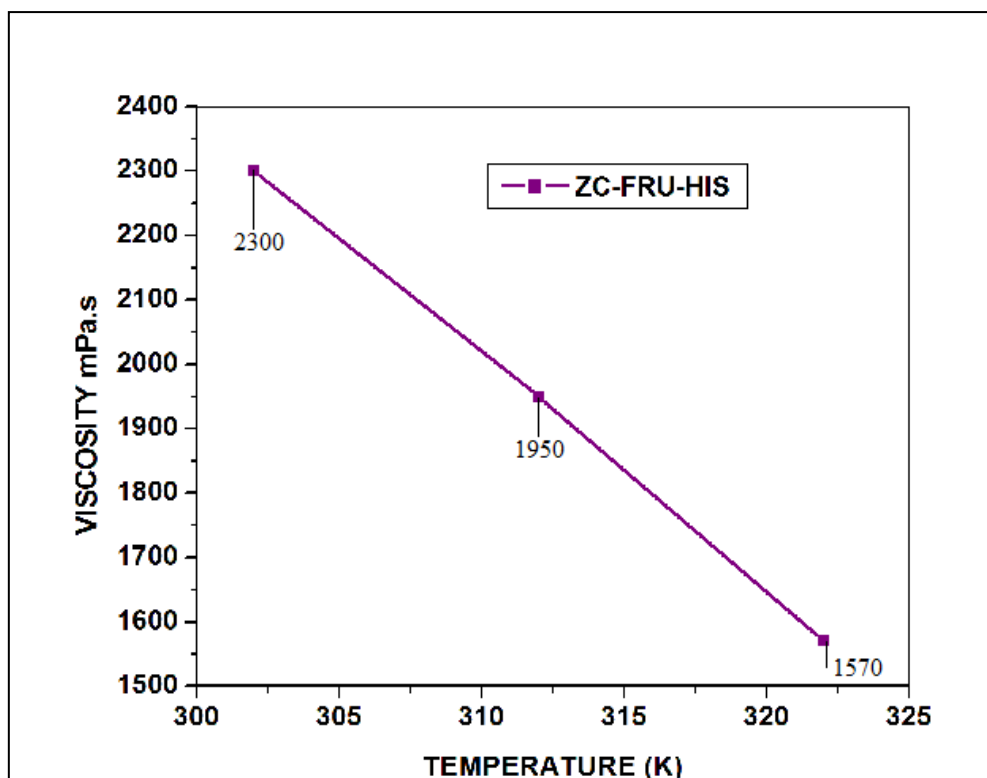


Figure 7.6.2 Viscosity of ZC-FRU-HIS TDES at Different Temperatures

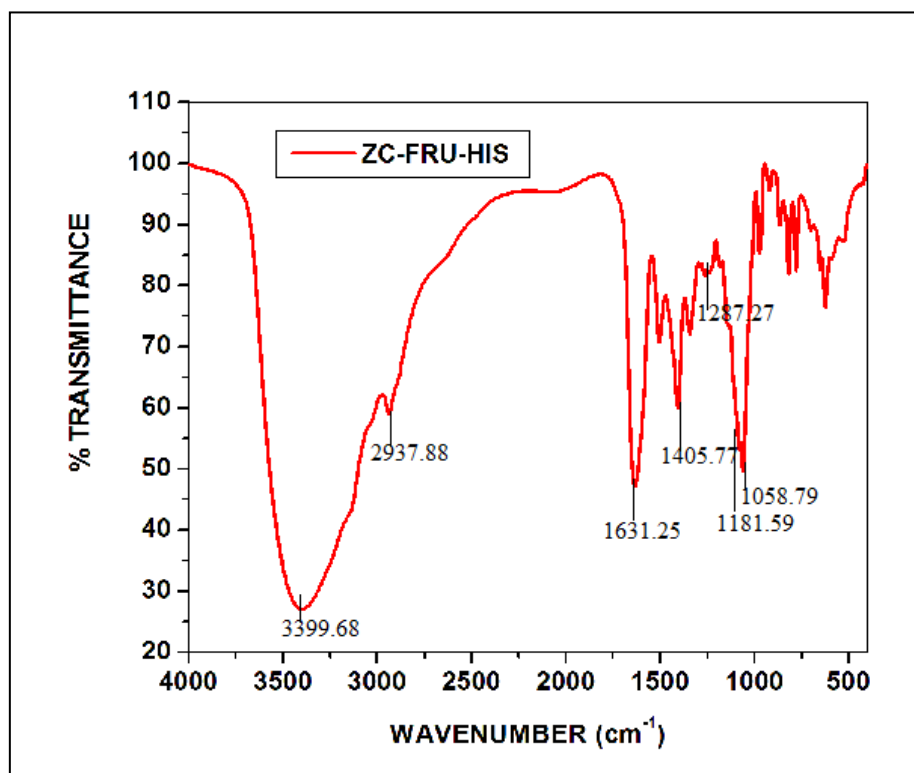


Figure 7.6.3 FTIR spectrum of ZC-FRU-HIS TDES





## **8. Manganese chloride-based Ternary Deep Eutectic Solvents (TDES)**

---

### **8.1 Introduction**

The formation of metal-based eutectics from metal salts or metal salt hydrate in combination with various hydrogen-bond donors (HBDs) <sup>[1]</sup> is known as Type IV deep eutectic solvent (DES). In this study, we had synthesized six types of ternary deep eutectic solvents by mixing manganese chloride, glucose/ fructose, and amino acids such as glutamine, glycine, and histidine as reported by Dai. Et.al <sup>[2]</sup>. The successfully synthesized ternary deep eutectic solvents were subjected to measure physical properties such as density, conductivity, pH, viscosity, and FTIR.

### **8.2 Preparation of Manganese Chloride-Glucose-Glutamine (MC-GLU-GLUT) TDES**

Manganese chloride, glucose, and glutamine at a mole ratio of 1:1:1 were dissolved in double distilled water and evaporated in a water bath till the constant weight was attained <sup>[2]</sup>. The mixture as a clear liquid was kept in a desiccator containing anhydrous CaCl<sub>2</sub> for about two weeks. As no turbidity developed during this time, the ternary DESs were subjected to physical property measurements such as density, pH, conductivity, and viscosity. The H-bonded interactions between the components were characterized using FTIR.

### **8.3 Preparation of Manganese Chloride-Fructose-Glutamine (MC-FRU-GLUT) TDES**

Manganese chloride, fructose, and glutamine at a mole ratio of 1:1:1 were dissolved in double distilled water and evaporated in a water bath till the constant weight was attained <sup>[2]</sup>. The mixture as a clear liquid was kept in a desiccator containing anhydrous CaCl<sub>2</sub> for about two weeks. As no turbidity developed during this time, the ternary DESs were

subjected to physical property measurements such as density, pH, conductivity, and viscosity. The H-bonded interactions between the components were characterized using FTIR.

#### **8.4 Preparation of Manganese Chloride-Glucose-Glycine (MC-GLU-GLY) TDES**

Manganese chloride, glucose, and glycine at a mole ratio of 1:1:1 were dissolved in double distilled water and evaporated in a water bath till the constant weight was attained [2]. The mixture as a clear liquid was kept in a desiccator containing anhydrous CaCl<sub>2</sub> for about two weeks. As no turbidity developed during this time, the ternary DESs were subjected to physical property measurements such as density, pH, conductivity, and viscosity. The H-bonded interactions between the components were characterized using FTIR.

#### **8.5 Preparation of Manganese Chloride-Fructose-Glycine (MC-FRU-GLY) TDES**

Manganese chloride, fructose, and glycine at a mole ratio of 1:1:1 were dissolved in double distilled water and evaporated in a water bath till the constant weight was attained [2]. The mixture as a clear liquid was kept in a desiccator containing anhydrous CaCl<sub>2</sub> for about two weeks. As no turbidity developed during this time, the ternary DESs were subjected to physical property measurements such as density, pH, conductivity, and viscosity. The H-bonded interactions between the components were characterized using FTIR.

#### **8.6 Preparation of Manganese Chloride-Glucose-Histidine (MC-GLU-HIS) TDES**

Manganese chloride, glucose, and histidine at a mole ratio of 1:1:1 were dissolved in double distilled water and evaporated in a water bath till the constant weight was attained [2]. The mixture as a clear liquid was kept in a desiccator containing anhydrous CaCl<sub>2</sub> for about two weeks. As no turbidity developed during this time, the ternary DESs were subjected to physical property measurements such as density, pH, conductivity, and

viscosity. The H-bonded interactions between the components were characterized using FTIR.

### **8.7 Preparation of Manganese Chloride-Fructose-Histidine (MC-FRU-HIS) TDES**

Manganese chloride, fructose, and glycine at a mole ratio of 1:1:1 were dissolved in double distilled water and evaporated in a water bath till the constant weight was attained [2]. The mixture as a clear liquid was kept in a desiccator containing anhydrous CaCl<sub>2</sub> for about two weeks. As no turbidity developed during this time, the ternary DESs were subjected to physical property measurements such as density, pH, conductivity, and viscosity. The H-bonded interactions between the components were characterized using FTIR.

## **8.8. Results and Discussion**

### **8.8.1 Characterization of Manganese Chloride-Glucose-Glutamine TDES**

#### **8.8.1.1 Density and Conductivity**

The density is the most important feature of a liquid. There is little known information about the TDES densities. The high viscous liquid will have low conductivity because it is affected by ion concentration [3-6]. At room temperature, MC-GLU-GLUT TDES has a density of 1.5296 g/cm<sup>3</sup> and a conductivity of 0.016 mS/cm.

#### **8.8.1.2 pH**

The pH scale is an important physical parameter that has a significant impact on chemical processes. Andrea Skulcova et al. [7] studied the effect of temperature on pH for a variety of DESs and discovered that as the temperature increased, pH values decreased. This study investigated the effect of temperature on the pH of newly formed DESs. The hydrogen-bond donor has a considerable impact on the pH of the final product, according to pH behavior research. The type of hydrogen bond donor determines the acidity of the

combination. The pH values of MC-GLU-GLUT TDES fall slightly as the temperature rises, as shown in Fig.8.1.1.

### **8.8.1.3 Viscosity**

Viscosity <sup>[8]</sup> replicates the interaction between molecules in a liquid mixture. The lower the viscosity of DES, the better it may be used as a solvent <sup>[1]</sup>. The viscosity of MC-GLU-GLUT TDES as a function of temperature is shown in Figure 8.1.2. As the temperature rises, the viscosity decreases dramatically.

### **8.8.1.4 FTIR spectrum of MC-GLU-GLUT TDES**

Figure 8.1.3 shows the FTIR spectrum of MC-GLU-GLUT TDES. The intermolecular O - H stretching of the alcoholic group causes a large peak at  $3389.97\text{cm}^{-1}$ <sup>[11]</sup>. The peak at  $1655.07\text{cm}^{-1}$  is due to amide C = O stretching and the peaks at  $1403.25\text{cm}^{-1}$  &  $1302.89\text{cm}^{-1}$ <sup>[9, 10]</sup> is due to the C - H bending of the methyl group of glucose. The C - OH stretching causes peaks between  $1079.65$  and  $1034.43\text{cm}^{-1}$ <sup>[10]</sup>.

## **8.8.2 Characterization of Manganese Chloride-Fructose-Glutamine TDES**

### **8.8.2.1 Density and Conductivity**

The density is the most important feature of a liquid. There is little known information about the TDES densities. The high viscous liquid will have low conductivity because it is affected by ion concentration <sup>[3-6]</sup>. At room temperature, MC-FRU-GLUT TDES has a density of  $1.5096\text{ g/cm}^3$  and a conductivity of  $0.018\text{mS/cm}$ .

### **8.8.2.2 pH**

The pH scale is an important physical parameter that has a significant impact on chemical processes. Andrea Skulcova et al. <sup>[7]</sup> studied the effect of temperature on pH for a variety of DESs and discovered that as the temperature increased, pH values decreased. This study investigated the effect of temperature on the pH of newly formed MC-FRU-GLUT TDES. The hydrogen-bond donor has a considerable impact on the pH of the final

product, according to pH behavior research. The type of hydrogen bond donor determines the acidity of the combination. The pH values of MC-GLU-GLUT TDES fall slightly as the temperature rises, as shown in Fig.8.2.1.

### **8.8.2.3 Viscosity**

Viscosity <sup>[8]</sup> replicates the interaction between molecules in a liquid mixture. The lower the viscosity of DES, the better it may be used as a solvent <sup>[1]</sup>. The viscosity of MC-FRU-GLUT TDES as a function of temperature is shown in Figure 8.2.2. As the temperature rises, the viscosity decreases dramatically.

### **8.8.2.4 FTIR spectrum of MC-FRU-GLUT TDES**

Figure 8.2.3 shows the FTIR spectrum of MC-FRU-GLUT TDES. The intermolecular O - H stretching of the alcoholic group causes a large peak at 3365.55  $\text{cm}^{-1}$ <sup>[1]</sup>. The peak at 1658.63 $\text{cm}^{-1}$  is due to amide C = O stretching and the peaks at 1411.33 $\text{cm}^{-1}$  & 1348.08  $\text{cm}^{-1}$ <sup>[9, 10]</sup> is due to the C - H bending of the methyl group of glucose. The C - OH stretching causes peaks between 1144.44 and 1059.99 $\text{cm}^{-1}$ <sup>[10]</sup>.

## **8.8.3 Characterization of Manganese Chloride-Glucose-Glycine TDES**

### **8.8.3.1 Density and Conductivity**

The density is the most important feature of a liquid. There is little known information about the TDES densities. The high viscous liquid will have low conductivity because it is affected by ion concentration <sup>[3-6]</sup>. At room temperature, MC-GLU-GLY TDES has a density of 1.5454  $\text{g}/\text{cm}^3$  and a conductivity of 0.058  $\text{mS}/\text{cm}$ .

### **8.8.3.2 pH**

The pH scale is an important physical parameter that has a significant impact on chemical processes. Andrea Skulcova et al. <sup>[7]</sup> studied the effect of temperature on pH for a variety of DESs and discovered that as the temperature increased, pH values decreased. This study investigated the effect of temperature on the pH of newly formed DESs. The

hydrogen-bond donor has a considerable impact on the pH of the final product, according to pH behaviour research. The type of hydrogen bond donor determines the acidity of the combination. The pH values of MC-GLU-GLY TDES fall slightly as the temperature rises, as shown in Fig.8.3.1.

### **8.8.3.3 Viscosity**

Viscosity <sup>[8]</sup> replicates the interaction between molecules in a liquid mixture. The lower the viscosity of DES, the better it may be used as a solvent <sup>[1]</sup>. The viscosity of MC-GLU-GLY TDES as a function of temperature is shown in Figure 8.3.2. As the temperature rises, the viscosity decreases dramatically.

### **8.8.3.4 FTIR spectrum of MC-GLU-GLY TDES**

Figure 8.3.3 shows the FTIR spectrum of MC-GLU-GLY TDES. The intermolecular O - H stretching of the alcoholic group causes a large peak at 3367.08  $\text{cm}^{-1}$ <sup>[11]</sup>. The peak at 1626.61 $\text{cm}^{-1}$  is due to amide C = O stretching and the peaks between 1445.37 $\text{cm}^{-1}$  & 1333.59  $\text{cm}^{-1}$ <sup>[9, 10]</sup> is due to the C - H bending of the methyl group of glucose. The C - OH stretching causes peaks between 1077.03 and 1033.33 $\text{cm}^{-1}$ <sup>[10]</sup>.

## **8.8.4 Characterization of Manganese Chloride-Fructose-Glycine TDES**

### **8.8.4.1 Density and Conductivity**

The density is the most important feature of a liquid. There is little known information about the TDES densities. The high viscous liquid will have low conductivity because it is affected by ion concentration <sup>[3-6]</sup>. At room temperature, MC-FRU-GLY TDES has a density of 1.4288  $\text{g}/\text{cm}^3$  and a conductivity of 0.0121  $\text{mS}/\text{cm}$ .

### **8.8.4.2 pH**

The pH scale is an important physical parameter that has a significant impact on chemical processes. Andrea Skulcova et al. <sup>[7]</sup> studied the effect of temperature on pH for a variety of DESs and discovered that as the temperature increased, pH values decreased.

This study investigated the effect of temperature on the pH of newly formed DESs. The hydrogen-bond donor has a considerable impact on the pH of the final product, according to pH behavior research. The type of hydrogen bond donor determines the acidity of the combination. The pH values of MC-FRU-GLY TDES fall slightly as the temperature rises, as shown in Fig.8.4.1.

#### **8.8.4.3 Viscosity**

Viscosity <sup>[8]</sup> replicates the interaction between molecules in a liquid mixture. The lower the viscosity of DES, the better it may be used as a solvent <sup>[1]</sup>. The viscosity of MC-FRU-GLY TDES as a function of temperature is shown in Figure 8.4.2. As the temperature rises, the viscosity decreases dramatically.

#### **8.8.4.4 FTIR spectrum of MC-FRU-GLY TDES**

Figure 8.4.3 shows the FTIR spectrum of MC-FRU-GLY TDES. The intermolecular O - H stretching of the alcoholic group causes a large peak at 3368.79  $\text{cm}^{-1}$ <sup>[1]</sup>. The peak at 1626.94 $\text{cm}^{-1}$  is due to amide C = O stretching and the peaks at 1448.20 $\text{cm}^{-1}$  & 1333.38  $\text{cm}^{-1}$ <sup>[9, 10]</sup> are due to the C - H bending of the methyl group of glucose. The C - OH stretching causes peaks between 1181.67 and 1059.24 $\text{cm}^{-1}$ <sup>[10]</sup>.

### **8.8.5 Characterization of Manganese Chloride-Glucose-Histidine TDES**

#### **8.8.5.1 Density and Conductivity**

The density is the most important feature of a liquid. There is little known information about the TDES densities. The high viscous liquid will have low conductivity because it is affected by ion concentration <sup>[3-6]</sup>. At room temperature, MC-GLU-HIS TDES has a density of 1.5014  $\text{g}/\text{cm}^3$  and a conductivity of 0.208  $\text{mS}/\text{cm}$ .

#### **8.8.5.2 pH**

The pH scale is an important physical parameter that has a significant impact on chemical processes. Andrea Skulcova et al. <sup>[7]</sup> studied the effect of temperature on pH for

a variety of DESs and discovered that as the temperature increased, pH values decreased. This study investigated the effect of temperature on the pH of newly formed DESs. The hydrogen-bond donor has a considerable impact on the pH of the final product, according to pH behaviour research. The type of hydrogen bond donor determines the acidity of the combination. The pH values of MC-GLU-HIS TDES fall slightly as the temperature rises, as shown in Fig.8.5.1.

### **8.8.5.3 Viscosity**

Viscosity <sup>[8]</sup> replicates the interaction between molecules in a liquid mixture. The lower the viscosity of DES, the better it may be used as a solvent <sup>[1]</sup>. The viscosity of MC-GLU-HIS TDES as a function of temperature is shown in Figure 8.5.2. As the temperature rises, the viscosity decreases dramatically.

### **8.8.5.4 FTIR spectrum of MC-GLU-HIS TDES**

Figure 8.5.3 shows the FTIR spectrum of MC-GLU-HIS TDES. The intermolecular O - H stretching of the alcoholic group causes a large peak at  $3400.36\text{cm}^{-1[1]}$ . The peak at  $1627.00\text{ cm}^{-1}$  is due to amide C = O stretching and the peak at  $1408.18\text{ cm}^{-1[9, 10]}$  is due to the C - H bending of the methyl group of glucose. The C - OH stretching causes peak at  $1078.37\text{ cm}^{-1[10]}$ .

## **8.8.6 Characterization of Manganese Chloride-Fructose-Histidine TDES**

### **8.8.6.1 Density and Conductivity**

The density is the most important feature of a liquid. There is little known information about the TDES densities. The high viscous liquid will have low conductivity because it is affected by ion concentration <sup>[3-6]</sup>. At room temperature, MC-FRU-HIS TDES has a density of  $1.4804\text{ g/cm}^3$  and a conductivity of  $0.006\text{ mS/cm}$ .



### 8.8.6.2 pH

The pH scale is an important physical parameter that has a significant impact on chemical processes. Andrea Skulcova et al. [7] studied the effect of temperature on pH for a variety of DESs and discovered that as the temperature increased, pH values decreased. This study investigated the effect of temperature on the pH of newly formed DESs. The hydrogen-bond donor has a considerable impact on the pH of the final product, according to pH behaviour research. The type of hydrogen bond donor determines the acidity of the combination. The pH values of MC-FRU-HIS TDES fall slightly as the temperature rises, as shown in Fig.8.6.1.

### 8.8.6.3 Viscosity

Viscosity [8] replicates the interaction between molecules in a liquid mixture. The lower the viscosity of DES, the better it may be used as a solvent [1]. The viscosity of MC-FRU-HIS TDES as a function of temperature is shown in Figure 8.6.2. As the temperature rises, the viscosity decreases dramatically.

### 8.8.6.4 FTIR spectrum of MC-FRU-HIS TDES

Figure 8.6.3 shows the FTIR spectrum of MC-FRU-HIS TDES. The intermolecular O - H stretching of the alcoholic group causes a large peak at  $3411.99\text{ cm}^{-1}$ [1]. The peak at  $1626.72\text{ cm}^{-1}$  is due to amide C = O stretching and the peak at  $1407.92\text{ cm}^{-1}$ [9, 10] is due to the C - H bending of the methyl group of glucose. The C - OH stretching causes peaks between  $1082.96$  and  $1059.66\text{ cm}^{-1}$ [10].

## 8.9. Conclusion

Six types of Manganese chloride based ternary deep eutectic solvents. The physical properties such as density, conductivity, pH, and viscosity. The FTIR spectra were taken for the characterization of hydrogen-bonded interactions.

## References

- [1]. Koon-Kee Kow, K Sirat, Novel manganese (II)-based deep eutectic solvents: Synthesis and physical properties analysis, *Chinese Chemical Letters*, 26 10 (2015) 1311 –1314.
- [2]. Y.T. Dai, J. van Spronsen, G.J. Witkamp, R. Verpoorte, Y.H. Choi, Natural deep eutectic solvents as new potential media for green technology, *Anal. Chim. Acta* 766 (2013) 61 – 68.
- [3]. Q. Cao; X. Lu; X. Wu; Y. Guo; Xu, L.; Fang, W. Density, Viscosity, and Conductivity of Binary Mixtures of the Ionic Liquid N-(2-Hydroxyethyl) piperazinium Propionate with Water, Methanol, or Ethanol, *Journal of Chemical & Engg Data* (2015) 60,3, 455-463.
- [4]. P. Wasserscheid and P. Welton eds., *Ionic Liquids in Synthesis*, Wiley-VCH Verlag, Weinheim, *Org. Proc. Res. Dev.* 2003, 7, 2, 223–224
- [5]. F. Endres, A. P. Abbott, D. R Mac Farlane eds., *Electrodeposition from Ionic liquids*, Wiley-VCH Verlag, Weinheim, 2008.
- [6]. A. P. Abbott, D. Boothby, G. Capper, D. L. Davies, R. Rasheed, Deep Eutectic Solvents Formed between Choline Chloride and Carboxylic Acids: Versatile Alternatives to Ionic Liquids, *J. Am. Chem. Soc.*, 126, 29, (2004). 9142–9147.
- [7]. Andrea Skulcova, Albert Russ, Michal Jablonsky, JozefSima, “pH of eutectic solvents,” *BioResources* 13(3), (2018) 5042 - 5051.
- [8]. W. J. Guo, Y. C. Hou, S. H. Ren, S. D. Tian, W. Z. Wu, Formation of deep eutectic solvents by phenols and choline chloride and their physical properties, *J. Chem. Eng. Data* 58 (2013) 866 – 872. <https://doi.org/10.1021/je300997v>
- [9]. Donald L. Pavia, Gary M. Lampman, George S. Kriz, *Introduction to Spectroscopy*, 3rd Edition, BROOKS/COLE, Thomson Learning, USA, 2001
- [10]. B.D. Mistry, *A Handbook of Spectroscopic Data*, Oxford Book Company, India, 2009.

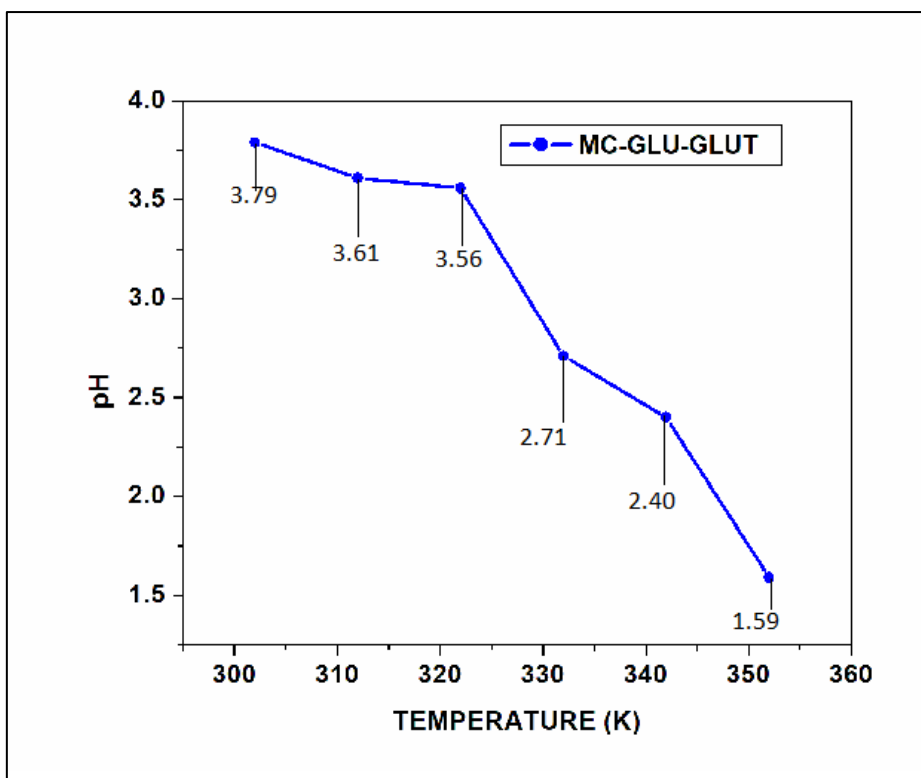


Figure 8.1.1 pH as a function against T of MC-GLU-GLUT

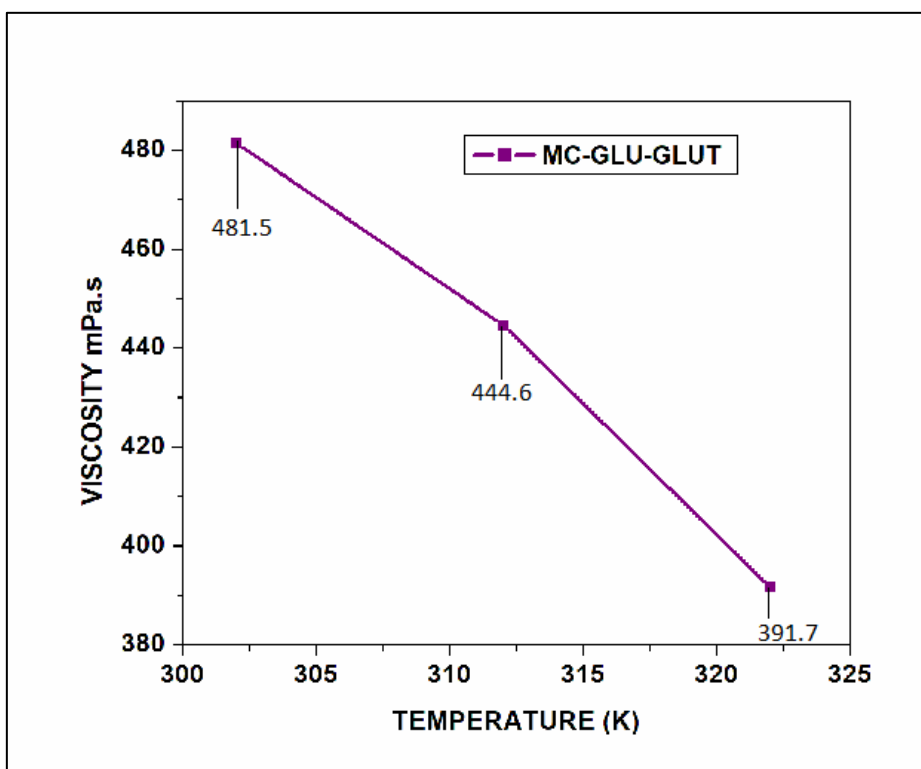


Figure 8.1.2. Viscosity of MC-GLU-GLUT TDES at different temperatures

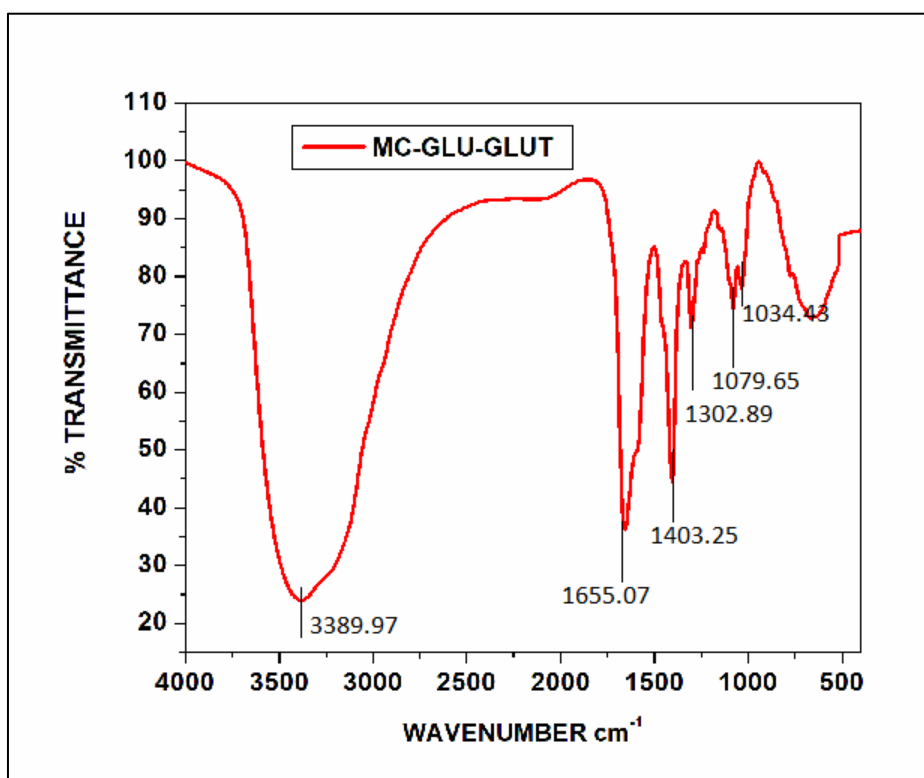


Figure 8.1.3 FTIR spectrum of MC-GLU-GLUT TDES

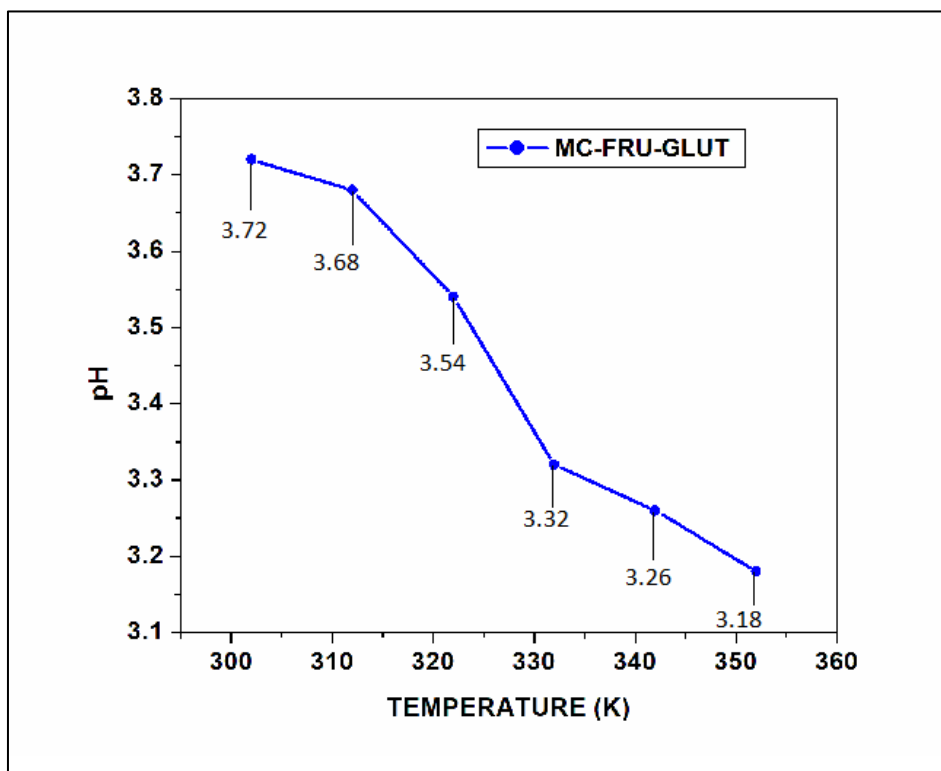


Figure 8.2.1 pH as a function against T of MC-FRU-GLUT TDES

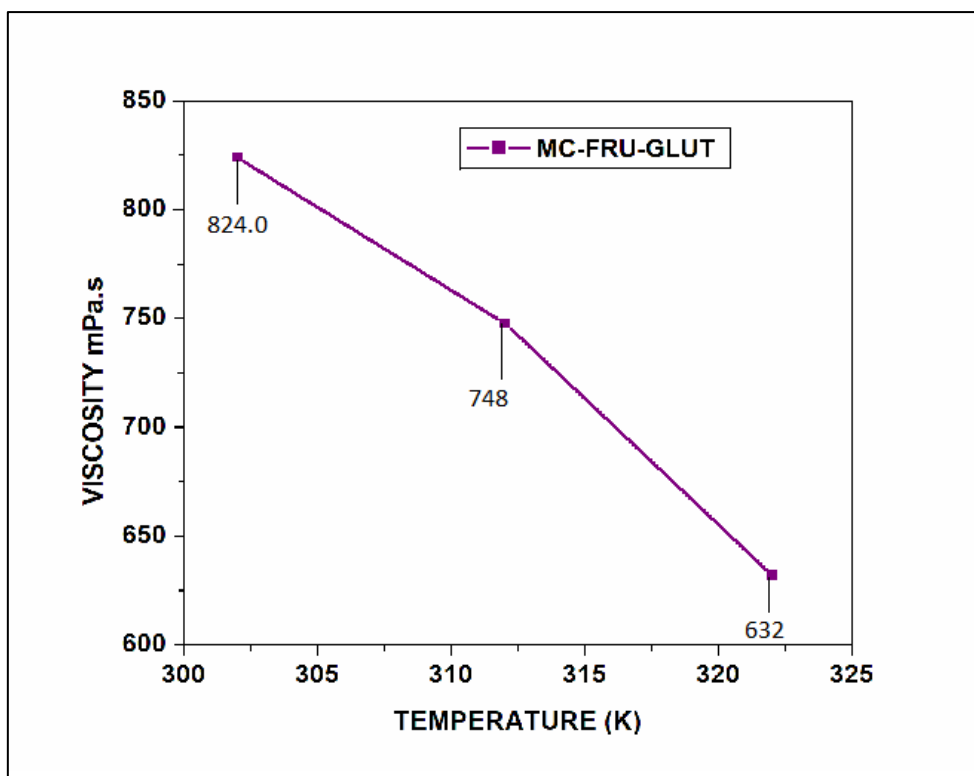


Figure 8.2.2 Viscosity of MC-FRU-GLUT TDES at different temperatures

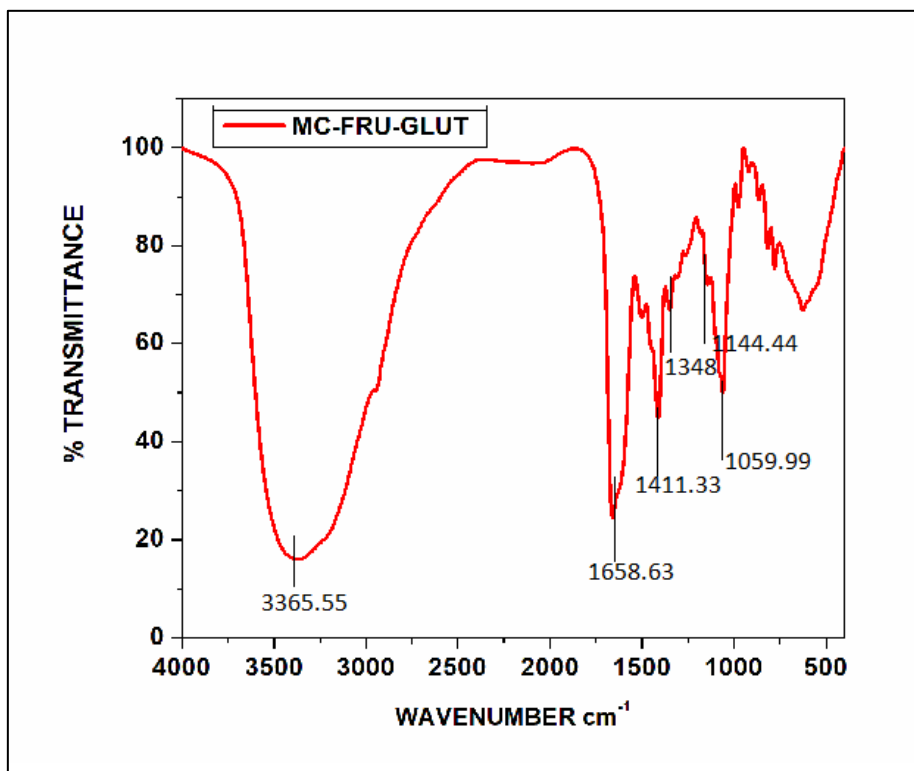


Figure 8.2.3 FTIR spectrum of MC-FRU-GLUT TDES

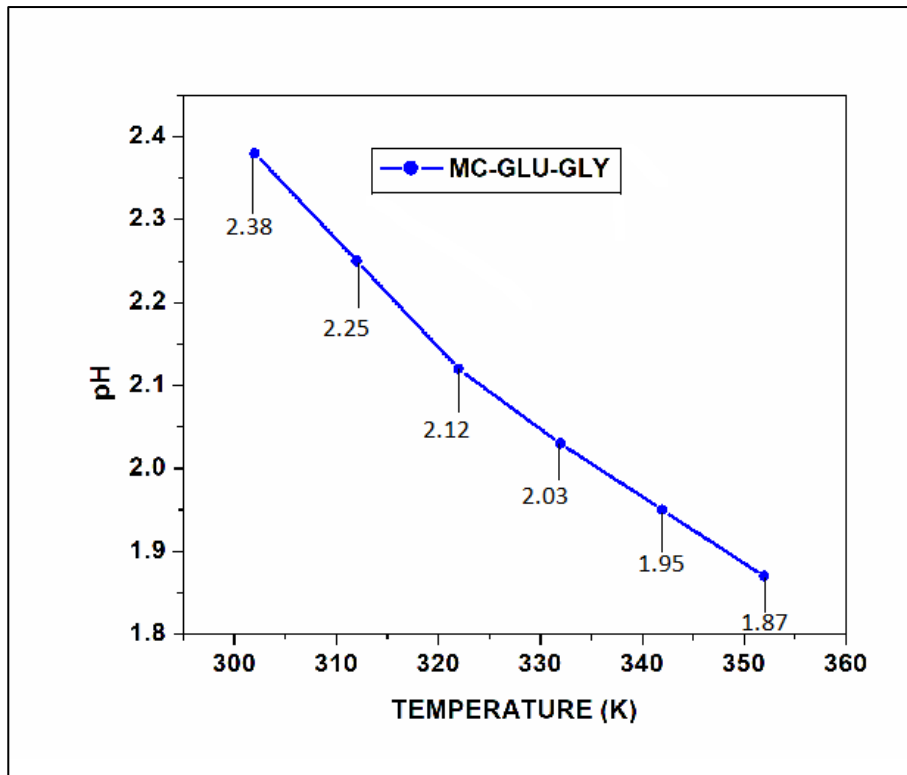


Figure 8.3.1 pH as a function against T of MC-GLU-GLY TDES

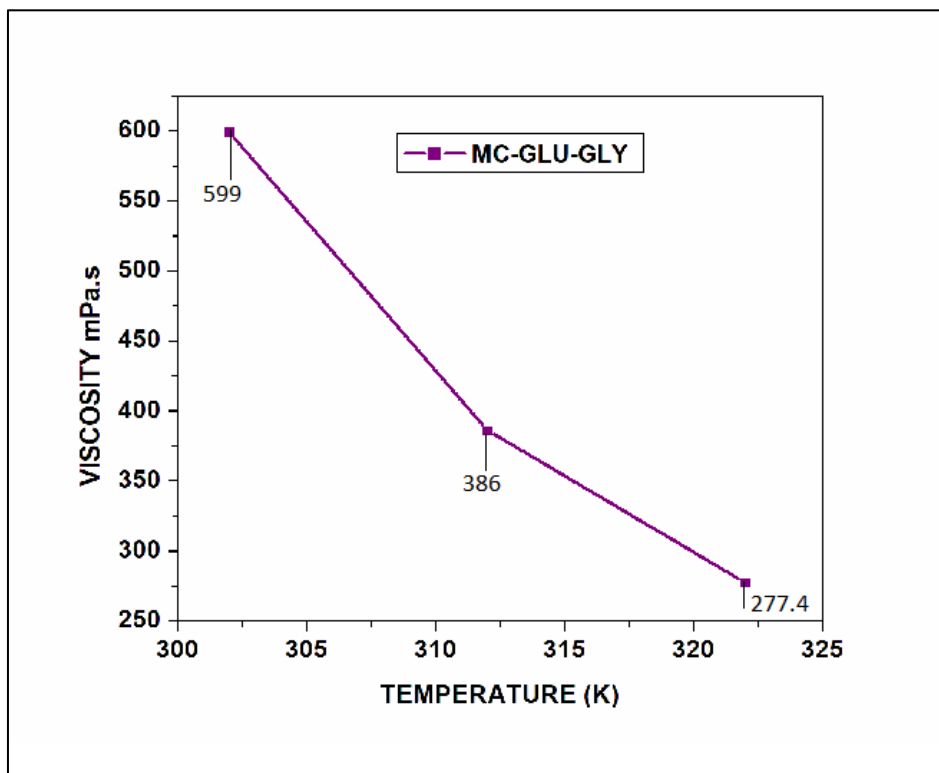


Figure 8.3.2 Viscosity of MC-GLU-GLY TDES at different temperatures

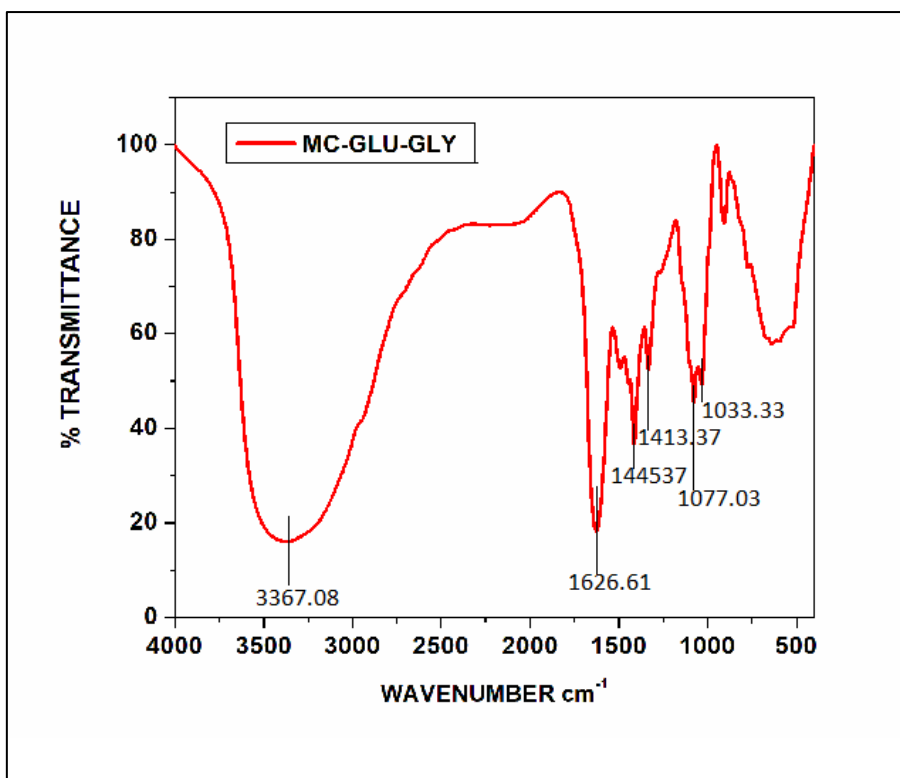


Figure 8.3.3 FTIR spectrum of MC-GLU-GLY TDES

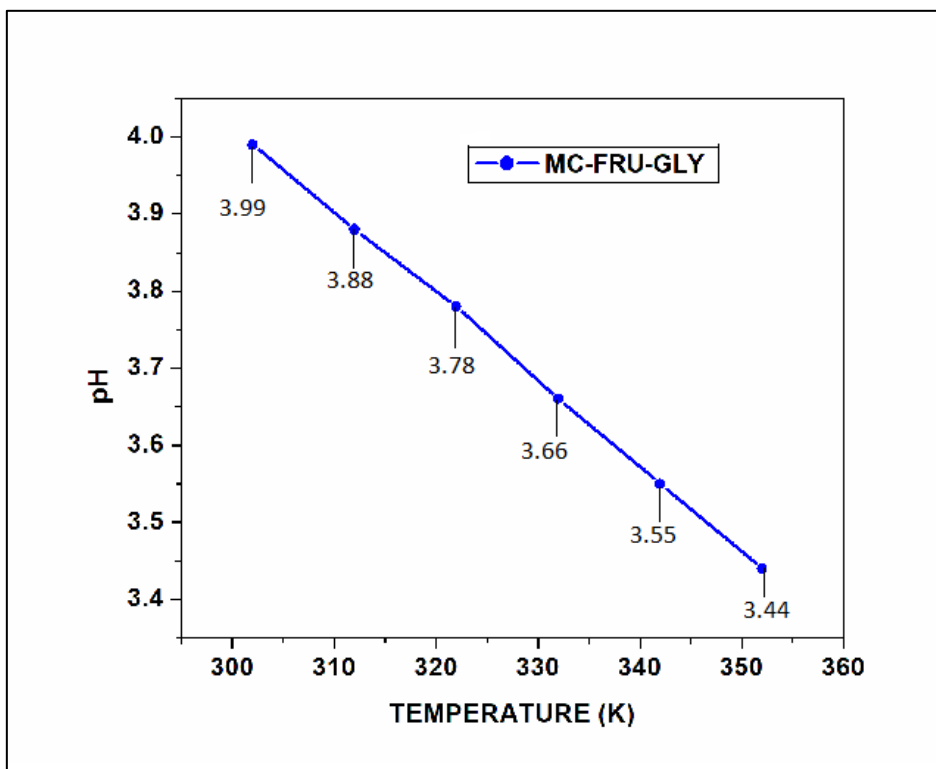


Figure 8.4.1 pH as a function against T of MC-FRU-GLY TDES

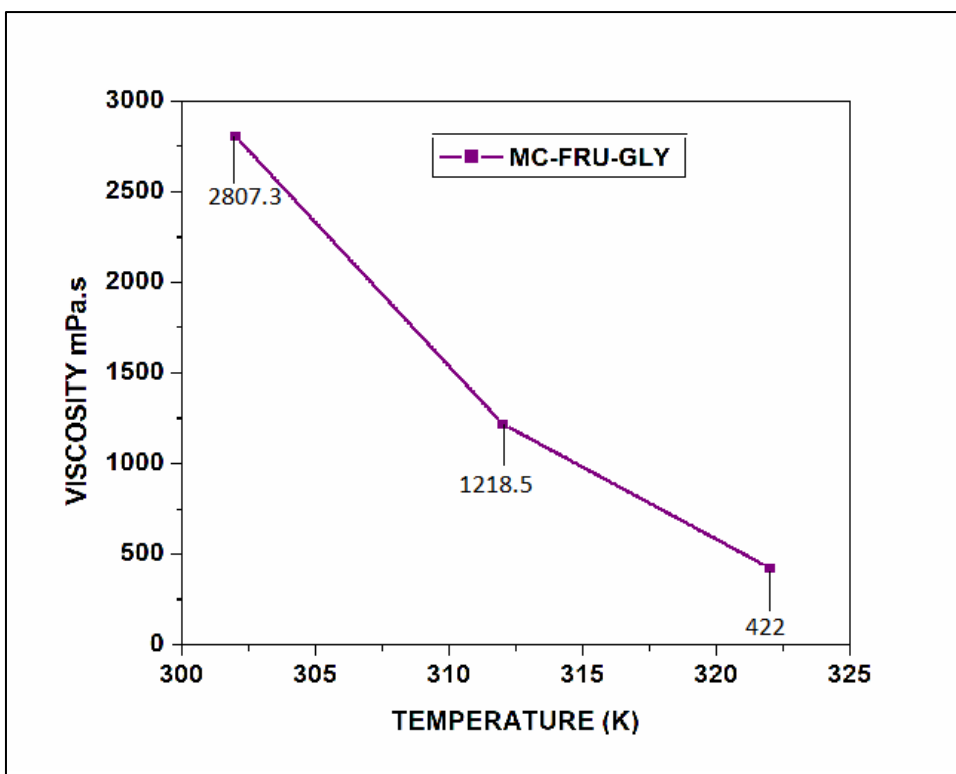


Figure 8.4.2 Viscosity of MC-FRU-GLY TDES at different temperatures

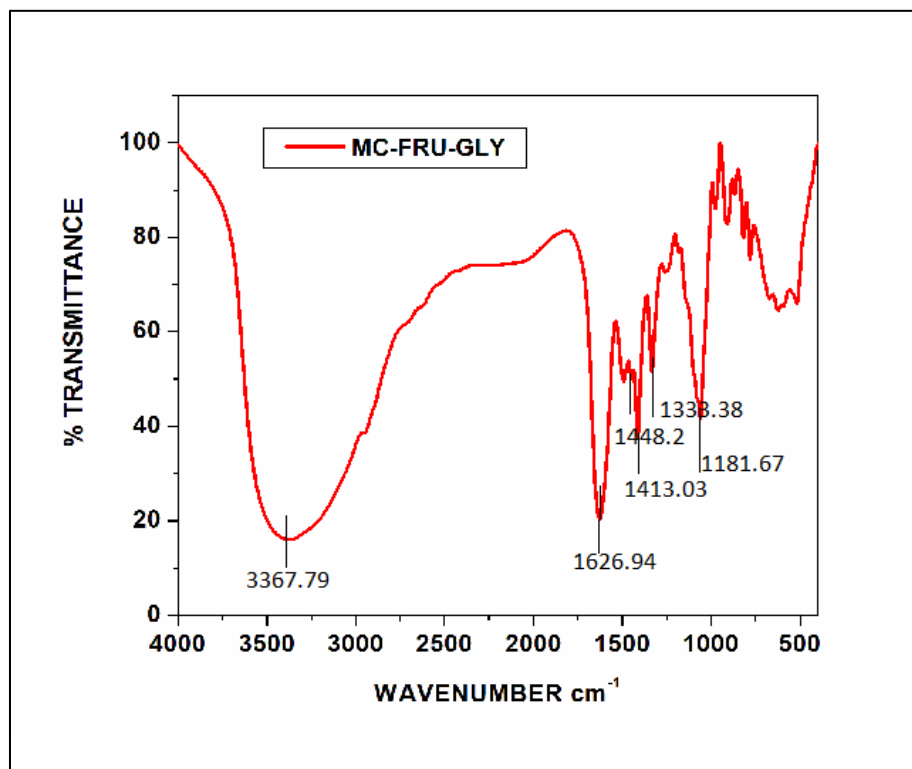


Figure 8.4.3 FTIR spectrum of MC-FRU-GLY TDES



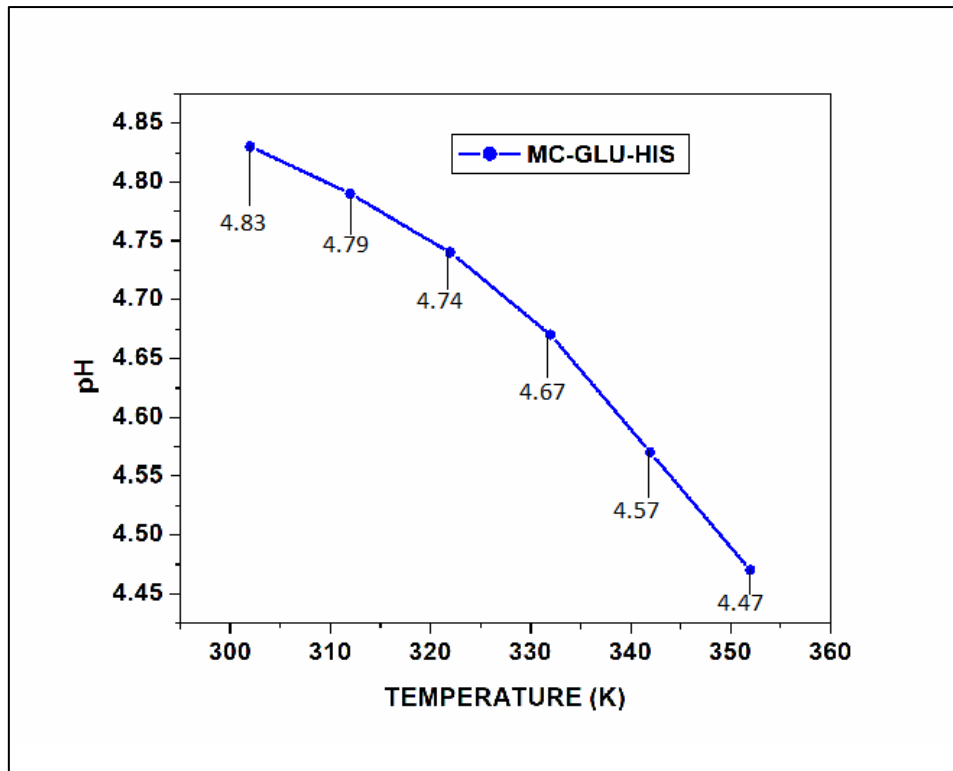


Figure 8.5.1 pH as a function against T of MC-GLU-HIS TDES

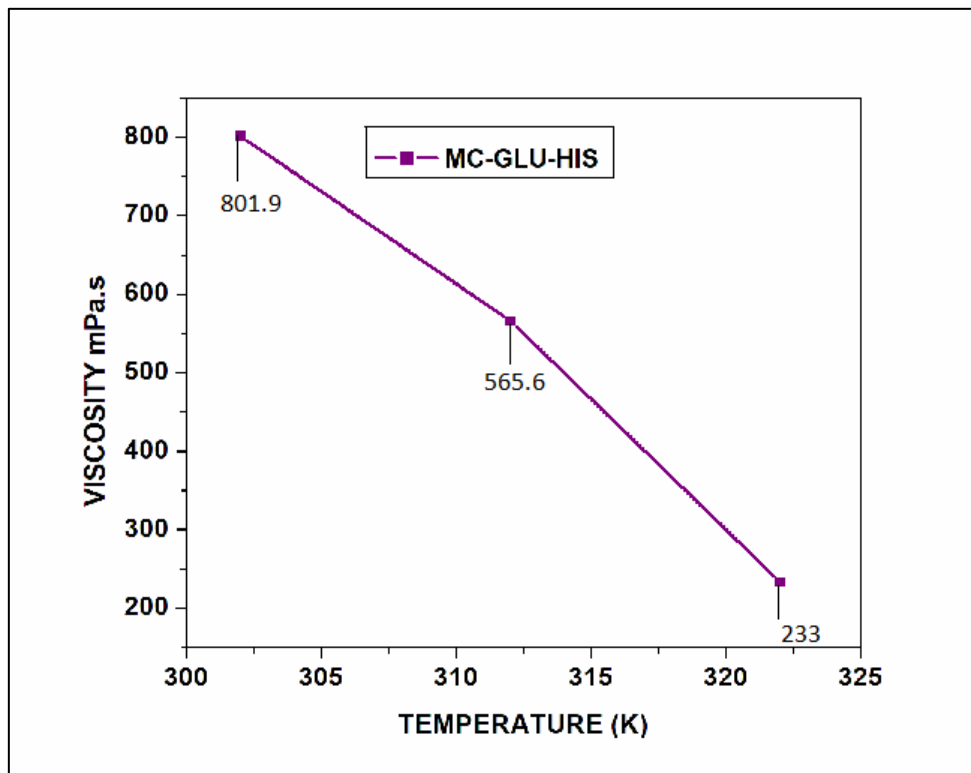


Figure 8.5.2 Viscosity of MC-GLU-HIS TDES at different temperatures

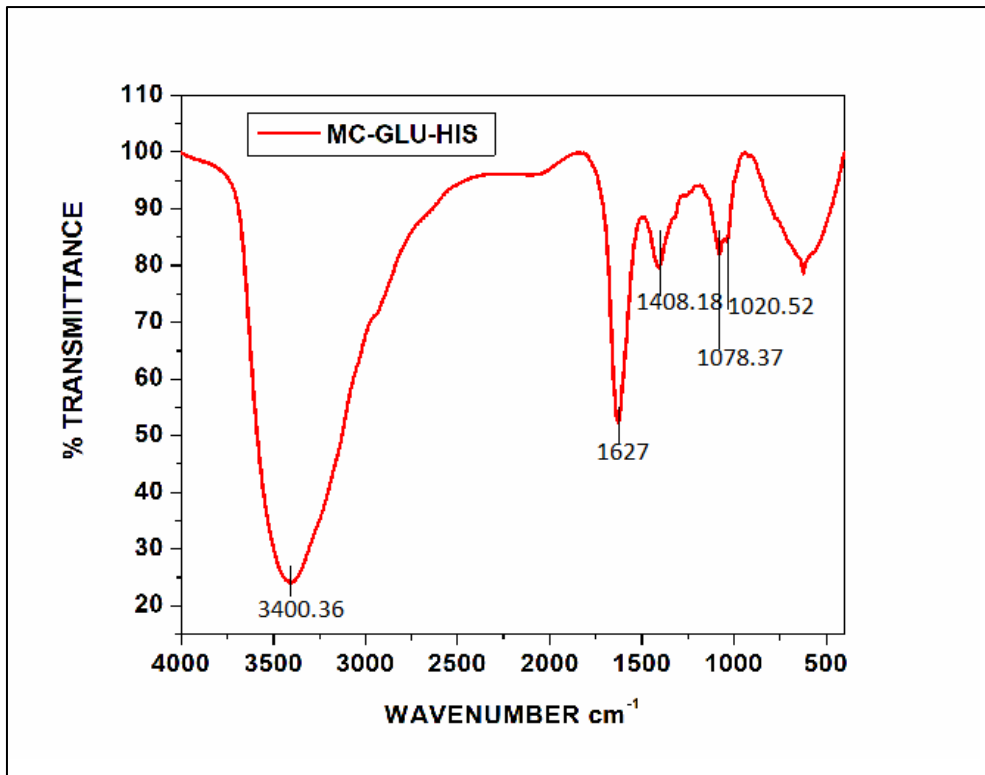


Figure 8.5.3 FTIR spectrum of MC-GLU-HIS TDES

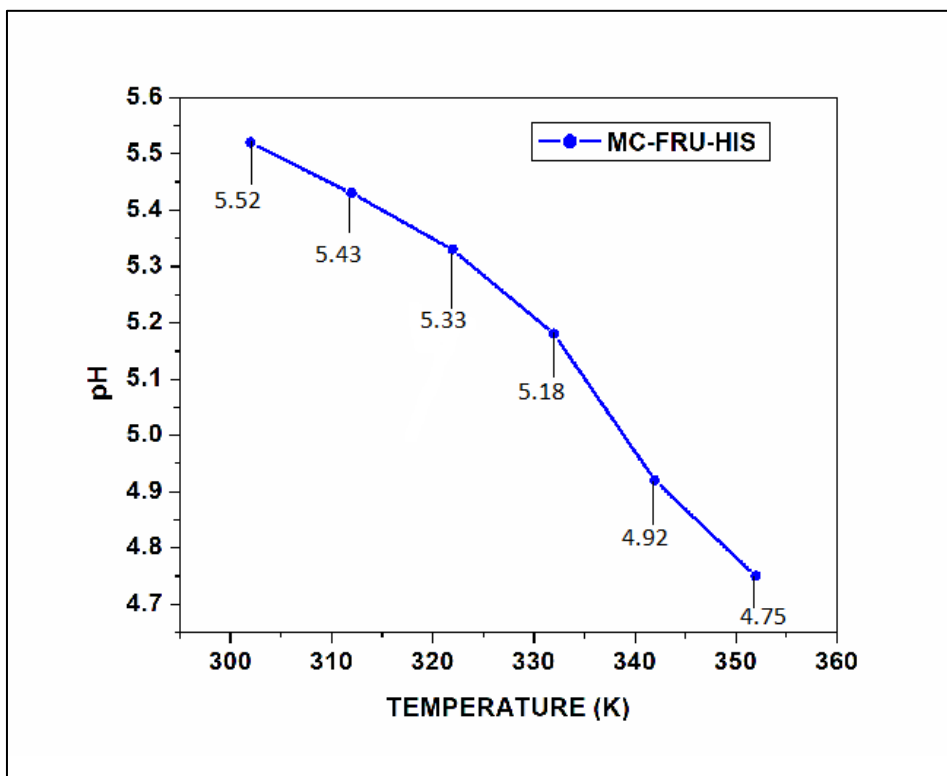


Figure 8.6.1 pH as a function against T of MC-FRU-HIS TDES

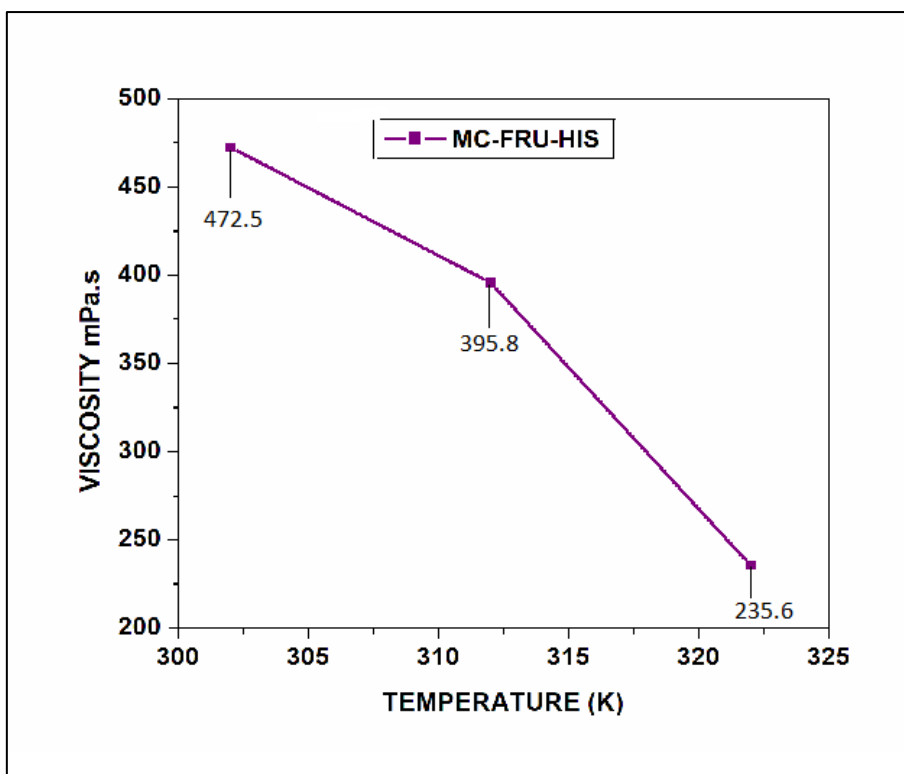


Figure 8.6.2 Viscosity of MC-FRU-HIS TDES at different temperatures

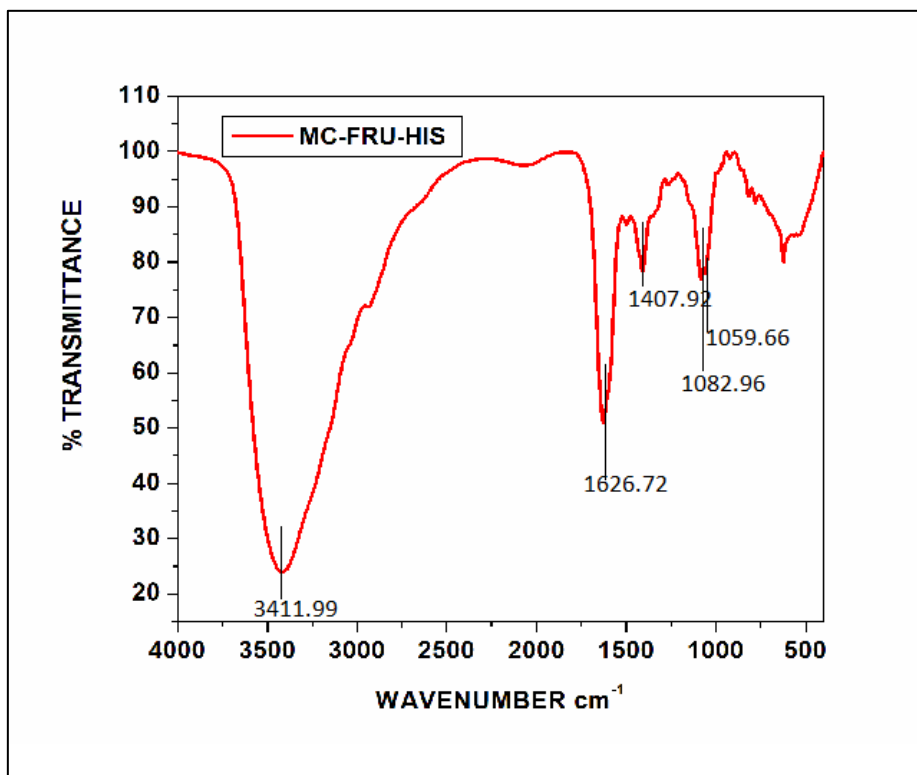


Figure 8.6.3 FTIR spectrum of MC-FRU-HIS TDES



## 9. Synthesis and characterization of Nanoparticles in Binary Deep Eutectic Solvents

---

### 9.1 Introduction

A nanoparticle is a tiny particle with a diameter of 1 to 100 nanometres. Nanoparticles, which are invisible to the naked eye, can have radically different physical and chemical properties than their bigger material counterparts. Nanoparticles have gotten a lot of attention in the scientific community and business in recent years because of their unusual physicochemical qualities, which are attributed to their small size and the high surface-area-to-volume ratio <sup>[1,2]</sup>. Because of its simplicity, solubility, inexpensive reagents, and fast reaction durations, the chemical reduction of copper (II) salts in an aqueous solution is one of the most versatile techniques <sup>[3]</sup>. Nanoparticles must be protected by adding surface-protecting stabilizing agents such as organic ligands, surfactants, or polymers that can form complexes with copper ions <sup>[4]</sup>. Among the many metallic nanoparticles used in biomedical applications, silver nanoparticles are one of the most important and fascinating nanomaterials. Scientists and technologists are interested in developing nano silver-based disinfectant products because of the unique properties of the high antimicrobial activity of silver nanoparticles <sup>[5]</sup>. Cadmium nanoparticles are used as a significant material in solar cells and light-emitting diodes <sup>[6]</sup>. Electrochemically, the solid-state of mercury nanoparticles were investigated, revealing unique characteristics. In the domains of electroanalytical chemistry and electrocatalysis, solid mercury nanoparticles have the potential to be very useful <sup>[7]</sup>.

In this work, we focussed on synthesizing the metal nanoparticles such as copper, silver, cadmium, mercury, and characterizing the synthesized nanoparticles by FTIR, UV, SEM, XRD, and EDAX techniques. We had synthesized copper, silver nanoparticles by

chemical reduction method and cadmium, mercury nanoparticles by chemical co-precipitation method.

## **9.2 Synthesis of copper nanoparticles in Malonic acid-based binary deep eutectic solvents**

Copper nanoparticles were synthesized in our prepared BDES such as MA-GLU BDES, MA-FRU BDES, and MA-GCL BDES separately using the chemical reduction method <sup>[3]</sup>. Nanoparticles were made by combining 10 ml of 0.01M Copper nitrate trihydrate [Cu (NO<sub>3</sub>)<sub>2</sub>.3H<sub>2</sub>O] with 15 ml of MA-GLU, MA-FRU, and MA - GCL BDES in separate beakers and stirring for 30 minutes at 1200 RPM with a magnetic stirrer. During vigorous stirring, about 8-10 ml of 0.01 M Hydrazine Hydride as a reducing agent was added drop by drop, followed by 20 ml of 1 M sodium hydroxide as a stabilizing agent was injected slowly into the mixture. The obtained copper oxide nanoparticles in two beakers were centrifuged, rinsed with deionized water, then methanol, and dried separately.

## **9.3 Synthesis of silver nanoparticles in Malonic acid-based binary deep eutectic solvents**

Silver nanoparticles were made by mixing 10 ml of 0.01 M silver nitrate [AgNO<sub>3</sub>] with 15 ml of MA-GLU BDES and MA-FRU BDES in separate beakers using the chemical reduction method <sup>[3]</sup> and stirring at 1200 RPM for 30 minutes with a magnetic stirrer. The reducing agent, 0.01 M sodium borohydride (about 8–10 ml) was added drop by drop under vigorous stirring, and a further 20 ml of stabilizing agent, 1 M sodium hydroxide was injected drop by drop using an injector. The silver oxide nanoparticles were centrifuged, then washed with deionized water, methanol, and finally dried.

#### **9.4 Synthesis of cadmium nanoparticles in Malonic acid-based binary deep eutectic solvents**

Cadmium nanoparticles were synthesized by mixing cadmium chloride with MA-GLU BDES & MA-FRU BDES separately in two beakers using the chemical co-precipitation method <sup>[8]</sup>. After mixing, they were stirred using a magnetic stirrer at 1200 RPM for 30 minutes. During the vigorous stirring, approximately 8-10 ml of 0.01 M Yellow Ammonium Sulfide was added drop by drop in the beakers. The precipitate of cadmium sulfide nanoparticles obtained was centrifuged, washed with deionized water followed by methanol, and dried.

#### **9.5 Synthesis of mercury nanoparticles in Malonic acid-based binary deep eutectic solvents**

Mercury nanoparticles were synthesized by mixing cadmium chloride with MA-GLU BDES & MA-FRU BDES separately in two beakers using the chemical co-precipitation method <sup>[8]</sup>. After mixing, they were stirred using a magnetic stirrer at 1200 RPM for 30 minutes. During the vigorous stirring, approximately 8-10 ml of 0.01 M Yellow Ammonium Sulfide was added drop by drop in the beakers. The precipitate of mercuric sulfide nanoparticles obtained was centrifuged, washed with deionized water followed by methanol, and dried.

#### **9.6 Synthesis of copper nanoparticles in Zinc chloride-based binary deep eutectic solvents**

Copper nanoparticles were synthesized in our prepared BDES such as ZC-GLU BDES and ZC-FRU BDES separately using the chemical reduction method <sup>[3]</sup>. Nanoparticles were made by combining 10 ml of 0.01M Copper nitrate trihydrate [Cu (NO<sub>3</sub>)<sub>2</sub>.3H<sub>2</sub>O] with 15 ml of ZC-GLU and ZC-FRU BDES in separate beakers and stirring for 30 minutes at 1200 RPM with a magnetic stirrer. During vigorous stirring, about 8-10

ml of 0.01 M Hydrazine Hydride as a reducing agent was added drop by drop, followed by 20 ml of 1 M sodium hydroxide as a stabilizing agent was injected slowly into the mixture. The obtained copper oxide nanoparticles in two beakers were centrifuged, rinsed with deionized water, then methanol, and dried separately.

### **9.7 Synthesis of silver nanoparticles in Zinc chloride-based binary deep eutectic solvents**

Silver nanoparticles were made by mixing 10 ml of 0.01 M silver nitrate [ $\text{AgNO}_3$ ] with 15 ml of ZC-GLU BDES and ZC-FRU BDES in separate beakers using the chemical reduction method <sup>[3]</sup> and stirring at 1200 RPM for 30 minutes with a magnetic stirrer. The reducing agent, 0.01 M hydrazine hydrate (about 8–10 ml) was added drop by drop under vigorous stirring, and a further 20 ml of stabilizing agent, 1 M sodium hydroxide was injected drop by drop using an injector. The silver oxide nanoparticles were centrifuged, then washed with deionized water, methanol, and finally dried.

### **9.8 Results and discussion**

The synthesized copper, silver nanoparticles were characterized by UV-Visible spectroscopy, Fourier transform infrared spectroscopy, Scanning electron microscopy, X-Ray diffraction pattern, and Energy dispersive X-ray analysis. Cadmium and mercury nanoparticles were characterized by UV-Visible spectroscopy, Fourier transform infrared spectroscopy, and Scanning electron microscopy.

#### **9.8.1 Characterization studies of copper nanoparticles in malonic acid-based binary deep eutectic solvents**

##### **9.8.1.1 UV-Visible spectra of copper oxide nanoparticles**

UV-Visible absorption spectra of copper oxide nanoparticles in ethanolic solution are shown in figure 9.1.1. The characteristic absorption peak of the copper metal was observed at 503 nm <sup>[9]</sup>. The broad peaks noticed at 503 and 470 nm in were assigned for



the copper oxide nanoparticles obtained in MA-GLU (Fig. 9.1.1a) and MA-FRU (Fig. 9.1.1 b) DES respectively <sup>[9]</sup>. So, it is concluded that copper nanoparticles were formed in MA-GLU and MA-FRU BDES. But the UV-Visible spectrum for the sample obtained in MA-GCL BDES did not give any surface plasmon peak around 400 – 600 nm as seen in the figure 9.1.1c and hence it is confirmed that no copper oxide nanoparticles formed in MA – GCL . This is due to fewer voids in MA-GCL BDES as it has high viscosity.

### **9.8.1.2 FTIR spectra of copper oxide nanoparticles**

The FTIR spectra in the range of 400 to 4000  $\text{cm}^{-1}$  for copper oxide nanoparticles prepared from MA-GLU and MA-FRU are reported in “a” and “b” of figure 9.1.2 respectively. The several peaks noticed in the range of 400 to 850  $\text{cm}^{-1}$  are correlated to Cu – O vibrations of CuO nanoparticles <sup>[10]</sup>. The sharp peak observed at 623  $\text{cm}^{-1}$  in both the spectra “a” and “b” clearly indicated the Cu – O stretching <sup>[11]</sup>. Here a few of the malonic acid molecules are capped on the surface of CuO nanoparticles. These are indicated by the peaks at 1042 and 1117  $\text{cm}^{-1}$  corresponding to the C – O stretching of the carboxylic acid group in both the spectra “a” and “b” of figure 9.1.2. The peak due to  $\text{CH}_2$  deformations of malonic acid is seen at 1384  $\text{cm}^{-1}$  in both spectra. The peak was noticed at 1600  $\text{cm}^{-1}$  denoted O – H bending of malonic acid. The peaks observed at 2854  $\text{cm}^{-1}$  and 2923  $\text{cm}^{-1}$  are due to C – O asymmetric stretching <sup>[11]</sup>. Further, the broad peaks seen around 3420  $\text{cm}^{-1}$  in both the spectra due to different vibrations modes of water molecules adsorbed on the surface of copper oxide nanoparticles <sup>[10]</sup>.

### **9.8.1.3 XRD patterns of copper oxide nanoparticles**

The powder x-ray diffraction patterns of copper oxide nanoparticles prepared from the deep eutectic solvents, MA-GLU and MA-FRU are given in “a” and “b” of figure 9.1.3 respectively. The XRD patterns give information about the grain size, structure, and phase cleanliness of the materials. In the case of CuO particle obtained in MA-GLU DES, the

diffraction peaks noticed at 36.4°, 43.3°, 50.4°, 61.4° and 74.1° are indexed as (034), (404), (440), (610) and (183) respectively. Similarly, the diffraction peaks seen at 36.6°, 43.2°, 50.4° and 74.1° are also indexed as (034), (404), (440) and (183) respectively for the CuO particles prepared using the MA-FRU BDES. This indexing corresponds to the orthorhombic structure of CuO [11]. The observed peaks are matching well with the JCPDC Card No. 77-1898. The grain size of CuO nanoparticles is determined by using the Debye–Scherer formula,

$$D = k \lambda / \beta \cos \theta$$

where D denotes the grain size, K refers to a constant,  $\lambda$  refers to the wavelength of X-ray used,  $\beta$  denotes the fullwidth half-maximum of the diffraction peaks and  $\theta$  is the angle of the diffraction [10]. By using this formula, the average grain size of CuO nanoparticles prepared from the BDES of MA-GLU is found to be 32 nm. Similarly, the average grain size of CuO nanoparticles prepared using the DES of MA-FRU is determined to be 58.66 nm.

#### **9.8.1.4 Morphological analysis of copper oxide nanoparticles by SEM**

The surface morphology and particle size of the CuO nanoparticles prepared using the BDESs have been analyzed by scanning electron microscope [10]. In figure 9.1.4, the SEM images of copper oxide nanoparticles prepared using MA-GLU BDES are labelled as “a” and “b” while the CuO nanoparticles obtained from the MA-FRU BDES are labelled as “c” and “d”. The morphology of CuO nanoparticles seems to be buds-like grains with an average diameter of 102.77 nm in the case of particles obtained from MA-GLU BDES. The CuO nanoparticles obtained in MA-FRU BDES look like a spongy scale-like morphology with an average diameter of 107.28 nm.

### **9.8.1.5 Energy Dispersive X-ray Analysis**

The elemental composition of the CuO nanoparticles was carried out by energy dispersive x-ray analysis (EDAX) spectroscopy <sup>[12]</sup>. In figure 9.1.5, it is given the EDAX spectrum of copper oxide nanoparticles synthesized using the DES of MA-GLU whereas the EDAX spectrum of CuO nanoparticles prepared using the DES of MA-FRU is denoted in figure 9.1.5 b. In figure 9.1.5 a, it is shown that the atomic percentage of Cu is 65.5 and O is 34.5, which revealed that pure CuO nanoparticles are formed in MA-GLU BDES. But in figure 9.1.5 b, it has been noticed that the atomic percentage of Cu, O, N and C are 5.8, 44.72, 28.66, and 20.82 respectively. Thus, it is observed that in the DES of MA-FRU, the more the atomic percentage of C and N due to the surface capping of malonic acid and adsorption of atmospheric nitrogen on CuO nanoparticles formed.

## **9.8.2 Characterization studies of silver nanoparticles in malonic acid-based binary deep eutectic solvents**

### **9.8.2.1 UV–Visible spectra of silver oxide nanoparticles**

UV–Visible spectroscopy is a very useful, consistent method for foremost nanoparticle characterization, as well as monitoring Ag<sub>2</sub>O NPs synthesis and stability <sup>[13]</sup>. In Ag<sub>2</sub>O NPs, conduction and valence bands are near together, allowing electrons to travel freely <sup>[14–17]</sup>. Due to the simultaneous oscillation of electrons of metal nanoparticles in resonance with light waves, these free electrons create a surface plasmon resonance (SPR) absorption band. According to Njagi et al <sup>[18]</sup>, this band corresponds to colloidal silver nanoparticle absorption in the 400–450 nm region due to surface plasmon vibration stimulation. In the event of Ag<sub>2</sub>O NPs formed in MA-GLU, a surface plasmon resonance peak (SPR) is visible in a strong absorption band around 430 nm, confirming the formation of Ag<sub>2</sub>O NPs, as suggested by W. Wei. et.al. <sup>[19]</sup>. In both the malonic acid-based solvents (MA-GLU, MA-FRU), the UV–visible spectrum of Ag<sub>2</sub>O NPs obtained in Fig. 9.2.1a &

Fig.9.2.1b clearly demonstrates a larger absorption throughout the entire UV–Visible light band of 200–800 nm <sup>[20]</sup>.

### 9.8.2.2 FTIR spectra of silver oxide nanoparticles

Silver oxide nanoparticles generated from Malonic acid-based solvents had FTIR spectra in the region of 4000 to 400  $\text{cm}^{-1}$ , as shown in ‘‘a’’ and ‘‘b’’ of Fig. 9.2.2. The Ag – O vibrations of  $\text{Ag}_2\text{O}$  nanoparticles are associated with multiple peaks observed in the region of 500 to 650  $\text{cm}^{-1}$ . The sharp peak around 542 and 544 and 1546.18  $\text{cm}^{-1}$  in the spectrum of malonic acid-based BDESs (Fig. 9.2.2a) clearly indicated Ag – O stretching <sup>[21]</sup>. The peak at 1543.52  $\text{cm}^{-1}$  is due to the N - O stretching vibration and at 1384.05  $\text{cm}^{-1}$  is due to the C - H bending vibration. The peaks observed at 2851  $\text{cm}^{-1}$  and 2921  $\text{cm}^{-1}$  are due to C – O asymmetric stretching. Furthermore, the broad peaks seen around 3420  $\text{cm}^{-1}$  in both spectra are due to the strong intermolecular bonded stretching of water molecules adsorbed on the surface of silver oxide nanoparticles <sup>[22]</sup>.

### 9.8.2.3 XRD analysis of silver oxide nanoparticles

The synthesized Ag NPs are characterized using X-Ray Diffraction analysis. The crystalline nature of the particles was confirmed by XRD, which showed intense peaks at  $2\theta$  values of 37.68, 43.89, 64.10, 77.08 in the case of NPs obtained in MA-GLU BDES Fig.9.2.3a and at 37.78, 43.95, 64.12, 77.10 in case of NPs obtained in MA-FRU BDES Fig. 9.2.3 b, both which indexed at planes (111), (200), (220), (311) of silver respectively <sup>[23]</sup>. The structure of  $\text{Ag}_2\text{O}$  nanoparticles is crystalline in nature and it is face-centered cubic in both cases. The observed peaks are matching well with JCPDC Card No. 89–3722. The Debye–Scherrer equation was used to calculate the average crystallographic size of silver nanoparticles,  $D = k\lambda / \beta \cos\theta$ . The average particle size obtained in the case of MA-GLU BDES is calculated to be 35 nm and in MA-FRU BDES is calculated to be 29 nm by measuring the breadth of (111) Bragg’s reflection <sup>[24]</sup>.

#### **9.8.2.4 SEM images of Ag<sub>2</sub>O nanoparticles**

Scanning electron microscopy was used to examine the morphological structure and particle size of Ag<sub>2</sub>O nanoparticles prepared using BDESs. In Fig. 9.2.4, the SEM images of silver oxide nanoparticles prepared using MA-GLU BDES are labeled as “a” and “b” while the Ag<sub>2</sub>O nanoparticles obtained from the MA-FRU BDES are labeled as “c” and “d”. The morphology of Ag<sub>2</sub>O nanoparticles seems to be polygonal beads shaped with an average diameter of 95.42 nm in the case of particles obtained from MA-GLU BDES and it seems to be irregular droplets shaped with an average diameter of 132.21 nm in the case of particles obtained from MA-FRU BDES.

#### **9.8.2.5 Energy Dispersive X-ray analysis**

The elemental components and also the relative abundance of the synthesized Ag<sub>2</sub>O NPs was determined by Energy Dispersive X-ray Analysis (EDAX), as shown in Fig.9.2.5. The purity and complete chemical composition of Ag<sub>2</sub>O NPs were revealed by the EDAX spectrum obtained in the case of MA-GLU (Fig. 9.2.5 designated as ‘a’). The percentage of Ag metal was discovered to be quite high. Because of surface Plasmon resonance, the reduced silver nanoparticles were submitted to EDAX analysis with an optical absorption characteristic peak at 3 keV [25]. Silver produced a strong signal on EDAX, showing that silver ions had been reduced to elemental silver. In comparison to oxygen, the EDAX study revealed that Ag has a major percentage relative composition of 77.98. (22.02). In the case of Ag<sub>2</sub>O NPs obtained via MA-FRU (Fig.9.2.5 designated as ‘b’), it was discovered that 100% of the product is made up of silver exclusively, with no other purity in the sample.

### **9.8.3 Characterization studies of cadmium nanoparticles in malonic acid-based binary deep eutectic solvents**

#### **9.8.3.1 UV-Visible spectra of Cadmium sulfide (CdS) nanoparticles**

The characteristic absorption peak of the cadmium metal was observed from 300 to 650 nm. The peaks were observed at 258 nm in MA-GLU BDES and at 410nm in MA-FRU BDES <sup>[26]</sup> as shown in Fig.9.3.1. CdS NPs are obtained due to their high viscosity. The large peaks created correlate to the surface plasmon resonance, showing that stable nanoparticles are present.

#### **9.8.3.2 FTIR spectrum of Cadmium sulfide nanoparticles**

FTIR spectra were measured to identify the functional groups and to confirm the formation of cadmium nanoparticles shown in Fig.9.3.2. The peak at  $3901.32\text{ cm}^{-1}$  corresponds to the free O - H group in the case of nanoparticles formed in MA-GLU BDES. The peak at  $2940.76\text{ cm}^{-1}$  is due to the C - H stretching vibration in the case of nanoparticles formed in MA-FRU BDES <sup>[27, 28]</sup>. The peaks at  $3399.80\text{ cm}^{-1}$  and  $3408\text{ cm}^{-1}$  are due to the O - H stretching group of both spectra. The peak in  $1717.27\text{ cm}^{-1}$  and  $1726\text{ cm}^{-1}$  corresponds to the C = O asymmetric stretching of both spectra <sup>[27, 28]</sup>. The peak at  $1587.44\text{ cm}^{-1}$  is due to the presence of a hydroxyl group of water. The peaks at  $1163.39\text{ cm}^{-1}$  correspond to the S - O bond and  $702.37\text{ cm}^{-1}$  is due to the S - S bond, at  $467.27\text{ cm}^{-1}$  <sup>[29]</sup> response to the formation of the Cd - S nanoparticles. There are some peaks around  $1300\text{ cm}^{-1}$  that correspond to C - H bending in both spectra <sup>[27,28]</sup>.

#### **9.8.3.3 SEM images of Cadmium sulfide nanoparticles**

The morphological structure and particle size of CdS nanoparticles are taken by Scanning electron microscopy. In Fig.9.3.3a the CdS nanoparticles seem to be a flower-like structure taken up to 200 nm in the case of particles obtained from MA-GLU BDES with an average diameter of 150nm. The CdS nanoparticles obtained in MA-FRU BDES

look like a disc-shaped structure taken up to 1 $\mu$ m with an average diameter of 130 nm shown in Fig.9.3.3b.

## **9.8.4 Characterization studies of mercury nanoparticles in malonic acid-based binary deep eutectic solvents**

### **9.8.4.1 UV-Visible spectra of mercury sulfide nanoparticles**

UV-Visible absorption spectra of mercury nanoparticles in DMSO solution are shown in figure 9.4.1. The characteristic absorption peak of the mercury metal was observed around 250 nm <sup>[30]</sup>. The peaks observed at 259.40 and 258.80 nm were assigned for the mercury sulfide nanoparticles obtained in MA-GLU BDES and MA-FRU BDES respectively. So, it is concluded that mercury nanoparticles were formed in MA-GLU and MA-FRU BDESs due to their high viscosity.

### **9.8.4.2 FTIR spectra of mercury sulfide nanoparticles**

In figure 9.4.2, FTIR spectrum for mercury sulfide nanoparticles shows a peak at 3428.97 $\text{cm}^{-1}$  & 3429.07  $\text{cm}^{-1}$  corresponds to the free O - H group in both spectra, and the peak at 2922.35 & 2922.88  $\text{cm}^{-1}$  is due to the presence of thiol groups in both spectra <sup>[31]</sup>. The peak at 1724.89  $\text{cm}^{-1}$  and 1719.10  $\text{cm}^{-1}$  corresponds to the C = O asymmetric stretching of both spectra. The peaks observed at 1384 to 1400 $\text{cm}^{-1}$  corresponds to the C - H bending vibration of both spectra. The peaks observed at 1618.93 $\text{cm}^{-1}$  & 1592.85 $\text{cm}^{-1}$  are due to the presence of two amide bands <sup>[31]</sup> and the peaks around 1200- 1000 $\text{cm}^{-1}$  corresponds to the S - O bond and peaks around 600 $\text{cm}^{-1}$  due to the C - S stretching vibration <sup>[32]</sup>. Further, there are some weak peaks also in both spectra.

### **9.8.4.3 Morphological analysis of mercury sulfide nanoparticles by SEM**

The surface morphology and particle size of the HgS nanoparticles prepared using the DESs have been analyzed by scanning electron microscope <sup>[33]</sup>. In figure 9.4.3, the SEM images of mercury sulfide nanoparticles prepared using MA-GLU DES are labeled as “a”

and “b” while the HgS nanoparticles obtained from the MA-FRU DES are labeled as “c” and “d”. The morphology of HgS nanoparticles seems to be a sponge-like structure taken up to 200 nm in the case of particles obtained from MA-GLU DES. The HgS nanoparticles obtained in MA-FRU DES look like a spherical-shaped structure taken up to 1  $\mu\text{m}$ .

### **9.8.5 Characterization studies of copper nanoparticles in zinc chloride-based binary deep eutectic solvents**

#### **9.8.5.1 UV-Visible spectra of copper nanoparticles**

Figure 9.5.1 shows the UV-visible absorption spectra of copper oxide nanoparticles in ethanolic solution. The characteristic absorption peak of copper was discovered at 550-570 nm <sup>[9,34]</sup>. The copper oxide nanoparticles obtained in ZC-GLU BDES (Fig. 9.5.1a) and MA-FRU (Fig. 9.5.1 b) BDES were assigned to the broad peaks at 503 and 470 nm in figure 9.5.1 <sup>[9,34]</sup>. As a result, copper nanoparticles were found in the MA-GLU and MA-FRU BDESs.

#### **9.8.5.2 FTIR spectra of copper nanoparticles**

The FTIR spectra in the range of 4000 to 400  $\text{cm}^{-1}$  for copper oxide nanoparticles prepared from ZC-GLU and ZC-FRU are reported in “a” and “b” of figure 9.5.2 respectively. The several peaks noticed in the range of 400 to 850  $\text{cm}^{-1}$  are correlated to Cu – O vibrations of CuO nanoparticles <sup>[10]</sup>. The sharp peak observed at 609  $\text{cm}^{-1}$  in both the spectra “a” and “b” clearly indicated the Cu – O stretching <sup>[11]</sup>. Here zinc chloride molecules are capped on the surface of CuO nanoparticles. These are indicated by the peaks at 1077.41 and 1078.16  $\text{cm}^{-1}$  corresponding to the C – O stretching of the carboxylic acid group in both the spectra “a” and “b” of figure 9.5.2. The peak due to  $\text{CH}_2$  deformations of malonic acid is seen at 1384  $\text{cm}^{-1}$  in both spectra. The peak was noticed at 1600  $\text{cm}^{-1}$  denoted O – H bending of malonic acid. The peaks observed at 2923.09  $\text{cm}^{-1}$  and 2924.66  $\text{cm}^{-1}$  are due to C – O asymmetric stretching <sup>[11]</sup>. Further, the broad peaks seen around 3436  $\text{cm}^{-1}$  in both



the spectra due to different vibrations modes of water molecules adsorbed on the surface of copper oxide nanoparticles <sup>[10]</sup>.

### 9.8.5.3 XRD patterns of copper oxide nanoparticles

The powder x-ray diffraction patterns of copper oxide nanoparticles prepared from the deep eutectic solvents, ZC-GLU and ZC-FRU are given in “a” and “b” of figure 9.5.3 respectively. The XRD patterns give information about the grain size, structure, and phase cleanliness of the materials. In the case of CuO particles obtained in ZC-GLU DES, there were no sharp diffraction peaks as they were a little amorphous structure. The diffraction peaks seen at 23.50°, 27.45°, 41.85° and 66.04° are indexed as (040), (021), (420), (300) respectively. Similarly, the diffraction peaks seen at 23.92°, 27.18°, 35.65° and 61.05° are also indexed as (101), (021), (240) and (220) <sup>[35]</sup> respectively for the CuO particles prepared using the ZC-FRU BDES. The grain size of CuO nanoparticles is determined by using the Debye–Scherer formula,

$$D = k \lambda / \beta \cos \theta$$

where D denotes the grain size, K refers to a constant,  $\lambda$  refers to the wavelength of X-ray used,  $\beta$  denotes the fullwidth half-maximum of the diffraction peaks and  $\theta$  is the angle of the diffraction <sup>[10]</sup>. By using this formula, the average grain size of CuO nanoparticles prepared from the BDES of ZC-GLU is found to be 25 nm. Similarly, the average grain size of CuO nanoparticles prepared using the DES of ZC-FRU is determined to be 52.54 nm.

### 9.8.5.4 Morphological analysis of copper oxide nanoparticles by SEM

The surface morphology and particle size of the CuO nanoparticles prepared using the ZC- BDESs have been analyzed by scanning electron microscope <sup>[10]</sup>. In figure 9.5.4, the SEM images of copper oxide nanoparticles prepared using ZC-GLU BDES are labelled as “a” and “b” while the CuO nanoparticles obtained from the ZC-FRU BDES are labelled

as “c” and “d”. The morphology of CuO nanoparticles seems to be grains with an average diameter of 65.29 nm in the case of particles obtained from ZC-GLU BDES. The CuO nanoparticles obtained in ZC-FRU BDES look like leaves-like morphology with an average diameter of 95.23 nm.

#### **9.8.5.5 Energy Dispersive X-ray Analysis**

The elemental composition of the CuO nanoparticles was carried out by energy dispersive x-ray analysis (EDAX) spectroscopy <sup>[12]</sup>. In figure 9.8.5, it is given the EDAX spectrum of copper oxide nanoparticles synthesized using the DES of ZC-GLU whereas the EDAX spectrum of CuO nanoparticles prepared using the DES of ZC-FRU is denoted in figure 9.5.5 b. In figure 9.5.5 a, it is shown that the atomic percentage of O is 74.49 and Cu is 20.73, which revealed that CuO nanoparticles are formed in ZC-GLU BDES. In figure 9.5.5 b, it has been noticed that the atomic percentage of Cu, O are 69.36 and 23.77 respectively. Thus, it is observed that in the ZC-BDES, there are some impurities due to surface capping of solvents.

#### **9.8.6 Characterization studies of silver nanoparticles in zinc chloride-based binary deep eutectic solvents**

##### **9.8.6.1 UV–Visible spectra of silver oxide nanoparticles**

The conduction and valence bands in Ag<sub>2</sub>O NPs are close together, allowing electrons to freely move <sup>[14–17]</sup>. These free electrons generate a surface plasmon resonance (SPR) absorption band due to the simultaneous oscillation of electrons of metal nanoparticles in resonance with light waves. This band corresponds to colloidal silver nanoparticle absorption in the 400–450 nm area due to surface plasmon vibration stimulation, according to Njagi et al <sup>[18]</sup>. A surface plasmon resonance peak (SPR) in a strong absorption band of about 300 nm is evident in the case of Ag<sub>2</sub>O NPs synthesized in ZC-GLU, 256 nm in the case of ZC-FRU confirming the formation of Ag<sub>2</sub>O NPs. The UV-

Visible spectra of silver oxide nanoparticles synthesized in ZC BDES are given in the figure.9.6.1

#### **9.8.6.2 FTIR spectra of silver oxide nanoparticles**

Silver oxide nanoparticles generated from Zinc chloride-based solvents had FTIR spectra in the region of 4000 to 400  $\text{cm}^{-1}$ , as shown in “a” and “b” of Fig.9.6.2. The Ag – O vibrations of  $\text{Ag}_2\text{O}$  nanoparticles are associated with multiple peaks observed in the region of 500 to 650  $\text{cm}^{-1}$ [21]. The peak due to glucose/fructose is seen at 1384  $\text{cm}^{-1}$  in the spectrum of zinc chloride-based DESs. The peak at 1543.52  $\text{cm}^{-1}$  is due to the N - O stretching vibration and at 1384.05  $\text{cm}^{-1}$  is due to the C - H bending vibration. The peaks observed at 2851  $\text{cm}^{-1}$  and 2921  $\text{cm}^{-1}$  are due to C – O asymmetric stretching. Furthermore, the broad peaks seen around 3420  $\text{cm}^{-1}$  in both spectra are due to the strong intermolecular bonded stretching of water molecules adsorbed on the surface of silver oxide nanoparticles [22].

#### **9.8.6.3 XRD patterns of silver oxide nanoparticles**

Ag nanoparticles obtained in the case of ZC-GLU BDES (Fig.9.6.3a) show intense peaks at 31.44°, 37.85°, 45.25°, 64.28 and 77.32 indexed at the planes of (110), (111), (110), (220) and (311) respectively, and in the case of ZC-FRU BDES (Fig.9.6.3 b) at 37.75°, 43.88°, 64.17°, and 77.13° indexed at the planes of (111), (200), (220), and (311) respectively. The structure of silver nanoparticles is crystalline in nature, and it is face-centered cubic in both cases. The average particle size obtained in the case of ZC-GLU BDES is calculated to be 44 nm, and in ZC-FRU BDES it is calculated to be 15 nm by measuring the breadth of (111) Bragg’s reflection.

#### **9.8.6.4 SEM images of silver oxide nanoparticles**

Scanning electron microscopy was used to examine the morphological structure and particle size of  $\text{Ag}_2\text{O}$  nanoparticles prepared using BDESs. The morphology of  $\text{Ag}_2\text{O}$

nanoparticles seems to be irregularly shaped with an average diameter of 110.27 nm in the case of particles obtained from ZC-GLU BDES (Fig.9.6.4. a,b) and it seems to be granular shaped with an average diameter of 185.99 nm in the case of particles obtained from ZC-FRU BDES (9.6.4.c,d).

#### **9.8.6.5 Energy Dispersive X-ray Analysis**

The weight percent composition of Ag<sub>2</sub>O NPs prepared in the case of ZC-GLU (Fig.9.6.5a) is 3.60, and other elements such as zinc, chlorine, and oxygen acted as capping agents bonded to the surface of the silver nanoparticles <sup>[36]</sup>. In the instance of ZC-FRU, Ag<sub>2</sub>O NPs were synthesized with a weight percent composition of 9.80, while other elements such as zinc, chlorine, silicon, and oxygen served as capping agents (Fig.9.6.5. b).

#### **9.9. Conclusion**

Using Malonic acid-based Binary Deep Eutectic Solvents and Zinc chloride-based Binary Deep Eutectic Solvents, Copper, Cadmium, Mercury, and Silver nanoparticles were successfully synthesized. The nanoparticles were characterized by many techniques. There were no nanoparticles formed in MA – GCL BDES as it has high viscosity. Viscosity is an important property for a solvent. When the level of water is high, the viscosity decreases. By this way, the particle size was controlled. The nanoparticles were synthesised in a simple and convenient manner. There was no surfactant and seed were needed for the formation of nanoparticles.

## References

- [1]. M. Sampath, R. Vijayan, E. Tamilarasu, A. Tamilselvan, and B. Sengottuvelan, “Green synthesis of novel jasmine bud-shaped copper nanoparticles,” *Journal of Nanotechnology*, vol. 2014, Article ID 626523, 7 pages, 2014.
- [2]. J.-G. Yang, S.-H. Yang, T. Okamoto, et al., “Synthesis of copper monolayer and particles at the aqueous-organic interface,” *Surface Science*, vol. 600, no. 24, pp. L318–L320, 2006.
- [3]. M. Abdulla-Al-Mamun, Y. Kusumoto, and M. Muruganandham, “Simple new synthesis of copper nanoparticles in water/acetonitrile mixed solvent and their characterization,” *Materials Letters*, vol. 63, no. 23, pp. 2007–2009, 2009.
- [4]. P. K. Khanna, S. Gaikwad, P. V. Adhyapak, N. Singh, and R. Marimuthu, “Synthesis and characterization of copper nanoparticles,” *Materials Letters*, vol. 61, no. 25, pp. 4711–4714, 2007.
- [5]. Quang Huy Tran et al, silver nanoparticles: synthesis, properties, toxicology, applications and perspectives, *Adv. Nat. Sci: Nanosci. Nanotechnol.* 4 033001, 2013.
- [6]. M.A. Malik, *Solid-State Materials, Including Ceramics and Minerals*, in *Comprehensive Inorganic Chemistry II (Second Edition)*, 2013.
- [7]. Villa Krishna Harika et.al., Sustainable existence of solid mercury (Hg) nanoparticles at room temperature and their applications, *Chem. Sci.*, 2021, 12, 3226-3238.
- [8]. R Aruna Devi et al., Synthesis, and Characterization of Cadmium Sulfide Nanoparticles by Chemical Precipitation Method *J Nanosci Nanotechnol.* 2015 Nov; 15(11):8434-9.
- [9]. Shikha Jain, Ankita Jain, Vijay Devra, Copper nanoparticles catalyzed oxidation of threonine by peroxomonosulfate, *Journal of Saudi chemical society* 18 (2014), 149 - 153.

- [10]. Tariq Jan, J. Iqbal, Umar Farooq, Asma Gul, Rashda Abbasi, Ishaq Ahmad, Maaza Malik, Structural, Raman and optical characteristics of Sn doped CuO nanostructures: A novel anticancer agent, *Ceramics International*, 41(10), Part A December 2015, 13074 – 79. <http://dx.doi.org/10.1016/j.ceramint.2015.06.080>
- [11]. A. Rita, A. Sivakumar, S. A. Martin Britto Dhas, Influence of shock waves on structural and morphological properties of copper oxide NPs for aerospace applications, *Journal of Nanostructure in Chemistry*, 9 (2019), 225 – 230. <https://doi.org/10.1007/s40097-019-00313-0>
- [12]. S. Kalaiarasi, P. Yogeswarai Nithya, Synthesis, characterization and electrochemical behavior of metal oxide nanoparticles *Cressa Cretica* whole plant, *Int. Journal of Advanced Scientific Research and Management*, Special Issue 4, 2019 (ICAMA-18), 105 – 109.
- [13]. M. Sastry, V. Patil, R. Sankar, *J. Phys. Chem. B.* 102 (1998) 1404–1410.
- [14]. R. Das, S.S. Nath, D. Chakdar, G. Gope, R.J. Bhattacharjee, *Nanotechnol.* 5 (2009) 1–6.
- [15]. Kreibig U., Vollmer M. Springer; Berlin, Germany: 1995.
- [16]. S. Link, M.A. Ei-Sayed, *Annu. Rev. Phys. Chem.* 54 (2003) 331–366.
- [17]. A. Tleb, C. Petit, M.P. Pileni, *J. Phys. Chem. B.* 102 (1998) 2214–2220.
- [18]. E.C. Njagi, H. Huang, L. Stafford, H. Genuino, et al., *Langmuir* 27 (2011) 264–271.
- [19]. W. Wei, X. Mao, L.A. Ortiz, D.R. Sadoway, *Journal of Materials Chemistry* 21 (2) (2011) 432–438.
- [20]. Manikandan, V., Velmurugan, P., Park, JH. et al. *3 Biotech* 7, 72 (2017).
- [21]. V. Ravichandran, G. Paluri, K.L. Kumar, B. R., Kokati Venkata, *Journal of Experimental Nanoscience* 11 (6) (2016) 445–458.
- [22]. J. Coates, R.A. Meyers, Ed., *Encyclopaedia of Analytical Chemistry* 12 (2000) 10815–10837.

- [23]. Vivek Dhand, L. Soumya, Somayajula Bharadwaj, Shilpa Chakra, *Materials Science and Engineering C* 58 (2015) 36–43.
- [24]. B. Ajitha, Y. Ashok Kumar Reddy, P. Sreedhara Reddy, *Spectrochim Acta Part A* 121 (2014) 164–172.
- [25]. S. Kaviya, J. Santhanalakshmi, B. Viswanathan, J. Muthumar, K. Srinivasan, *Spectrochimica Acta Part A: Molecular and Biomolecular Spectroscopy* 79 (2011) 594–598.
- [26]. Malarkodi C., Rajeshkumar S., Paulkumar K., Jobitha G G., Vanaja M., and Annadurai G., “Biosynthesis of semiconductor nanoparticles by using sulfur-reducing bacteria *Serratia nematodiphila*”, *Advances in Nano Research.*, 1(2). 83-91. 2013.
- [27]. Donald L. Pavia, Gary M. Lampman, George S. Kriz, *Introduction to spectroscopy*, 3rd Edition, BROOKS/COLE, Thomson Learning, USA, 2001
- [28]. B.D. Mistry, *A Handbook of Spectroscopic Data*, Oxford Book Company, India, 2009.
- [29]. Preeti Sahare, *Synthesis, and Characterization of Cds Nanoparticle*, *International Journal of Engineering Research & Technology (IJERT)* ISSN: 2278-0181, NCANA - 2018 Conference Proceedings.
- [30]. N. Jassim Mohammed et.al.; *Synthesis and Characterization of Mercuric Sulfide Nanoparticles Thin Films by Pulsed Laser Ablation (PLA) in Distilled Water (DW)*; *Iranian Journal of Materials Science & Engineering* Vol. 17, No. 3, (2020)
- [31]. Satyavati et.al., *Biosynthesis and Characterization of Mercuric Sulfide nanoparticles produced by Bacillus cereus MRS-1*; *Indian Journal of Experimental Biology*; vol 51; pp 973-978;(2013)
- [32]. Asep Bayu Dani Nandiyanto et.al.; *How to Read and Interpret FTIR Spectroscopy of Organic Material*; *Indonesian Journal of Science & Technology* 4 (1); pp97-118; (2019)

- [33]. Peter A. Ajibade. et.al; Synthesis and Characterization of Metal Sulfides Nanoparticles /Poly (methyl methacrylate) Nanocomposites; Hindawi Publishing Corporation International Journal of Polymer Science Volume 2014, Article ID 752394.
- [34]. Arnim Henglein, Formation and Absorption Spectrum of Copper Nanoparticles from the Radiolytic Reduction of  $\text{Cu}(\text{CN})_2^-$ , J. Phys. Chem. B 2000, 104, 6, 1206–1211
- [35]. M.C.Morris, H.F. McMurdie, E.H.Evans, B. Paretzkin, H.S.Parker, Standard X-ray Diffraction powder patterns Sec-21
- [36]. Abiola Grace Femi-Adepoju, Adewum Oluwasogo Dada, PMC article; Heliyon 5(4) : (2019) e01543.



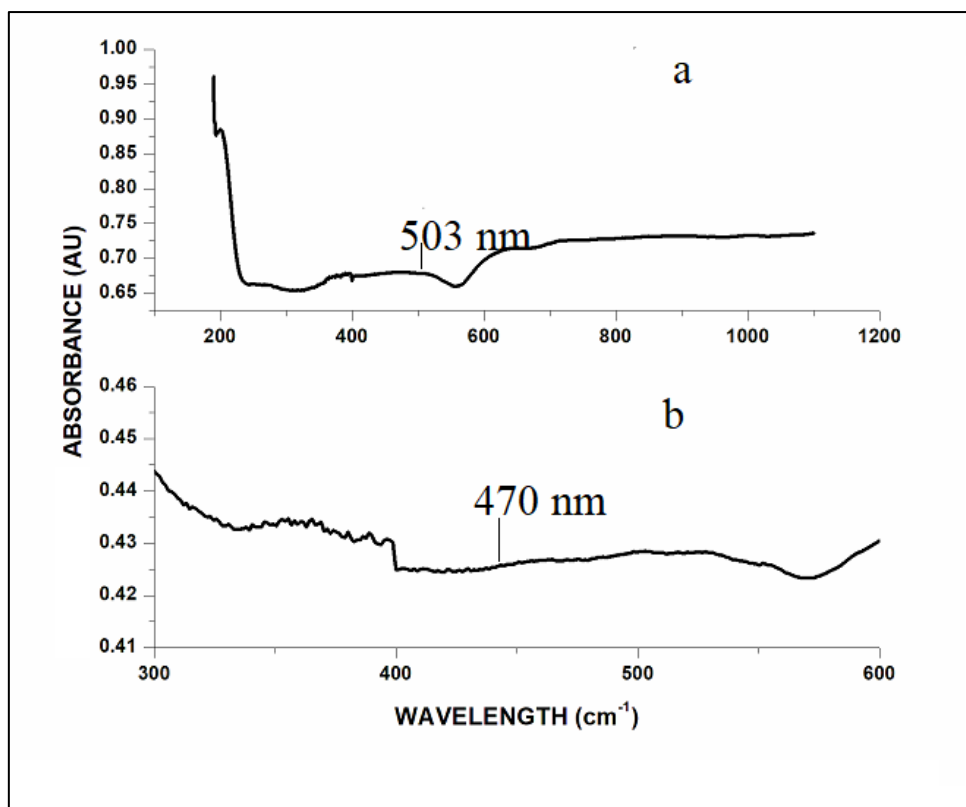


**Figure 9.1.1. UV-Visible spectra of copper oxide nanoparticles obtained using (a) Malonic acid - Glucose BDES (b) Malonic acid – Fructose BDES**

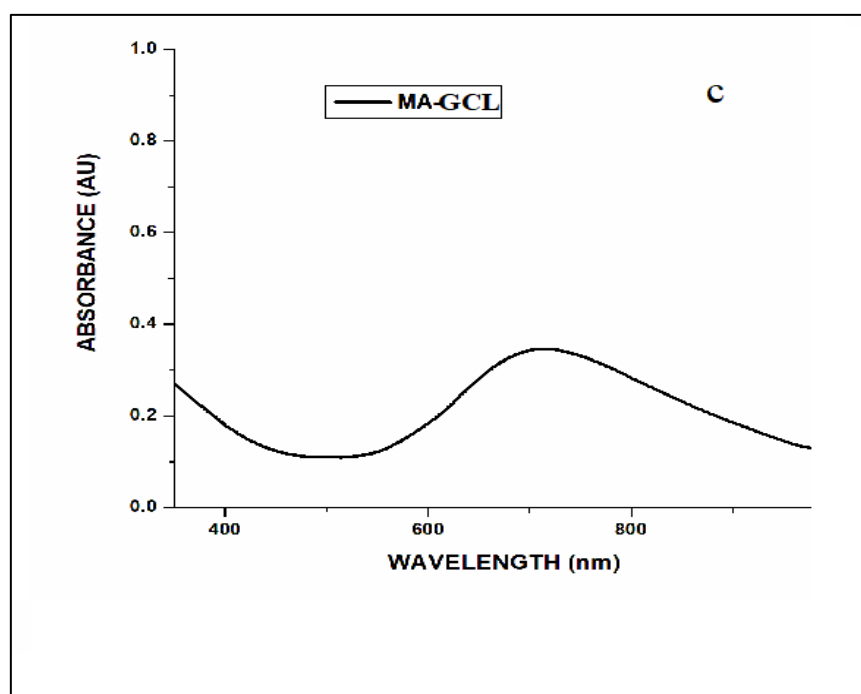


**Figure 9.1.1. c UV-Visible spectra of copper oxide nanoparticles obtained using Malonic acid - Glycerol BDES**

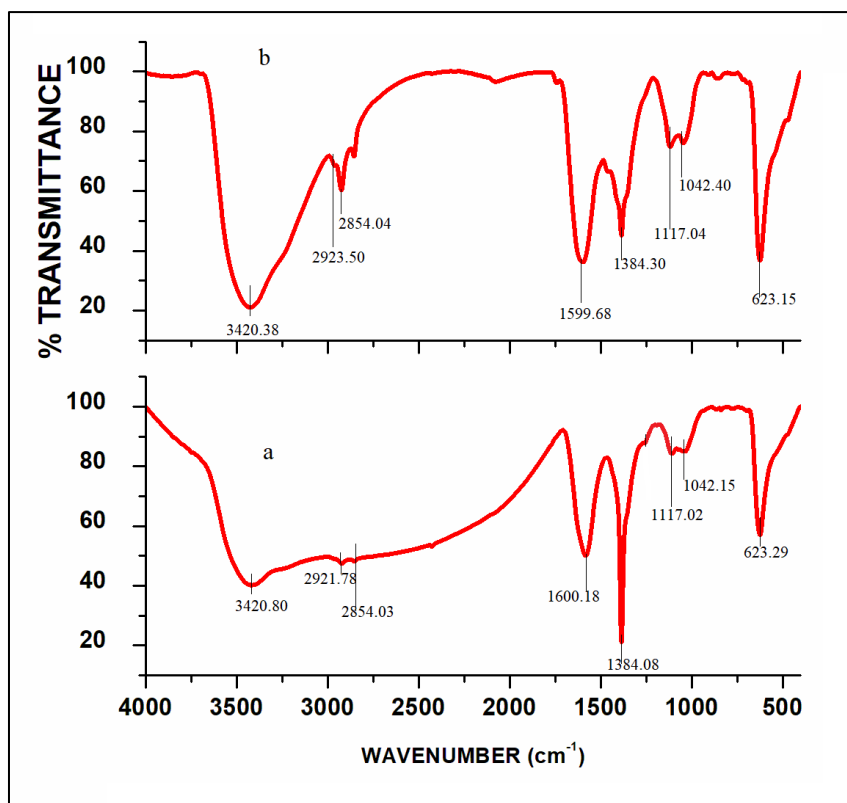


**Figure 9.1.2 FTIR spectra of copper oxide nanoparticles obtained using (a) Malonic acid - Glucose BDES (b) Malonic acid – Fructose BDES**

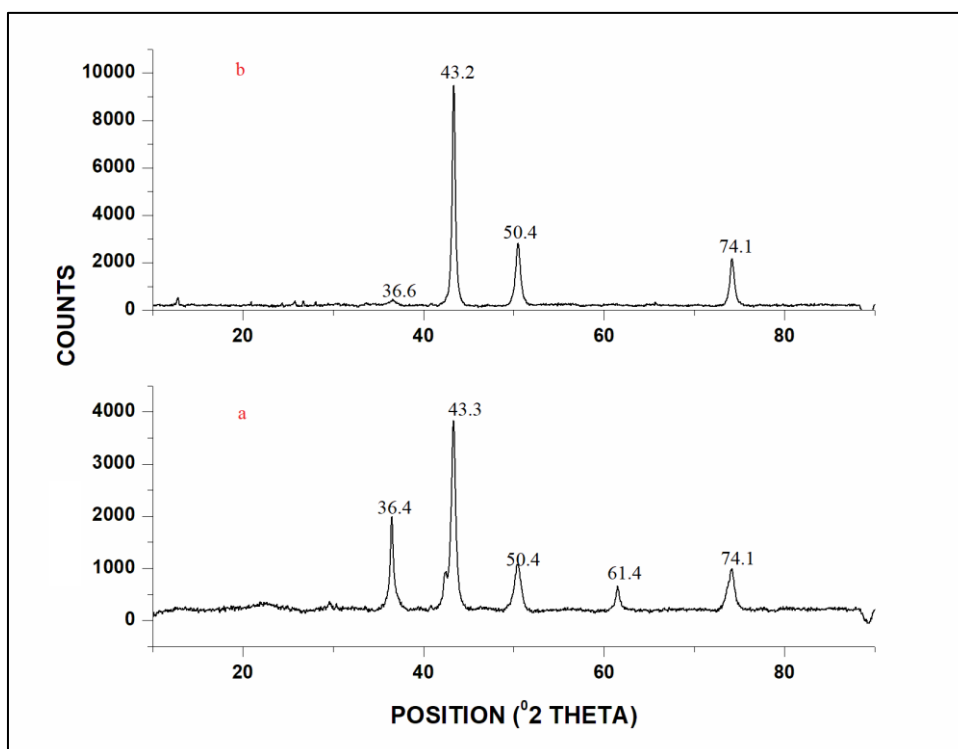


**Figure 9.1.3 XRD patterns of copper oxide nanoparticles obtained using (a) Malonic acid Glucose BDES and (b) Malonic acid – Fructose BDES**

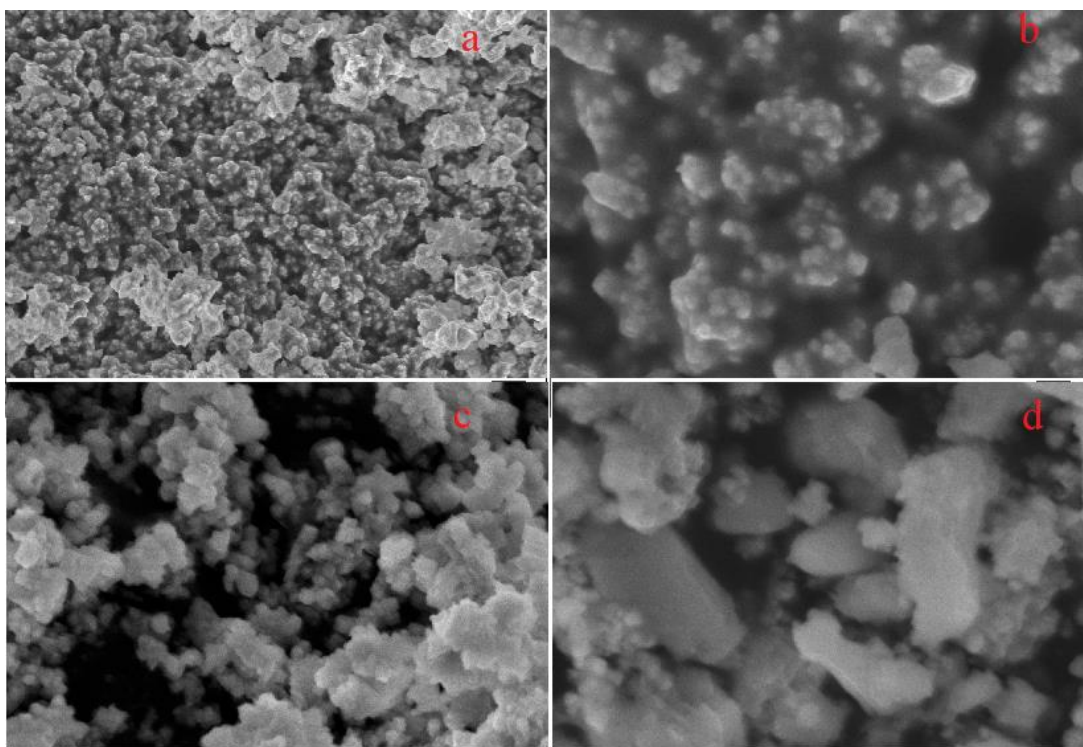


**Figure 9.1.4 SEM images of copper oxide nanoparticles obtained using (a) Malonic acid Glucose BDES and (b) Malonic acid – Fructose BDES**

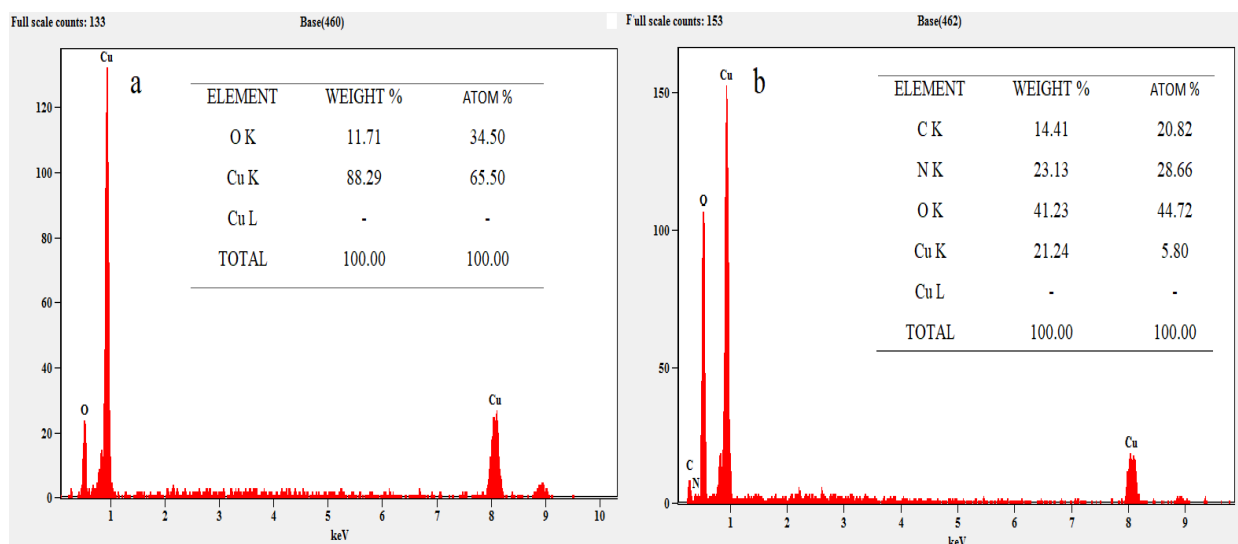


**Figure 9.1.5 EDAX Spectra of copper oxide nanoparticles obtained using (a) Malonic acid –Glucose BDES and (b) Malonic acid – Fructose BDES**

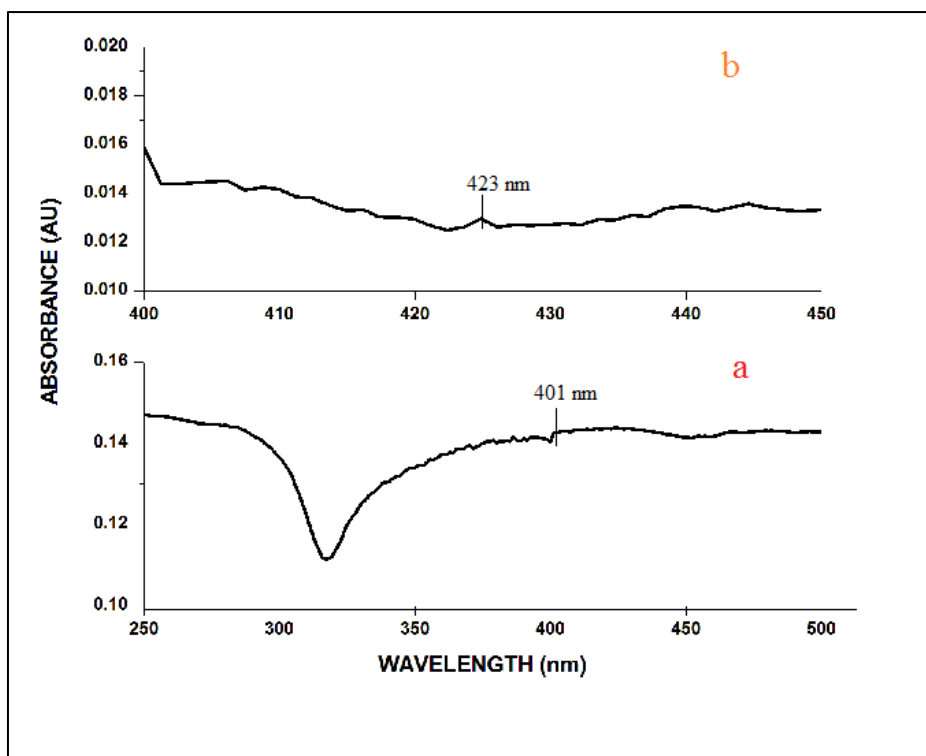
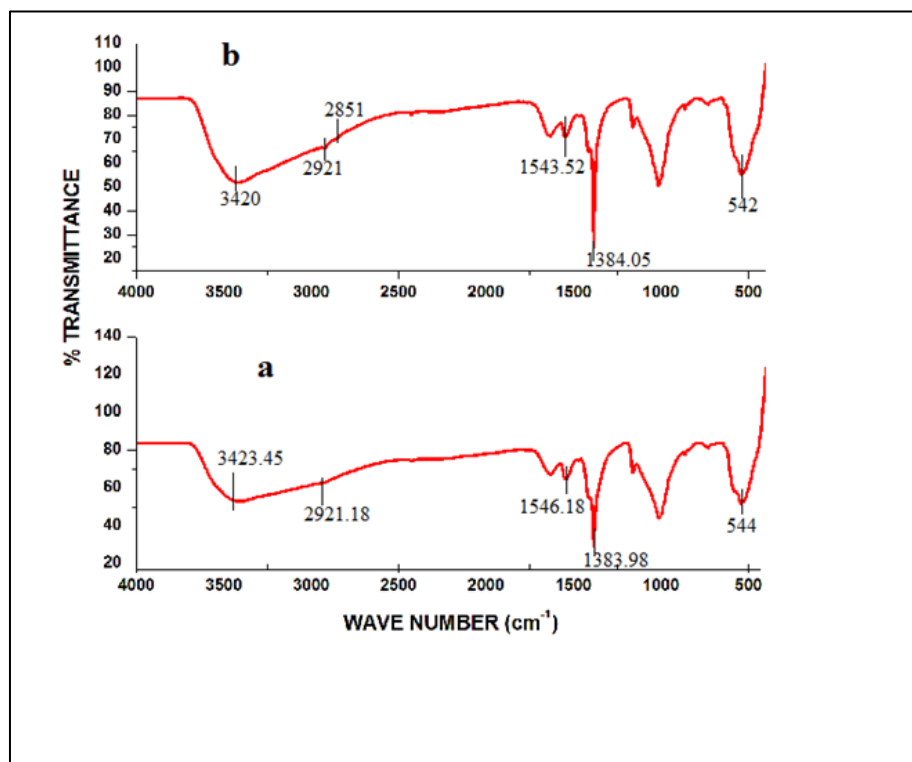


**Figure 9.2.1 UV-Visible spectra of silver oxide nanoparticles obtained using (a) Malonic - Glucose BDES (b) Malonic acid – Fructose BDES**



**9.2.2. FTIR spectra of silver oxide nanoparticles obtained using (a) Malonic - Glucose BDES (b) Malonic acid – Fructose BDES**

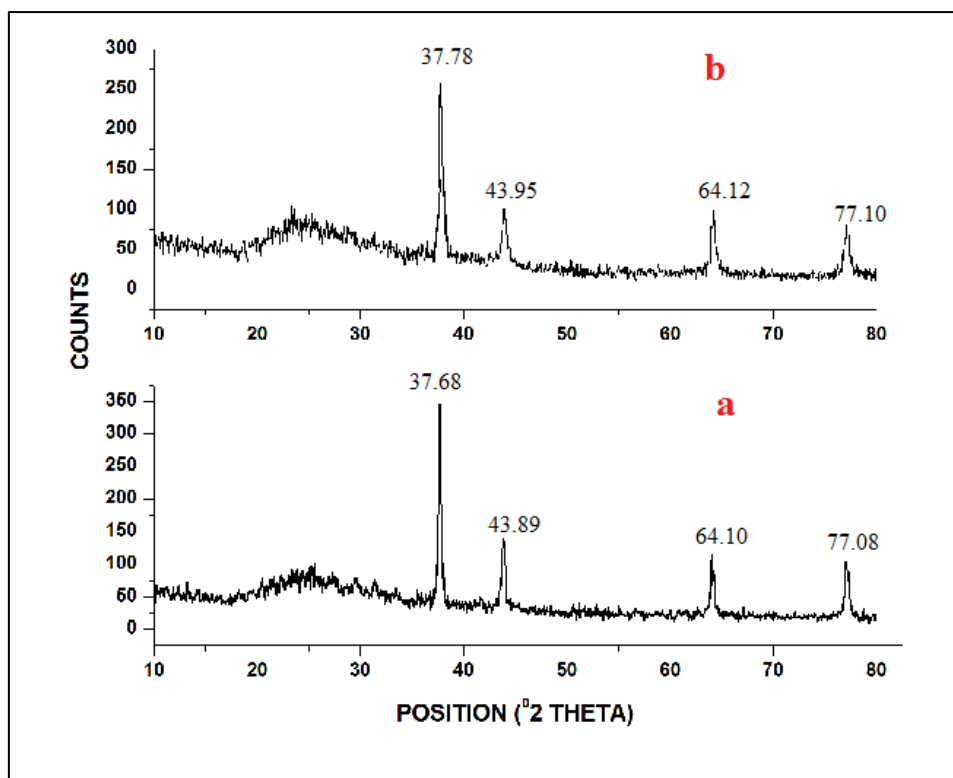


**Figure 9.2.3 XRD patterns of silver oxide nanoparticles obtained using (a) Malonic - Glucose BDES (b) Malonic acid – Fructose BDES**

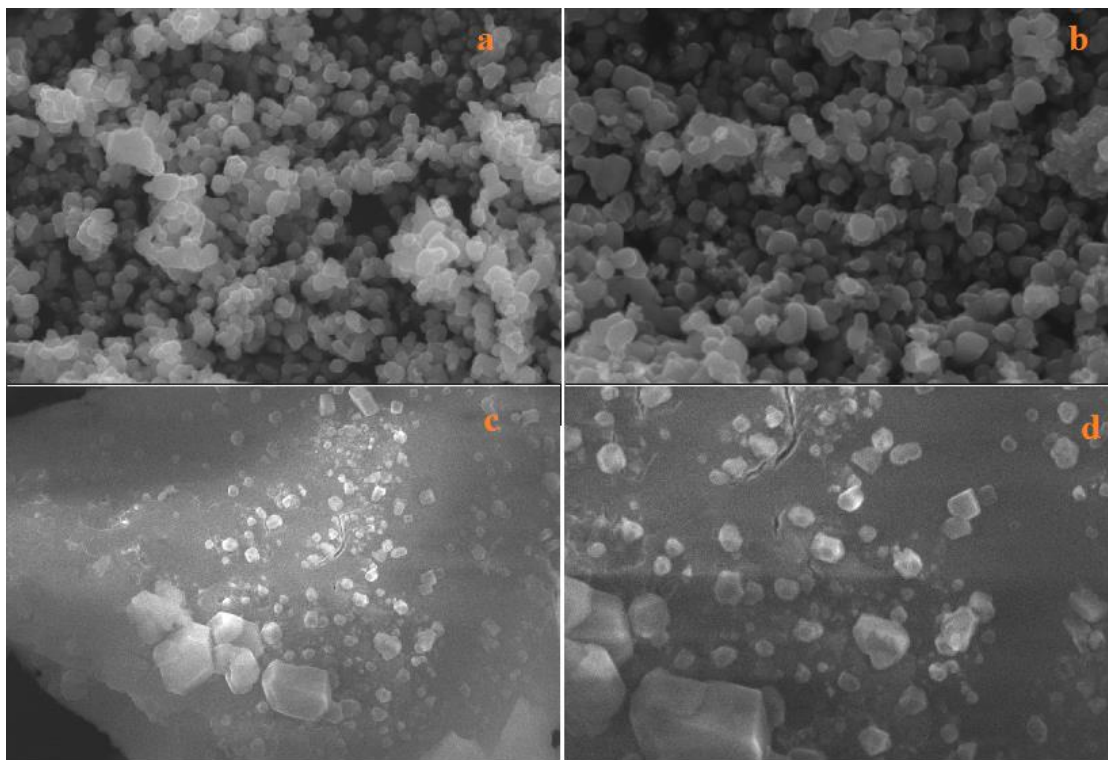


**Figure 9.2.4 SEM images of silver oxide nanoparticles obtained using (a) Malonic - Glucose BDES (b) Malonic acid – Fructose BDES**

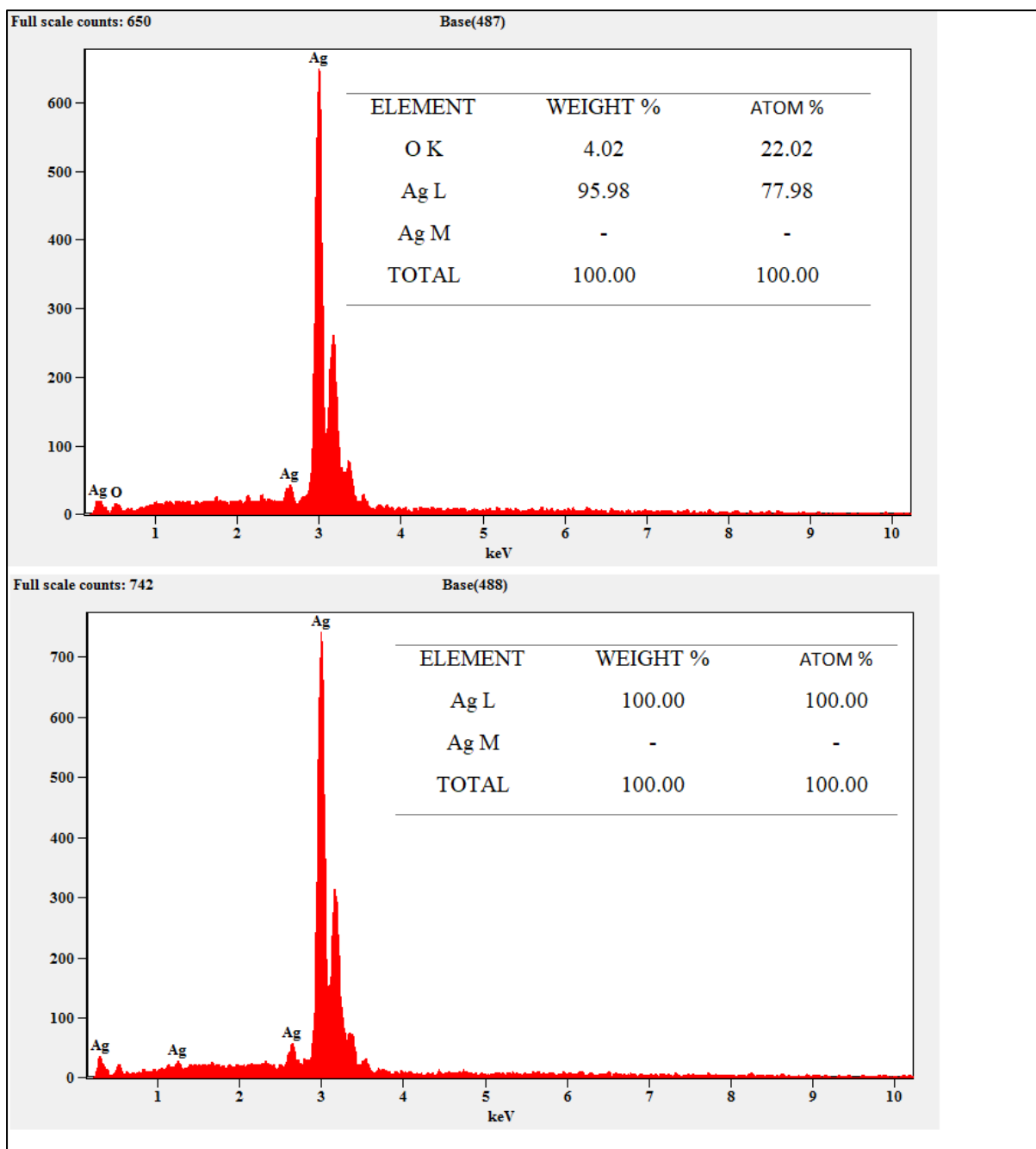


**Figure 9.2.5 EDAX spectra of silver oxide nanoparticles obtained using (a) Malonic - Glucose BDES (b) Malonic acid – Fructose BDES**

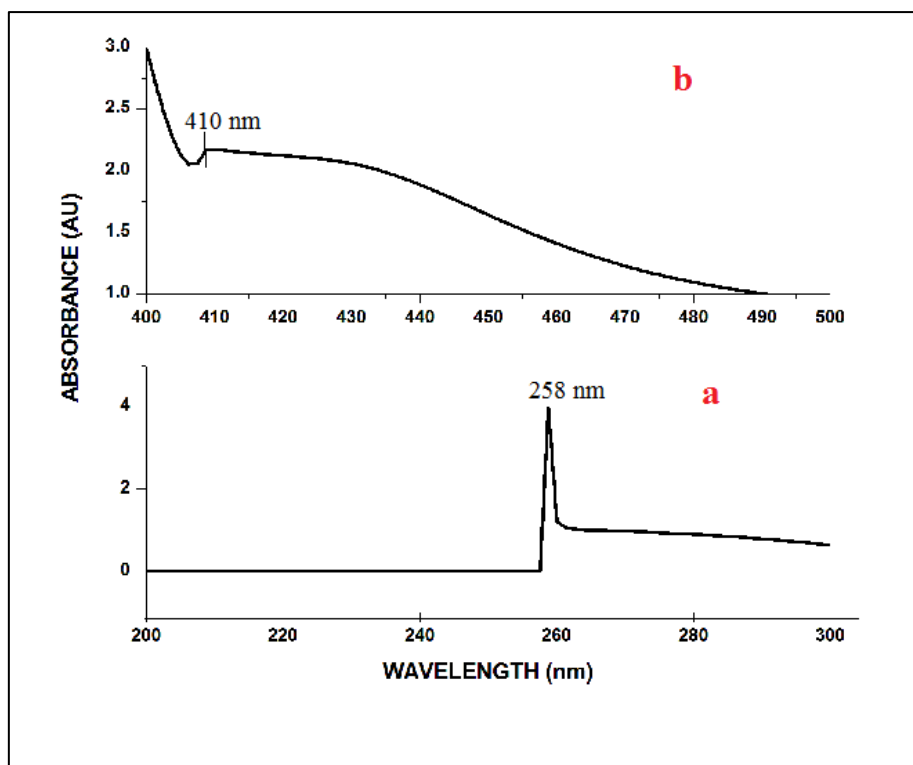


Figure 9.3.1 UV-Visible spectra of Cadmium sulfide nanoparticles obtained using (a) Malonic - Glucose BDES (b) Malonic acid – Fructose BDES

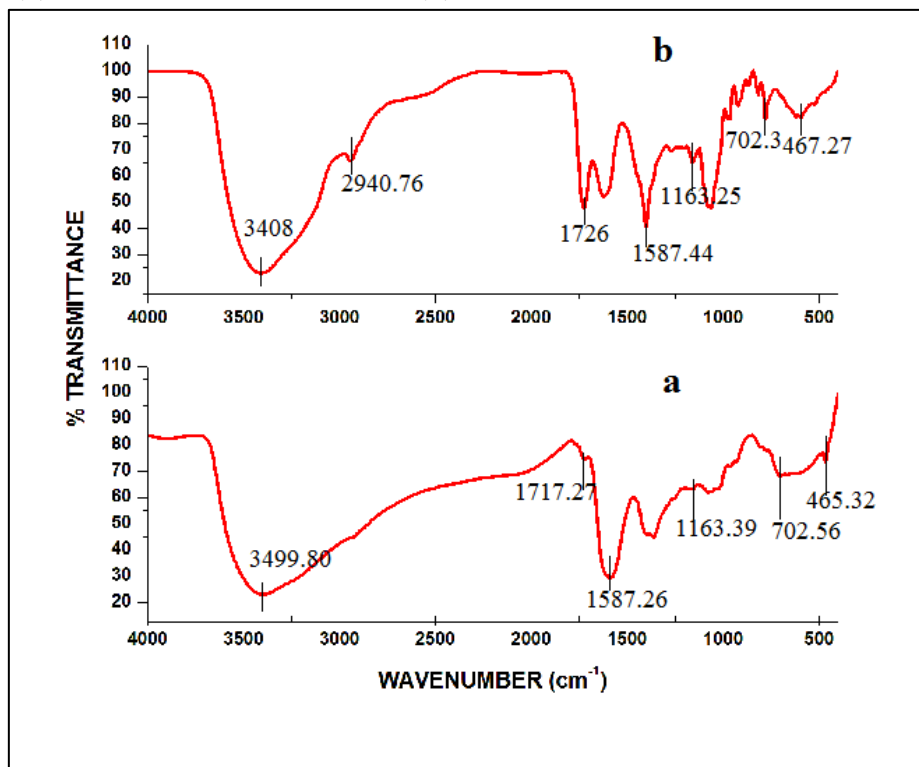
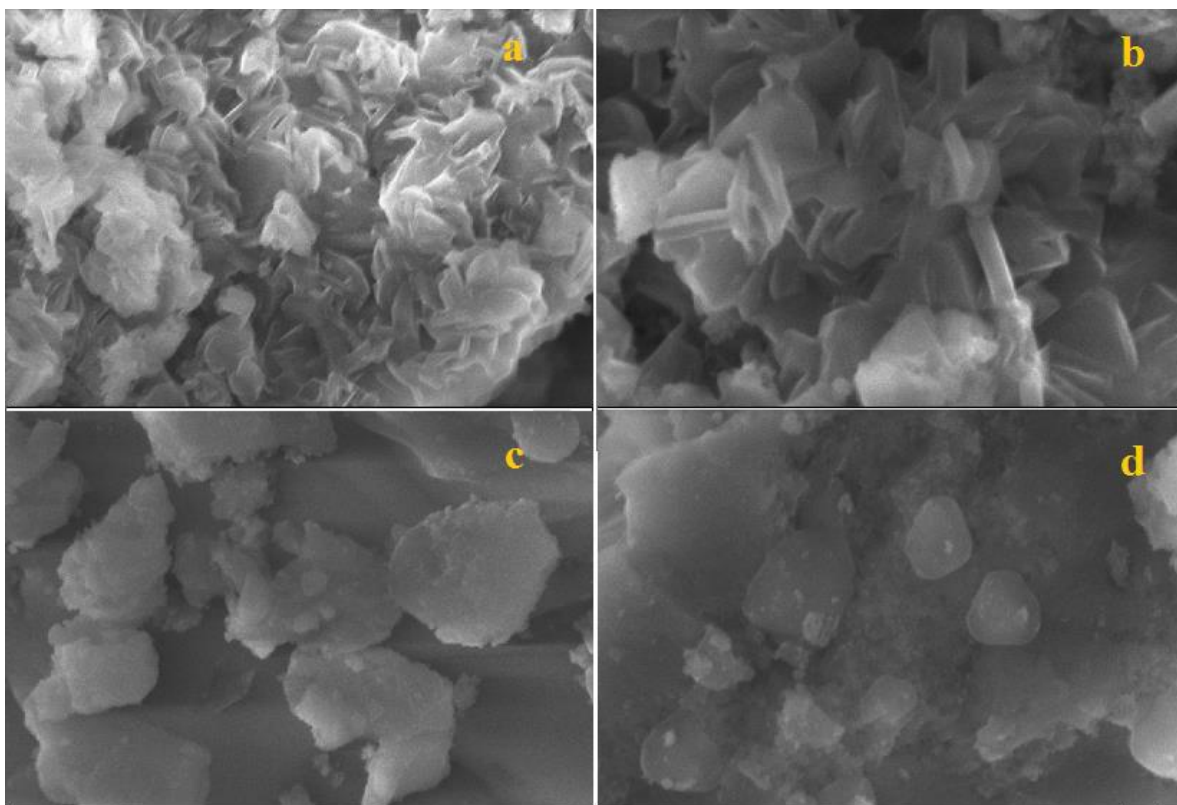
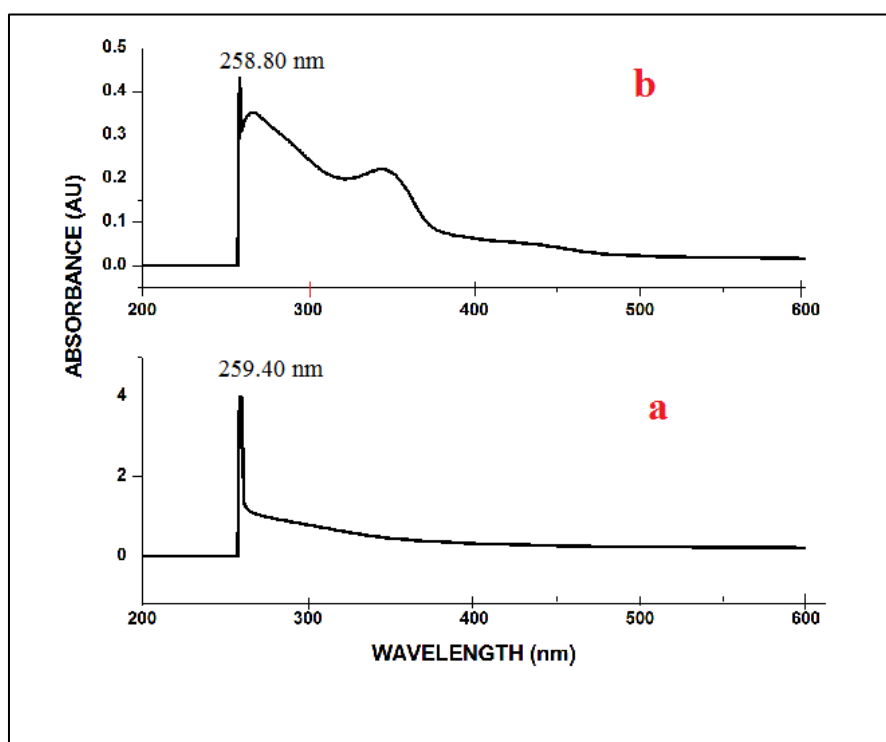


Figure 9.3.2. FTIR spectra of Cadmium sulfide nanoparticles obtained using (a) Malonic - Glucose BDES (b) Malonic acid – Fructose BDES

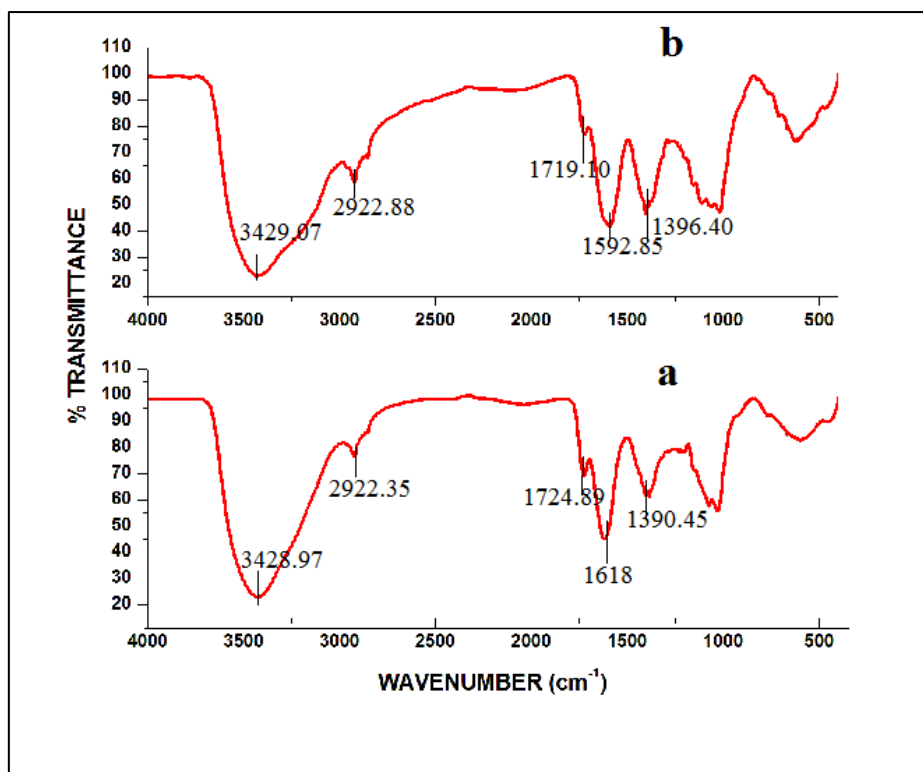


**Figure 9.3.3 SEM images of Cadmium sulfide nanoparticles obtained using (a) Malonic - Glucose BDES (b) Malonic acid – Fructose BDES**



**Figure 9.4.1. UV-Visible spectra of Mercury sulfide nanoparticles obtained using (a) Malonic - Glucose BDES (b) Malonic acid – Fructose BDES**





**9.4.2. FTIR spectra of Mercury sulfide nanoparticles obtained using (a) Malonic - Glucose BDES (b) Malonic acid – Fructose BDES**

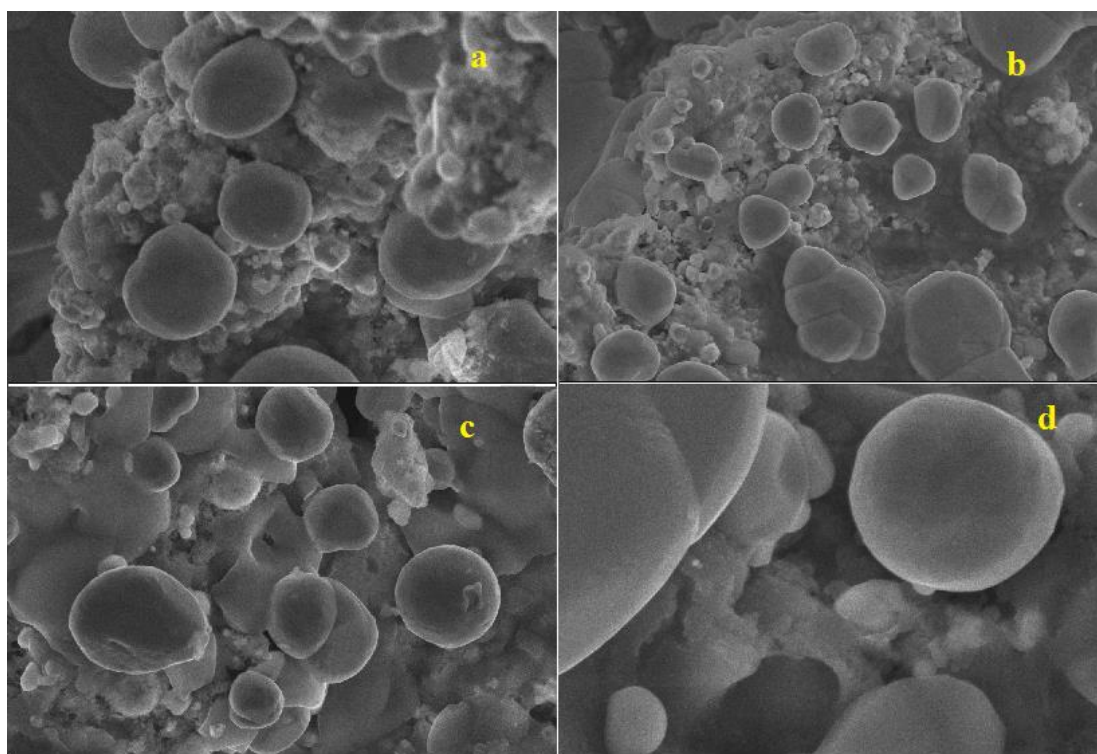


**Figure 9.4.3. SEM images of Mercury sulfide nanoparticles obtained using (a) Malonic - Glucose BDES (b) Malonic acid – Fructose BDES**

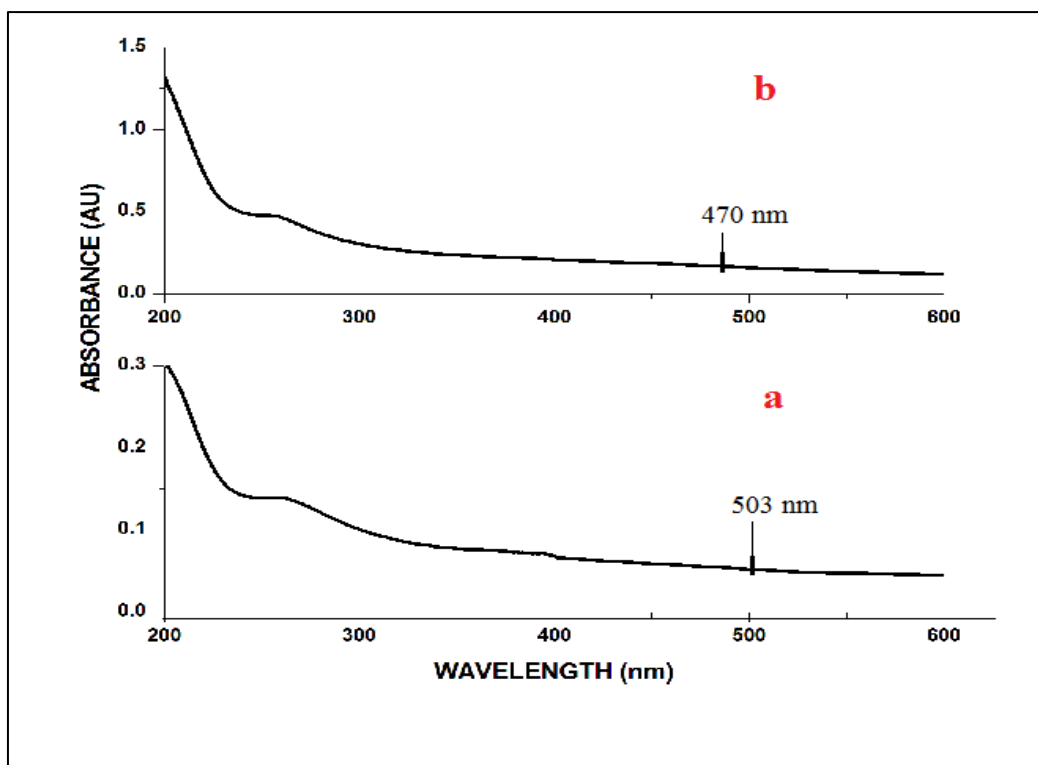


Figure 9.5.1. UV-Visible spectra of copper nanoparticles obtained using (a) Zinc chloride - Glucose BDES (b) Zinc chloride – Fructose BDES

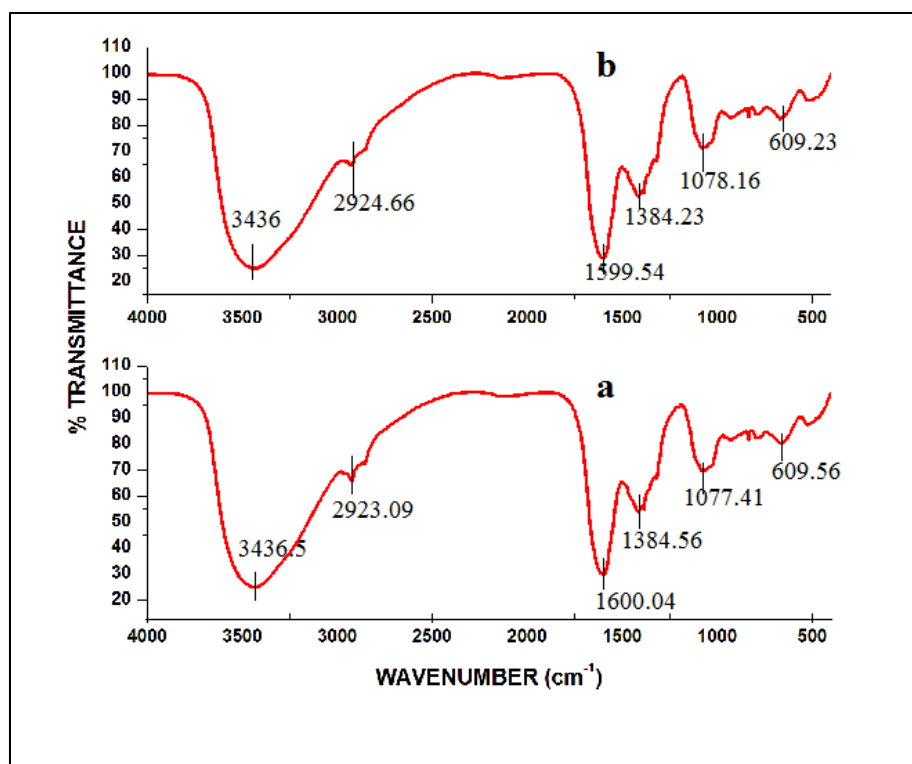
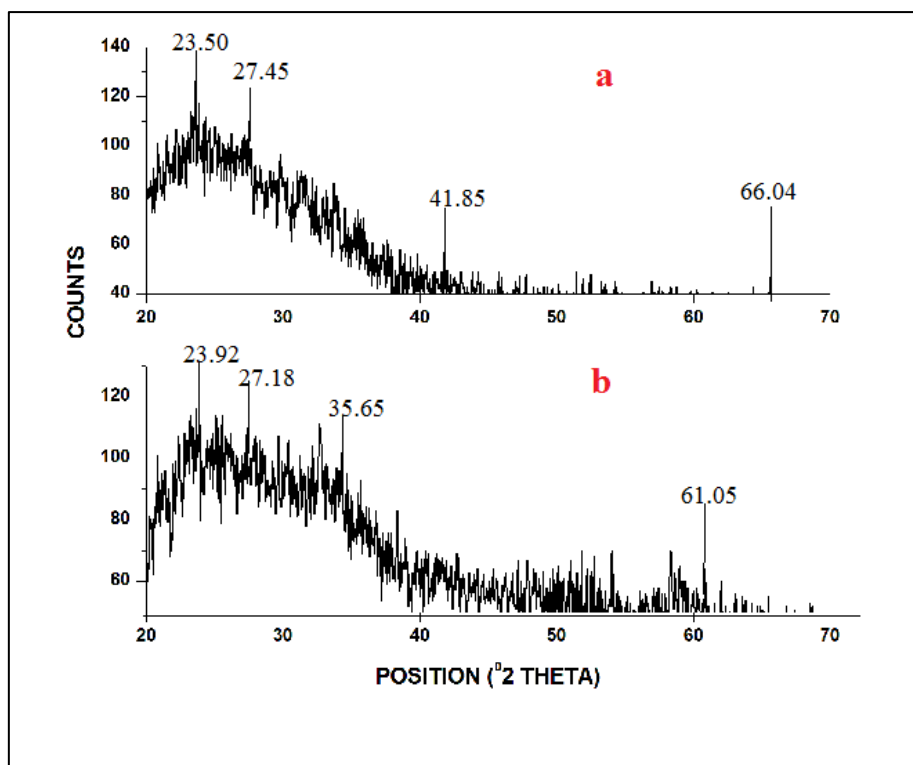
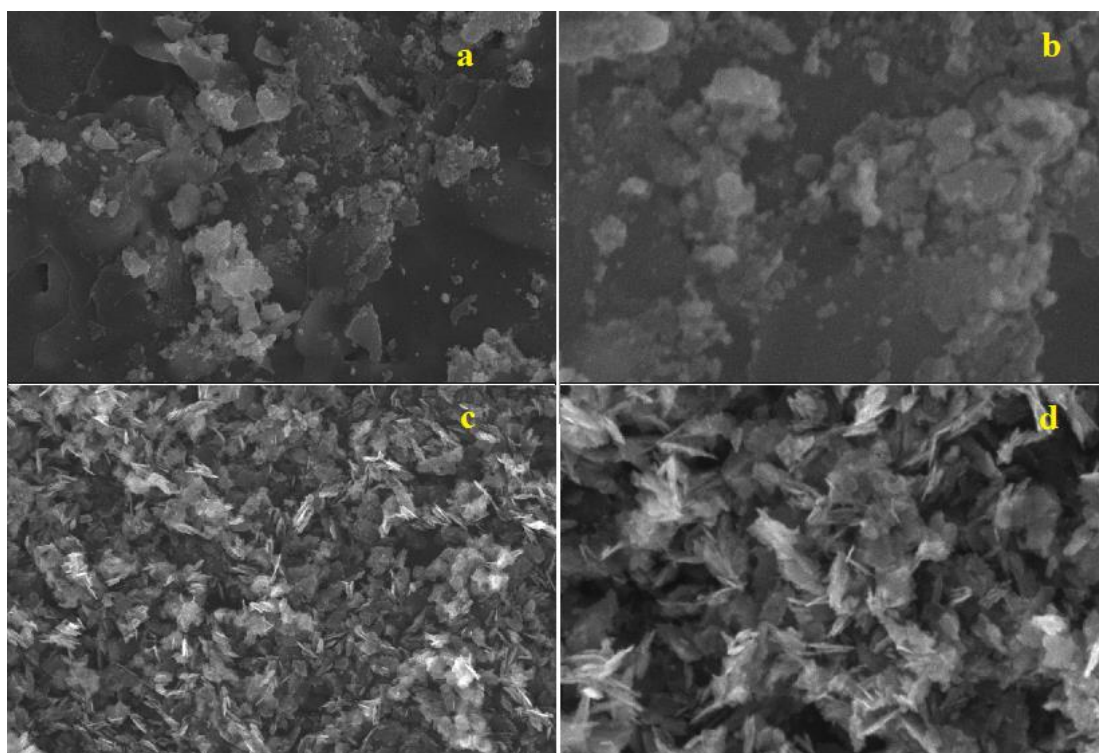


Figure 9.5.2. FTIR spectra of copper nanoparticles obtained using (a) Zinc chloride - Glucose BDES (b) Zinc chloride – Fructose BDES



**Figure 9.5.3. XRD patterns of copper nanoparticles obtained using (a) Zinc chloride - Glucose BDES (b) Zinc chloride – Fructose BDES**



**Figure 9.5.4. SEM images of copper nanoparticles obtained using (a) Zinc chloride - Glucose BDES (b) Zinc chloride – Fructose BDES**

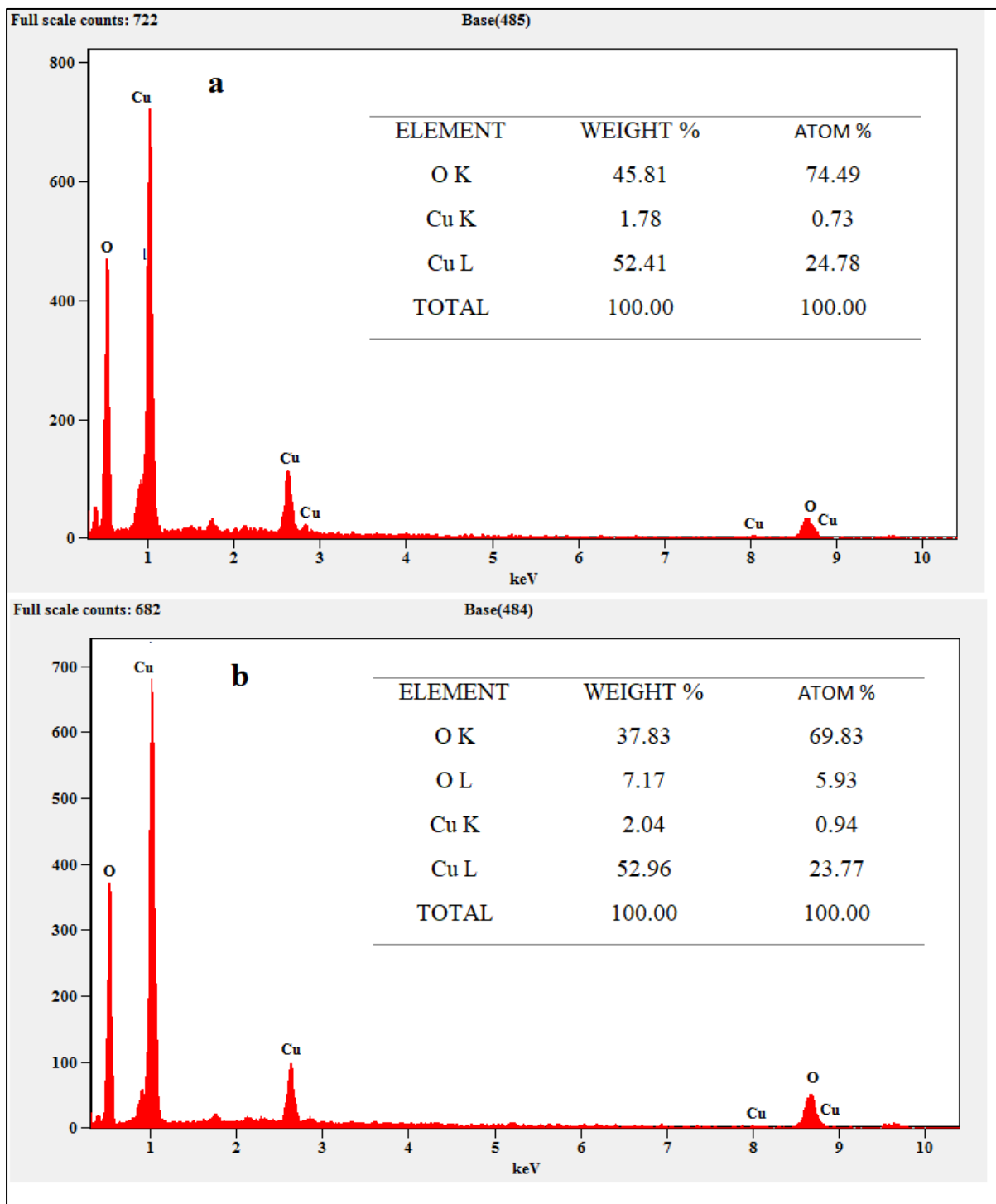


**Figure 9.5.5. EDAX spectra of copper nanoparticles obtained using (a) Zinc chloride - Glucose BDES (b) Zinc chloride – Fructose BDES**

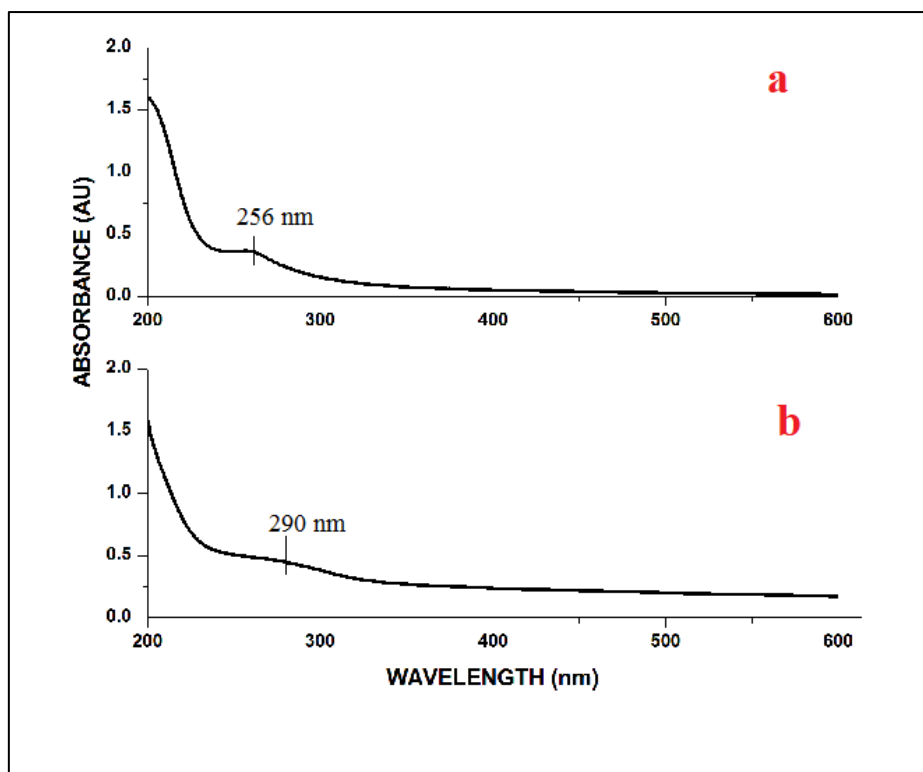


**Figure 9.6.1. UV-Visible spectra of silver nanoparticles obtained using (a) Zinc chloride - Glucose BDES (b) Zinc chloride – Fructose BDES**

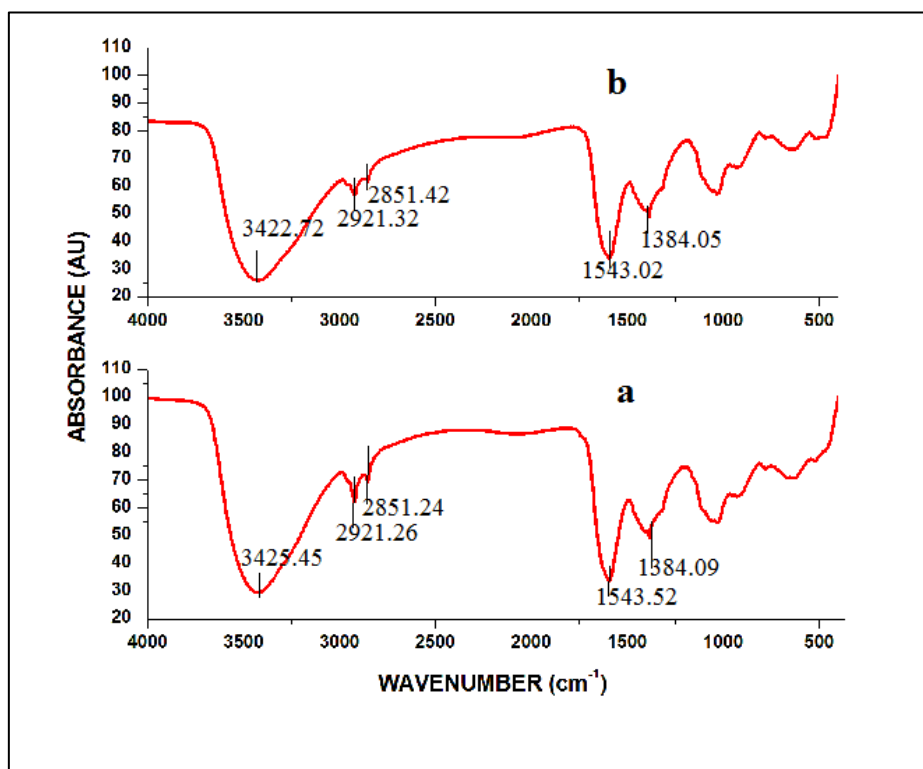


**Figure 9.6.2. FTIR spectra of silver nanoparticles obtained using (a) Zinc chloride - Glucose BDES (b) Zinc chloride – Fructose BDES**

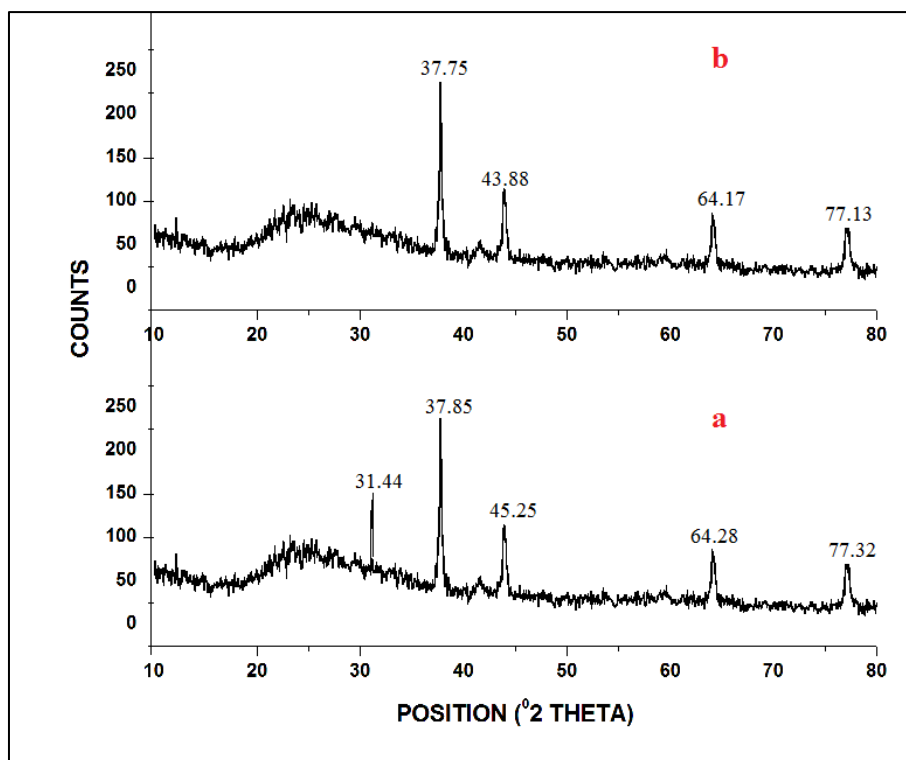


**Figure 9.6.3. XRD patterns of silver nanoparticles obtained using (a) Zinc chloride - Glucose BDES (b) Zinc chloride – Fructose BDES**

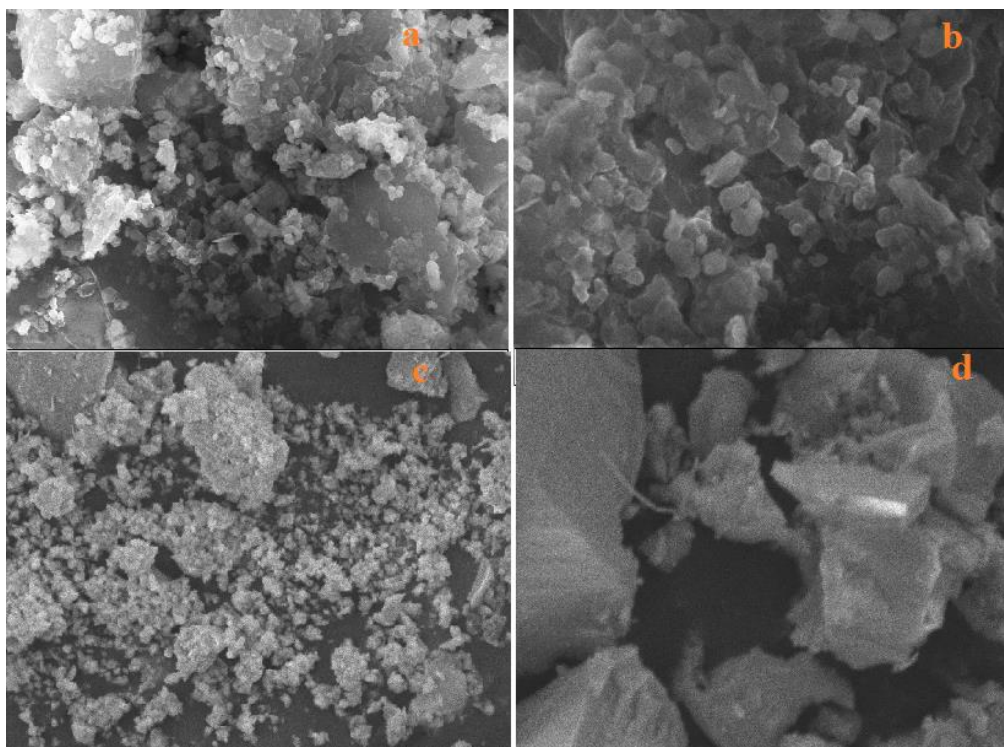


**Figure 9.6.4. SEM images of silver nanoparticles obtained using (a) Zinc chloride - Glucose BDES (b) Zinc chloride – Fructose BDES**

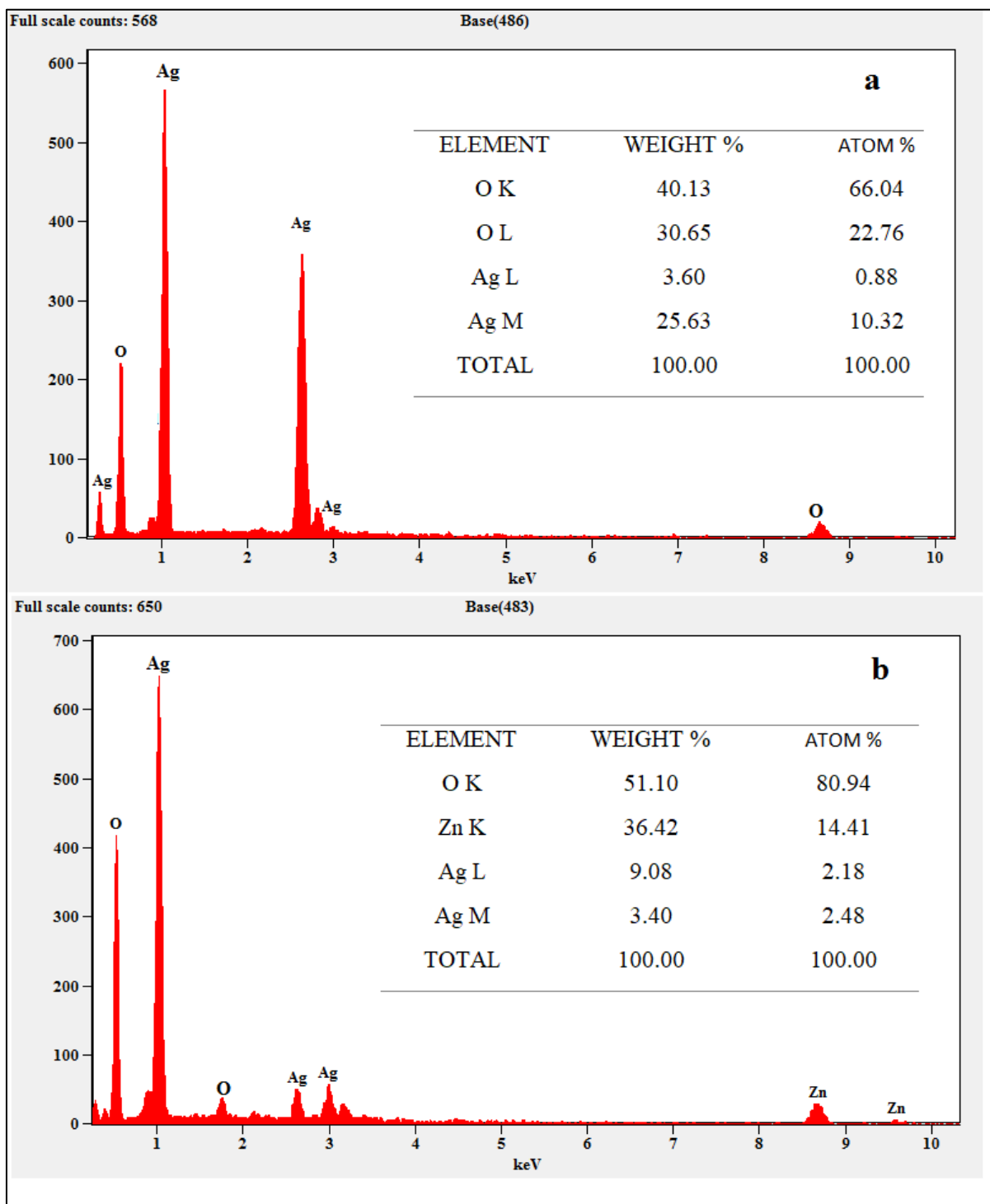


**Figure 9.6.5. EDAX spectra of silver nanoparticles obtained using (a) Zinc chloride - Glucose BDES (b) Zinc chloride – Fructose BDES**





## **10. Synthesis and characterization of nanoparticles using Ternary Deep Eutectic Solvents**

---

### **10.1. Introduction**

Nanotechnology is a future era in material science that develops and upgrades particle qualities like size and morphology, allowing non-materials to enter future high-quality material construction in practically all fields <sup>[1]</sup>. Nanotechnologies have been employed to create targeted medication carriers based on nanoparticles <sup>[2]</sup>. Because of their physicochemical properties, metal nanoparticles have a large specific surface area and a high fraction of surface atoms <sup>[3, 4]</sup>. Catalytic activities, optical and electrical properties, antimicrobial qualities, and magnetic properties are among them <sup>[5,6]</sup>. Because of its simplicity, solubility, inexpensive reagents, and fast reaction durations, the chemical reduction of copper (II) salts in an aqueous solution is one of the most versatile techniques <sup>[7]</sup>. Among the many metallic nanoparticles used in biomedical applications, silver nanoparticles are one of the most important and fascinating nanomaterials. Scientists and technologists are interested in developing nano silver-based disinfectant products because of the unique properties of the high antimicrobial activity of silver nanoparticles <sup>[8]</sup>.

In this work, we used chemical reduction to make copper and silver nanoparticles. FTIR, UV, SEM, XRD, and EDAX techniques to characterize the synthesized nanoparticles such as copper and silver.

### **10.2. Synthesis of copper nanoparticles in Malonic acid-sugar-amino acids based ternary deep eutectic solvents**

Copper nanoparticles were synthesized in our prepared TDES such as MA-GLU-GLY TDES, MA-FRU-GLY TDES, MA-GLU-HIS TDES, and MA-FRU-HIS TDES separately using the chemical reduction method <sup>[9]</sup>. Nanoparticles were made by combining

10 ml of 0.01M Copper sulfate pentahydrate [CuSO<sub>4</sub>.5H<sub>2</sub>O] with 15 ml of all TDESs in four separate beakers and stirring for 30 minutes at 1200 RPM with a magnetic stirrer. During vigorous stirring, about 8-10 ml of 0.01 M Hydrazine Hydrate as a reducing agent was added drop by drop, followed by 20 ml of 1 M sodium hydroxide as a stabilizing agent was injected slowly into the mixture. The obtained copper oxide nanoparticles in the beakers were centrifuged, rinsed with deionized water, then methanol, and dried separately.

### **10.3. Synthesis of silver nanoparticles in Malonic acid-sugar-amino acids based ternary deep eutectic solvents**

Silver nanoparticles were synthesized in our prepared TDES such as MA-GLU-GLUT TDES, and MA-FRU-GLUT TDES separately using the chemical reduction method<sup>[9]</sup>. Nanoparticles were made by combining 10 ml of 0.01M silver nitrate [AgNO<sub>3</sub>] with 15 ml of the above-mentioned two TDESs in two separate beakers and stirring for 30 minutes at 1200 RPM with a magnetic stirrer. During vigorous stirring, about 8-10 ml of 0.01 M sodium borohydride as a reducing agent was added drop by drop, followed by 20 ml of 1 M sodium hydroxide as a stabilizing agent was injected slowly into the mixture. The obtained silver oxide nanoparticles in the beakers were centrifuged, rinsed with deionized water, then methanol, and dried separately.

### **10.4 Synthesis of silver nanoparticles in Zinc chloride-sugar-amino acids based ternary deep eutectic solvents**

Silver nanoparticles were made by mixing 10 ml of 0.01 M silver nitrate [AgNO<sub>3</sub>] with 15 ml of ZC-GLU-GLUT TDES, MA-FRU-GLUT TDES, ZC-GLU-GLY TDES, MA-FRU-GLY TDES, ZC-GLU-HIS TDES, MA-FRU-HIS TDES in separate six beakers using the chemical reduction method<sup>[3]</sup> and stirring at 1200 RPM for 30 minutes with a magnetic stirrer. The reducing agent, 0.01 M sodium borohydride (about 8–10 ml) was added drop by drop under vigorous stirring, and a further 20 ml of stabilizing agent, 1 M

sodium hydroxide was injected drop by drop using an injector. The silver oxide nanoparticles were centrifuged, then washed with deionized water, methanol, and finally dried.

### **10.5. Synthesis of copper nanoparticles in Manganese chloride-sugar-amino acids based ternary deep eutectic solvents**

Copper nanoparticles were synthesized in our prepared TDES such as MC-GLU-GLY TDES, MC-FRU-GLY TDES, MC-GLU-HIS TDES, MC-FRU-HIS TDES, MC-GLU-GLUT TDES, and MC-FRU-GLUT TDES separately using the chemical reduction method <sup>[9]</sup>. Nanoparticles were made by combining 10 ml of 0.01M Copper chloride dihydrate [ $\text{CuCl}_2 \cdot 2\text{H}_2\text{O}$ ] (for glucose-based TDESs) and Copper acetate monohydrate [ $\text{Cu}(\text{COOCH}_3)_2 \cdot \text{H}_2\text{O}$ ] (for fructose-based TDESs), with 15 ml of all TDESs in six separate beakers and stirring for 30 minutes at 1200 RPM with a magnetic stirrer. During vigorous stirring, about 8-10 ml of 0.01 M Hydrazine Hydrate as a reducing agent was added drop by drop, followed by 20 ml of 1 M sodium hydroxide as a stabilizing agent was injected slowly into the mixture. The obtained copper oxide nanoparticles in the beakers were centrifuged, rinsed with deionized water, then methanol, and dried separately.

### **10.6. Results and discussion**

The synthesized copper, silver nanoparticles were characterized by UV-Visible spectroscopy, Fourier transform infrared spectroscopy, Scanning electron microscopy, X-Ray diffraction pattern, and Energy dispersive X-ray analysis.

#### **10.6.1 Characterization studies of copper nanoparticles in malonic acid-sugar-amino acids based ternary deep eutectic solvents**

##### **10.6.1.1 UV-Visible spectra of copper oxide nanoparticles**

UV-Visible absorption spectra of copper oxide nanoparticles in ethanolic solution are shown in figure 10.1.1. The characteristic absorption peak was assigned at 398 nm and

399 nm for the copper oxide nanoparticles obtained in MA-GLU-GLY (Fig. 10.1.1a) and MA-FRU-GLY (Fig. 10.1.1 b) DES respectively <sup>[10]</sup>. The characteristic absorption peak was assigned at 397 nm and 398 nm for the copper oxide nanoparticles obtained in MA-GLU-HIS (Fig. 10.1.1c) and MA-FRU-HIS (Fig. 10.1.1d) DES respectively <sup>[10]</sup>. So, it is concluded that copper nanoparticles were formed in malonic acid-based ternary DES.

#### **10.6.1.2 FTIR spectra of copper oxide nanoparticles**

The FTIR spectra in the range of 4000 to 400  $\text{cm}^{-1}$  for copper oxide nanoparticles prepared from MA-GLU-GLY, MA-FRU-GLY, MA-GLU-HIS, and MA-FRU-HIS are reported in “a”, “b”, “c”, and “d” of figure 10.1.2 respectively. The several peaks noticed in the range of 400 to 850  $\text{cm}^{-1}$  are correlated to Cu – O vibrations of CuO nanoparticles <sup>[11]</sup>. The sharp peak observed around 600  $\text{cm}^{-1}$  of all the spectra clearly indicated the Cu – O stretching <sup>[12]</sup>. Here a few of the malonic acid molecules are capped on the surface of CuO nanoparticles. The peaks around 1300 – 1000  $\text{cm}^{-1}$  correspond to the C – O stretching of the carboxylic acid group in figure 10.1.2. The peaks due to  $\text{CH}_2$  deformations of malonic acid are seen around 1385  $\text{cm}^{-1}$  in all spectra. The peaks noticed at 1627.71  $\text{cm}^{-1}$ , 1603.01  $\text{cm}^{-1}$ , 1629.94  $\text{cm}^{-1}$  denoted the O – H bending of malonic acid in the figure 10.1.2 “a, c, d” spectra. The peaks were observed at 2852.26  $\text{cm}^{-1}$ , 2850.57  $\text{cm}^{-1}$ , 2925.02  $\text{cm}^{-1}$ , and 2850.19  $\text{cm}^{-1}$  are due to C – O asymmetric stretching <sup>[12]</sup>. Further, the broad peaks seen around 3400  $\text{cm}^{-1}$  in all the spectra are due to different vibrations modes of water molecules adsorbed on the surface of copper oxide nanoparticles <sup>[11]</sup>.

#### **10.6.1.3 XRD patterns of copper oxide nanoparticles**

The powder x-ray diffraction patterns of copper oxide nanoparticles prepared from the deep eutectic solvents, MA-GLU-GLY, MA-FRU-GLY, MA-GLU-HIS, and MA-FRU-HIS are given in “a, b, c, d” of figure 10.1.3 respectively. The XRD patterns give information about the grain size, structure, and phase cleanliness of the materials. In the

case of CuO particle obtained in MA-GLU-GLY TDES, the diffraction peaks noticed at 42.9°, 50.2°, and 73.9° are indexed as (111), (200), and (220) respectively. The diffraction peaks seen at 42.9°, 50.2°, and 73.8° are also indexed as (111), (200), and (220) respectively for the CuO particles prepared using the MA-FRU-GLY TDES. This indexing corresponds to the fcc structure of CuO and the peaks are matching well with JCPDC card no:04-0836 [13]. The diffraction peaks seen at 37.7°, 40.6°, 54.8°, and 69.56° are also indexed as (111), (200), (211) and (301) respectively for the CuO particles prepared using the MA-FRU-HIS TDES. The diffraction peaks seen at 32.7°, 47.4°, 59.2°, and 68.2° are also indexed as (034), (404), (440) and (183) respectively for the CuO particles prepared using the MA-FRU-HIS TDES. This indexing corresponds to the orthorhombic structure of CuO [11]. The observed peaks are matching well with the JCPDC Card No. 77-1898. The grain size of CuO nanoparticles is determined by using the Debye–Scherer formula,

$$D = k \lambda / \beta \cos \theta$$

where D denotes the grain size, K refers to a constant,  $\lambda$  refers to the wavelength of X-ray used,  $\beta$  denotes the fullwidth half-maximum of the diffraction peaks and  $\theta$  is the angle of the diffraction [11]. By using this formula, the average grain size of CuO nanoparticles prepared from the TDES of MA-GLU-GLY and MA-FRU-GLY are found to be 15.454 nm. Similarly, the average grain size of CuO nanoparticles prepared using the TDES of MA-GLU-HIS and MA-FRU-HIS are determined to be 22.15 nm and 10.4 nm respectively.

#### **10.6.1.4 Morphological analysis of copper oxide nanoparticles by SEM**

The surface morphology and particle size of the CuO nanoparticles prepared using the BDESs have been analyzed by scanning electron microscope [10]. In figure 10.1.4.1, the SEM images of copper oxide nanoparticles prepared using MA-GLU-GLY TDES are labelled as “a” and “b” while the CuO nanoparticles obtained from the MA-FRU-GLY

TDES are labelled as “c” and “d”. In figure 10.1.4.2, the SEM images of copper oxide nanoparticles prepared using MA-GLU-HIS TDES are labelled as “e” and “f” while the CuO nanoparticles obtained from the MA-FRU-HIS TDES are labelled as “g” and “h”. The morphology of CuO nanoparticles seems to be clusters of grains with an average diameter of 121.3 nm in the case of particles obtained from MA-GLU-GLY TDES and in MA-FRU-GLY TDES seems to be scale like structure with an average diameter of 113.85nm. The CuO nanoparticles obtained in MA-GLU-HIS and MA-FRU TDES look like a trigonal beads-like morphology and worm like morphology with an average diameter of 245.5 nm and 98.67nm respectively.

#### **10.6.1.5 Energy Dispersive X-ray Analysis**

The elemental composition of the CuO nanoparticles was carried out by energy dispersive x-ray analysis (EDAX) spectroscopy<sup>[14]</sup>. In figure 10.1.5 a, it is given the EDAX spectrum of copper oxide nanoparticles synthesized using the DES of MA-GLU-GLY TDES whereas the EDAX spectrum of CuO nanoparticles prepared using the DES of MA-FRU-GLY TDES is denoted in figure 10.1.5 b. In figure 10.1.5c, it is given the EDAX spectrum of copper oxide nanoparticles synthesized using the DES of MA-GLU-HIS TDES whereas the EDAX spectrum of CuO nanoparticles prepared using the DES of MA-FRU-HIS TDES is denoted in figure 10.1.5 d. In figure 10.1.5 a, it is shown that the atomic percentage of Cu is 66.62 and O is 33.38, which revealed that pure CuO nanoparticles are formed in MA-GLU-GLY TDES. But in figure 10.1.5 b, it has been noticed that the atomic percentage of Cu, O, and C are 17.51, 16.97, and 65.52 respectively. In figure.10.1.5 c, the atomic percentage of Cu, N, O, and C is 30.89, 35.36, 32.45, and 1.30. In figure. 10.1.5 d, the atomic percentage of Cu, N, O, and C is 30.89, 35.36, 32.45, and 1.30. It is confirmed that the atmospheric nitrogen and the carbon atoms of malonic acid are capped on the CuO nanoparticles obtained in MA-GLU-HIS and MA-FRU-HIS TDES.

## **10.6.2 Characterization studies of silver nanoparticles in malonic acid-sugar-amino acids based ternary deep eutectic solvents**

### **10.6.2.1 UV-Visible spectra of silver oxide nanoparticles**

UV-Visible absorption spectra of silver nanoparticles in ethanolic solution are shown in figure 10.2.1. The characteristic absorption peak of the silver metal was observed between 461 and 467 nm were assigned for silver nanoparticles obtained in MA-GLU-GLUT and MA-FRU-GLUT ternary deep eutectic solvents respectively [15, 16].

### **10.6.2.2 FTIR spectra of silver oxide nanoparticles**

Silver nanoparticles generated from Malonic Acid-Glucose-Glutamine and Malonic Acid-Fructose-Glutamine TDESs had FTIR spectra in the region of 4000 to 400  $\text{cm}^{-1}$ , as shown in Fig. 10.2.2. The spectrum shows different peaks at 3431.57  $\text{cm}^{-1}$ - N-H stretching; 2921.68  $\text{cm}^{-1}$ - O-H stretching; 2851.67  $\text{cm}^{-1}$ - aldehydic C-H stretching of glucose; 1596.55  $\text{cm}^{-1}$ - C-C stretching; the peaks found at 1383  $\text{cm}^{-1}$  are due to the silver nanoparticles in case of MA-GLU-GLUT TDES. The spectrum shows different peaks at 3430.29  $\text{cm}^{-1}$ - N-H stretching; 2922.23  $\text{cm}^{-1}$ - O-H stretching; 2851.62  $\text{cm}^{-1}$ - aldehydic C-H stretching of glucose; 1595.85  $\text{cm}^{-1}$ - C-C stretching; 1383.95  $\text{cm}^{-1}$  are due to silver nanoparticles. There are some prominent peaks in the fingerprint region [17, 18, 19, 20, 21].

### **10.6.2.3 XRD patterns of silver oxide nanoparticles**

The crystalline structure of silver nanoparticles are predicted using X-Ray Diffraction analysis, which showed intense peaks at  $2\theta$  values of 37.69°, 43.85°, 64.15°, 77.16° in case of silver nanoparticles obtained in MA-FRU-GLUT TDES( Fig.10.2.3 a) and at 37.78°, 43.95°, 64.12°, 77.11° in case of silver nanoparticles obtained in MA-GLUU-GLUT TDES (Fig.10.2.3 b), both which indexed at planes (111), (200), (220), (311) of silver respectively [22]. The structure of the obtained nanoparticles is crystalline in nature, and it is face centered cubic in both cases. The observed peaks are matching well

with JCPDC Card No. 89-3722. The Debye–Scherrer equation was used to calculate the average crystallographic size of silver nanoparticles,  $D=0.9\lambda/\beta\cos\theta$ . The average particle size obtained is calculated to be 30nm by measuring the breadth of (111) Bragg's reflection in both solvents [23].

#### **10.6.2.4 Morphological analysis of silver oxide nanoparticles by SEM**

To examine the morphological structure and particle size of silver nanoparticles, Scanning Electron Microscopy was used. In Fig.10.2.4, the SEM images of the obtained silver nanoparticles prepared using MA-GLU-GLUT TDES are labeled as "a" and "b" while the silver nanoparticles obtained from MA-FRU-GLUT TDES are labeled as "c" and "d". The morphology of silver nanoparticles seems to be sponge like structure with an average diameter of 83.05nm in the case of particles obtained from MA-GLU-GLUT TDES and it seems to grain shaped with an average diameter of 97.85nm in the case of particles obtained from MA-FRU-GLUT TDES.

#### **10.6.2.5 Energy Dispersive X-ray Analysis**

The elemental composition and the purity of the obtained silver nanoparticles are confirmed by Energy Dispersive X-ray Analysis. EDAX spectrum reveals strong signal in the silver region and silver nanoparticles formation were confirmed. Metallic silver nanoparticles generally show optical absorption peak approximately at 3 KeV [24] due to surface plasmon resonance. The percent composition of silver is high in MA-FRU-GLUT TDES as compared to MA-GLU-GLUT TDES. Silver (80.12%) was the major constituent element and oxygen (19.06%) as shown in Fig.10.2.5b. In MA-GLU-GLUT TDES, the silver composition is low (19.59%) and oxygen is high (66.68%) as shown in Fig.10.2.5a. some impurities are acting as capping agents of silver nanoparticles [25].



### **10.6.3 Characterization studies of silver nanoparticles in zinc chloride-sugar-amino acids based ternary deep eutectic solvents**

#### **10.6.3.1 UV-Visible spectra of silver oxide nanoparticles**

UV-Visible absorption spectra of silver nanoparticles in ethanolic solution are shown in figure 10.3.1. The reduction of silver ions present in the solution of silver nitrate with TDESs was observed using UV-Visible spectroscopy with wavelengths ranging from 200 to 800nm. The UV-Visible spectra show surface plasmon resonance peaks around 397-432nm<sup>[26, 27]</sup> of silver nanoparticles synthesized in ZC-GLU-GLY, ZC-FRU-GLY and ZC-GLU-GLUT TDESs. The silver nanoparticles obtained in ZC-FRU-GLUT, ZC-GLU-HIS, and ZC-FRU-HIS TDESs show peak at 273nm, 296nm and 297nm respectively.

#### **10.6.3.2 FTIR spectra of silver oxide nanoparticles**

Figure 10.3.2 shows the FTIR spectra of silver nanoparticles generated in all ZC based TDESs. The hydroxyl and amine stretching vibrations in the TDESs cause peaks spanning from 3200 to 3600cm<sup>-1</sup><sup>[12]</sup>. C-H stretching is responsible for the peaks about 2920- 2930 cm<sup>-1</sup>. N-H bending from TDESs is represented by the peaks around 1600 cm<sup>-1</sup><sup>[21]</sup>. The C-O stretching of the alcohol group of solvents causes peaks about 1100cm<sup>-1</sup>. In all solvents, the silver nanoparticles show peaks around 1383cm<sup>-1</sup><sup>[28]</sup>, and peaks around 577cm<sup>-1</sup><sup>[29]</sup> are caused by Ag-O vibrations because the nanoparticles are covered by oxygen.

#### **10.6.3.3 XRD patterns of silver oxide nanoparticles**

The crystalline structure of silver nanoparticles are predicted using X-Ray Diffraction analysis, which showed intense peaks at 2θ values of 32.02°, 46.02°, 54.34°, 67.07°, 76.67° in case of silver nanoparticles obtained in ZC-GLU-GLY TDES( Fig.10.3.3 a), at 32.02°, 46.02°, 54.34°, 77.06° in case of silver nanoparticles obtained in ZC-FRU-GLY TDES (Fig.10.3.3b), at 31.73°, 45.73°, 54.54°, 76.37° in case of silver nanoparticles

obtained in ZC-GLU-GLUT TDES (Fig.10.3.3c), at 32.02°, 46.02° in case of silver nanoparticles obtained in ZC-FRU-GLUT TDES (Fig.10.3.3d), at 32.02°, 46.02°, 54.34°, 77.18° in case of silver nanoparticles obtained in ZC-GLU-HIS TDES (Fig.10.3.3e), at 31.73°, 45.73°, 54.54°, 75.98° in case of silver nanoparticles obtained in ZC-FRU-HIS TDES (Fig.10.3.3f). This was also evident in many studies when the XRD pattern included the relevant 2° range [30, 31]. The silver nanoparticles indexed at planes (111), (200), (220), (311) which are like JCPDS file no.89-3722 [22]. The structure of the obtained nanoparticles is crystalline in nature, and it is face-centered cubic in all cases. The Debye–Scherrer equation was used to calculate the average crystallographic size of silver nanoparticles,  $D=0.9\lambda/\beta\cos\theta$ . The average particle size obtained is calculated to be 30nm by measuring the breadth of (111) Bragg's reflection in all solvents [23].

#### **10.6.3.4 Morphological analysis of silver oxide nanoparticles by SEM**

To examine the morphological structure and particle size of silver nanoparticles, Scanning Electron Microscopy was used. In Fig.10.3.4.1, the SEM images of the obtained silver nanoparticles prepared using ZC-GLU-GLY TDES are labeled as "a" and "b" while the silver nanoparticles obtained from ZC-FRU-GLY TDES are labeled as "c" and "d". In Fig.10.3.4.2, the SEM images of the obtained silver nanoparticles prepared using ZC-GLU-GLUT TDES are labeled as "a" and "b" while the silver nanoparticles obtained from ZC-FRU-GLUT TDES are labeled as "c" and "d". In Fig.10.3.4.3, the SEM images of the obtained silver nanoparticles prepared using ZC-GLU-HIS TDES are labeled as "a" and "b" while the silver nanoparticles obtained from ZC-FRU-HIS TDES are labeled as "c" and "d". The morphology of silver nanoparticles seems to be spherical shape with an average diameter of 189 nm in the case of particles obtained from ZC-GLU-GLY TDES and it seems to disc shaped with an average diameter of 226 nm in the case of particles obtained from ZC-FRU-GLY TDES. Likewise, the morphology of silver nanoparticles obtained

from ZC-GLU-GLUT TDES and ZC-FRU-GLUT TDES seem to be irregular in shape, clavor shape with an average diameter of 150nm and 192 nm respectively. The morphology of silver nanoparticles seems to be irregular shaped with an average diameter of 99.64 nm and triangular prism like structure with an average diameter of 58.48 nm in case of ZC-GLU-HIS and ZC-FRU-HIS TDESs respectively.

#### **10.6.3.5 Energy Dispersive X-ray Analysis**

The elemental composition and the purity of the obtained silver nanoparticles are confirmed by Energy Dispersive X-ray Analysis. EDAX spectrum in figure. 10.3.5 reveals strong signal in the silver region and silver nanoparticles formation were confirmed. Metallic silver nanoparticles generally show optical absorption peak approximately at 3 KeV <sup>[24]</sup> due to surface plasmon resonance. The atomic percentage of Ag, Cl, O is 35.74, 32.32, 31.94 in case of silver nanoparticles obtained from ZC-GLU-GLY TDES. The atomic percentage of Ag, Cl, O and C is 16.14, 15.28, 12.63, and 55.95 in case of silver nanoparticles obtained from ZC-FRU-GLY TDES. The atomic percentage of Ag, Cl, O and Zn is 16.36, 32.15, 38.93, and 12.56 in case of silver nanoparticles obtained from ZC-GLU-GLUT TDES. The atomic percentage of Ag, Cl, O, C, and Zn is 1.81, 9.82, 29.34, 49.94, and 9.10 in case of silver nanoparticles obtained from ZC-FRU-GLUT TDES. The atomic percentage of Ag, Cl, O and Zn is 4.02, 11.45, 75.81, and 8.72 in case of silver nanoparticles obtained from ZC-GLU-HIS TDES. The atomic percentage of Ag, Cl, O and Zn is 3.25, 11.09, 76.80, and 8.87 in case of silver nanoparticles obtained from ZC-FRU-HIS TDES. The silver nanoparticles were capped by some atmospheric elements such as carbon, oxygen and by the TDESs <sup>[25]</sup>.

## **10.6.4 Characterization studies of copper nanoparticles in manganese chloride-sugar-amino acids based ternary deep eutectic solvents**

### **10.6.4.1 UV-Visible spectra of copper oxide nanoparticles**

UV-Visible absorption spectra of copper oxide nanoparticles in ethanolic solution are shown in figure 10.4.1. The characteristic absorption peak was assigned at 236 nm and 393 nm for the copper oxide nanoparticles obtained in MC-GLU-GLY (Fig. 10.4.1a) and MC-FRU-GLY (Fig. 10.4.1 b) DES respectively <sup>[10]</sup>. The characteristic absorption peak was assigned at 547 nm and 360 nm for the copper oxide nanoparticles obtained in MC-GLU-GLUT (Fig. 10.4.1c) and MC-FRU-GLUT (Fig. 10.4.1d) TDES respectively <sup>[10]</sup>. The copper oxide nanoparticles show an absorption peak at 397nm in the case of Cu NPs obtained from MC-GLU-HIS TDES.

### **10.6.4.2 FTIR spectra of copper oxide nanoparticles**

The FTIR spectra in the range of 4000 to 400  $\text{cm}^{-1}$  for copper oxide nanoparticles prepared from MC-GLU-GLY, MC-FRU-GLY, MC-GLU-GLUT, MC-FRU-GLUT, and MA-FRU-HIS are reported in “a”, “b”, “c”, “d” and “e” of figure 10.4.2 respectively. The several peaks noticed in the range of 400 to 850  $\text{cm}^{-1}$  are correlated to Cu – O vibrations of CuO nanoparticles <sup>[11]</sup>. The sharp peak observed around 700  $\text{cm}^{-1}$  of all the spectra clearly indicated the Cu – O stretching <sup>[12]</sup>. Here a few of the malonic acid molecules are capped on the surface of CuO nanoparticles. The peaks around 1300 – 1000  $\text{cm}^{-1}$  correspond to the C – O stretching of the carboxylic acid group in figure 10.4.2. The peaks due to  $\text{CH}_2$  deformations of malonic acid are seen around 1385  $\text{cm}^{-1}$  in all spectra. The peaks noticed at 1614.20  $\text{cm}^{-1}$ , 1603.25  $\text{cm}^{-1}$ , 1611.44  $\text{cm}^{-1}$ , 1619  $\text{cm}^{-1}$ , 1602.23  $\text{cm}^{-1}$  denoted the O – H bending of malonic acid. The peaks were observed at 2926.10  $\text{cm}^{-1}$ , 2922.38  $\text{cm}^{-1}$ , 2937.62  $\text{cm}^{-1}$  are due to C – O asymmetric stretching <sup>[12]</sup>. Further, the broad peaks seen around 3400

cm<sup>-1</sup> in all the spectra are due to different vibrations modes of water molecules adsorbed on the surface of copper oxide nanoparticles <sup>[11]</sup>.

#### 10.6.4.3 XRD patterns of copper oxide nanoparticles

The powder x-ray diffraction patterns of copper oxide nanoparticles prepared from the deep eutectic solvents, MC-GLU- GLY, MC-FRU-GLY, MC-GLU-GLUT, MC-FRU-GLUT and MC-GLU-HIS are given in “a, b, c, d, e” of figure 10.4.3 respectively. The XRD patterns give information about the grain size, structure, and phase cleanliness of the materials. In the case of CuO particle obtained in MC-GLU-GLY TDES, the diffraction peaks noticed at 42.91°, 49.72°. The diffraction peaks seen at 43.87°, 53.17° for the CuO particles prepared using the MC-FRU- GLY TDES. This indexing corresponds to the fcc structure of CuO and the peaks are matching well with JCPDC card no:04-0836 <sup>[13]</sup>. The diffraction peaks are seen at 37.7°, 40.6°, 54.8°, and 69.56° are also indexed as (111), (200), (211) and (301) respectively for the CuO particles prepared using the MA-GLU- GLUT TDES. The diffraction peaks are seen at 31.87°, 52.29°, are also indexed as (034), (440) for the CuO particles prepared using the MA-FRU-GLUT TDES. The diffraction peaks are seen at 44.83°, 50.46°, 65.14°. This indexing corresponds to the orthorhombic structure of CuO <sup>[11]</sup>. The observed peaks are matching well with the JCPDC Card No. 77- 1898. The grain size of CuO nanoparticles is determined by using the Debye–Scherer formula,

$$D = k \lambda / \beta \cos \theta$$

where D denotes the grain size, K refers to a constant, λ refers to the wavelength of X-ray used, β denotes the fullwidth half-maximum of the diffraction peaks and θ is the angle of the diffraction <sup>[11]</sup>. By using this formula, the average grain size of CuO nanoparticles prepared from the MC based TDES are determined to be 20nm.

#### **10.6.4.4 Morphological analysis of copper oxide nanoparticles by SEM**

The surface morphology and particle size of the CuO nanoparticles prepared using the BDESs have been analyzed by scanning electron microscope <sup>[10]</sup>. In figure 10.4.4.1, the SEM images of copper oxide nanoparticles prepared using MC-GLU-GLY TDES are labelled as “a” and “b” while the CuO nanoparticles obtained from the MC-FRU-GLY TDES are labelled as “c” and “d”. In figure 10.4.4.2, the SEM images of copper oxide nanoparticles prepared using MC-GLU-GLUT TDES are labelled as “a” and “b” while the CuO nanoparticles obtained from the MC-FRU-GLUT TDES are labelled as “c” and “d”. In figure 10.4.4.3, the SEM images of copper oxide nanoparticles prepared using MC-GLU-HIS TDES are labelled as “a” and “b”. The morphology of CuO nanoparticles seems to be rod shaped with an average diameter of 115.3 nm in the case of particles obtained from MC-GLU-GLY TDES and in MC-FRU-GLY TDES seems to be spherical shaped with an average diameter of 123.65nm. The CuO nanoparticles obtained in MC-GLU-GLUT and MC-FRU-GLUT TDES look like leaves-like morphology and cylindrical shaped morphology with an average diameter of 150.5 nm and 108.27nm respectively. The CuO nanoparticles obtained in MC-GLU-HIS TDES look like disc shaped morphology with an average diameter of 198.26nm.

#### **10.6.4.5 Energy Dispersive X-ray Analysis**

The elemental composition of the CuO nanoparticles was carried out by energy dispersive x-ray analysis (EDAX) spectroscopy <sup>[14]</sup>. In figure 10.4.5 a, it is given the EDAX spectrum of copper oxide nanoparticles synthesized using the DES of MC-GLU-GLY TDES whereas the EDAX spectrum of CuO nanoparticles prepared using the DES of MC-FRU-GLY TDES is denoted in figure 10.5.5 b. In figure 10.5.5c, it is given the EDAX spectrum of copper oxide nanoparticles synthesized using the DES of MC-GLU-GLUT whereas the EDAX spectrum of CuO nanoparticles prepared using the DES of MC-FRU-

GLUT TDES is denoted in figure 10.5.5 d. In figure 10.5.5e, it is given the EDAX spectrum of copper oxide nanoparticles synthesized using the DES of MC-GLU-HIS. In figure 10.5.5 a, it is shown that the atomic percentage of Cu is 66.62, O is 33.38, Mn is 6.57, and Cl is 20.25. In figure 10.5.5 b, it has been noticed that the atomic percentage of Cu, O, Cl, and C are 17.20, 79.65, 2.87, and 0.28 respectively. In figure.10.5.5 c, the atomic percentage of Cu, Mn, O, and C is 17.90, 5.47, 59.73, and 16.90. In figure. 10.5.5 d, the atomic percentage of Cu, Mn, O, and Cl is 10.80, 16.50, 70.07, and 2.63. In figure. 10.5.5 e, the atomic percentage of Cu, Mn, O, and Cl is 6.56, 20.01, 70.85, and 2.58. It is confirmed that the atmospheric oxygen and the carbon atoms of malonic acid and the solvents are capped on the CuO nanoparticles obtained in MC-based TDES [25].

## **10.7. Conclusion**

Seventeen types of nanoparticles were synthesized successfully using malonic acid, zinc chloride and manganese chloride-based ternary deep eutectic solvents. The copper and silver nanoparticles were characterized by techniques such as UV spectroscopy, FTIR spectroscopy, X-Ray diffraction, Scanning Electron Microscopy, and Energy Dispersive X-ray Analysis. The copper nanoparticle synthesized from MC-FRU-HIS TDES was sticky in nature. The nanoparticles were synthesised in a simple and convenient manner. There was no surfactant and seed were needed for the formation of nanoparticles. The size of the particles formed was controlled by varying proportions of the water present in the TDESs.

## References

- [1]. Kaviya S, Viswanathan B. "Green synthesis of silver nanoparticles using *Polyalthia longifolia* leaf extract along with D-sorbitol". *Journal of nanotechnology*. 2011;1-5.
- [2]. Falanga, A, Vitiello M.T., Cantisani M, Tarallo R, Guarnieri D, Mignogna E, Netti, P, Pedone C, Galdiero M, Galdiero S. "A peptide derived from herpes simplex virus type 1 glycoprotein H: Membrane translocation and applications to the delivery of quantum dots". *Nanomedicine*. 2011; 10(1016)4-9.
- [3]. Catauro M, R.M., De Gaetano FD, Marotta A. "sol-gel processing of drug delivery materials and release kinetics". *J Mater Sci Mater Med*. 2005; 16(3):261-265.
- [4]. Crabtree JH, B.R, Siddiqi RA, Huen IT, Handott LL, Fishman A. "The efficacy of silver-ion implanted catheters in reducing peritoneal dialysis-related infections". *Perit Dial Int*. 2003; 23(4):368-374.
- [5]. Krolikowska A, Michota A, Bukowska J, "SERS studies on the structure of thioglycolic acid monolayers on silver and gold". *Surf Sci*. 2003; 532:227-232.
- [6]. Zhao G, S.J., "Multiple parameters for the comprehensive evaluation of the susceptibility of *Escherichia coli* to the silver ion". *Biometals*. 1998; 11:27.
- [7]. M. Abdulla-Al-Mamun, Y. Kusumoto, and M. Muruganandham, "Simple new synthesis of copper nanoparticles in water/acetonitrile mixed solvent and their characterization," *Materials Letters*, vol. 63, no. 23, pp. 2007–2009, 2009.
- [8]. Quang Huy Tran et al, silver nanoparticles: synthesis, properties, toxicology, applications and perspectives, *Adv. Nat. Sci: Nanosci. Nanotechnol*. 4 033001, 2013.
- [9]. Shikha Jain, Ankita Jain, Vijay Devra, Copper nanoparticles catalyzed oxidation of threonine by peroxomonosulfate, *Journal of Saudi chemical society* 18 (2014), 149 - 153.
- [10]. Tariq Jan, J. Iqbal, Umar Farooq, Asma Gul, Rashda Abbasi, Ishaq Ahmad, Maaza Malik, Structural, Raman and optical characteristics of Sn doped CuO nanostructures: A



novel anticancer agent, *Ceramics International*, 41(10), Part A December 2015, 13074 – 79. <http://dx.doi.org/10.1016/j.ceramint.2015.06.080>

[11]. A. Rita, A. Sivakumar, S. A. Martin Britto Dhas, Influence of shock waves on structural and morphological properties of copper oxide NPs for aerospace applications, *Journal of Nanostructure in Chemistry*, 9 (2019), 225 – 230. <https://doi.org/10.1007/s40097-019-00313-0>

[12]. Donald L. Pavia, Gary M. Lampman, George S. Kriz, *Introduction to Spectroscopy*, 3rd Edition, BROOKS/COLE, Thomson Learning, USA, 2001

[13]. Raja, Mohan, Subha, J., Ali, Fathilah Binti, and Ryu, Sung Hun (2008)'Synthesis of Copper Nanoparticles by Electroreduction Process', *Materials and Manufacturing Processes*,23:8,782 — 785

[14]. R. Das, S.S. Nath, D. Chakdar, G. Gope, R.J. Bhattacharjee, *Nanotechnol.* 5 (2009) 1–6.

[15]. Rabab M. Elamawi, Raida E. Al-Harbi &Awatif A. Hendi, Biosynthesis and characterization of silver nanoparticles using *Trichoderma longibrachiatum* and their effect on phytopathogenic fungi, *Egyptian Journal of Biological Pest Control*, 28, 28 (2018)

[16]. François Eya'ane Meva, Marcelle Loretta Segnou, Cecile Okalla Ebongue, Agnes Antoinette Ntumba, Philippe Belle Ebanda Kedi, Vandi Deli, Marie-Annie Etoh, Emmanuel Mpondo Mpondo, Spectroscopic synthetic optimizations monitoring of silver nanoparticles formation from *Megaphrynium macrostachyum* leaf extract, *Brazilian J. of Pharmacognosy, Revista Brasileira de Farmacognosia*, 26, 5, (2016), 640-646

[17]. Preetha Devaraj, Prachi Kumari, Chiron Aarti, Arun Renganathan, Synthesis and Characterization of Silver Nanoparticles Using Cannonball Leaves and Their Cytotoxic Activity against MCF-7 Cell Line, *Journal of Nanotechnology*, 2013, (2013).

[18]. *Infrared Spectral Interpretation* by Brian Smith, CRC Press, 1999

- [19]. Infrared Spectroscopy: Fundamentals and Applications by Barbara Atuart, John Wiley&Sons, Ltd., 2004
- [20]. Interpretation of Infrared Spectra, A Practical Approach by John Coates in Encyclopedia of Analytical Chemistry pp. 10815-10837, John Wiley&Sons Ltd, Chichester, 2000
- [21]. Wan Khaima Azira Wan Mat Khalir, Kamyar Shameli, Seyed Davoud Jazayeri, Nor Azizi Othman, Nurfatehah Wahyuny Che Jusoh and Norazian Mohd Hassan, Biosynthesized Silver Nanoparticles by Aqueous Stem Extract of *Entada spiralis* and Screening of Their Biomedical Activity, *Front. Chem.*, (2020)
- [22]. Vivek Dhand, L. Soumya, Somayajula Bharadwaj, Shilpa Chakra; Green synthesis of silver nanoparticles using *Coffea arabica* seed extract and its antibacterial activity; *Materials Science and Engineering C* 58 (2015) 36–43
- [23]. Ajitha B, Ashok Kumar Reddy Y, Sreedhara Reddy P. Biogenic nano-scale silver particles by *Tephrosia purpurea* leaf extract and their inborn antimicrobial activity; *Spectrochim Acta Part A*; 121: (2014); 164–172
- [24]. S. Kaviya, J. Santhanalakshmi, B. Viswanathan, J. Muthumar, K. Srinivasan; Biosynthesis of silver nanoparticles using citrus *sinensis* peel extract and its antibacterial activity; *Spectrochimica Acta Part A: Molecular and Biomolecular Spectroscopy*, 79 (2011), pp. 594-598
- [25]. Abiola Grace Femi-Adepoju, Adewumi Oluwasogo Dada, Green synthesis of silver nanoparticles using terrestrial fern (*Gleichenia Pectinata* (Willd.) C. Presl.): characterization and antimicrobial studies; *PMC article; Heliyon* 5(4) :(2019) e01543.
- [26]. Michael Ndikau, Naumih M. Noah, Dickson M. Andala, Eric Masika, Green Synthesis and Characterization of Silver Nanoparticles Using *Citrullus lanatus* Fruit Rind

Extract, International Journal of Analytical Chemistry, vol. 2017, Article ID 8108504, (2017).

[27]. Anandalakshmi.K., Venugopal, J. & Ramasamy, V. Characterization of silver nanoparticles by green synthesis method using *Petalium murex* leaf extract and their antibacterial activity. *Appl Nanosci* 6, 399–408 (2016).

[28]. Pannerselvam Balashanmugam, Pudupalayam Thangavelu Kalaichelvan, Biosynthesis characterization of silver nanoparticles using *Cassia roxburghii* DC. The aqueous extract, and coated on cotton cloth for effective antibacterial activity, *Int J Nanomedicine.*; 10(Suppl 1): 87–97. (2015)

[29]. Ravichandran, V. Paluri, G. Kumar, K. Loganathan, and B. R. Kokati Venkata, A novel approach for the biosynthesis of silver oxide nanoparticles using aqueous leaf extract of *Callistemon lanceolatus* (Myrtaceae) and their therapeutic potential; *Journal of Experimental Nanoscience*, 11 ,6, 445–458, (2016).

[30]. Jeeva K, Thiyagarajan M, Elangovan V, Geetha N, Venkatachalam P (2014b) *Caesalpinia coriaria* leaf extracts mediated biosynthesis of metallic silver nanoparticles and their antibacterial activity against clinically isolated pathogens. *Ind Crops Prod* 52:714–720

[31]. Kumar V, Yadav SK (2009) Plant mediated synthesis of silver and gold nanoparticles and their applications. *J Chem Technol Biotechnol* 84:151–157.

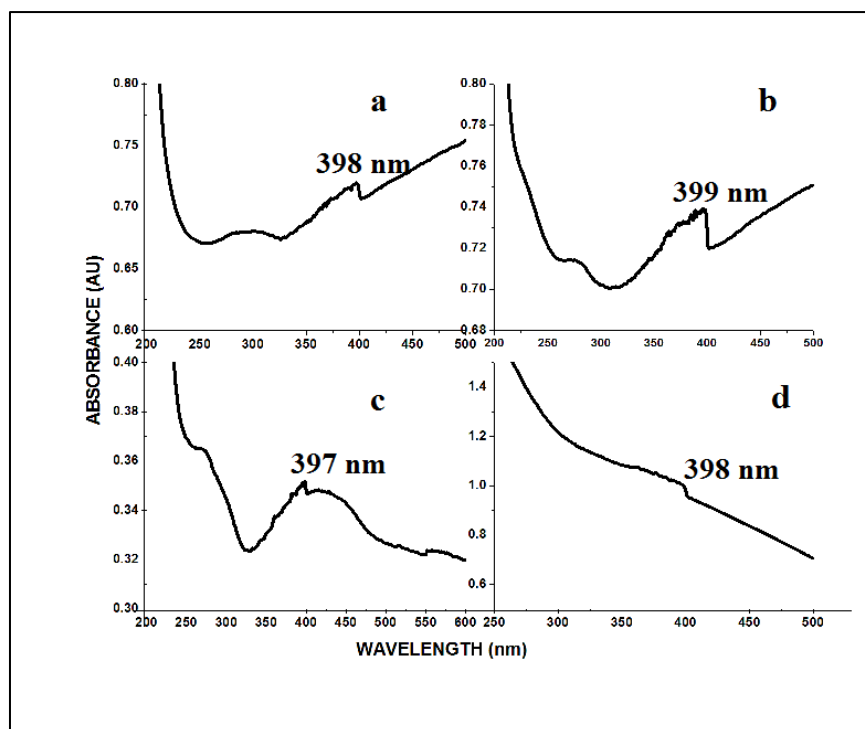


**Figure. 10.1.1.** UV-Visible spectra of copper oxide nanoparticles obtained using  
 (a) Malonic acid - Glucose – Glycine (MA – GLU - GLY) TDES  
 (b) Malonic acid – Fructose- Glycine (MA – FRU - GLY) TDES  
 (c) Malonic acid – Glucose – Histidine (MA – GLU - HIS) TDES  
 (d) Malonic acid – Fructose- Histidine (MA -FRU – HIS) TDES

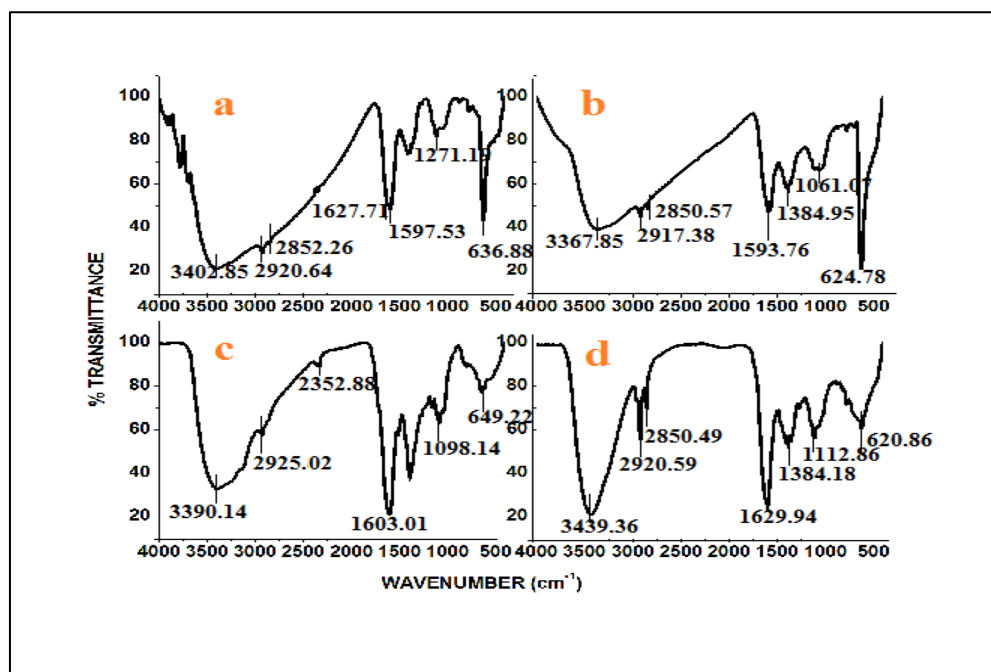


**Figure. 10.1.2.** FTIR spectra of copper oxide nanoparticles obtained using  
 (a) Malonic acid - Glucose – Glycine (MA – GLU - GLY) TDES  
 (b) Malonic acid – Fructose - Glycine (MA – FRU - GLY) TDES  
 (c) Malonic acid – Glucose – Histidine (MA – GLU - HIS) TDES  
 (d) Malonic acid – Fructose - Histidine (MA -FRU – HIS) TDES

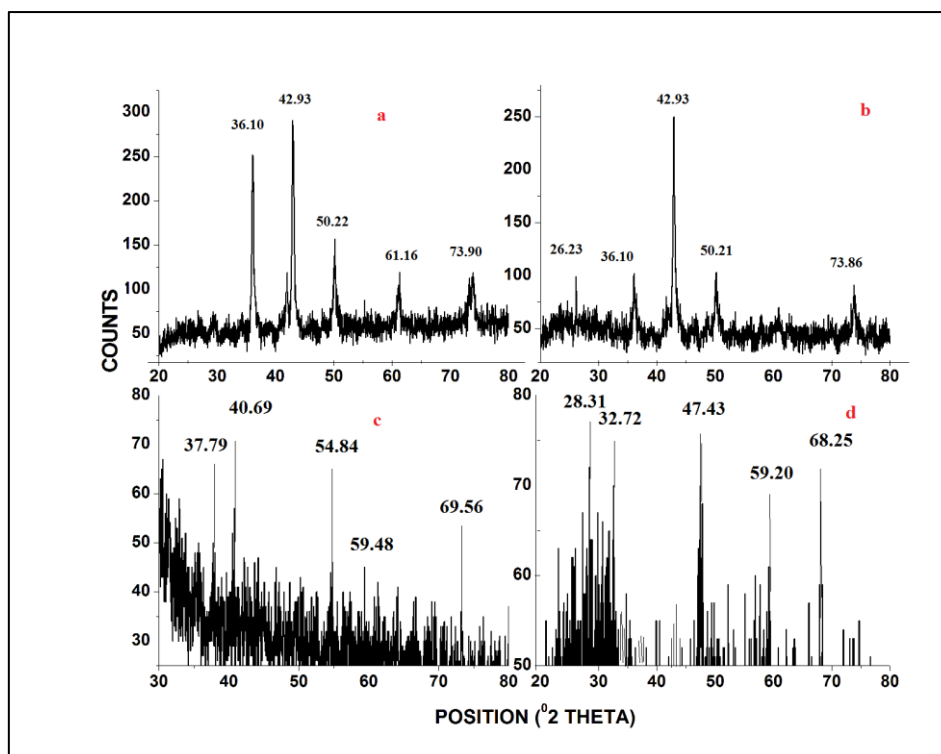


**Figure. 10.1.3. XRD patterns of copper oxide nanoparticles obtained using**  
 (a) Malonic acid - Glucose – Glycine (MA – GLU - GLY) TDES  
 (b) Malonic acid – Fructose- Glycine (MA – FRU - GLY) TDES  
 (c) Malonic acid – Glucose – Histidine (MA – GLU - HIS) TDES  
 (d) Malonic acid – Fructose- Histidine (MA -FRU – HIS) TDES

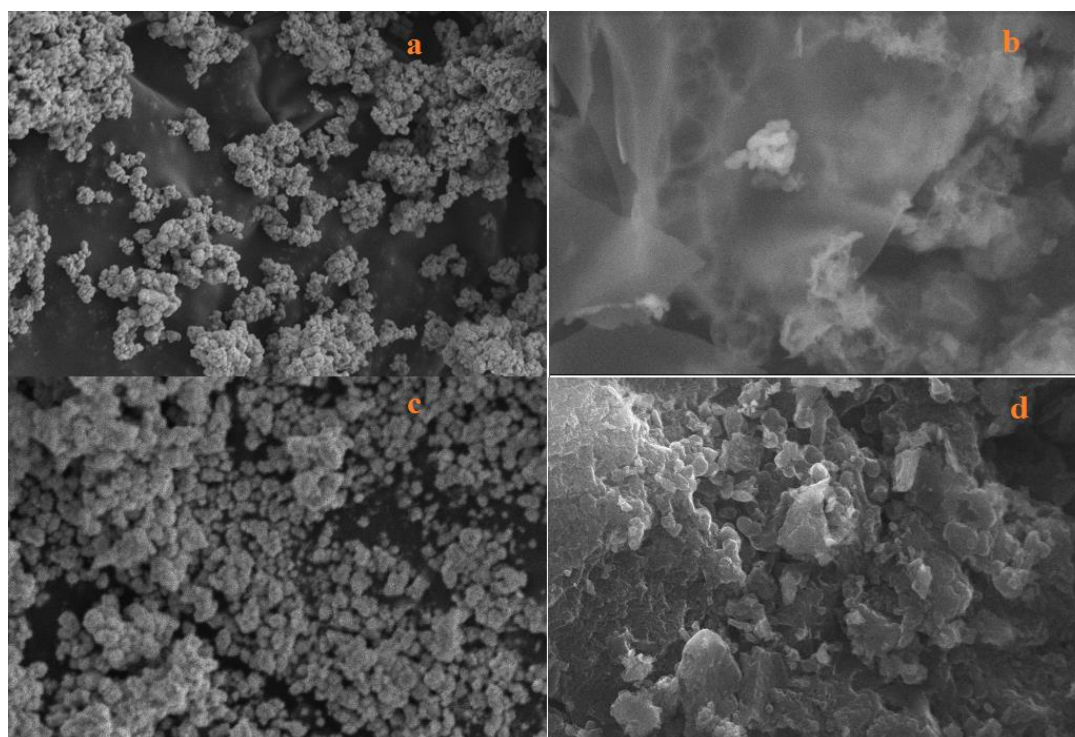


**Figure. 10.1.4.1. SEM images of copper oxide nanoparticles obtained using**  
 (a), (b) Malonic acid - Glucose – Glycine (MA – GLU - GLY) TDES  
 (c), (d) Malonic acid – Fructose- Glycine (MA – FRU - GLY) TDES

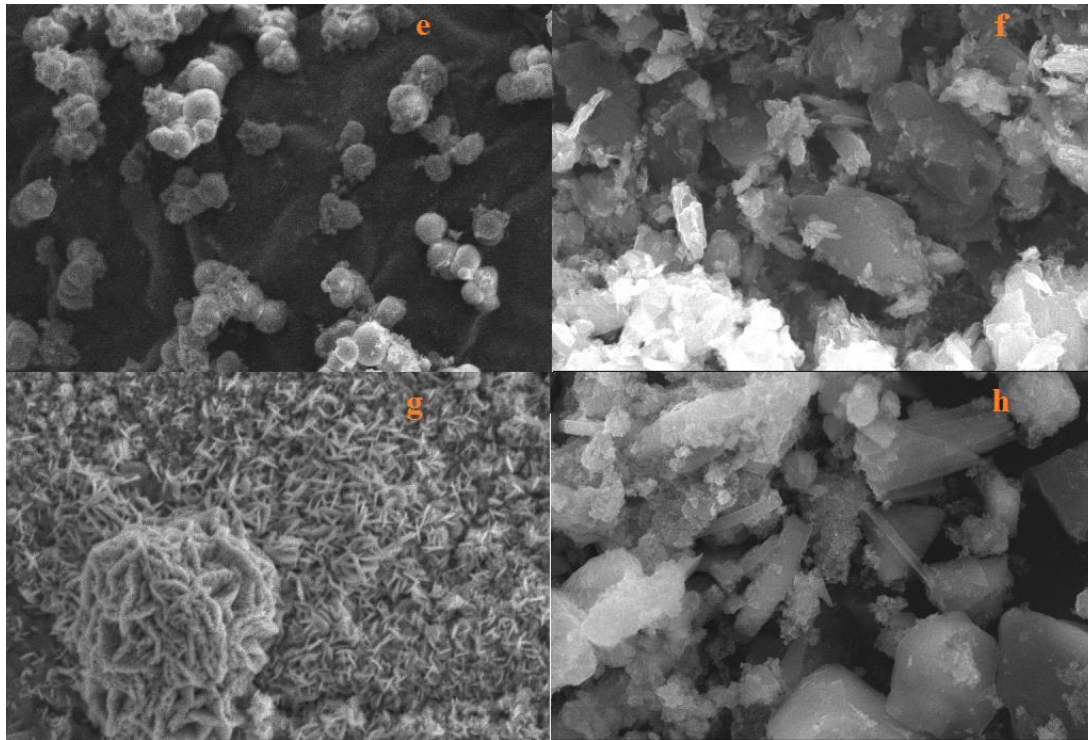


**Figure. 10.1.4.2 SEM images of copper oxide nanoparticles obtained using (e), (f) Malonic acid – Glucose – Histidine (MA – GLU - HIS) TDES (g), (h) Malonic acid – Fructose- Histidine (MA -FRU – HIS) TDES**

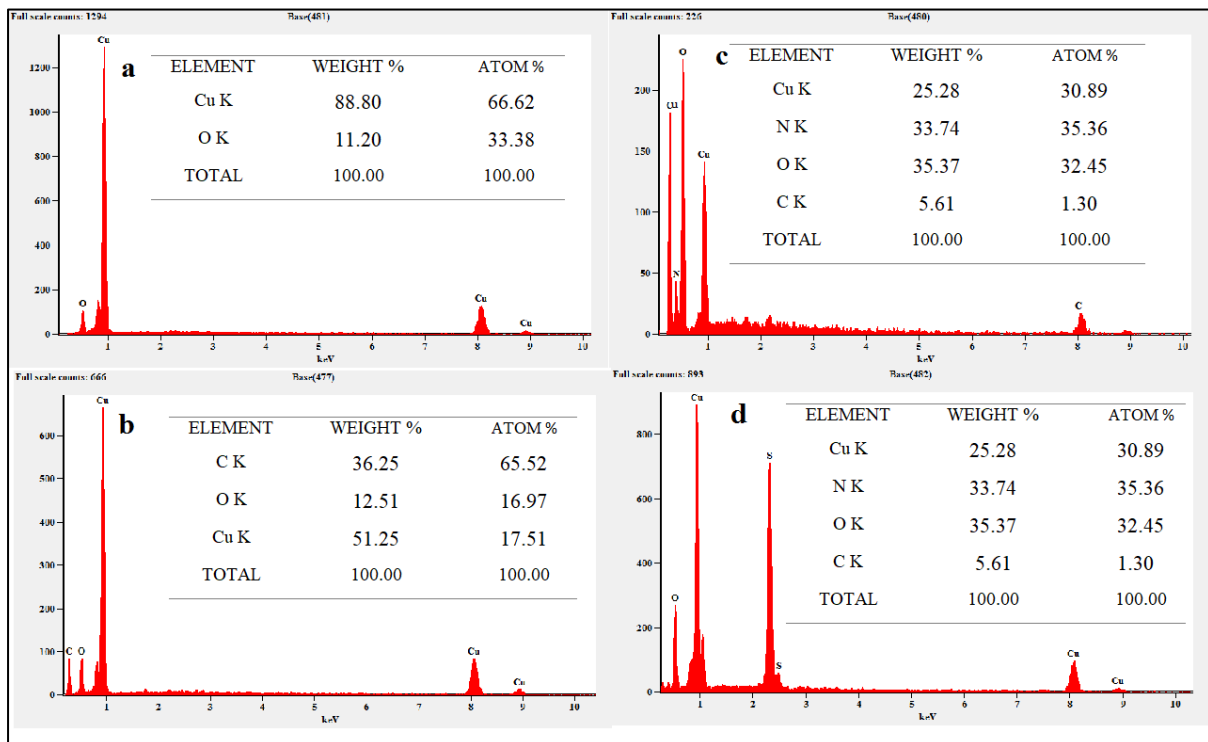


**Figure. 10.1.5. EDAX spectra of copper oxide nanoparticles obtained using (a) Malonic acid - Glucose – Glycine (MA – GLU - GLY) TDES (b) Malonic acid – Fructose- Glycine (MA – FRU - GLY) TDES (c) Malonic acid – Glucose – Histidine (MA – GLU - HIS) TDES (d) Malonic acid – Fructose- Histidine (MA -FRU – HIS) TDES**

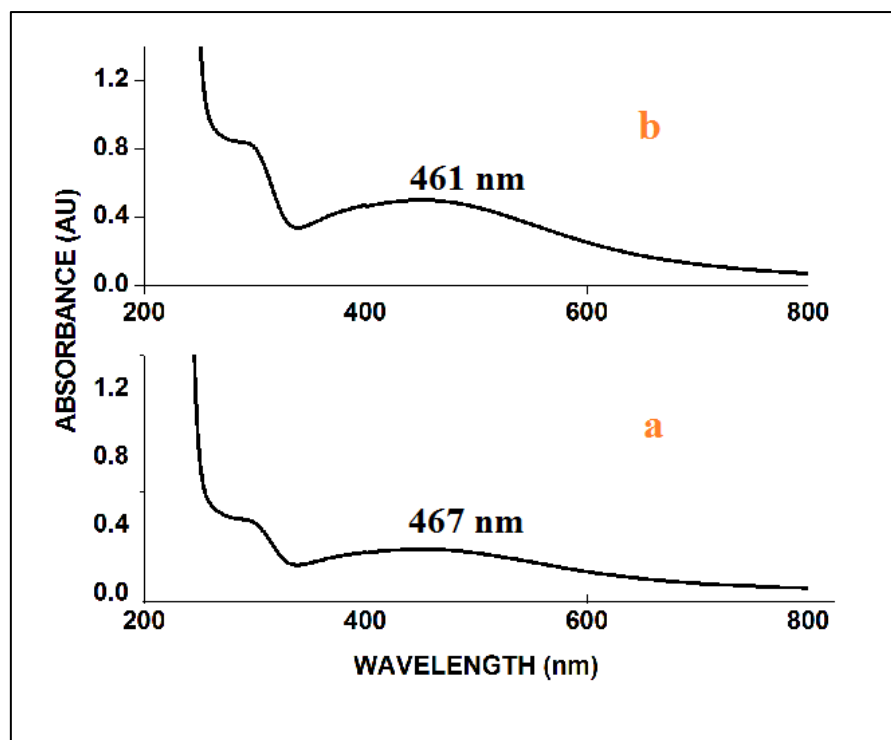


**Figure. 10.2.1. UV-Visible spectra of silver oxide nanoparticles obtained using**  
**(a) Malonic acid - Glucose – Glutamine (MA – GLU - GLUT) TDES**  
**(b) Malonic acid – Fructose- Glutamine (MA – FRU - GLUT) TDES**

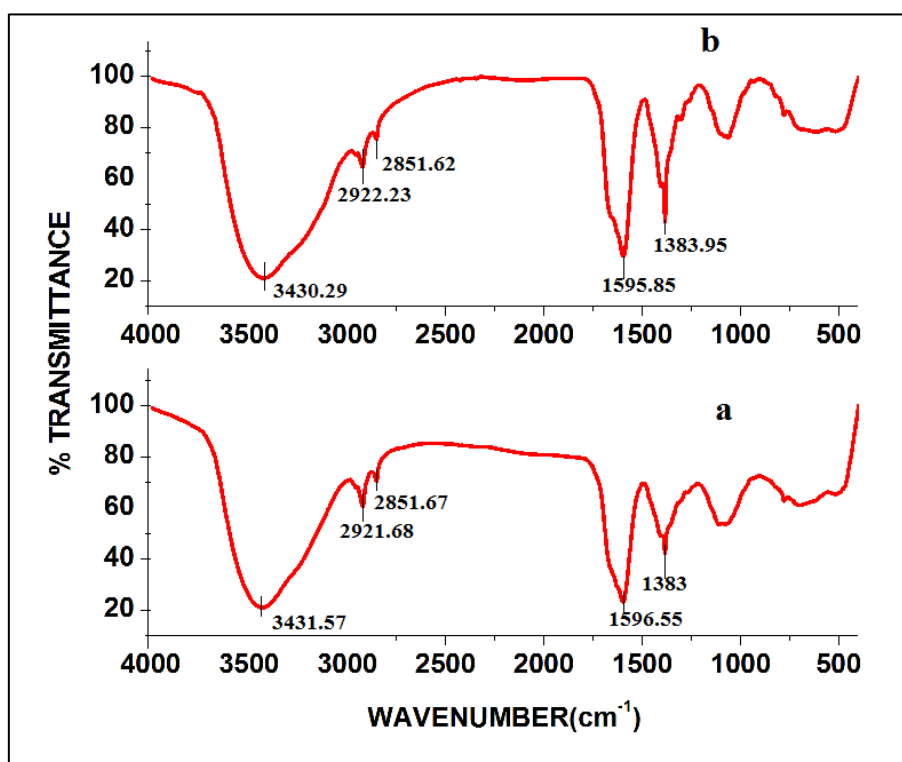


**Figure. 10.2.2. FTIR spectra of silver oxide nanoparticles obtained using**  
**(a) Malonic acid - Glucose – Glutamine (MA – GLU - GLUT) TDES**  
**(b) Malonic acid – Fructose- Glutamine (MA – FRU - GLUT) TDES**



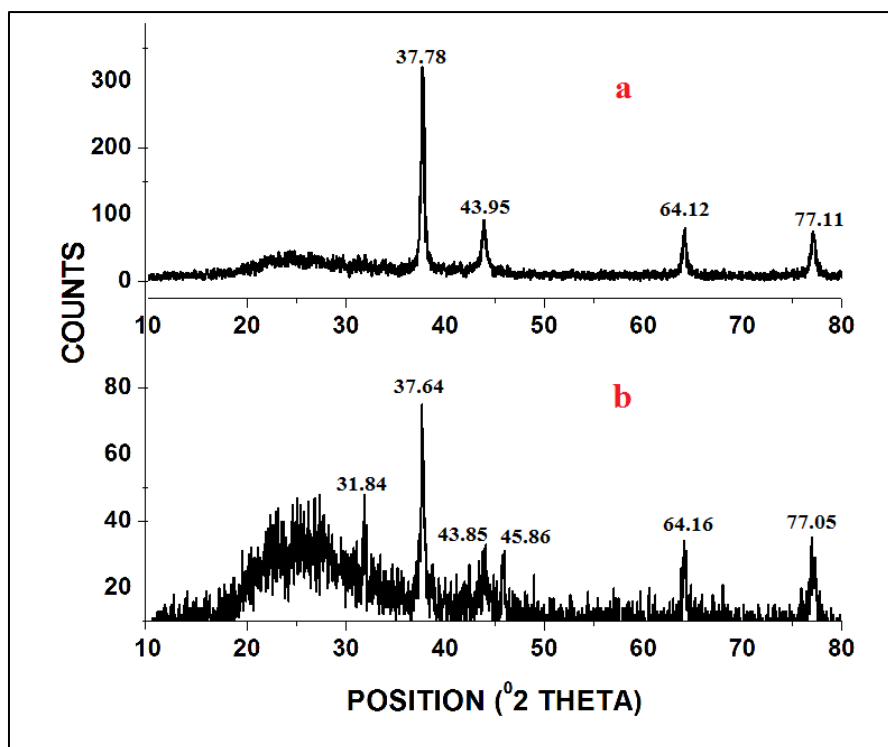


**Figure. 10.2.3. XRD patterns of silver oxide nanoparticles obtained using**  
 (a) Malonic acid - Glucose – Glutamine (MA – GLU - GLUT) TDES  
 (b) Malonic acid – Fructose- Glutamine (MA – FRU - GLUT) TDES

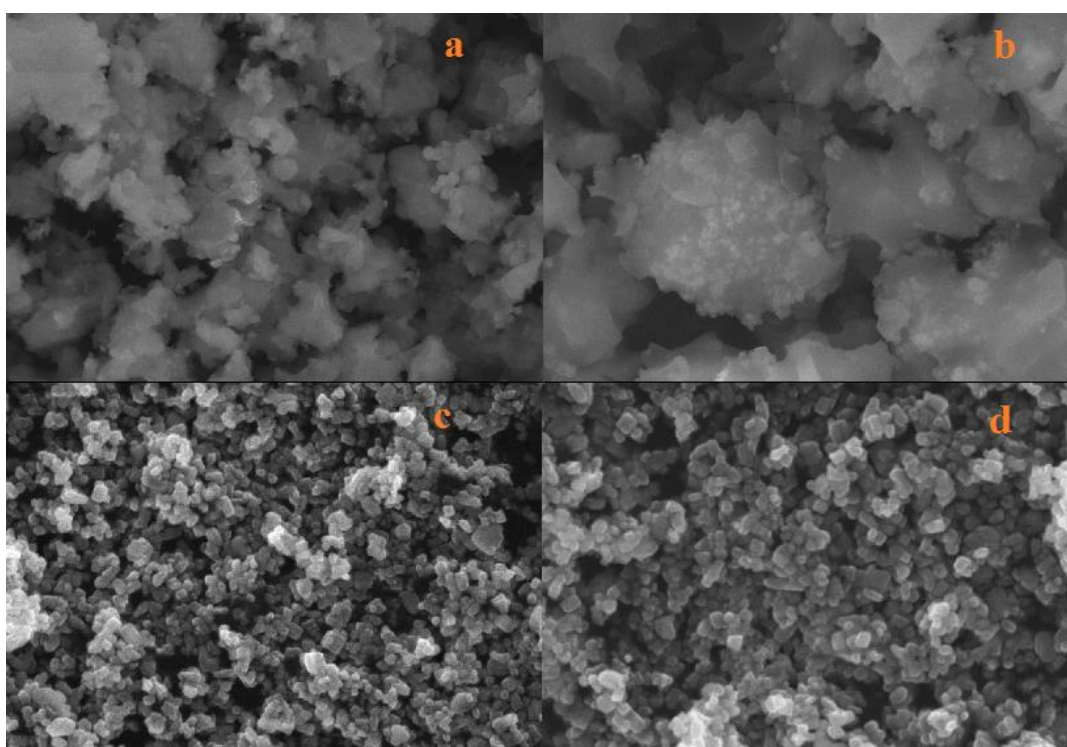


**Figure. 10.2.4. SEM images of silver oxide nanoparticles obtained using**  
 (a) (b) Malonic acid - Glucose – Glutamine (MA – GLU - GLUT) TDES  
 (c) (d) Malonic acid – Fructose- Glutamine (MA – FRU - GLUT) TDES



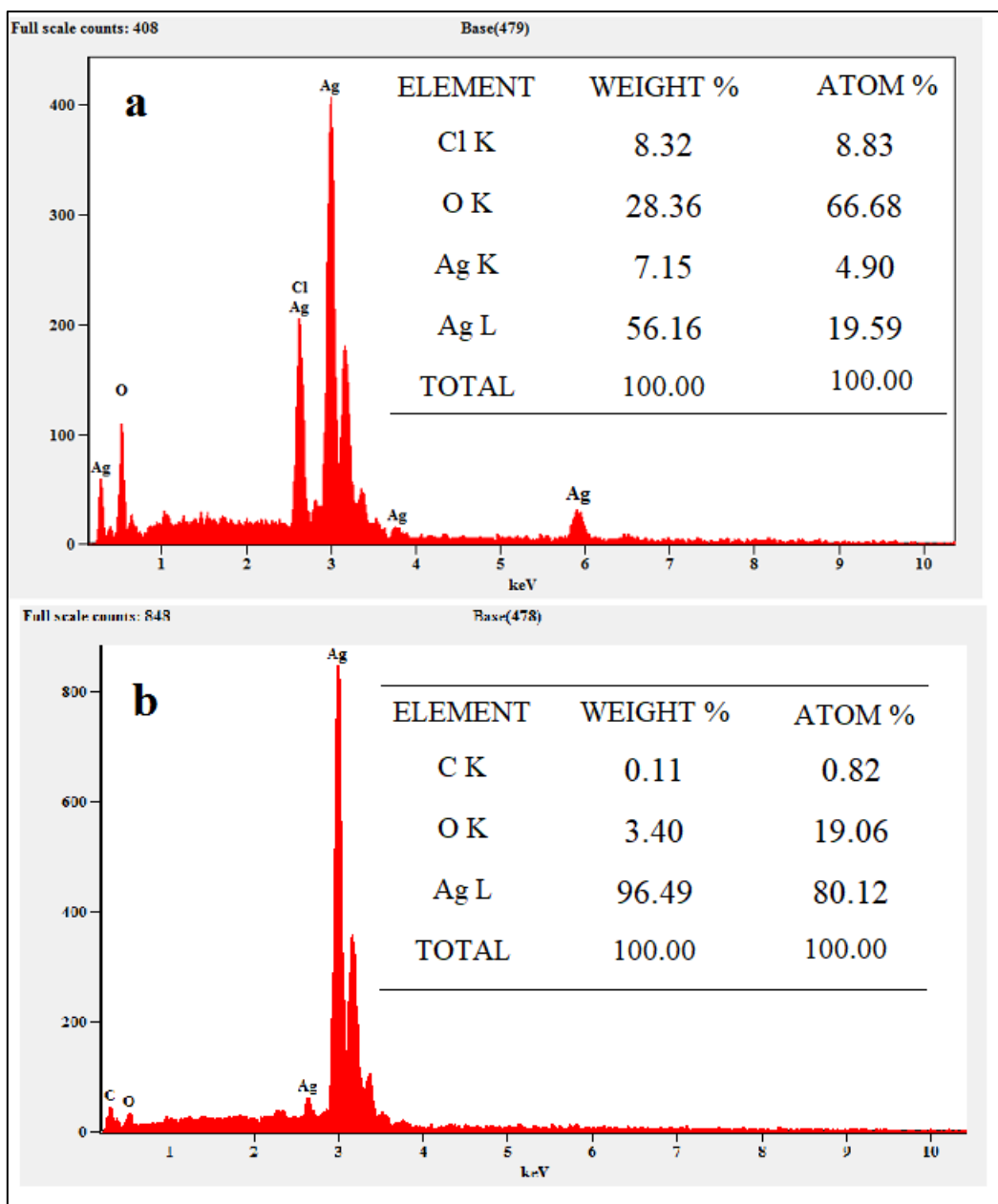


**Figure. 10.2.5. EDAX spectra of silver oxide nanoparticles obtained using**  
**(a) Malonic acid – Fructose- Glutamine (MA – FRU - GLUT) TDES**  
**(b) Malonic acid - Glucose – Glutamine (MA – GLU - GLUT) TDES**

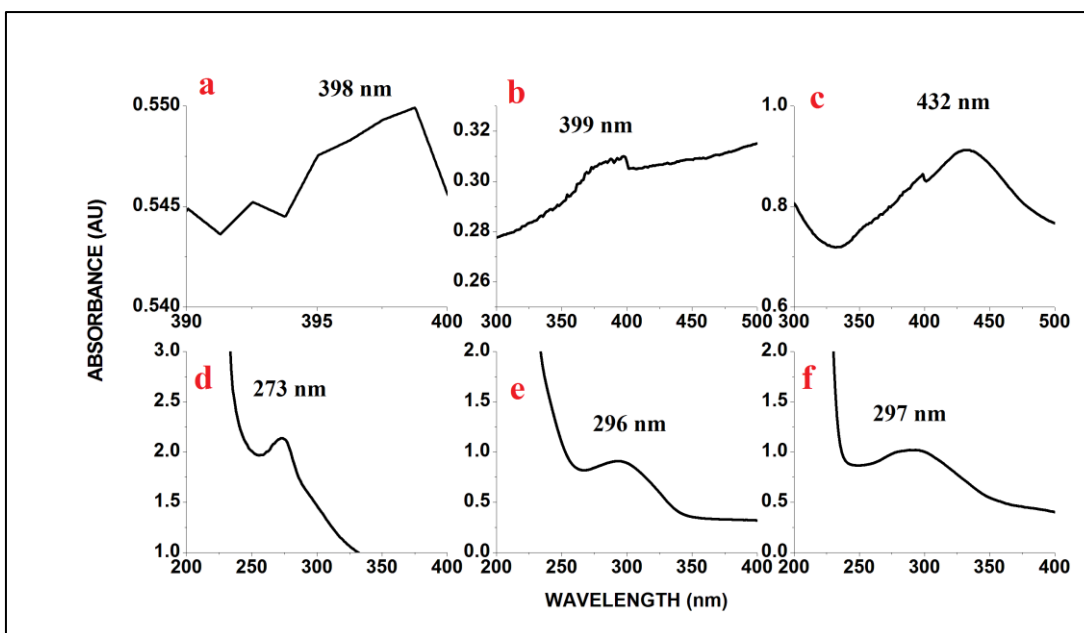


**Figure. 10.3.1. UV-Visible spectra of silver oxide nanoparticles obtained using**  
 (a) Zinc chloride - Glucose – Glycine (ZC – GLU - GLY) TDES  
 (b) Zinc chloride – Fructose- Glycine (ZC – FRU - GLY) TDES  
 (c) Zinc chloride – Glucose – Glutamine (ZC – GLU - GLUT) TDES  
 (d) Zinc chloride – Fructose- Glutamine (ZC -FRU – GLUT) TDES  
 (e) Zinc chloride – Glucose – Histidine (ZC – GLU - HIS) TDES  
 (f) Zinc chloride – Fructose- Histidine (ZC -FRU – HIS) TDES

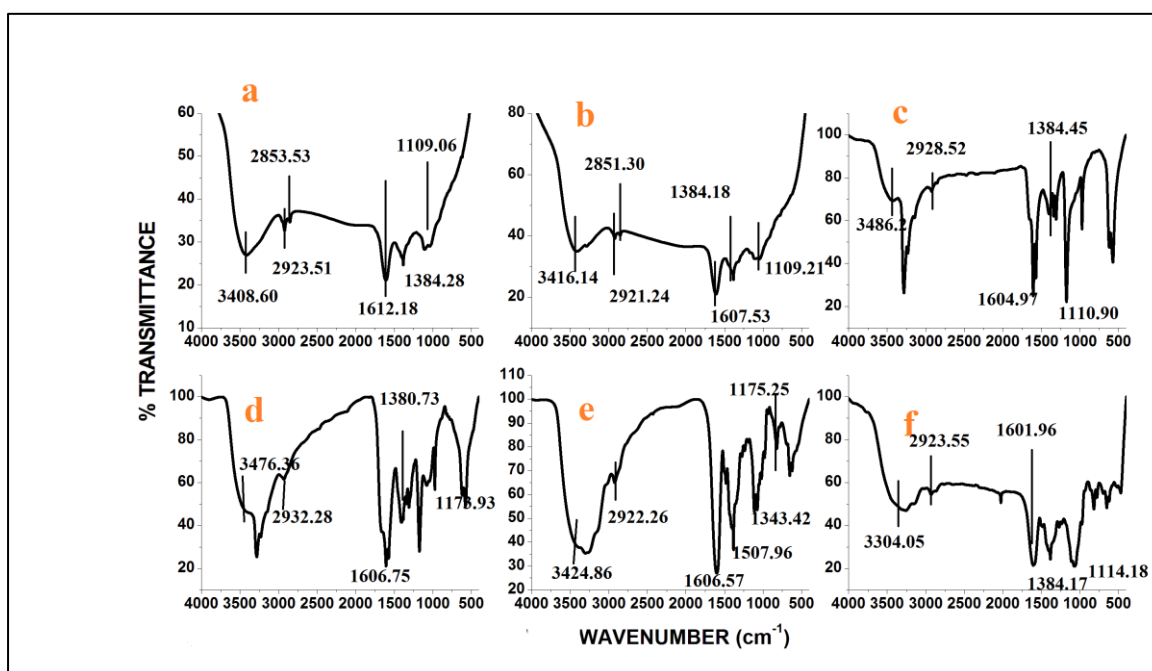


**Figure. 10.3.2. FTIR spectra of silver oxide nanoparticles obtained using**  
 (a) Zinc chloride - Glucose – Glycine (ZC – GLU - GLY) TDES  
 (b) Zinc chloride – Fructose- Glycine (ZC – FRU - GLY) TDES  
 (c) Zinc chloride – Glucose – Glutamine (ZC – GLU - GLUT) TDES  
 (d) Zinc chloride – Fructose- Glutamine (ZC -FRU – GLUT) TDES  
 (e) Zinc chloride – Glucose – Histidine (ZC – GLU - HIS) TDES  
 (f) Zinc chloride – Fructose- Histidine (ZC -FRU – HIS) TDES

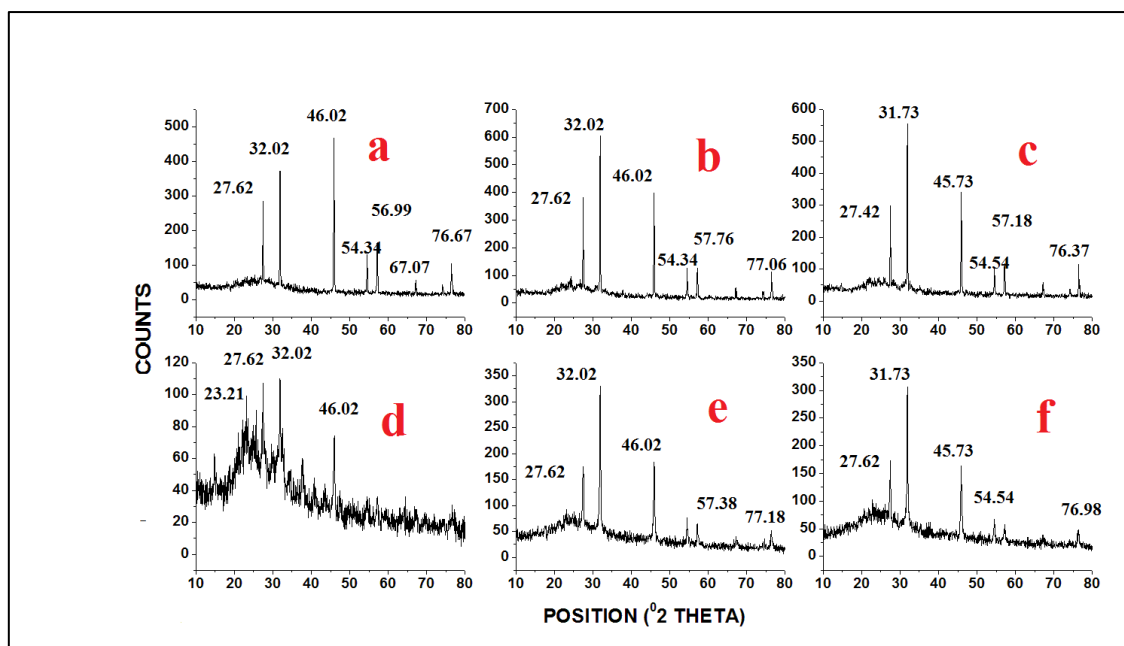


**Figure. 10.3.3. XRD patterns of silver oxide nanoparticles obtained using**  
 (a) Zinc chloride - Glucose – Glycine (ZC – GLU - GLY) TDES  
 (b) Zinc chloride – Fructose- Glycine (ZC – FRU - GLY) TDES  
 (c) Zinc chloride – Glucose – Glutamine (ZC – GLU - GLUT) TDES  
 (d) Zinc chloride – Fructose- Glutamine (ZC -FRU – GLUT) TDES  
 (e) Zinc chloride – Glucose – Histidine (ZC – GLU - HIS) TDES  
 (f) Zinc chloride – Fructose- Histidine (ZC -FRU – HIS) TDES

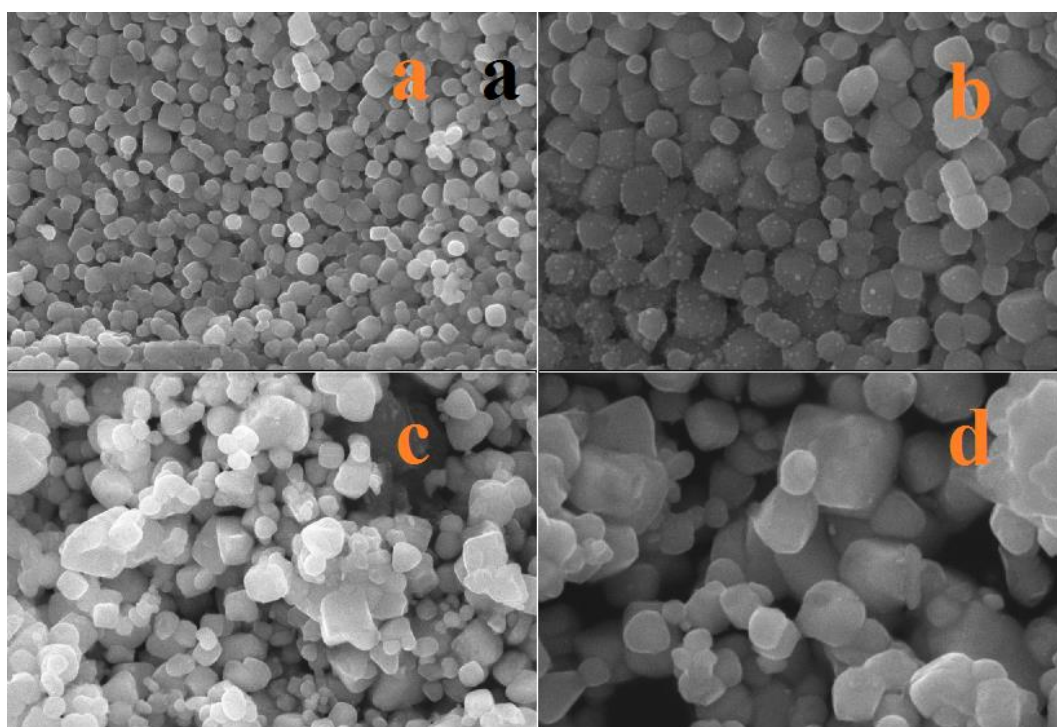


**Figure. 10.3.4.1 SEM images of silver oxide nanoparticles obtained using**  
 (a) (b) Zinc chloride - Glucose – Glycine (ZC – GLU - GLY) TDES  
 (c) (d) Zinc chloride – Fructose- Glycine (ZC – FRU - GLY) TDES

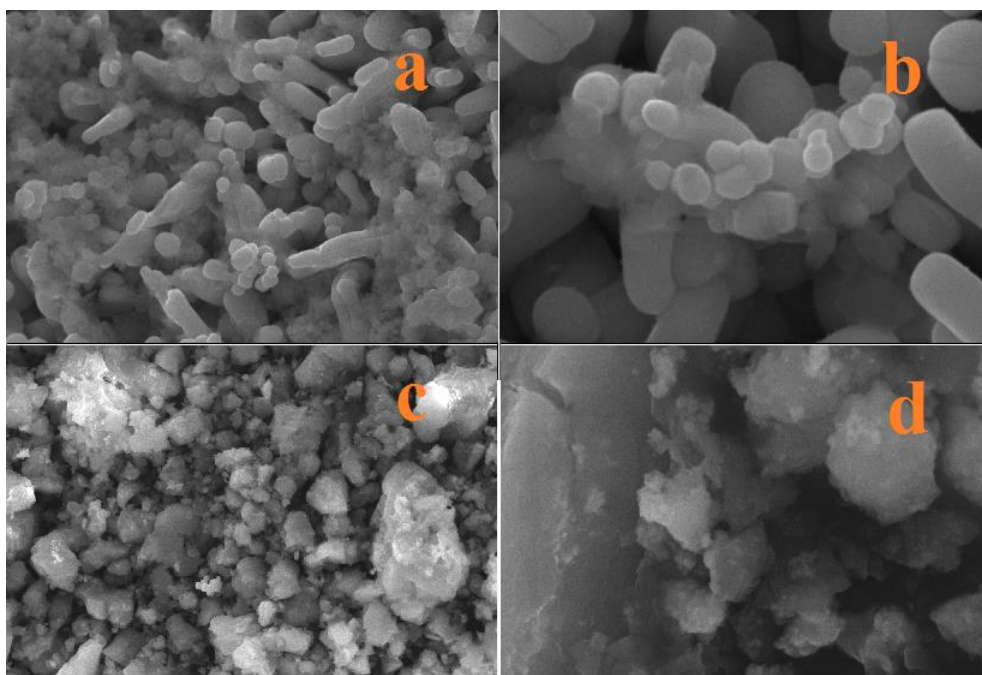


**Figure. 10.3.4.2 SEM images of silver oxide nanoparticles obtained using**  
 (a) (b) Zinc chloride - Glucose – Glutamine (ZC – GLU - GLUT) TDES  
 (c) (d) Zinc chloride – Fructose- Glutamine (ZC – FRU - GLUT) TDES

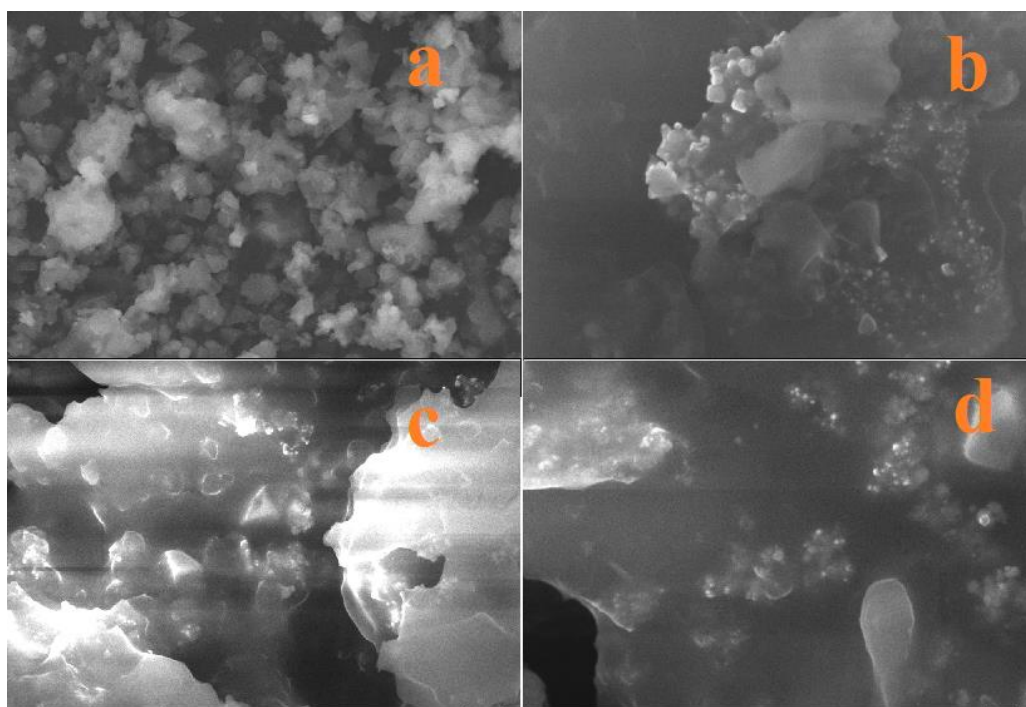


**Figure. 10.3.4.3 SEM images of silver oxide nanoparticles obtained using**  
 (a) (b) Zinc chloride - Glucose – Histidine (ZC – GLU - HIS) TDES  
 (c) (d) Zinc chloride – Fructose- Histidine (ZC – FRU - HIS) TDES

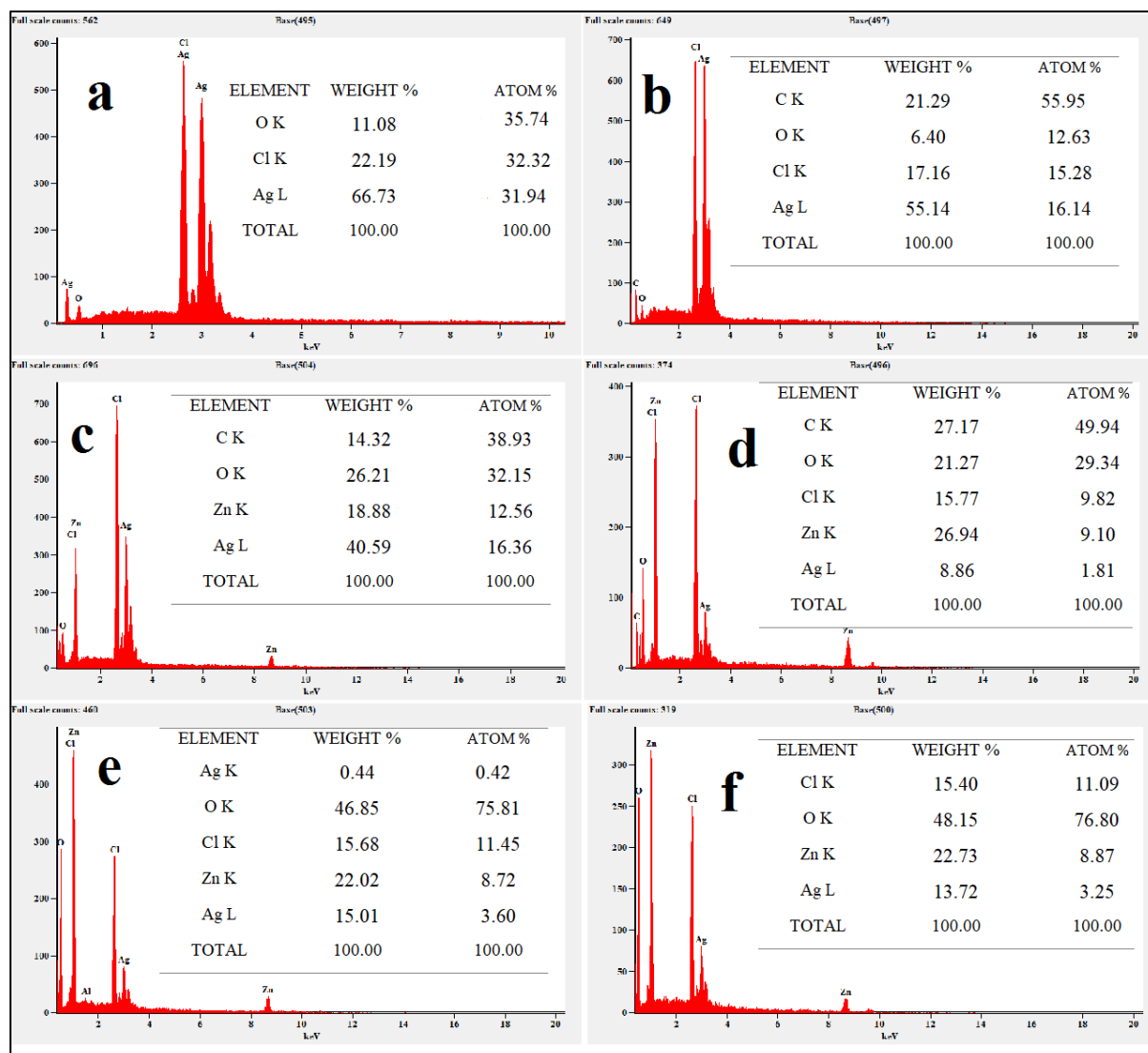


**Figure. 10.3.5. EDAX spectra of silver oxide nanoparticles obtained using**  
**(a) Zinc chloride - Glucose – Glycine (ZC – GLU - GLY) TDES**  
**(b) Zinc chloride – Fructose- Glycine (ZC – FRU - GLY) TDES**  
**(c) Zinc chloride – Glucose – Glutamine (ZC – GLU - GLUT) TDES**  
**(d) Zinc chloride – Fructose- Glutamine (ZC -FRU – GLUT) TDES**  
**(e) Zinc chloride – Glucose – Histidine (ZC – GLU - HIS) TDES**  
**(f) Zinc chloride – Fructose- Histidine (ZC -FRU – HIS) TDES**

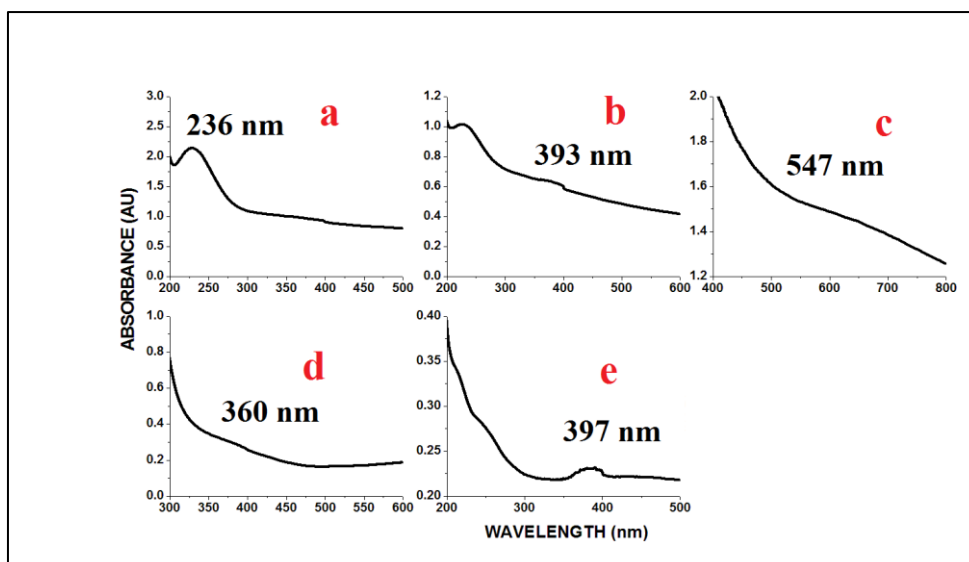


**Figure. 10.4.1. UV spectra of copper oxide nanoparticles obtained using**  
 (a) Manganese chloride - Glucose – Glycine (MC – GLU - GLY) TDES  
 (b) Manganese chloride – Fructose- Glycine (MC – FRU - GLY) TDES  
 (c) Manganese chloride – Glucose – Glutamine (MC – GLU - GLUT) TDES  
 (d) Manganese chloride – Fructose- Glutamine (MC -FRU – GLUT) TDES  
 (e) Manganese chloride – Glucose – Histidine (MC – GLU - HIS) TDES

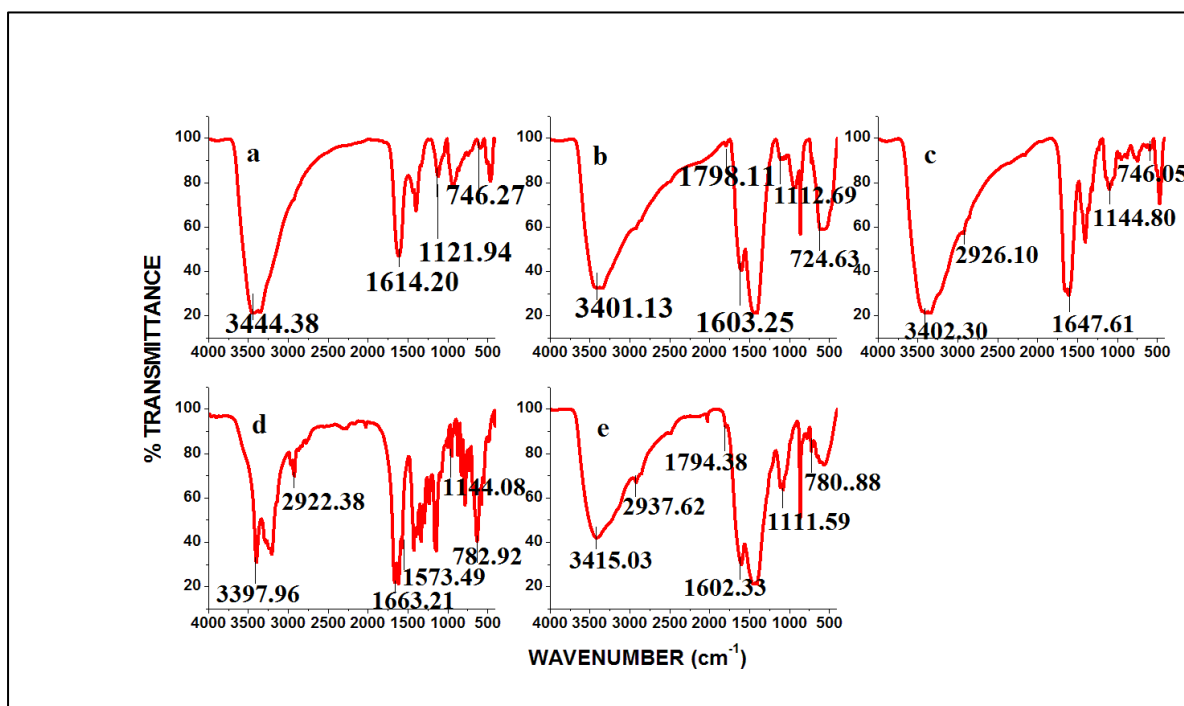


**Figure. 10.4.2. FTIR spectra of copper oxide nanoparticles obtained using**  
 (a) Manganese chloride - Glucose – Glycine (MC – GLU - GLY) TDES  
 (b) Manganese chloride – Fructose- Glycine (MC – FRU - GLY) TDES  
 (c) Manganese chloride – Glucose – Glutamine (MC – GLU - GLUT) TDES  
 (d) Manganese chloride – Fructose- Glutamine (MC -FRU – GLUT) TDES  
 (e) Manganese chloride – Glucose – Histidine (MC – GLU - HIS) TDES



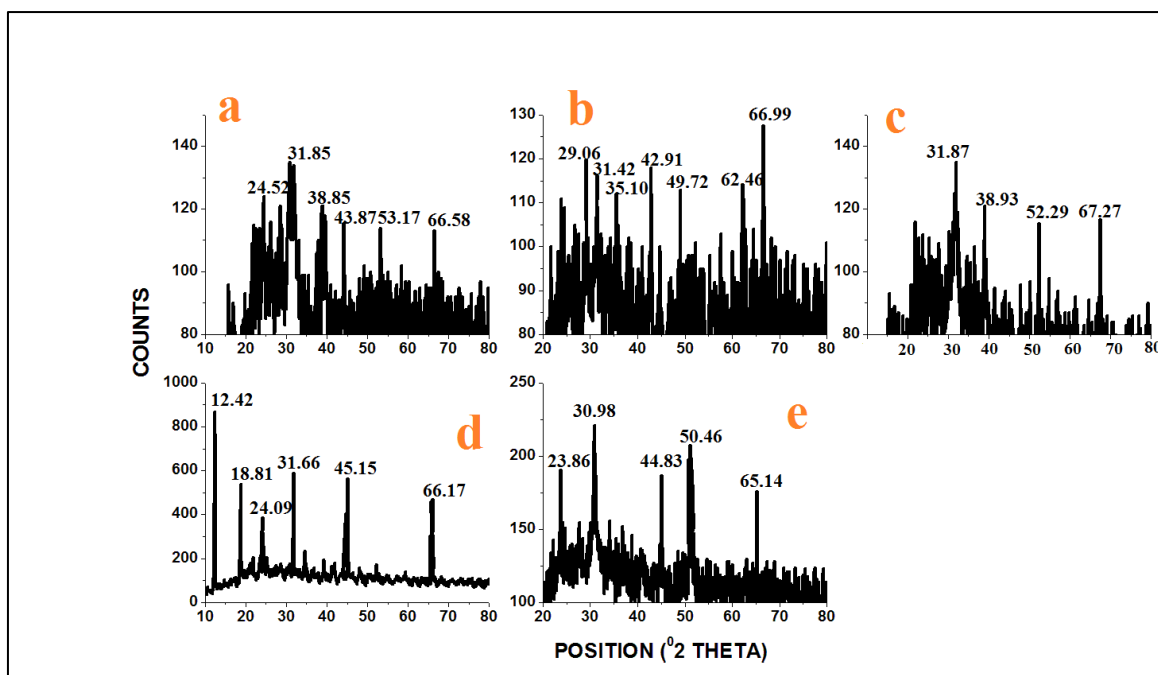


**Figure. 10.4.3. XRD Patterns of copper oxide nanoparticles obtained using**  
 (a) Manganese chloride - Glucose – Glycine (MC – GLU - GLY) TDES  
 (b) Manganese chloride – Fructose- Glycine (MC – FRU - GLY) TDES  
 (c) Manganese chloride – Glucose – Glutamine (MC – GLU - GLUT) TDES  
 (d) Manganese chloride – Fructose- Glutamine (MC -FRU – GLUT) TDES  
 (e) Manganese chloride – Glucose – Histidine (MC – GLU - HIS) TDES

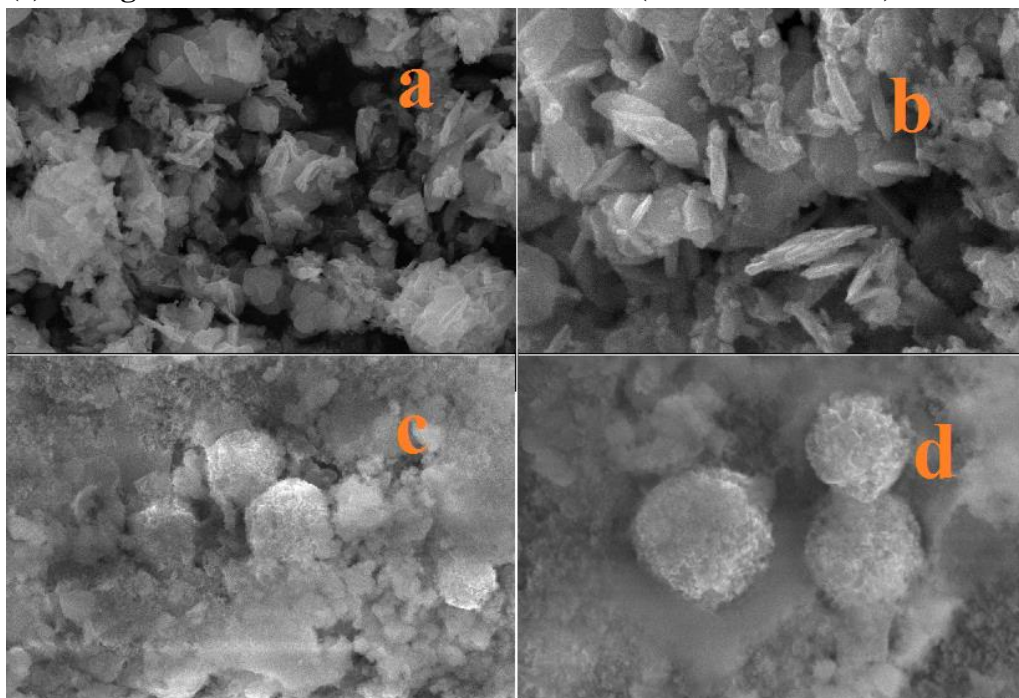


**Figure. 10.4.4.1 SEM images of copper oxide nanoparticles obtained using**  
 (a) (b) Manganese chloride - Glucose – Glycine (MC – GLU - GLY) TDES  
 (c) (d) Manganese chloride – Fructose- Glycine (MC – FRU - GLY) TDES

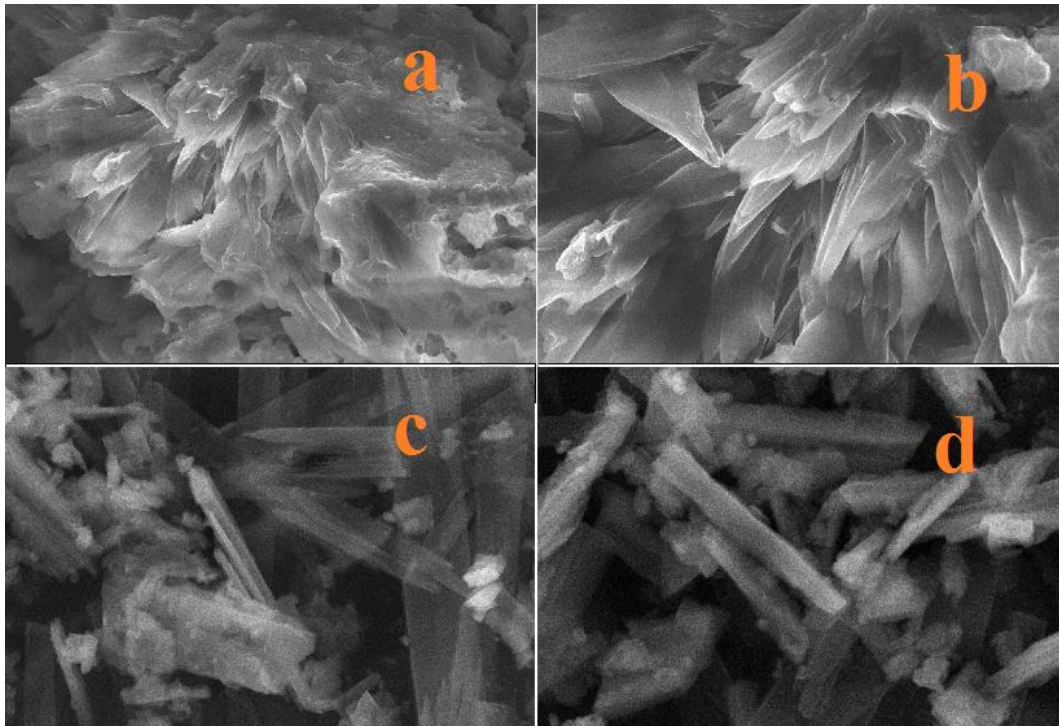


**Figure. 10.4.4.2 SEM images of copper oxide nanoparticles obtained using**  
**(a) (b) Manganese chloride - Glucose – Glutamine (MC – GLU - GLUT) TDES**  
**(c) (d) Manganese chloride – Fructose- Glutamine (MC – FRU - GLUT) TDES**

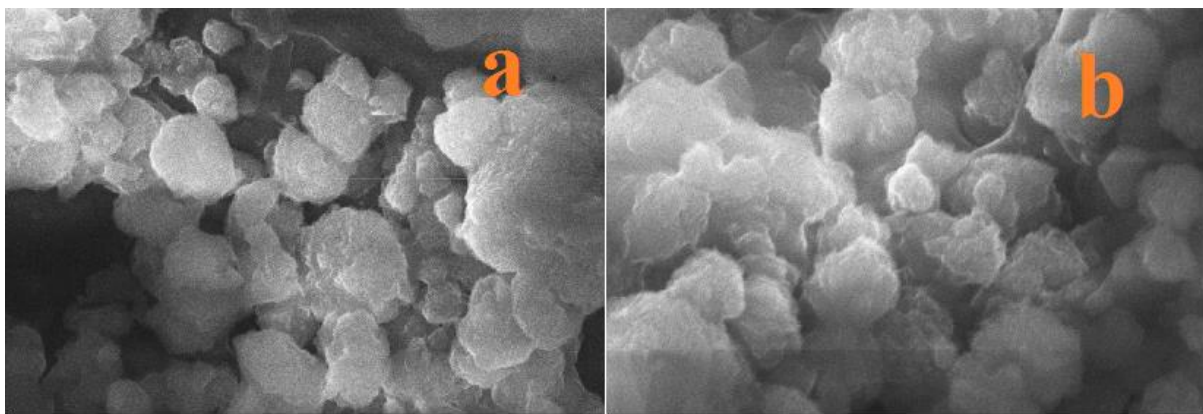


**Figure. 10.4.4.3 SEM images of copper oxide nanoparticles obtained using**  
**(a) (b) Manganese chloride - Glucose – Histidine (MC – GLU - HIS) TDES**



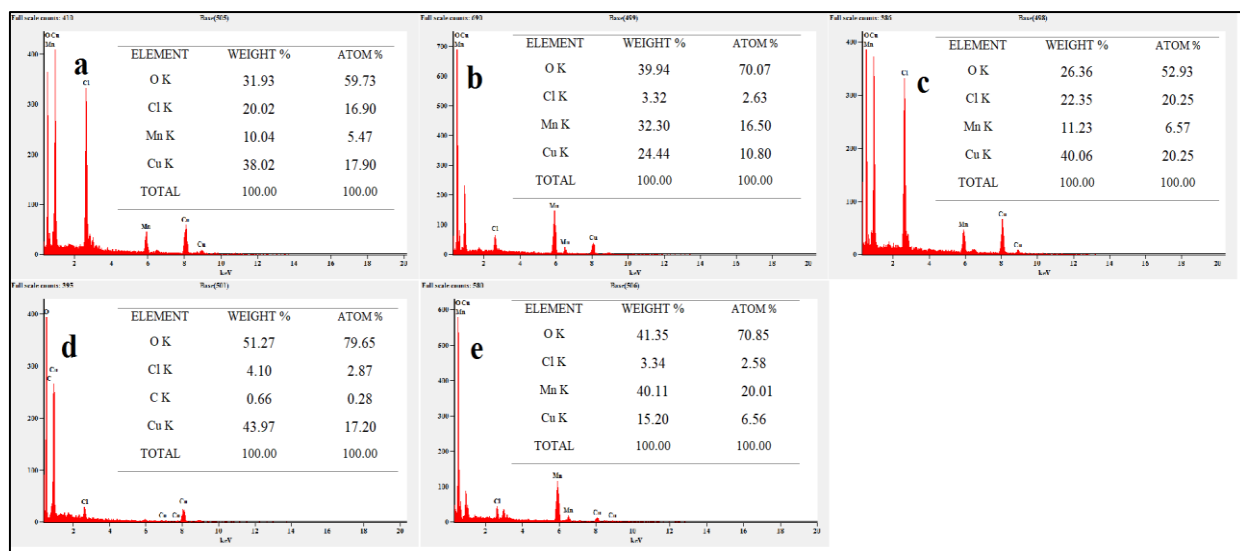


**Figure. 10.4.5. EDAX spectra of copper oxide nanoparticles obtained using**  
**(a) Manganese chloride - Glucose – Glycine (MC – GLU - GLY) TDES**  
**(b) Manganese chloride – Fructose- Glycine (MC – FRU - GLY) TDES**  
**(c) Manganese chloride – Glucose – Glutamine (MC – GLU - GLUT) TDES**  
**(d) Manganese chloride – Fructose- Glutamine (MC -FRU – GLUT) TDES**  
**(e) Manganese chloride – Glucose – Histidine (MC – GLU - HIS) TDES**



## 11. Antimicrobial studies of some nanoparticles

---

### 11.1 Introduction

The rise of nanotechnology in recent decades has sparked a great interest in research into the antibacterial properties of nanoscale metals. Metallic NPs with a lower concentration have a higher antibacterial and antifungal action <sup>[1]</sup>. Antimicrobial agents are compounds that can kill microorganisms without giving any toxic effects to the surrounding areas. Antibacterial compounds are utilized in a variety of industries, including textiles, water disinfection, food packaging, and medicine <sup>[2]</sup>. The antimicrobial effects of different metallic nanoparticles such as Alumina <sup>[3-5]</sup>, silver <sup>[6,7]</sup>, magnesium <sup>[8-10]</sup>, and zinc oxide <sup>[11, 12]</sup> have been widely studied. In our study, we focussed to find the antimicrobial activities of some of our synthesized nanoparticles. Using few copper and silver nanoparticles, the antibacterial and the antifungal activities were studied respectively.

### 11.2 Antibacterial studies of copper nanoparticles

The antibacterial activity of synthesized copper nanoparticles was tested against a variety of bacteria, including Gram-positive and Gram-negative bacteria. Copper is a commonly available metal that is required by most living organisms as a trace element. Copper nanoparticles have a wide range of applications; this metal has also been employed as a potential antibacterial agent since antiquity. The anti-microbial activity was performed by the disc diffusion method followed by NCCLS <sup>[13]</sup> and Awoyinka et al. <sup>[14]</sup>.

#### 11.2.1. Growth of bacterial media

The bacteria used in this study were Gram-positive bacteria: *Staphylococcus aureus* (MTCC 3160), *Bacillus subtilis* (MTCC 441), and Gram-negative bacteria: *Escherichia coli* (MTCC 732), *Pseudomonas aeruginosa* (MTCC 741) obtained from Microbial type culture collection (MTCC) at the Institute of Microbial Technology (IMTECH),

Chandigarh, India. The basic culture medium used for the growth of bacteria is nutrient agar Hi media. In 1000 mL distilled water, dissolve 28.0 g of nutrient agar Hi media, boil, mix them completely. Then it was autoclaved at 15 lbs, 121°C for 15 minutes to sterilize. After that, it was poured into sterile Petri plates. In a Roux bottle, a loop containing each of the bacteria was suspended in around 10ml of physiological saline to maintain living tissues. Then these were traced onto the appropriate culture slants and incubated for 24 hours at 37°C. When growth was observed after the incubation period, the tubes were stored at 2-8° C until used <sup>[15]</sup>.

### **11.2.2 Preparation of dried filter paper discs**

The standard solution of Chloramphenicol is used to compare the antibacterial activities with the sample solutions. The sample solutions were prepared by weighing 10mg of the copper nanoparticles in 10ml of deionized water. Then the filter paper discs were loaded with these standard and sample solutions of various concentrations after the paper was sterilized in hot air <sup>[15]</sup>.

### **11.2.3. Antimicrobial assay**

The bacteria were inoculated, distributed, and allowed to dry for 10 minutes on a hardened agar plate. To evenly inoculate the whole surface of the Nutrient agar plates, a sterile cotton swab was dipped into a standardized microorganism's test suspension. Then, on Nutrient agar plates, inoculums containing each bacterial strain were dispersed. 50µl, 100µl, and 150µl of each sample solution were put into sterile filter paper discs, and 30µl of the standard solution was applied. The plates were incubated for 24 hours at 37°C. Triplicates of each sample were tested. The mean diameter of the zone of inhibition around the disc in millimeters, measured using a millimeter scale, was used to measure the antibacterial potential of test samples of copper nanoparticles synthesized in MA-GLU and

MA-FRU <sup>[15]</sup>. The measured values were expressed as Mean  $\pm$  SD for triplicates as tabulated in Table 11.1.

The antibacterial activities were tested for the copper nanoparticles using the disc diffusion method. The results revealed that the tested samples showed a significant reduction in the growth of each bacteria. The growth inhibition of bacteria from the copper NPs obtained using MA-GLU is more than that from MA-FRU. There is a significant increase in the inhibition when the concentrations of the sample solutions increase. The nanoparticles show comparatively growth inhibition activity, which is like the standard taken, Chloramphenicol. The images of the zone of inhibition of the copper nanoparticles synthesized in MA-GLU, MA-FRU were shown in Figures 11.1.1 and 11.1.2.

### **11.3. Antifungal studies of Silver Nanoparticles**

Silver nanoparticles are well-known for having excellent antimicrobial action against different pathogens such as bacteria, viruses, and fungus <sup>[16]</sup>. Antifungal <sup>[17]</sup>, anti-inflammatory <sup>[18]</sup>, and anti-viral <sup>[19]</sup> characteristics are all common uses for silver nanoparticles. This study aims to determine the antifungal activity of the synthesized silver nanoparticles against *Candida albicans* and *Aspergillus niger* strains by the disc diffusion method followed by NCCLS <sup>[13]</sup> and Awoyinka et al. <sup>[14]</sup>.

#### **11.3.1. Growth of fungal media**

The fungi used in this study were *Candida albicans* (MTCC 183) and *Aspergillus niger* (MTCC 10180) obtained from Microbial type culture collection (MTCC) at the Institute of Microbial Technology (IMTECH), Chandigarh, India. The basic culture medium used for the growth of fungi is Potato Dextrose Agar (PDA-Himedia). In 1000 mL distilled water, dissolve 28.0 g of PDA-Himedia, boil, mix them completely. Then it was autoclaved at 15 lbs, 121°C for 15 minutes to sterilize using tartaric acid. After that, it was poured into sterile Petri plates. In a Roux bottle, a loop containing each of the bacteria was

suspended in around 10ml of physiological saline to maintain living tissues. Then these were traced onto the appropriate culture slants and incubated for 48 hours at 25°C. When growth was observed after the incubation period, the tubes were stored at 2-8° C until used [15].

### **11.3.2 Preparation of dried filter paper discs**

The standard solution of Fluconazole is used to compare the antifungal activities with the sample solutions. The sample solutions were prepared by weighing 10mg of the silver nanoparticles in 10ml of DMSO. Then the filter paper discs were loaded with these standard and sample solutions of various concentrations after the paper was sterilized in hot air [15].

### **11.3.3. Antimicrobial assay**

The fungi were inoculated, distributed, and allowed to dry for 10 minutes on a hardened PDA-Himedia plate. To evenly inoculate the whole surface of the PDA-Himedia plates, a sterile cotton swab was dipped into a standardized microorganism's test suspension. Then, on PDA-Himedia plates, inoculums containing each fungal strain were dispersed. 50µl, 100µl, and 150µl of each sample solution were put into sterile Whatman no:1 filter paper disc, and 30µl of the standard solution was applied. The plates were incubated for 24 hours at 37°C. Triplicates of each sample were tested. The mean diameter of the zone of inhibition around the disc in millimeters, measured using a millimeter scale, was used to measure the antifungal potential of test samples of silver nanoparticles synthesized in MA-GLU-GLUT and MA-FRU-GLUT [15]. The measured values were expressed as Mean ± SD for triplicates as tabulated in Table 11.2.

The antifungal activities were assayed both in solvents and silver nanoparticles. The results revealed that the tested samples showed a significant reduction in the growth of *Candida albicans*. The growth inhibition of *Candida albicans* from MA-GLU-GLUT TDES

and MA-FRU-GLUT TDES were found to be  $3.50\pm 0.24\text{mm}$  and  $2.70\pm 0.18\text{mm}$  respectively and their activities in silver nanoparticles were found to be  $6.70\pm 0.46\text{mm}$  and  $4.90\pm 0.34\text{mm}$  which is like the standard taken, Fluconazole. There is a significant decrease in the growth of *Aspergillus niger* both in solvents and silver nanoparticles than *Candida albicans*. The growth inhibition of *Aspergillus niger* from MA-GLU-GLUT and MA-FRU-GLUT were found to be  $3.00\pm 0.21\text{mm}$  and  $2.40\pm 0.16\text{mm}$  respectively and their activities in silver nanoparticles were found to be  $5.50\pm 0.38\text{mm}$  and  $4.00\pm 0.28\text{mm}$  which is like the standard taken, Fluconazole. Among the tested samples, the highest growth inhibition activity is observed from the silver nanoparticles than the solvents as shown in Fig. 11.2.1 and 11.2.2.

#### **11.4 Conclusion**

Some synthesized nanoparticles were studied by antimicrobial activities using Disc Diffusion Method. The copper nanoparticles were studied for antibacterial activities and the silver nanoparticles were studied for antifungal activities. The synthesized nanoparticles show anti – activities against some bacteria and fungi. Copper nanoparticles obtained using MA-GLU BDES taken as  $150\mu\text{l}$  show significant antibacterial activities on *Escherichia coli*. Comparatively the copper nanoparticles show highest inhibition effect on gram positive and gram negative bacteriae as the standard taken, Chloramphenicol. Silver nanoparticles had a significant anti- fungal effect on the growth of *Candida albicans* which was comparable to the standard taken, Flucanazole. Among the silver nanoparticles obtained using MAGGT and MAFGT TDESs, the silver nanoparticles using MAGGT has highest growth inhibition activity than the silver nanoparticles using MAFGT.

## References

- [1]. Kon K, Rai M (2013) Metallic nanoparticles: mechanism of antibacterial action and influencing factors. *J Comp Clin Path Res* 2: 160-174.
- [2]. Hajipour MJ, Fromm KM, Ashkarran AA, de Aberasturi DJ, de Larramendi IR, et al. (2012) Antibacterial properties of nanoparticles. *Trends Biotechnol* 30: 499-511.
- [3]. Buckley JJ, Gai PL, Lee AF, Olivi L, Wilson K (2008) Silver carbonate nanoparticles stabilized over alumina nanoneedles exhibiting potent antibacterial properties. *Chem Commun* 18:4013-4015.
- [4]. Chang Q, Yan L, Chen M, He H, Qu J (2007) Bactericidal mechanism of Ag/Al<sub>2</sub>O<sub>3</sub> against *Escherichia coli*. *Langmuir* 23: 11197-11199.
- [5]. Geoprincy G, Gandhi N, Renganathan S (2012) Novel antibacterial effects of alumina nanoparticles on *Bacillus cereus* and *Bacillus subtilis* in comparison with antibiotics. *Int J Pharm Pharm Sci* 4: 544-548.
- [6]. Marambio-Jones C, Hoek EM (2010) A review of the antibacterial effects of silver nanomaterials and potential implications for human health and the environment. *J Nanopart Res* 12: 1531-1551.
- [7]. Sotiriou GA, Pratsinis SE (2010) Antibacterial activity of nanosilver ions and particles. *Environ Sci Technol* 44: 5649-5654.
- [8]. Jin T, He Y (2011) Antibacterial activities of magnesium oxide (MgO) nanoparticles against foodborne pathogens. *J Nanopart Res* 13: 6877-6885.
- [9]. Lellouche J, Friedman A, Lellouche JP, Gedanken A, Banin E (2012) Improved antibacterial, and antibiofilm activity of magnesium fluoride nanoparticles obtained by water-based ultrasound chemistry. *Nanomedicine: Nanotechnology, Biology and Medicine* 8: 702-711.



- [10]. Dong C, He G, Zheng W, Bian T, Li M, et al. (2014) Study on antibacterial mechanism of Mg(OH)<sub>2</sub> nanoparticles. Mater Lett 134: 286-289.
- [11]. Espitia PJ, Soares ND, dos Reis Coimbra JS, de Andrade NJ, et al. (2012) Zinc oxide nanoparticles: synthesis, antimicrobial activity, and food packaging applications. Food Bioprocess Tech 5: 1447-1464.
- [12]. Liu Y, He L, Mustapha A, Li H, Hu ZQ, et al. (2009) Antibacterial activities of zinc oxide nanoparticles against Escherichia coli O157: H7. J Appl Microbiol 107:1193-1201.
- [13]. NCCLS. (1993) National Committee for Clinical Laboratory Standards. Performance standards for antimicrobial disc susceptibility tests. PA: NCCLS Publications 25.
- [14]. Awoyinka, O.A., Balogun I.O. and Ogunnow, A.A. (2007). Phytochemical screening and *in vitro* bioactivity of *Cnidioscolus aconitifolius* (Euphorbiaceae). J. Med. Plant Res, 1: 63-95.
- [15]. P. Jegajeevanram, N.M.I. Alhaji, Antimicrobial Activity of *Tagetes Erecta* flower and Mango Ginger Rhizome Extracts. World Journal of Science and Research. 1(3): 65-70 (2016).
- [16]. Franci, G., Falanga, A., Galdiero, S., Palomba, L., Rai, M., Morelli, G., et al. Silver nanoparticles as potential antibacterial agents. Molecules 20, (2015). 8856–8874.
- [17]. Medda, S., Hajra, A., Dey, U., Bose, P., and Mondal, N. K. Biosynthesis of silver nanoparticles from Aloe vera leaf extract and antifungal activity against *Rhizopus* sp. and *Aspergillus* sp. Appl. Nanosci. 5, (2015),875–880.
- [18]. Hebeish, A., El-Rafie, M., El-Sheikh, M., Seleem, A. A., and El-Naggar, M. E. Antimicrobial wound dressing and anti-inflammatory efficacy of silver nanoparticles. Int. J. Biol. Macromol. 65, (2014)., 509–515.

[19]. Bekele, A. Z., Gokulan, K., Williams, K. M., and Khare, S. Dose and size-dependent antiviral effects of silver nanoparticles on feline calicivirus, a human norovirus surrogate. *Foodborne Pathog. Dis.* 13, (2016), 239–244.

**Table 11.1. Comparison of antibacterial activity of copper nanoparticles obtained using Malonic Acid-Glucose (MA-GLU) and Malonic Acid-Fructose (MA-FRU) sample solutions with a standard solution, Chloramphenicol (Std).**

Bacterial strains	Solvent	Samples at different concentrations			Std.	Control
		50µL	100 µL	150 µL	30 µL	50 µL
<i>Escherichia coli</i>	MA-GLU	3.50±0.24	6.35±0.44	9.80±0.68	12.20±0.85	0.00±0.00
	MA-FRU	3.35±0.23	6.20±0.43	9.50±0.66	12.25±0.85	0.00±0.00
<i>Pseudomonas aeruginosa</i>	MA-GLU	3.05±0.21	5.90±0.41	9.10±0.63	11.20±0.78	0.00±0.00
	MA-FRU	3.00±0.21	5.75±0.40	9.00±0.63	11.25±0.78	0.00±0.00
<i>Staphylococcus aureus</i>	MA-GLU	3.25±0.22	6.20±0.43	9.40±0.65	11.30±0.79	0.00±0.00
	MA-FRU	3.10±0.21	6.00±0.42	9.25±0.64	11.40±0.79	0.00±0.00
<i>Bacillus subtilis</i>	MA-GLU	2.80±0.19	5.60±0.39	8.70±0.60	11.00±0.77	0.00±0.00
	MA-FRU	2.50±0.17	5.45±0.38	8.50±0.59	11.10±0.77	0.00±0.00

**Table 11.2. Comparison of antifungal activity of silver nanoparticles obtained using Malonic Acid-Glucose- Glutamine (MA-GLU-GLUT) and Malonic Acid-Fructose- Glutamine (MA-FRU-GLUT) sample solutions with a standard solution, Fluconazole (Std).**

Fungal strains	Solvent	Samples	Std.	Control	
		30µL	30 µL	30 µL	
<i>Candida albicans</i>	MA-GLU-GLUT	3.50±0.24	6.70±0.46	7.10±0.49	0.20±0.01
	MA-FRU-GLUT	2.70±0.18	4.90±0.34	6.90±0.48	0.10±0.01
<i>Aspergillus niger</i>	MA-GLU-GLUT	3.00±0.21	5.50±0.38	7.00±0.49	0.20±0.01
	MA-FRU-GLUT	2.40±0.16	4.00±0.28	6.80±0.47	0.20±0.01

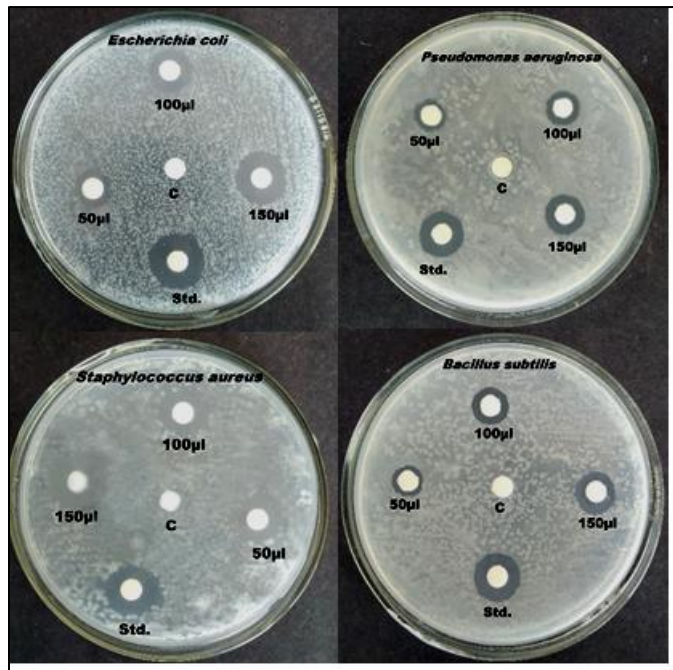


**Figure.11.1.1** Images of the zone of inhibition at various concentrations of copper nanoparticles obtained using MA-GLU

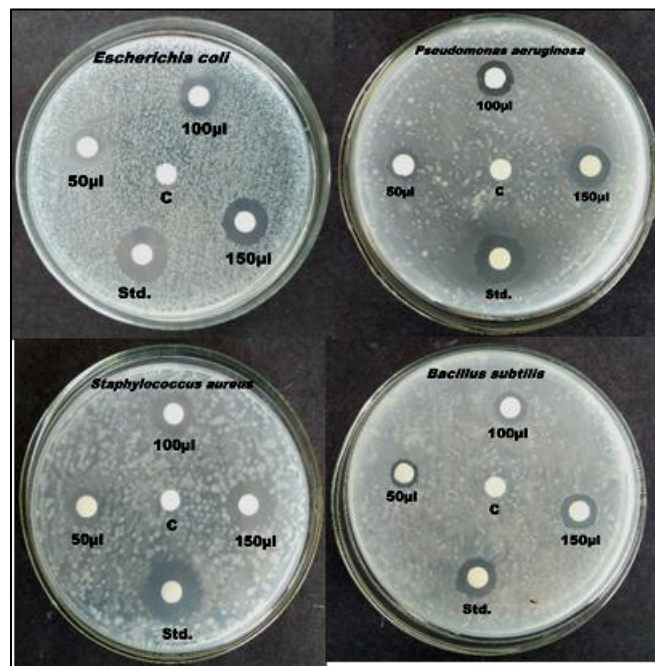


**Figure.11.1.2** Images of the zone of inhibition at various concentrations of copper nanoparticles obtained using MA-FRU

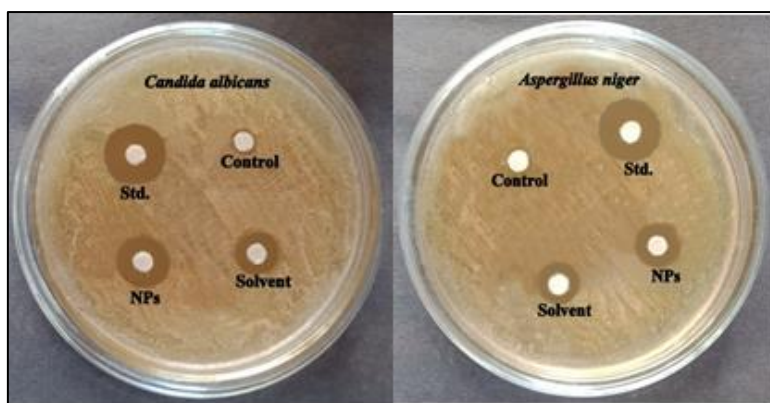


**Figure.11.2.1** Images of the zone of inhibition at various concentrations of silver nanoparticles obtained using MA-GLU-GLUT

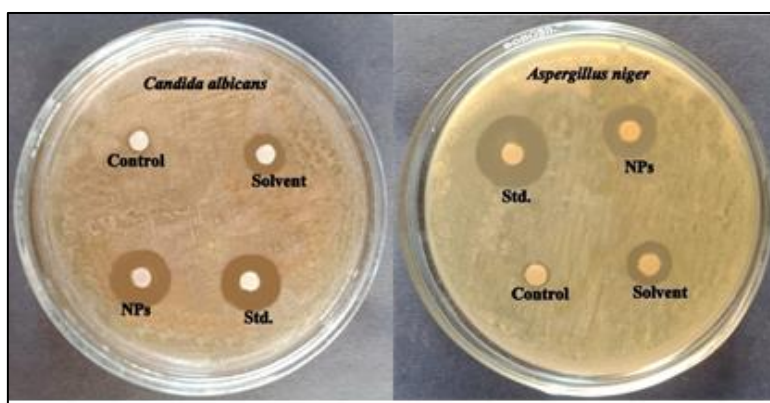


**Figure.11.2.2** Images of the zone of inhibition at various concentrations of silver nanoparticles obtained using MA-FRU-GLUT



## 12.1 Summary and conclusion

---

In this investigation, we had used a common method, evaporating method to develop novel deep eutectic solvents. Nine types of binary deep eutectic solvents and eighteen types of ternary deep eutectic solvents were successfully synthesized and their physical properties such as pH, viscosity, conductivity, density were measured and the bonding interactions between the materials taken were also characterized by FTIR. The binary deep eutectic solvents are far better than ternary deep eutectic solvents as they are clear liquids for more than two weeks and their viscosities are not so high. The three binary deep eutectic solvents such as MA – GCL, ZC – LA, MC – CA are more viscous than other deep eutectic solvents. Except the above three, others are stable until 100°C. The binary and ternary deep eutectic solvents are well suitable for using as greener solvents.

We used the chemical reduction method for the synthesis of copper, silver nanoparticles, and the chemical co-precipitation method for the synthesis of cadmium, mercury nanoparticles using our prepared DESs. These methods are simple and very convenient as no surfactant or seed needed for the formation of nanoparticles. The size of the particle was controlled by adjusting the amount of water. The formation of nanoparticles was confirmed by UV, FTIR, XRD, SEM, and EDAX techniques. The method used for the synthesise of nanoparticles is a simple and eco-friendly method. We had got many nanoparticles as efficient, and these nanoparticles were used for the studies of antibacterial, antifungal activities.

We had studied antimicrobial activities for some specified solvents and nanoparticles. The nanoparticles show more anti-microbial activities than their respective solvents used for the synthesis of the nanoparticles. Notably, silver nanoparticles show more activity toward the microorganisms than copper nanoparticles.

Viscosity is an important property to be used as solvents. The liquids with a moderate viscosity are well suitable for the synthesis of nanoparticles due to the availability of fewer voids. If the solvents are too viscous, it is difficult to dissolve the materials in them and there is less possibility for the formation of nanoparticles. For this reason, there was no formation of nanoparticles in Malonic acid- glycerol binary deep eutectic solvent. It is confirmed by UV-Visible spectroscopy. During the preparation of copper nanoparticles in Zinc chloride- Lactic acid, the particles were crystallized, and the solubility of crystals in various solvents. But the crystals were dissolved. So, we had not taken for further investigations.

The copper nanoparticles in Manganese chloride- fructose- histidine ternary deep eutectic solvents yield sticky products. So, these nanoparticles were not considered for further characterization studies.

In summary, it was observed that the simple method for both the preparation of deep eutectic solvents and the synthesis of nanoparticles are the advantages of our study. The nanoparticles also show more antimicrobial behaviours than solvents, which is a beneficial added to our investigation.

## **12.2 Future perceptive of the work**

- Investigation of some other deep eutectic solvents by combining various hydrogen-bonded donors with metal salts.
- Applying these solvents for various organic reactions.
- For synthesizing different nanoparticles such as Zinc, Manganese, Zirconium using these solvents.
- To check the antimicrobial studies for the remaining nanoparticles.
- To study the physical properties such as surface tension for these deep eutectic solvents.



- To study the industrial applications of these deep eutectic solvents.
- To check the reusability and recyclability of deep eutectic solvents.



## List of articles published as in the UGC listed Scopus indexed peer-reviewed journals

---

1. K. Sarjuna, D. Ilangeswaran; Preparation of some zinc chloride-based deep eutectic solvents and their characterization, *Materials Today: Proceedings* 33 (2020) 2767–2770.  
<https://doi.org/10.1016/j.matpr.2020.02.080>.
2. K. Sarjuna, D. Ilangeswaran; Preparation and Physico-Chemical studies of Ag<sub>2</sub>O nanoparticles using newly formed Malonic acid and ZnCl<sub>2</sub>-based Deep Eutectic Solvents. *Materials today: proceedings*; 49 (2022) 2943–2948.  
<https://doi.org/10.1016/j.matpr.2021.11.355>.
3. K. Sarjuna, D. Ilangeswaran; Synthesis and Characterization of Silver Nanoparticles Using Zinc Chloride-Sugar-Amino Acids Based Novel Ternary Deep Eutectic Solvents; *ECS transactions*. (Accepted)
4. K. Sarjuna, D. Ilangeswaran; Synthesis and characterization of copper (II) Oxide nanoparticles using newly developed Malonic acid-based deep eutectic solvents and their antibacterial activity; *International Journal of Nanoscience* (Under considerations).
5. K. Sarjuna, D. Ilangeswaran; Synthesis of some metal/metal sulfide nanoparticles using a superior dissolvable media- Malonic acid (MA) based Deep Eutectic Solvents [DES]; *Abstracts of International Conferences & Meetings (AICM); Krispon Advancing science; Volume-1, Issue-5, 2021* 14DOI: <https://doi.org/10.5281/zenodo.5371643>
6. K. Sarjuna, D. Ilangeswaran; Synthesis and Characterization of Silver Nanoparticles Using Zinc Chloride-Sugar-Amino Acids Based Novel Ternary Deep Eutectic Solvents: Silver Nanoparticles- Characterization; *SPAST Abstracts*, 1(01).  
<https://spast.org/techrep/article/view/193>

7. K. Sarjuna, D. Ilangeswaran; Silver Nanoparticles: Synthesis in newly formed Ternary Deep Eutectic Solvent Media, Characterization, and their Antifungal activity; Current Nanomaterials; ( Under consideration ).

### **List of papers presented in the international conferences**

---

1. D. Ilangeswaran and K. Sarjuna, “Synthesis and Characterization of newer sugar based deep eutectic solvents”, Frontier Areas in Chemical Technologies (FACTS-2017) organized by Department of Industrial Chemistry, Alagappa University, Karaikudi, Tamilnadu, India held during 6<sup>th</sup> to 8<sup>th</sup> July 2017.
2. D. Ilangeswaran and K. Sarjuna, “Synthesis and Characterization of newly developed Mn<sup>2+</sup> and Zn<sup>2+</sup> based deep eutectic solvents”, International Conference on Recent Trends in Synthetic Methods and Material Chemistry (RTSMC-2018) organized by Department of chemistry, Annamalai University, Annamalai Nagar, Tamilnadu, India held during 2<sup>nd</sup> & 3<sup>rd</sup> February 2018.
3. K. Sarjuna and D. Ilangeswaran, “Malonic acid-based deep eutectic solvents- A better solvent media for the synthesis of some metal/metal sulfide nanoparticles”, International Conference on Frontiers in Chemical and Material Sciences (ICFCMS-2020), organized by Department of chemistry, The Gandhigram Rural Institute, Gandhigram, Tamilnadu, India held during 24<sup>th</sup> & 25<sup>th</sup> February 2020.
4. K.Sarjuna, D. Ilangeswaran; “Synthesis of some metal/metal sulfide nanoparticles using a superior dissolvable media- Malonic acid (MA) based Deep Eutectic Solvents [DES]”, the International Online conference on NanoMaterials (ICN 2021) held at Mahatma Gandhi University, Kottayam, Kerala, India during 09<sup>th</sup> -11<sup>th</sup> April 2021.

5. K.Sarjuna, D. Ilangeswaran; “Synthesis and characterization of copper oxide nanoparticles using greener solvents- Malonic acid- Sugar - Amino acids based Deep Eutectic Solvents”, the International Conference on Smart Materials Chemistry (CHEMSMAT 2021) organized by the Department of Chemistry, St. Joseph’s College, Tiruchirapalli, Tamilnadu, India held during 29<sup>th</sup> -31<sup>st</sup> July 2021.
6. K.Sarjuna, D. Ilangeswaran; “Synthesis And Characterization Of Silver Oxide Nanoparticles Using Newly Formed Malonic Acid And Zinc Chloride-Based Deep Eutectic Solvents” International Conference On “ Innovative Research In Applied Engineering And Computing Methodologies (ICIRAEK2K21)” organized by Department of Electronics And Communication Engineering, Syed Ammal Engineering College, Ramanathapuram, Tamilnadu, India held during 13<sup>th</sup> & 14<sup>th</sup> August 2021.
7. K. Sarjuna, D. Ilangeswaran; “Synthesis and Characterization of Silver Nanoparticles Using Zinc Chloride-Sugar-Amino Acids Based Novel Ternary Deep Eutectic Solvents: Silver Nanoparticles- Characterization”, International Conference on Technologies for Smart Green Connected Societies (ICTSGS-2021), online worldwide led by Yamagata University Japan held during 29<sup>th</sup> & 30<sup>th</sup> November 2021.